ENGINEERING COLORECTAL CANCER MODELS FOR MECHANISTIC STUDIES AND THERAPEUTICS

A Dissertation

Presented to the Faculty of the Graduate School

of Cornell University

In Partial Fulfillment of the Requirements for the Degree of

Doctor of Philosophy

By Huanhuan Chen

August 2014

ENGINEERING COLORECTAL CANCER MODELS FOR MECHANISTIC STUDIES AND THERAPEUTICS

Huanhuan Chen, Ph. D.

Cornell University 2014

ABSTRACT

Current orthotopic xenograft models of colorectal cancer (CRC) require survival surgery and do not robustly form tumors in liver, the most common site of metastasis in patients. In the work described in the thesis chapter 2, we used chemokine-targeting to develop cell line and primary patient-derived xenograft models that recapitulate the vast majority of common human somatic CRC mutations as primary gastrointestinal (GI) tumors in mice without requiring surgery. Importantly, we utilize early-stage mouse blastocyst microinjection techniques to extend this approach and model primary human CRCs in immunoproficient mouse hosts. Next, we show that primary GI tumors can inducibly and robustly metastasize to liver. Finally, we demonstrate that human CRC liver metastases *in vivo* have higher levels of DKK4 and NOTCH signaling and are more chemoresistant than paired sub-cutaneous xenografts. Overall, we anticipate that this experimental system can help improve our mechanistic understanding of human primary CRC progression to liver metastasis and provide a more physiological model than sub-cutaneous xenografts for pre-clinical drug screening.

Refined cancer models are urgent to bridge the gap between cell-line or animal based research and clinical research. In thesis chapter 3, we described an organotypic colon cancer model which was generated from human native matrix and have

pathophysiologically recapitulated the natural features of progression from APC-dependent *in situ* neoplasia to sub-mucosal invasive adenoma in colorectal cancer (CRC)-associated genetic pathways. To identify invasion-driver genes, we performed a forward genetic screen using *Sleeping Beauty (SB)* transposon- based mutagenesis in the *ex vivo* CRC model. This screen identified 39 candidate genes, all of which are listed in TCGA CRC dataset. 17 of them, including TCF7L2, TWIST2, MSH2, DCC and EPHB1,2, most likely drive invasion of CRC through cooperation with mutant APC. Among the remaining genes that have not previously been implicated in CRC, seven out of ten were functionally validated to significantly promote the growth, migration or invasion of colon cells. This piece of work demonstrated the utility of ex vivo human-originated models with transposon-based mutagenesis and provided a new system for studying the biology of cancer.

BIOGRAPHICAL SKETCH

Huanhuan Joyce Chen was born in Pingyang, Wenzhou, China where her grandfather was the county mayor, father was the county sheriff and mother was a civil servant. She loved to spend much time in childhood with her grand grandmother, who had been a nun in the hometown Temple for more than sixty years. Affected by Buddhism at her young age, huanhuan became intrigued with the origins of human life and this seeded her interests in life science.

Upon the encouragement and supports of her parents, Huanhuan decided to study pharmaceutical sciences at Zhejiang University in Hangzhou. After seven years of academic life enriched with activities in literature club, being a volunteer in pharmacy stores, road trips covering most area in Zhejiang and struggling for the balance between studying majors and preparing for GRE, she graduated with both Bachelor degree and Master degree in pharmacology in the August of 2003. Her interests in cancer research came through when she worked as a research assistant for Professor Daoxing Peng and made an exciting discovery that the anti-malarial drugs also can inhibit cancer growth and angiogenesis by suppressing cellular iron influx. She published four papers on this work with each paper cited to date in more than 150 citations and was awarded as a young investigator grant in Zhejiang province.

After married Jason Chen, Huanhuan moved to New York City and her son Jace was born in the fall of 2006. After taking care of Jace and working to support her family for four years, Huanhuan resumed her academic life by enrolling in PhD program in Biomedical Engineering at Cornell University in 2010, with hopes of doing research in

cellular and tissue engineering for studying oncology. She was mentored by Professor Steven M Lipkin in studying colorectal cancer biology and by Professors Xiling Shen and Michael L Shuler in modeling oncology. She successfully defended her dissertation on June 24th in 2014.

With forever love to my grandparents and son

ACKNOWLEDGEMENTS

First and foremost I would like to thank my thesis advisor, Professor Xiling Shen, for his mentorship throughout my graduate study. He encouraged me to pursue my passion and cross the traditional boundaries into interdisciplinary research while guiding me with his advice, feedback and support. He has also been generously supporting my professional development and his encouragement and advice helped me win the National Science Foundation (NSF) fellowship.

I am deeply indebted to my biology minor advisor, Professor Steven Lipkin at Weill Cornell medical college, for guiding me into the fields of cancer biology, for providing me with most research resources he could get, for his amazing patience, for sharing his knowledge and ideas, for seeing the potential of my work, and for his always encouragements, trusts and reliability when I encountered every difficulty in my research.

My many thanks also go to my engineering minor advisor, Professor Michael Shuler, for sharing his wisdom, engineering expertise, and resources. He serves as an inspirational role model with his open-mindedness towards research, his unconditional support of junior researches, and his long, celebrated career that focuses on innovation and impact. I will carry these invaluable assets with me for the rest of my career.

I would also like to thank my committee member, Professor Robert Weiss, for his generous advice, suggestions and comments that have contributed greatly to my research progress and thesis.

I am very thankful to my collaborator lab, Professors Nancy Jenkins and Neal Copeland, and their postdoc Dr. Zhubo Wei, at Methodist Hospital Research Institute, for helps in designing projects, data analysis, and technical supports in transposon mutagenesis system and helps with my proposal for the National Cancer Institute (NCI)-PSOC grant. I also would like to thank Professors Rita Serda and Steven Curley and their graduate student David Savage, at Methodist Hospital Research Institute, for their helpful advice and comments on my PS-OC grant proposal.

I am very thankful to my great colleagues and collaborators without whom I could not get any piece of my research work done: to Dr. Pengcheng Bu and his wife, graduate student Lihua Wang, for discussing projects with me, inspiring enthusiasm in my research and their readiness to help; to Dr. Jian Sun for great helps in solving all of the tough problems in genetic analyses, and being extremely patient in teaching bioinformatics to me; to Myra Arcilla, Nikolai Rakhilin and Paula Miller, the three lab mangers in Lipkin, Shen and Shuler labs respectively, for their unselfish helps and preparing my experiments; to Professor Winfried Edelmann and Harry Hou at Albert Einstein College of Medicine, for developing the amazing idea and technique of mouse blastocyst injection with human cancer cells; to Professor Robert Edwards at University of California, Irvine, for helpfulness in colon cancer pathology; to professor Nozomi Nishimura and her two-photon imaging group for providing the fascinating in vivo tumor imaging; to professor John Schimenti and his mouse genetics facility for the technique supports of mouse blastocyst injection; to Professor Shuibing Chen and her postdoc Dr. Miguel Crespo, at Weill Cornell medical college, for providing the precious iPSC cells and IRB approval for my projects, to Asmita Bhattaharya for teaching me molecular

cloning and reading-proof for my manuscript, to Belinda Floyd, Susan Payne and Jackie Creque at Cornell Biomedical Engineering (BME) for administrative assistance, and many others who have offered helps.

I am also indebted to both my families in China and in New York City, for their unconditional love, support, encouragements and sacrifices throughout my ups and downs. I took many adventures into uncharted waters during my PhD research and professional development because I always knew that I could fall back to the safe harbor provided by my family, who has been stretching to provide me with financial and emotional support. Specially, I dedicated this thesis to the memory of my grandfather, Jiazhang Wu, whose role in my life was, and remains immense. Last but not the least, I wrote the thesis to my dear husband, Jason Chen, and son, Jace Chen, who have been with me for all of the time and made it the best time in my life.

TABLE OF CONTENTS

BACKGROUND

Colorectal cancer (CRC) is a major public health source of morbidity and mortality. Approximately 5% of the population in western world will develop colorectal malignancies during their lifetime and 25% of CRC patients eventually die from metastatic disease [1, 4]. Thus, it is urgent for research to enhance our ability to diagnosis, prevent and treat this disease. To improve patient outcome largely depends on precisely interdicting the mechanisms of metastasis and developing therapy targeting the mechanisms.

Genetics of Colorectal Cancer

Each disease stage during CRC progression develops distinct pathological features [27]. Firstly, inappropriate proliferation cause colon stem or progenitor cells to transform into colon cancer stem cells, which start with adenoma formation and evolve into carcinoma *in situ*. Then, pre-invasive CRCs, by accumulating more genetic mutations, acquire the ability to invade through the submucosa and muscularis, and metastasize out of the colon microenvironment niche and in the distant organs.

In the CRC molecular etiology, each clinical stage highly correlates with sequential accumulations of mutations in major genes [1, 10]. CRC generally can be divided into two classes based on the genetic background displaying chromosomal instability (CIN) or microsatellite instability (MSI), in which CIN phenotype occurs in 80-90% CRC cases. CRCs displaying CIN frequently harbor loss-of-function mutations in adenomatous polyposis coli (APC) which is believed to be the initial event to transform normal colon epithelium into pedunculated adenomatous polyps through up-regulating *WNT* signaling.

Then additional somatic mutations occur to drive malignant transformation of pedunculated adenomatous polyps to invasive and metastatic adenocarcinomas [5, 10, 27]. The “Vogelstein model” [11, 28] described oncogene KRAS/BRAF mutations promote the early stage adenoma to late stage adenoma, and further mutations in DCC, TP53, and abrogation of the TGF-β pathway, including mutations in SMAD4 and TGFBR2, are thought to occur later in CRC progression, transforming the adenoma to a carcinoma. Although colorectal cancer (CRC) progression appears to be characterized by high-frequency mutations, such as KRAS, SMAD, TP53, many low-frequency mutations are also believed to contribute to the disease development. The advance in secondary generation sequencing has accelerated the identification of genetic alterations in human cancers in whole-genome scale and comprehensive molecular studies such as TCGA (The Cancer Genome Atlas) [1] have provided a broad range of insights with an unprecedented level of molecular resolution into the precise molecular alterations that drive human CRC pathogenesis and progression.

Chemokine Network with CRC

Chemokines, family members of cytokines, are 8- to 12-KD polypeptides that when binding to specific G protein – coupled chemokine receptors, activate signaling cascades guiding cell migration toward chemokine ligand gradients. Chemokine-regulating cell movements play critical roles in immunity, embryonic development, angiogenesis, wound healing and involved in the physiological events of central nervous system, and skeletal muscle. Chemokine signaling pathways are essential to the functions of immune system, mediating various types of immune cells trafficking between the secondary lymph sites and the regions of inflammation [17, 19, 21, 22].

The connection between inflammation and cancer has been well-established and more and more recent studies indicate that chemokines play key roles in both driving and preventing cancer progression [3, 6, 14, 15, 16]. Many human cancers have a complex chemokine network that regulates the extent and phenotype of the infiltrating leukocytes, as well as have an effect on tumor growth, survival, migration, and angiogenesis. Cancer cells can produce chemokines to regulate immune cell behaviors, and alter inflammation microenvironment which in turn effects cancer progression. Cancer cells also can express chemokine receptors and thus directly guide themselves into targeted organs and develop metastases. Interestingly, studies indicate that adaptive immune cells have the potential to limit tumor progression. Galon and colleagues demonstrated that the presence of CD8+ T cells infiltrate is associated with the absence of early metastatic processes in patients with melanoma, ovarian cancer and CRC [20]. In contrast, the persistence of active innate immune responses, such as the chronic inflammation at tumor sites, has been implicated with poor clinical outcome [2, 7].

Chemokine ligand CCL25 and receptor CCR9 are unique and critical to intestinal immune system. Intestinal epithelial cells secrete CCL25 to attract CCR9 expressing lymphocytes into gut for immune function [19]. Evidence shows [3, 15, 16, 23] that gut produced CCL25 regulate CCR9+ melanoma or ovarian cancer cells to spread metastases in intestines. However, how the CCR9-CCL25 axis interacts with colon cancer under native intestinal conditions has been poorly understood. My first project [8] described in chapter 1 of the dissertation for the first time reveal a new function for

CCR9-CCL25 axis to inhibit CRC invasion and metastasis and describe a novel *in vivo* experimental system to study CRC mechanisms.

Animal models of CRC

Animal models capitulating features of specific human CRC are invaluable tools necessary to study carcinogenesis, the specific molecular mechanisms of colon cancer, to test potential preventive and therapeutic strategies, and to translate the research hypotheses derived from cell models into the results under physiologically – relevant conditions. However, one of the major limitations in current experimental system for studying CRC is the absence of refined animal models to bridge the gaps in translational research.

A genetically engineered mouse model (GEMM, transgenetic mice) is one of the most used in vivo models for cancer study. However, it has some weakness: First, only some of major genes relevant to human CRC have been to date modified to make GEMM with floxed alleles, enabling specifically targeting the colon epithelial cells. The lack of mice with variant floxed gene alleles limits the generation of GEMM with either intestine-specific or inducible genetic modifications. Second, almost all of whole-body gene-modified or chemical-induced models develop tumors outside the colon or with colon cancer as a minor phenotype. Thus, due to its over-simple genetic background, GEMM hardly captures all the features of the genetic mutations and epigenetic regulations in human CRC diseases. For example, mouse screens for cooperating mutations are not always concordant with TCGA results to identify the most common mutations, genomic rearrangements and epigenetic in the corresponding human cancer.

Subcutaneous xenograft models, the current workhorse for drug screening, lack the native gut microenvironment and the property of distant metastasis, thus lead to many false positive drugs that can cure mice but fail in patients [4]. Surgical implantation of CRC cells under the kidney capsule, or orthotopic implantation through intra-cecum or rectal injection overcomes this limitation. However, injection needle tracts create potential artifacts for cell egress, disturb the extracellular matrix and artificially generate a local inflammatory microenvironment, which confound the research results. Additionally, we currently do not have robust, consistent models of CRC liver metastasis from primary intestinal sites. Advance methods are required to model more accurately CRC metastasis and improve therapeutics.

In my second project described in the chapter 2, we used chemokine-targeting to develop cell line and primary patient-derived xenograft models that recapitulate the vast majority of common human somatic CRC mutations as primary gastrointestinal (GI) tumors in mice without requiring surgery. Importantly, we utilize early-stage mouse blastocyst microinjection techniques to extend this approach and model primary human CRCs in immunoproficient mouse hosts. We anticipate that this experimental system can help improve our mechanistic understanding of human primary CRC progression to liver metastasis and provide a more physiological model than sub-cutaneous xenografts for pre-clinical drug screening.

Transposon-Mediated Mutagenesis System

Transposons are discrete DNA elements including transposon and transposase, which have the unique ability to change their genomic position through “cut and paste”

mechanism [12, 13]. The Tc1/ mariner transposons are the most wide-spread transposons found in nature and have little insertion site preference, except that they always integrate into a TA dinucleotide. Ivics and colleagues genetically engineered a synthetic transposase, *SB10*, which can precisely mobilize the Tc1/ mariner elements in all the major types of vertebrate cells. This transposon system was named Sleeping Beauty *(SB). SB* Transposon-based insertional mutagenesis (TIM) provides an alternative high-throughput platform for cancer gene discovery [24, 25]. To our knowledge, the *SB*-TIM system has been considered non-biased, efficient, and thus the best mutagenesis system to date to simulate somatic mutations in cancer models.

Copeland & Jenkins Lab, one of our collaborators [9], developed a new mutagenic transposon T2/Onc2, which could up-regulate the expression of oncogenes or inactivate tumor suppressor genes. T2/Onc2 has been used to model many types of mouse cancers through introducing into the mouse germ line by microinjection, and the transgenic lines carrying enough high copy numbers of the transposon genes were selected to develop mouse tumors in multiple organs. Several research groups reported that *SB* inducing somatic-cell insertional mutagenesis in mice was successfully used for the identification of novel cancer genes and signaling pathways through forward genetics screen. The T2/Onc mobilization driven by the gastrointestinal tract-specific Villin promoter (Vil-Cre) can generate intestine-specific mutagenesis in APC ^{min} mouse models and this tissue-specific TIM system has been used for the identification of novel driver genes causing CRC progression through cooperation of APC mutations.

<u>Decellularization – Recellularization in Tissue Engineering</u>

Extracellular matrix (ECM) consists of the proteins and other biomolecules produced by cells, with cells made up the whole tissues. Each tissue has tissue-specific dynamically reciprocal communication in that cells response to the signals of ECM to regulate cellular behaviors and the cells in turn alter the composition of ECM and thus the entire tissue-specific microenvironment and so on. Similar to normal tissues, ECM and tissue microenvironment also play critically important roles in cancer initiation, promotion and progression. Studying cancer cells in 3D tissue context can produce more comprehensive and physiologically relevant results with concordance of translation to the clinical research.

The advance in tissue engineering and regenerative medicine shed more light on the technology of isolating the whole tissue matrix through efficient removal of cellular components. Through acid, enzyme or detergent-based methods, several groups have successfully in generating acellular organs of heart, lung, liver and kidney, with some further attempts to orthotopic transplantation of the organ constructs by recellularization. The decellularized matrix preserves the main proteins and biomolecules in ECM and retains complex tissue-specific geometry and structure including relative intact vasculature, thus provides an ideal culture platform for cancer cells to grow, form shapes and maintain cell-cell, cell-ECM interactions. Recently, Mishera and colleagues have developed ex vivo lung cancer models by growing several human lung cancer cell lines (A549, H1299 and H460) in the acellular rat lung matrix and the lung cancer cells grown in the matrix had features similar to the original human lung cancer.

In the chapter 3, we described, to our knowledge, the first ex vivo colon cancer model engineered from the native human colon tissue matrix using the decellularization-

recellularization techniques. Furthermore, we applied the CRC models combined with TIM in studying cancer genetics.

Currently large-scale and high-throughput genetic sequencing have facilitated the identification of genetic alterations in human cancers. However, because tumor heterogeneously evolves and numerous passenger mutations confound the footprints of driver alterations, most cancer studies using reverse genetics yield numerous and complex genetic candidates, making it difficult to identify the driver genes [5]. Another major obstacle to distinguish drivers from passengers rises from technical limitations of existing experimental systems. Conventional cell culture models as research platforms lack the capacity to maintain multiple-cellular interactions and tissue-specific microenvironment, which are required for tumor progression. Animal models are short of appropriate resolution and sensitivity to track the dynamics of cancer malignant transition. Animal study can also show considerable differences from humans with regard to requirements for oncogenic transformation. To bypass the above difficulties, we engineered ex vivo human CRC models with transposon-based mutagenesis that allowed us to perform rapid forward genetics study in human-originated colon tissues for exploring novel CRC-driver genes and improve the understanding of CRC biology. This work is described in chapter 3 in the dissertation.

REFERENCES

1. *Comprehensive molecular characterization of human colon and rectal cancer.* Nature, 2012. **487**(7407): p. 330-7.

2. Allavena, P., et al., *The Yin-Yang of tumor-associated macrophages in neoplastic progression and immune surveillance.* Immunol Rev, 2008. **222**: p. 155-61.

3. Amersi, F.F., et al., *Activation of CCR9/CCL25 in cutaneous melanoma mediates preferential metastasis to the small intestine.* Clinical cancer research : an official journal of the American Association for Cancer Research, 2008. **14**(3): p. 638-45.

4. Arrowsmith, J., *Trial watch: Phase II failures: 2008-2010.* Nat Rev Drug Discov, 2011. **10**(5): p. 328-9.

5. Bozic, I., et al., *Accumulation of driver and passenger mutations during tumor progression.* Proc Natl Acad Sci U S A, 2010. **107**(43): p. 18545-50.

6. Burger, J.A. and T.J. Kipps, *CXCR4: a key receptor in the crosstalk between tumor cells and their microenvironment.* Blood, 2006. **107**(5): p. 1761-7.

7. Cao, Z., et al., *Angiocrine factors deployed by tumor vascular niche induce B cell lymphoma invasiveness and chemoresistance.* Cancer Cell, 2014. **25**(3): p. 350-65.

8. Chen, H.J., et al., *Chemokine 25-induced signaling suppresses colon cancer invasion and metastasis.* J Clin Invest, 2012. **122**(9): p. 3184-96.

9. Copeland, N.G. and N.A. Jenkins, *Harnessing transposons for cancer gene discovery.* Nat Rev Cancer, 2010. **10**(10): p. 696-706.

10. de Lau, W., N. Barker, and H. Clevers, *WNT signaling in the normal intestine and colorectal cancer.* Frontiers in bioscience : a journal and virtual library, 2007. **12**: p. 471-91.

11. Fearon, E.R. and B. Vogelstein, *A genetic model for colorectal tumorigenesis.* Cell, 1990. **61**(5): p. 759-67.

12. Ivics, Z., et al., *Molecular reconstruction of Sleeping Beauty, a Tc1-like transposon from fish, and its transposition in human cells.* Cell, 1997. **91**(4): p. 501-10.

13. Ivics, Z., et al., *Transposon-mediated genome manipulation in vertebrates.* Nat Methods, 2009. **6**(6): p. 415-22.

14. Johnson, E.L., et al., *CCR9 interactions support ovarian cancer cell survival and resistance to cisplatin-induced apoptosis in a PI3K-dependent and FAK-independent fashion.* J Ovarian Res, 2010. **3**: p. 15.

15. Johnson, E.L., et al., *CCL25-CCR9 interaction modulates ovarian cancer cell migration, metalloproteinase expression, and invasion.* World J Surg Oncol, 2010. **8**: p. 62.

16. Johnson-Holiday, C., et al., *CCL25 mediates migration, invasion and matrix metalloproteinase expression by breast cancer cells in a CCR9-dependent fashion.* Int J Oncol, 2011. **38**(5): p. 1279-85.

17. Kabelitz, D. and D. Wesch, *Features and functions of gamma delta T lymphocytes: focus on chemokines and their receptors.* Critical reviews in immunology, 2003. **23**(5-6): p. 339-70.

18. Kopan, R. and M.X. Ilagan, *The canonical Notch signaling pathway: unfolding the activation mechanism.* Cell, 2009. **137**(2): p. 216-33.

19. Meurens, F., et al., *Expression of TECK/CCL25 and MEC/CCL28 chemokines and their respective receptors CCR9 and CCR10 in porcine mucosal tissues.* Vet Immunol Immunopathol, 2006. **113**(3-4): p. 313-27.

20. Pages, F., et al., *Effector memory T cells, early metastasis, and survival in colorectal cancer.* N Engl J Med, 2005. **353**(25): p. 2654-66.

21. Peled, A., O. Wald, and J. Burger, *Development of novel CXCR4-based therapeutics.* Expert opinion on investigational drugs, 2012. **21**(3): p. 341-53.

22. Rettig, M.P., et al., *CXCR4 and mobilization of hematopoietic precursors.* Methods in enzymology, 2009. **460**: p. 57-90.

23. Sharma, P.K., et al., *CCR9 mediates PI3K/AKT-dependent antiapoptotic signals in prostate cancer cells and inhibition of CCR9-CCL25 interaction enhances the cytotoxic effects of etoposide.* Int J Cancer, 2010. **127**(9): p. 2020-30.

24. Starr, T.K., et al., *A Sleeping Beauty transposon-mediated screen identifies murine susceptibility genes for adenomatous polyposis coli (Apc)-dependent intestinal tumorigenesis.* Proc Natl Acad Sci U S A, 2011. **108**(14): p. 5765-70.

25. Su, Q., et al., *A DNA transposon-based approach to validate oncogenic mutations in the mouse.* Proc Natl Acad Sci U S A, 2008. **105**(50): p. 19904-9.

26. Trobridge, P., et al., *TGF-beta receptor inactivation and mutant Kras induce intestinal neoplasms in mice via a beta-catenin-independent pathway.* Gastroenterology, 2009. **136**(5): p. 1680-8 e7.

27. Vermeulen, L., et al., *Single-cell cloning of colon cancer stem cells reveals a multi-lineage differentiation capacity.* Proceedings of the National Academy of Sciences of the United States of America, 2008. **105**(36): p. 13427-32.

28. Wood, L.D., et al., *The genomic landscapes of human breast and colorectal cancers.* Science, 2007. **318**(5853): p. 1108-13.

CHAPTER 1

The Chemokine 25/Chemokine Receptor 9 Axis Suppresses Colon Cancer Invasion and Metastasis

(Contribution: Steven Lipkin, Huanhuan Chen and Xiling Shen designed the project; Huanhuan Chen, Robert Edwards and Serena Tucci performed experiments; Steven Lipkin, Huanhuan Chen, Xiling Shen wrote the manuscript; Winfried Edelmann and Zeynep H. Gümüş helped with project discussion.)

INTRODUCTION

Colorectal cancer is a leading cause of cancer death worldwide. CRC progresses through multiple distinct stages in its evolution. Morphologically, inappropriate proliferation and anti-apoptosis cause formation of adenomas, which evolve into pre-invasive carcinoma *in situ*. Then, pre-invasive CRCs acquire the ability to invade through the submucosa and muscularis, metastasize, and survive outside the colon microenvironment niche [1-3]. Mechanistically, mutations activating WNT signaling in transformed colon cancer cells are an early event [4-6]. Subsequently, mutations in KRAS, TGFBR1, BRAF, TP53, DNA mismatch repair genes, FBXW7, NOTCH, PI3 Kinase and other signaling pathways accumulate to promote CRC tumor progression to invasive and metastatic disease [7-11]. As 5-year survival for early stage CRC is ~90% vs. ~15% for metastatic CRC, understanding in great detail the mechanisms that regulate the transition from indolent (adenomas and carcinoma *in situ*) to locally invasive early clinical stage(stage I-II) and metastatic later stage(stage III/IV) CRC is critical to improving patient outcomes[12].

Chemokines are a family of secreted ligands that play important roles in regulating lymphocyte intra- and intercellular signaling, anti-apoptosis and trafficking between different organs, such as bone marrow and intestinal mucosa[13]. The G-protein coupled chemokine receptor CCR9 and its ligand CCL25 comprise a signaling axis that is particularly important for the small intestine and colon. Small intestine and colon epithelial cells produce CCL25 [14-17]. This attracts circulating CCR9+ T cells to intravasate into the gut towards the CCL25 source.CCL25 binding promotes CCR9 $G_{\beta\gamma}$ interaction with PI-3 kinase, which initiates a downstream cascade activating AKT

kinase. AKT phosphorylates several targets, including GSK3B, promoting T cell proliferation, anti-apoptosis and mucosal immunity [14, 15, 18-20]. In addition to producing CCL25, small intestine and colon epithelial cells also express CCR9. Small intestinal epithelial cell CCR9 increases local immune response, while colonic epithelial cell CCR9 reduces inflammation, possibly by acting as a CCL25 “sink”[15]. Furthermore, melanoma, ovarian, breast and prostate adenocarcinomas express CCR9 [21-25]. This is proposed to play a role in tumor cell anti-apoptosis and proliferation. Overall, these findings show that CCL25/CCR9 plays a variety of important roles in different cell types, including several cancers.

Here, we reveal a novel role for CCR9 to inhibit colorectal cancer invasion and metastasis. Compared to normal colon mucosa, CCR9 is upregulated in adenomas and pre-invasive colorectal cancers. In contrast, CCR9 expression is subsequently downregulated in invasive and metastatic CRCs. Because the commonly used colorectal cancer cell lines we tested were CCR9-, we searched for new cell culture models and found that both primary colorectal cancer cell cultures and CCIC lines made from early stage tumors are CCR9+. *In vivo*, systemically injected CCR9+ early stage CCIC spontaneously form orthotopic colon and small intestinal xenografts, which has never been observed with any previous CRC cell line, while commonly used colorectal cancer cell lines (as has been described in the literature) and CCR9- CCIC form only extra-intestinal tumors. Blocking the CCR9-CCL25 axis inhibits CCIC intestine/colon tumor formation while increasing extra-intestinal tumor multiplicity. Finally, we show that NOTCH signaling, which stimulates CRC invasion and metastasis, promotes CCR9 proteosomal degradation, inhibits CCL25 dependent AKT signaling and increases extra-

intestinal colorectal cancer tumors. Overall, these data provide insights into the mechanism by which CCR9/CCL25 promotes colon-localized, early stage colorectal cancer growth while inhibiting invasion and metastasis, its suppression by NOTCH signaling in late stage colorectal cancer, and provide a novel *in vivo* model system to study CRC tumor progression in the native colon microenvironment.

RESULTS

CCR9 is upregulated in pre-invasive CRC and downregulated in invasive and metastatic CRC

To understand the expression pattern of CCR9 in colorectal cancer, we immunostained representative sections from patient tumors. Cases varied in clinical stage from adenoma to carcinoma *in situ* (Tis) to transmural involvement (T4). CCR9 staining intensity was scored for normal crypt epithelium and neoplastic tissue from each involved layer of the colon wall (**Figure 1**). Consistent with previous studies, CCR9 is expressed in normal colonocytes essentially throughout the entire crypt. To quantify CCR9 staining intensity, we used a histopathology scoring system ranging from 0-3. Normal colon epithelium had a mean staining intensity of 1.60±0.04, n=55. CCR9 staining in adenomatous foci was significantly increased (2.26±0.06, n=46) vs. normal tissue. In contrast, staining intensity progressively decreased in carcinoma *in situ*(2.03±0.08, n=19), and in carcinomas invasive into the submucosa (1.47±0.06, n=44) and muscle wall (1.13±0.08, n=42; all $p < 0.001$) (**Figure 1 A-I**). Additionally, we quantified CCR9 expression in primary CRC culture by FACS. Consistently, high percentages (~90%) of early stage (I/II) primary CRC cells areCCR9+, while much lower percentages of late stage (III/IV) invasive or metastatic CRCs (~10%) are CCR9+ (**Figure 1 J**). Overall, CCR9 levels are highest in non-invasive tumors (adenomas and in situ carcinomas) and progressively downregulated in submucosal invasive, muscle invasive and metastatic colorectal cancer tumors, consistent with a potential role for CCR9 to suppress invasion and metastasis.

To understand CCR9's role in colorectal cancer, we tested several commonly used colorectal cancer cell lines (HCT116, RKO, SW480 and LoVo) and found very low or undetectable CCR9 protein levels (**Figure 1 K,L**). In contrast, we found that several colon cancer initiating cell lines (CCIC) derived from early-stage/colon-localized (American Joint Committee on Cancer stage I/II) CRC patients [26, 27] generally have robust CCR9 protein expression. In contrast, CCIC lines derived from later stage (III/IV) patients whose tumors had spread beyond the colorectum have much lower CCR9 expression. This suggested that CCIC lines derived from early stage/colon-localized colorectal cancer patients might be a useful system for mechanistic studies of CCR9. Additionally, while only correlative, these data are consistent with immunohistochemistry that CCR9 protein levels are more closely associated with earlier stage CRC tumors that have less invasive and metastatic potential vs. later stage tumors with poorer prognosis.

Stage I/II CCIC form orthotopic xenograft CRC tumors in the colon and small intestine CCL25 produced by small intestine and colon epithelial cells attracts circulating CCR9+ T lymphocytes [28]. To understand the *in vivo* role of CCR9 in colorectal cancer, we injected CCIC lines systemically into the tail vein of immunodeficient mice (NOG mice). 73.3% of mice injected with early stage CCIC became moribund and developed average of 3.7 tumors in intestine/colon at mean 8.55 weeks post-inoculation (**Table 1**). Of mice that developed gastrointestinal (GI) tumors, 69% had tumors in both small intestine and colon, 19% only in colon and 12% only in small intestine (**Figure 2 H**). No upper GI or rectal tumors were seen. Many of these

tumors caused intestinal obstructions and pneumatosis coli (gas in the intestine from bacterial stasis and dysmotility secondary to obstruction) (**Figure 2 A,B**), pathologies often seen in patients with obstructing primary colorectal cancer adenocarcinomas. Evaluation of other organs showed that 35.6% of mice developed an average of 126 extra-intestinal tumor foci, mostly lung, and all were in mice that also carried intestine/colon tumors. In contrast, mice injected with CCIC derived from later stage tumors or commonly used colorectal cancer cell lines SW480 or LoVo formed tumors only outside the small intestine and colon (**Figure 2 H,I**). Similar to CCIC dermal xenografts and the vast majority of human primary and metastatic colorectal cancer tumors, CCIC colon/intestine and extra-GI tumors have adenocarcinoma morphology containing distorted crypt-like structures (**Figure 2 D-F**).

Mice injected with either early or late stage CCIC also became moribund at significantly earlier times post-inoculation vs. commonly used CRC cell lines ($P<0.001$) (**Supplemental Figure 1**). The colon/intestine tumors we observed could have arisen directly from early stage CCIC, or indirectly by stimulating endogenous mouse intestinal tumorigenesis. We systemically injected and tracked early stage CCIC carrying the PGK promoter driving constitutive expression of an eGFP reporter. First, we tested whether these tumors contained human DNA. PCR using two different human centromeric repeat sequences from genomic DNA isolated from intestine/colon tumors showed that they contain human DNA (**Figure 3 A**). Next, we examined the lower GI tract from mice carrying early stage CCIC colon/intestine tumors for eGFP fluorescence. This revealed that GI tumors consist of eGFP+ cells (**Figure 3 B, C, D**), indicating that the colon/ intestine tumors were formed by early stage CCIC in mouse hosts. As anticipated, the

intestine and colon sites where tumors formed expressed Ccl25 while sites of ex-GI tumors, such as lung, did not have detectable levels (**Figure 3 F, G**). Interestingly, early stage GI CCIC tumors were CCR9+ whereas ex-GI tumors were CCR9- (**Figure 3E**).

Stage I/II primary CRC cultures and CCIC show CCL25 dependent chemotaxis

To understand the role of the CCR9/CCL25 axis in primary colorectal cancer cells, we cultured tumor cells directly from patient tumors. Cells were sorted for expression of the colorectal cancer marker carcinoembryonic antigen (CEA) and plated in Boyden chambers. Consistently, more primary early stage colorectal cancer cultured cells migrated toward the chamber compartment containing recombinant CCL25 than mock control ($p<0.001$) (**Figure 4 A, B**) while SW480 did not. Migrated primary early stage colorectal cancer cells were double immunopositive (yellow) for CEA (red) and CCR9 (green) (**Figure 4 C**). Similarly, consistent with our *in vivo* xenograft studies, more early stage CCIC migrated *in vitro* towards a chamber containing CCL25 vs. a mock control while this activity overall was much lower for experiments with late stage CCIC (**Figure 4 D-F**). Altogether, these data show that both CCR9+ early stage colorectal cancer cells and CCIC functionally chemotax towards CCL25.

Inhibiting the CCR9/CCL25 axis reduces CCIC colon/intestine tumor formation

To test the role of CCR9 in CCIC orthotopic colon/intestine xenograft formation, we performed cell sorting for CCR9 and systemically injected CCR9+ or CCR9- early stage CCIC (**Supplemental Figure 5A**). Mice injected with CCR9+ CCIC had a high incidence of colon/ intestine tumors (both sites produce CCL25), whereas CCR9- CCIC

had low incidence (P<0.001) (**Table 2**). The mean number of colon/intestine tumors in mice injected with CCR9+ CCIC was also significantly higher than mice injected with CCR9- CCIC. At the same time, the incidence and mean number of tumors outside the colon/intestine were significantly higher in mice injected with CCR9- vs. CCR9+ CCIC (**Table 2**).

To confirm the role of CCR9/CCL25, we used anti-CCL25 antibodies to inhibit bioavailable intestinal CCL25. Pre-treating mice with anti-CCL25 antibodies before and concurrent with early stage CCIC injection reduced colon/intestine tumor multiplicity (**Supplemental Figure 5A**). Anti-CCL25 antibody treatment also trended towards reduced colon/ intestine tumor incidence and increased ex-GI incidence and multiplicity, although these differences were not statistically significant (**Table 2**). Additionally, we used CCR9 short hairpin RNA (shRNA) knockdown in CCIC. Mice injected with CCR9 shRNA knockdown CCIC had lower incidence, mean number of colon/intestine tumors and higher mean extra-intestinal tumors vs. mice injected with CCIC expressing a control shRNA (**Table 2** and **Supplemental Figure 2B**). The overall survival of mice injected with anti-Ccl25 antibodies or CCR9 shRNA knockdown CCIC was also significantly longer vs. control (**Table 2** and **Supplemental Figure 2C**).

The CCR9/CCL25 axis regulates CCIC metastasis out of the GI tract

To understand whether CCR9/CCL25 regulates CCIC metastasis out of the GI tract, we performed three sets of experiments involving antagonism of CCL25/CCR9 signaling after GI tumor initiation. First, we injected mice with CCR9+ CCIC, waited 3 weeks for colon/intestinal tumors to form and then treated mice with anti-Ccl25 antibodies. This

significantly increased both the incidence and multiplicity of CCIC ex-GI tumors (**Table 3, Supplemental Figure 3D, Supplemental Figure 4 and Supplemental Figure 5B**). Second, we injected CCR9+ CCIC with doxycycline inducible expression of anti-CCR9 or control shRNA. Approximately 3 weeks after injection, we administered doxycycline to induce CCR9 knockdown. This also significantly increased ex-GI CCIC tumor incidence and multiplicity (**Table 3**,**Supplemental Figure 3, Supplemental Figure 4, and Supplemental Figure 5B**). Third, we created HCT116 (which are CCR9-) sub-lines that stably express CCR9 (HCT116 $^{CCR9+}$) and used IVIS imaging to monitor the sites of tumor formation after tail vein injection. While HCT116 cells form ex-GI tumors, HCT116 $^{CCR9+}$cells in contrast form GI tumors in addition to ex-GI tumors. Interestingly, stable expression of CCR9 also reduces the overall burden of ex-GI tumors, as quantified by IVIS photon counting (**Supplemental Figure 6**). Altogether, these studies are consistent with CCL25/CCR9 antagonism causing CCIC in the intestine and colon to migrate outside the GI microenvironment and form additional ex-GI tumors.

CD26 and SNAL1 are associated with colorectal cancer migration and metastasis[29-31]. To understand whether they could play a role in CCIC migration outside the GI tract, we used shRNA to knock down expression of CD26 or SNAL1 by ~70% (**Supplemental Figure 2A**). However, neither of these gene knockdowns affected colon/intestine or ex-GI CCIC tumor formation, or survival of mice systemically injected with CCIC (**Supplemental Figure 2 B, C.**).

CCR9/CCL25 stimulates AKT signaling and cell proliferation in stage I/II CRC primary culture and CCIC

Our hematogenous xenograft studies show that CCR9+ early stage CCIC formed colon/intestinal tumors while CCR9- cells formed ex-GI tumors. To understand the signaling mechanisms regulated by CCL25/CCR9, we performed gene expression profiling of FACS sorted CCR9+ and CCR9- early stage CCIC (both treated with CCL25) with the Wafergen Human Oncology Panel Chip. Mapping all known interactions between differentially expressed genes to the Ingenuity Pathway Analysis mammalian interaction database revealed a network of CCR9/CCL25 upregulated oncogenic transcriptional regulators associated with cell proliferation, including FOS, FOSL1, JUN, EGR1 and ETS1 ($p=9.86e^{-12}$), directly downstream of AKT and NOTCH signaling pathways (**Figure 5 A**).To test whether CCL25/CCR9 regulates AKT signaling in CRC, we treated early stage primary colorectal cancer or CCIC cells with CCL25 and assayed for phospho-Ser473 AKT, a biomarker of activated AKT signaling. CCL25 treatment increased the number of phospho-Ser473^{+} and Thr 308 CCIC (**Figure 5 B-D**), consistent with activation of AKT signaling.

NOTCH signaling downregulates CCL25/CCR9 AKT signaling and chemotaxis

NOTCH signaling plays an important role in both normal intestine and CCIC.NOTCH signaling is activated by *JAGGED* 1 (*JAG1)* and *Delta-like* ligand binding to NOTCH receptors. This activates multiple proteolytic cleavage events [32, 33], after which the NOTCH receptor intracellular domain (NICD) is released and translocates to the nucleus. NICD interacts with the DNA-binding protein *RBPJκ*, which recruits co-activators and stimulates expression of NOTCH target genes including *HES* family genes[32]. Recently, an important new role for NOTCH signaling in promoting CRC invasion and metastasis was demonstrated [11, 34]. Because CCR9/CCL25 is

associated with early stage, colon-localized CRCs, we compared NOTCH signaling levels in FACS sorted CCR9+ and CCR9^{-} early stage CCIC treated with CCL25. NICD and *HES1*, biomarkers of active NOTCH signaling, were significantly higher in CCR9- vs. CCR9+ CCIC (**Supplemental Figure 8 A**). Confirming these data, we FACS sorted CCIC expressing eGFP under the control of a NOTCH responsive promoter containing multiple *RBPJ* binding sites (GFP-NOTCH) (**Supplemental Figure 7A**). GFP-NOTCH High early stage CCIC had lower levels of CCR9 and phospho-AKT (and higher levels of NICD and *HES1*) than GFP-NOTCH Low cells (**Supplemental Figure 8B**). Next, we treated stage I/II CCIC with a high concentration of *JAG1*. *JAG1* treatment increased CCIC NICD, *HES1* and the number of GFP-NOTCH+ cells (**Supplemental Figure 7 C** and **Supplemental Figure 8B**). *JAG1* also downregulated CCR9 protein levels (**Figure 8C**), consistent with a role for NOTCH as an upstream regulator of CCR9/CCL25 in colorectal cancer. To understand the mechanism of CCR9 downregulation by NOTCH signaling, we analyzed CCR9 mRNA and (co-treated with the proteosomal inhibitor PS-341), protein levels.CCR9 mRNA levels in two CCIC lines did not change in response to NOTCH activation, as measured by qPCR. In contrast, when cells were co-treated with the proteosomal inhibitor PS-341, CCR9 protein levels increased (**Figure 6 A, B**). Overall, these data are consistent with a mechanism whereby NOTCHlowers CCR9 protein levels by increasing its proteosomal degradation. Functionally, we found that *JAG1* inhibited CCL25 induced AKT phosphorylation and that co-incubation of CCIC with *JAG1* inhibited CCIC chemotaxis towards CCL25 (**Figure 6 C,D**). Similarly, in a migration assay, addition of CCL25 to the upper chamber inhibited migration to 5% serum in the lower chamber, and co-incubation with *JAG1* antagonized migration

stimulated by CCL25 (**Supplemental Figure 8D, E**). We did observe that addition of CCL25 downregulated NOTCH2 receptor levels. However, CCL25 did not downregulateNOTCH signaling as assayed by NICD and *HES1* protein levels (data not shown). Therefore, these data are consistent with NOTCH acting upstream of CCR9/CCL25 to inhibit AKT and migration, but that this interaction is not reciprocal.

NOTCH signaling promotes CCIC tumor formation outside the colon and intestine

Our *in vitro* studies are consistent with the NOTCH pathway acting upstream of CCR9/CCL25 to inhibit its function. To understand the *in vivo* role of NOTCH on the CCR9/CCL25 axis in CCIC, we used CCIC expressing a GFP-NOTCH reporter. We FACS sorted these CCIC into GFP-NOTCH High and Low cell populations, and injected cells systemically into the tail vein of immunodeficient mice. Consistent with the role of NOTCHto promote colorectal cancer invasion and metastasis[11], GFP-NOTCH High CCIC formed significantly more tumors outside the colon/intestine than GFP-NOTCH low CCIC (**Figure 6 E and Supplemental Figure 7 C.**). Conversely, GFP-NOTCH High CCIC formed significantly fewer intestine/colon tumors than GFP-NOTCH Low CCIC. Overall, these data are consistent with an *in vivo* role for NOTCH signaling to inhibit CCR9/CCL25 signaling in CCIC and promote invasion, metastasis and tumor formation at sites outside the GI tract.

DISCUSSION

Chemokines regulate anti-apoptosis, migration, recruitment of tumor associated cells, metastasis and trafficking for many cancers [13]. The CCR9/CCL25 axis specifically regulates gut mucosal immunity. CCL25 is produced by small intestine and colon epithelia, which recruit to the gut circulating CCR9+ T and dendritic cells, increases AKT signaling and prevents T lymphocyte apoptosis[14-17]. Here, we demonstrate an unexpected role for GI epithelium produced CCL25 to suppress CRC invasion and metastasis. The great majority of colonocytes express both CCR9 and CCL25 [15]. Compared to normal human colon, CCR9 is upregulated in adenomas and early stage CRC, but downregulated in invasive and metastatic CRC (**Figure 1**). Early stage colorectal cancers have better prognosis and less metastatic potential than late stage tumors. Both early stage primary tumor cells and CCIC demonstrate CCL25-dependent upregulation of AKT signaling, chemotaxis and proliferation (**Figure 4**). In colorectal cancer patients, AKT signaling (particularly in tumors carrying PIK3CA mutations) is associated with a good prognosis and is inversely correlated with later stages[35]. Conversely, NOTCH signaling is associated with CRC invasion and metastasis[11, 34] (**Figure 6**). Overall, our data are consistent with a model (**Supplemental Figure 9**) whereby pre-invasive (adenoma, carcinoma in situ) colorectal cancer cells upregulate CCR9 levels. Paracrine CCL25 produced by surrounding colon epithelium stimulates proliferation and anti-apoptosis signaling that contributes to increased tumor size, and likely superficial tumor spread along mucosal margins. This is accomplished mechanistically through upregulating AKT signaling and a downstream network of oncogenic transcription factors that promote proliferation. As tumors progress, some

cells upregulate NOTCH signaling. During this transition, upregulation of NOTCH signaling drives proliferation, taking over for CCL25/CCR9 signaling. This causes an “invasive switch” that stimulates CCR9 proteosomal degradation, inhibits CCR9/ CCL25 signaling, promotes NOTCH driven invasion and ultimately metastasis[34]. Consistent with this model, NOTCH signaling is higher in CCR9- vs. CCR9+ CCIC. Consequently, late stage invasive and metastatic colorectal cancer tumors do not express CCR9, as there is no proliferative advantage if CCL25 is absent from the microenvironment of metastatic sites. Overall, our data provide insights into the regulation of colorectal cancer tumor progression by the CCL25/CCR9 mechanism and the evolution of pre-invasive to invasive and metastatic CRC cells. Our data also suggests that CCR9 may be a useful prognostic marker to distinguish indolent from invasive and metastatic colorectal cancer.

Which NOTCH ligands are most important for stimulating CCR9 downregulation? Because there are multiple roles for NOTCH signaling in colorectal cancer, including roles in tumorigenesis, progression, chemoresistance and angiogenesis, and because there are five canonical NOTCH ligands, additional non-canonical NOTCH ligands (e.g. DLKs) that influence signaling levels, and post-translational modification of these ligands by glycosyltransferases (e.g. POFUT1) that affect their ability to bind to different NOTCH receptors[11, 32, 36-47], the answer is complex . The multiple roles of NOTCH signaling in normal colon homeostasis, different CRC mechanisms and the large diversity of possible ligands makes the association of individual ligands with NOTCH driven colorectal cancer progression by in situ hybridization or immunohistochemistry difficult both to study and interpret. However, it is important to note that previous studies

have shown that the NOTCH ligand DLL4 is upregulated in vascular endothelial cells located within colorectal cancers, but not in endothelium adjacent to normal mucosa [44]. Furthermore, some colorectal cancer cells themselves express NOTCH ligands such as JAG1 or DLK1 and are able to stimulate paracrine signaling [48, 49], in addition to expression of JAG1, JAG2, DLL1 and DLL4 ligands by normal colon epithelial cells. Therefore, while the overall situation is complex because of the multiple roles of NOTCH signaling in colorectal cancer, it is most likely that DLL4, JAG1, and possibly DLK-1, play the most important roles in CCR9 downregulation.

The chemokine receptor CXCR4 plays an important role in the homing and retention of hematopoietic stem cells within the bone marrow microenvironment [50]. Targeted disruption of CXCR4 signaling results in rapid mobilization of hematopoietic stem cells into the peripheral circulation [51-55]. The finding that downregulation of CCL25/CCR9 signaling can increase colorectal cancer migration out of the intestine/colon is therefore analogous to thesituation with CXCL12/CXCR4 and hematopoietic stem cells. Furthermore, because CXCL12 (also called SDF1α) is implicated in metastasis of multiple tumor types (with more than 700 citations in Medline on this topic) including colorectal cancer, we tested ex-GI CCIC tumors and found that they can express CXCR4 at high levels (**Supplemental Figure 10**). Overall, these findings are consistent with a potential colorectal cancer chemokine driven “metastatic switch,” during tumor progression. In future studies it will be important to evaluate this potential metastasis mechanism. Experimental approaches could include carefully designed experiments tracking colon cancer cell CCR9 vs. CXCR4 cell surface membrane protein levels in CCIC and other mouse models of stochastic colon cancer metastasis[56], for example

by FACS, to see if expression of these specific chemokine receptors are mutually exclusive, and whether CXCR4 correlates with NOTCH signaling upregulation [11]. Alternatively, new techniques using dual wavelength luciferase reporter genes driven respectively by the CCR9 or CXCR4 promoters could be monitored *in vivo* in surgical models of colon cancer metastasis [57]. Another approach would be to use dual immunofluorescence for CCR9 and CXCR4 to screen tissue microarray biospecimens from both early and late stage colorectal cancers to evaluate for mutual exclusivity of their expression in tumor progression. Overall, these experiments could create a strong rationale to repurpose existing CXCL12/ CXCR4 antagonists that are used for hematopoietic stem cell mobilization for clinical trials to inhibit colorectal cancer metastasis.

The commonly used colorectal cancer cell lines we tested express little or no CCR9. When injected systemically in mice, some lines can form tumors outside the GI tract. However, no spontaneous orthotopic colon/intestine tumor formation has ever been reported previously with any colorectal cancer cell line. Precisely why these commonly used cell lines do not express CCR9 is unknown. We speculate that this may reflect their long term *in vitro* culture in the absence of CCL25.

Since our novel *in vivo* orthotopic CRC tumor formation system models the transition directly from GI-localized neoplasms to metastatic carcinomas, the CCIC lines described here have the potential to be a useful model to identify important “driver” mutations, epigenetic changes and signaling pathways that regulate pre-invasive to invasive and metastatic CRC progression, with less confounding by the high background “passenger” mutation rates seen in advanced CRC tumors.

Functional CCR9 responsive to CCL25 is expressed by multiple tumor types, including prostate, ovarian, breast and pancreatic adenocarcinomas and melanomas [21-24, 58]. The role of CCR9 in these cancer types is unclear. One possibility is that a driving force is the upregulation of AKT signaling and cell proliferation. Because some chemokine receptors bind multiple ligands, we speculate additional CCR9 ligands may exist that play a role in these tumor types. Alternatively, CCR9 could cause constitutive activity even in the absence of ligand in these tumors (perhaps from somatic activating mutations) or paracrine CCL25 could be produced by infiltrating lymphocytes. Future experiments in these other tumors will be required to understand the precise role of CCR9 in these contexts outside of the intestine and colon.

METHODS

Histology and Immunohistochemistry Representative sections from patient CRC specimens were immunostained for CCR9 using a 1:150 dilution of anti-human CCR9 (Abcam #ab38564) with antigen retrieval and peroxidase-based detection. Cases varied in clinical stage from in situ carcinomas (Tis) to transmural involvement (T4). For each case, CCR9 staining intensity was assessed (range 0-3) for normal crypt epithelium, and neoplastic tissue from each involved layer of the colon wall using double blank scoring method. Intensity ± S.E.M. is shown.

Cell Culture. AJCC clinical stage I/II (referred to here as early) and stage III/IV (late) CCIC lines were generated using colon cancer "stem" cell culture conditions of Vermeulen et al [59] with several modifications as previously described by our lab[27]. Briefly, CRC patient fresh primary and metastastic tumor biospecimens were extensively washed with PBS, minced, and incubated at 37°C with collagenase. Cells were then strained through 40-μm filter and cultured as "colonospheres" [59]. Colonospheres were cultured in ultralow-attachment flasks in DMEM/F12 containing nonessential amino acids penicillin (500 U/ml), streptomycin (500 mg/ml), and amphotericin B (1.25 mg/ml) and heparin (4 μg/mL; Sigma). Changes from [59]included increased concentrations of epidermal growth factor (40 ng/mL), and basic fibroblast growth factor (20 ng/mL) and the addition of B27 supplement (Invitrogen). Cells were incubated at 37°C and 5% CO2. Cells were cloned as single cells, expanded and frozen in DMSO. With these conditions clonal cultured colonospheres were considered to be CCIC based on the following criteria: (1) 50+% FACS positive status for CD44, CD133 and ALDH1 (tested individually)[26], (2) 1:1,000-1:10,000 cell ability to form

subcutaneous xenografts in NOG mice, (3) capable of serial self-renewal in sub-cutaneous xenografts assays, (4) ability to form subcutaneous xenograft tumors with adenocarcinoma histomorphology. Additionally, CCIC were also noted to express LGR5, NOTCH 1,2 receptors, JAG1, DLL4 and nuclear β-catenin (consistent with expression of WNT target genes such as CD44 andLGR5). CCR9/ALDH1 co-expressing cells are also observed (data not shown).

Primary CRC culture Primary CRC culture used the method of collagenase /dispase enzyme digestion with slight modification, as previously described [60, 61]. Fresh samples of CRC were collected in DMEM/F12 supplemented with 10% FBS and 2% penicillin/streptomycin, immediately after patient operative resection. Tissue was dissected free of fat and blood clots and rinsed 5 times with PBS supplemented with 2% penicillin/streptomycin. Then tissue was minced into approximately1 mm fragments and digested in DMEM/F12 containing collagenase type XI (150 U/ml, Sigma, St. Louis, MO), dispase neutral protease (40 μg/ml, Roche Applied Science) and 1% FBS, stirring at 37°C for 30 min. After centrifugation, cells were re-suspended in the CCIC culture medium containing 5% FBS, 1% penicillin/streptomycin and cultured in the ultra low-attachment flashes for a short time (1-2 passages), then the cell culture was shifted into complete CCIC medium without FBS. FACS with ESA was used to purify CRC and cells within 5 passages were used for following experiments.

CCR9 constitutive and inducible knockdown;Snail or CD26 knockdown in CCIC and *NOTCH* reporter CCIC The lentiviral vector pEco-CMV-H1-shRNA-GFP encoding

a shRNA hairpin sequence (CCR9: 5'-CTTGTACTGGCTCGTGTTCAT; Snail: 5'-GAGCTGCAGGACTCTATCCA; CD26: 5'- CATTCCTACACAGCTTCATAT) was used for CCR9, Snail or CD26 expression knockdown and the lentiviral vectors pEco-CMV-H1-GFP (GenTargetInc, San Diego, CA) and pEco-CMV-H1-scrambled-shRNA-GFP served as controls. To generate the lentiviral vectors, the above plasmids were transfected into HEK293T cells with the Genetargetlentivirus packaging mix (GenTargetInc, San Diego, CA) according to the manufacturer's protocol. For CCR9 tetracycline inducible knockdown, the same shRNA hairpin sequence against CCR9 gene was inserted into pLenti-H1-shRNA-RSV (GFP-Puro) vector (GenTargetInc, San Diego, CA) and packaged into lentivirus particles as the same previous procedure, which were used together with another TetR expression lentivirus (RFP-Bsd) (GenTargetInc, San Diego, CA) to infect CCICs. After antibiotic selection and GFP/RFP dual FACS purification, the CCR9 shRNA knockdown can be induced by1ug/ml (in vitro) or 1mg/ml (in vivo) doxycycline. NOTCH signaling reporter CCIC was generated by infecting CCIC with pCignalLenti RBP-Jk Reporter (GFP) ready lentivirus (SABiosciences, Inc.). After infecting CCIC lines with these lentiviral vectors, stable knockdown clones were obtained through antibiotic selection of blasticidin (Invitrogen, Carlsbad, CA). The efficiency of the CCR9, SNAIL or CD26 knockdown in CCIC was verified by Western Blotting and efficiency of NOTCH signaling reporter was tested by 2 μg/ml Jagged-1[62-64] (AnaSpec) treatment following by GFP-FACS sorting.

CCIC xenograft tumor formation in colon/intestine and other organs 0.5-1 x 10^6CCIC or common CRC cells were injected into 6-8 weeks old non-obese

diabetic/severe combined immunodeficient (NOD/SCID) mice (Jackson Laboratory, Bar Harbor, Maine) by tail vein injection. Tumor incidence was monitored 2-3x weekly. When mice became moribund, they were sacrificed immediately, necropsy performed and tumors harvested using a dissecting microscope. For ex vivo GFP imaging of tumor tissues, lentiviral infection by the pEco-CMV-GFP vector was used to generate CCIC lines that stably express GFP and maintained in puromycin selection. 10^6 of these fluorescent CCIC were systemically injected as described above. Intestinal tissues harvested at the time of sacrifice were analyzed for GFP expression with Cri Maestro Imaging Systems (Cambridge Research & Instrumentation Inc, Woburn, MA).

For the CCR9 study, native CCICs, CCICs with CCR9, Snail (SNAL1) or CD26 knockdown (or commonly used CRC cell lines such as HCT116, etc. as indicated), CCR9+ CCIC with CCR9 inducible knockdown were intravenously inoculated into the 6-8 weeks old NOD/SCID mice by tail vein. Mice that became moribund were sacrificed immediately, whereas the rest were closely monitored for 16 weeks before sacrifice. To test whether CCL25 antibody could inhibit the CCL25-CCR9 GI homing mechanism *in vivo*, a dose of 100 ug goat anti-mouse CCL25 neutralization antibody (R&D systems, Cat# AF-481-NA), was IP administrated to each mouse twice (the same dose and schedule as used in [65]). As a negative control, a dose of 100 ug Goat IgG (R&D systems) was administered to each mouse in the control group. Then 1 x 10^6CCIC were injected into the mice 8 hours after or with the injection of the antibody. To test whether extra-GI metastasis is induced by CCR9/CCL25 signaling blockade, CCL25 neutralization antibody with the same dose was IP administrated to each mouse every

three days or 1 mg/ml doxycycline in drinking water was given to mice every other days starting from the fourth week after CCIC inoculation until mice get moribund.

Genomic DNA extraction and semi-quantitative PCR

Genomic DNA from CCIC culture, lung and intestinal adenomas normal tissues, or mouse tail was extracted using a tissue DNA extraction kit (Qiagen, Valencia CA). Semi-quantitative PCR was done followed by DNA gel electrophoresis. Human centromeric repeat loci were used as markers to detect human cells in harvested mouse tissues. Primer sequence pairs used are (1) 5'-GAGTGCACATTCAGACAAGACCC-3' and 5'- CCATTAGAGAGCTTTCCTCATTGC-3'or (2) 5'-CGTGTGTTTTTGGTTACTTCTCCCC- 3' and 5'-CTTAGCCATTGCCCATTGATGGA- 3'.

Quantitative real-time PCR

Total RNAs from cells were extracted by using RNeasy Kit (Qiagen, Valencia CA). 2 μg of total RNAs were reverse-transcribed into cDNA by using RT first stand kit (SA Biosciences) and RNA levels, normalized to GAPDH as the comparative CT (cycling threshold)= CT (target)- CT (control), were analyzed by the iCycler (Bio-Rad).

Primer pairs used are (1) GAPDH 5'-ACAGTCAGCCGCATCTTCTT-3' and 5'-AATGAAGGGGTCATTGATGG-3'; (2) HES 15'- ACGACACCGGATAAACCAAA-3' and 5'-CGGAGGTGCTTCACTGTCAT-3'; (3) CCR9 5'-CACAGACTTCACAAGCCCTA-3 and 5'-GTACAAGGGTGGGAGGAAAT-3' .

Transwell migration assay

Transwell Boyden chambers (BD Pharmingen Mountain View, CA) of 8-μm pore size were used to evaluate primary CRC cell and CCIC migration *in vitro*. Primary CRC cells or CCICs were seeded at a density of 5 x 10^5 per well into the upper chamber. CCIC

culture medium as described above with 100 ng/ml recombinant mouse CCL25 protein (R&D systems Inc; Minneapolis, MA) or 5% FBS was loaded into the lower chamber. Chambers of cells were incubated in 37^{o}C and 5 % CO_2 conditions for 8-12 hours. At the time of harvest, cells remaining inside the upper chambers were removed while cells attached to the lower surface of the membrane were fixed and stained with hexamethylpararosaniline chloride (Crystal violet) (Sigma, St Louis, MO) or immunofluorescence staining with anti-CCR9 or CEA antibodies, followed by imaging analyses.

SmartChip RT-PCR Procedures and Functional Analysis

Early stage CCIC were FACS sorted into CCR9+ and CCR9- subpopulations. 24 hours afterwards, cells were treated with100ng/ml human CCL25 for 30 min. RNA was extracted from both populations using PureLink RNA Mini kit (Invitrogen) and analyzed using the SmartChip Real-Time PCR System (WaferGen Biosystems, Fremont, CA). Briefly, cDNA was prepared using 1 ug of total RNA per sample per manufacturer's recommendation. A PCR cocktail containing SYBR Green I dye and the equivalent of 1000 ng of starting RNA for each sample was loaded onto the SmartChip Human Oncology V2 Panel (containing 1,296 unique real-time PCR reactions in quadruplicate for a total of 5,184 reactions/sample). The volume was 100 nL with an equivalent of 96 pg of RNA loaded per reaction. Forty cycles of real-time PCR were performed on the SmartChip Cycler collecting both raw Ct and Tm of each gene and sample for data analysis. A data quality screen on amplification, Tm curves, and Ct and Tm variability was performed to remove any outlier data. All-means normalization was performed on quadruplicate PCRs and delta-delta Ct calculations were used to determine fold change

in expression. Genes either with a log2 fold change by a factor of greater than 1.8 (that correlates to ~3.3 fold or higher), or expressed in only one sample with min raw of Ct of 24.99 were deemed significantly differentially expressed between CCR9- and CCR9+ early stage CCIC cells.The complex biological processes that differentiate between CCR9- and CCR9+ CCIC were examined in the context of biomolecular networks. The interaction network shown in Figure 5 was generated with Ingenuity Pathway Analysis (IPA), a web-delivered application used to discover, visualize and explore relevant networks (www.ingenuity.com). Gene symbol identifiers and log2 fold changes of differentially expressed genes were uploaded to IPA, each identifier was mapped to its corresponding gene object in the IPA Knowledgebase and direct interactions were queried only between these gene objects. The direct interaction network of differentially expressed genes between CCR9- and CCR9+ CCIC was manually integrated with signaling proteins known to be involved in the CCR9/CCL25 pathway.

Statistics Summary

All experiments were done with four to eight samples per group, unless otherwise indicated, and all results were derived from at least five independent experiments. Values are expressed as mean ± SEM. For Student's t test, a 2-tailed test was used. A *p* value less than 0.05 was considered significantly. Statistical calculations were performed with the Statistical Package for the Social Sciences version 11.5 software (SPSS Inc, Chicago, IL) or GraphPad. The statistical test used for each figure or table panel is indicated.

Study Approval

All primary CRC tissues in this study were taken from I-IV stage CRCs collected by the Weill Cornell Colon Cancer Biobank, approved by the Institutional Review Board (IRB) of Weill Cornell Medical College. All animal protocols in this study were approved by the institutional animal welfare and use committee of Weill Cornell Medical College, Cornell University.

Acknowledgements We thank other members of the Lipkin laboratory and Drs. Marian Waterman, Kambiz Afrasiabi and Wenhong Shen for helpful discussions. This work was supported by R01 CA098626, R21 CA122937,R01 GM095990, NSF 1106153, NSF 2011131053, the HRH Prince Alwaleed Bin Talal Bin Abdulaziz Alsaud Institute for Computational Biomedicine, the Coffrin Center for Biomedical Information at Weill Cornell Medical College and a generous donation by Matthew Bell.

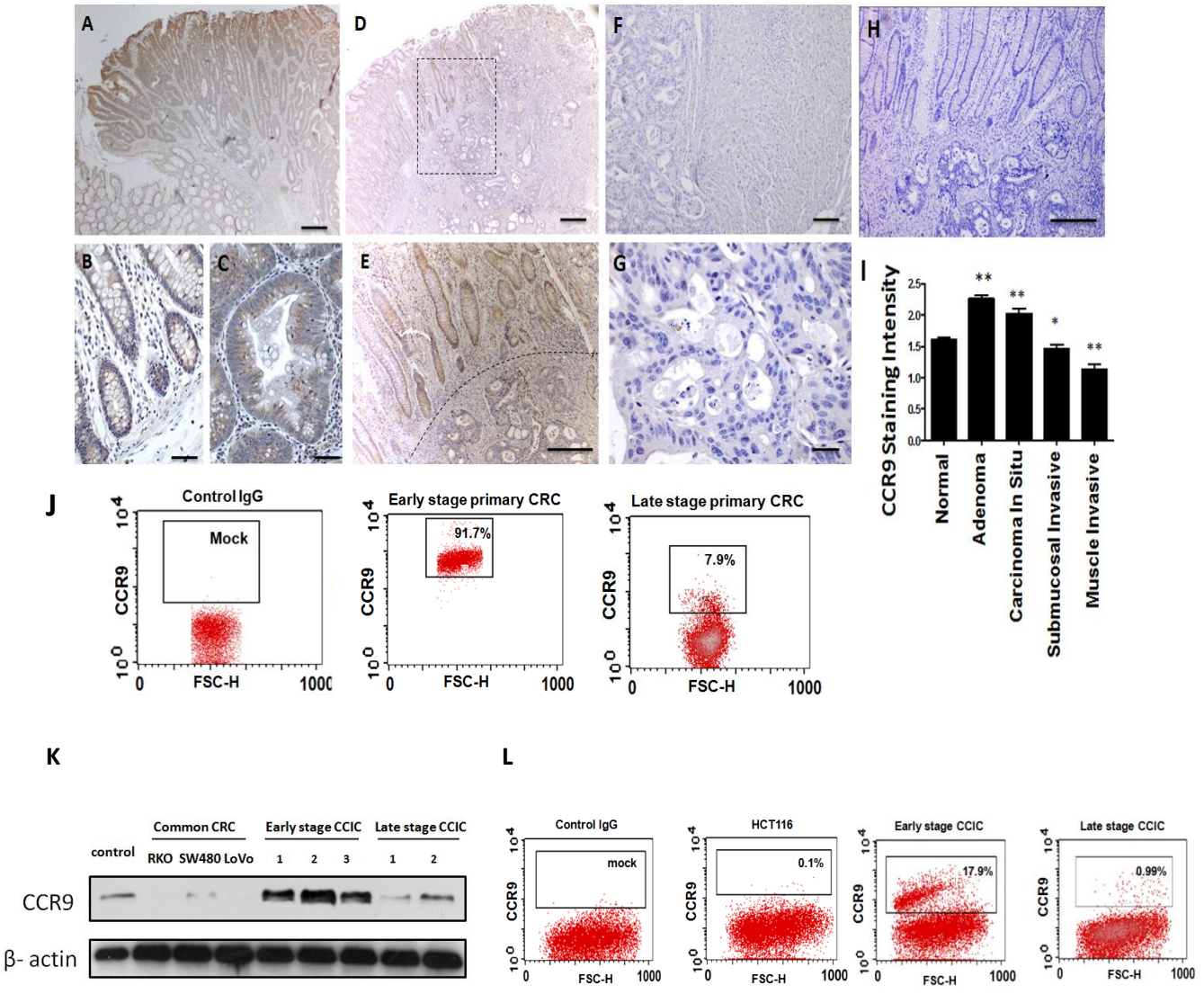

Figure 1. CCR9 is expressed in early stage CRC and early stage colon cancer initiating cells (CCIC). CCR9 protein in normal colon epithelium (**B**), pre-invasive (**A&C**), invasive (**D&E**) and liver metastatic (**F&G**) CRCs are shown by immunohistochemistry with anti-human CCR9 and developed by DAB (brown). Dotted line in **E** indicates the boundary between normal epithelium (CCR9+) and invasive CRC (CCR9-).**(H)**, negative control with control IgG; Scale bars, 100μ in **A,D,F**; 50 μ in **E,G,H**; 10 μ in **B,C (I)** CCR9 expression levels by immunohistochemistry scoring. Error bars indicate SEM. * and ** indicate statistical difference with P < 0.001 and P<0.01, respectively, compared to normal colon. **(J)** FACS quantification of membrane and cytoplasmic CCR9+ cells in early or late stage primary CRCs. Gates are set for high CCR9+ signal intensity.**(K)** Western blot of CCR9 protein levels in common CRC lines (RKO, SW480, LoVo), 3 early stage CCIC lines (Stage I/II) and 2 late stage CCIC lines (Stage III/IV), β-actin is loading control. Lymphoma cells are used as a positive control for CCR9.(**L)** FACS quantification of cell surface membrane CCR9+ cells in common CRC lines (HCT116 as representative), early stage CCIC and late stage CCIC (early stage CCIC1 and late stage CCIC1 as representative).

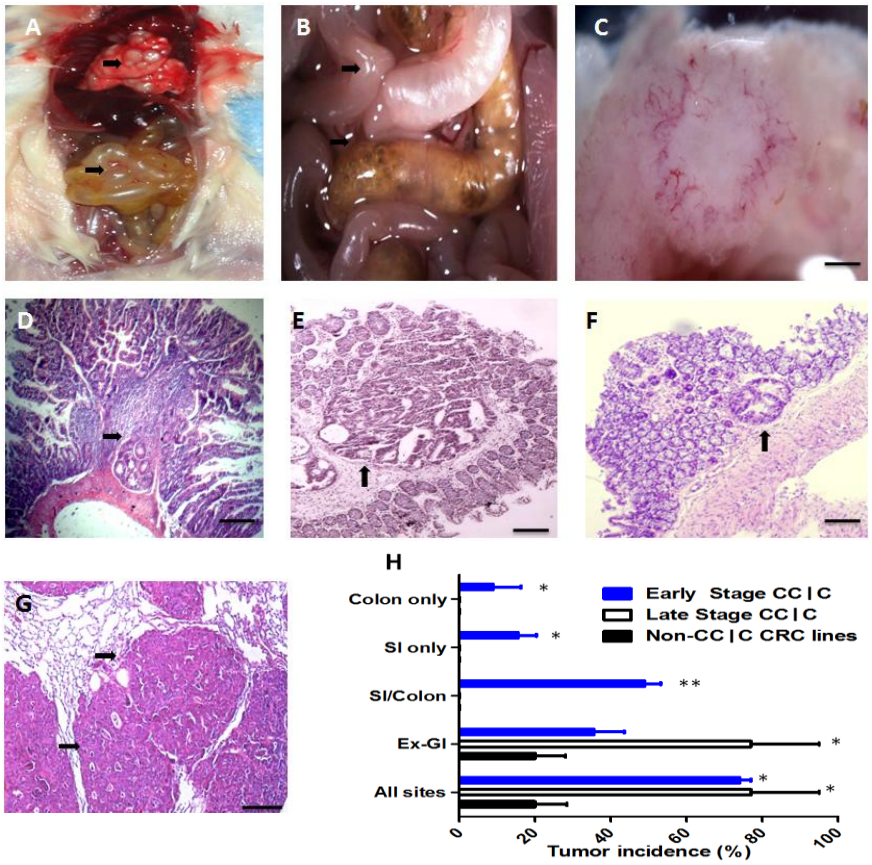

Figure 2.Early stage CCIC form orthotopic xenograft tumors in mouse intestine, colon and other sites. (A) Post-mortem analysis of NOD/SCID mice with tail vein-injected CCIC (4X). Arrows show CCIC tumors in lung (white spots; upper part of photo) and intestine (lower part of photo). Small bowel is distended and inflamed. **(B)**Close up of mouse abdomen showing (1) distended small intestine loop proximal to CCICtumor obstruction with adhesion to adjacent (non-obstructed and grossly normal) small intestine loop and (2) Pneumatosisintestinalis from bacterial stasis in right colon proximal to another CCIC obstruction.**(C**) High low power light microscopy close up of CCIC jejunal adenocarcinoma, Scale bars, 0.5 mm. Multiple CCIC tumors with histopathology in small intestine (**D**), colon (**E&F**) and lung (**G**). Arrow denotes adenocarcinomas in **D-G**. Scale bars,100µ. (**H**)Xenograft tumor incidence by site of implantation mice injected with CCIC or CRC cell lines. * P< 0.01 and **P< 0.001 compared to non-CCIC. Error bars indicate S.E.M.

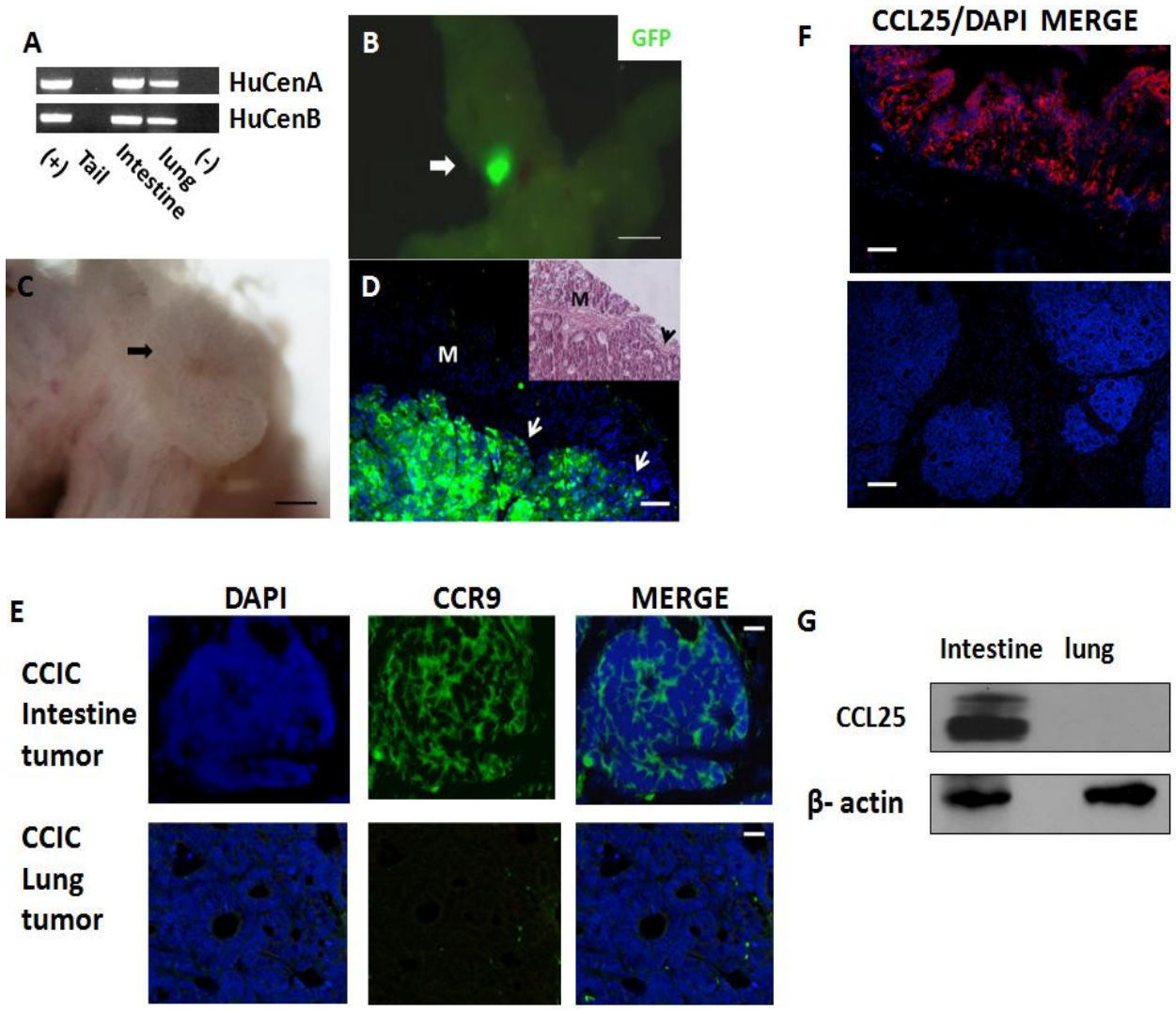

Figure 3.CCIC colon and intestinal tumors consist of human cells and are CCR9 positive. (**A**). PCRof human centromeric repeat sequences from DNA extracted from CCIC (positive control), CCIC injected mouse tail, intestine, lung tissue and no DNA control (negative control). **(B**). Maestro GFP imaging system images of intestinal tumor of PGK-eGFP expressing CCIC. Scale bars, 0.5 cm.**(C**).Light microscopy close up of eGFP+ CCIC tumor in (**B**).Scale bars, 0.5 mm.(**D**). Anti-GFP-immunofluorescence imaging of CCIC intestinal tumor with adenocarcinoma morphology. Left upper window shows H+E staining of the same intestinal tumor as control. Arrows indicated eGFP+ cells. **M**, mucosa. Scale bars, 100μ. (**E**). CCR9 immunofluorescence of CCIC intestinal and lung tumors.CCR9 protein was detected by anti-human CCR9 antibody (green) and nuclei were stained with DAPI (blue). Scale bars, 50 μ. (**F**).CCL25 immunofluorescence in mouse intestine and lung.CCL25 expression was detected by anti-mouse CCL25 antibody (red) and nuclei were stained with DAPI (blue). Scale bars, 100 μ. (**G**). Anti-CCl25 antibody western blot showing CCL25 expression in mouse intestine but not lung. β-actin is loading control.

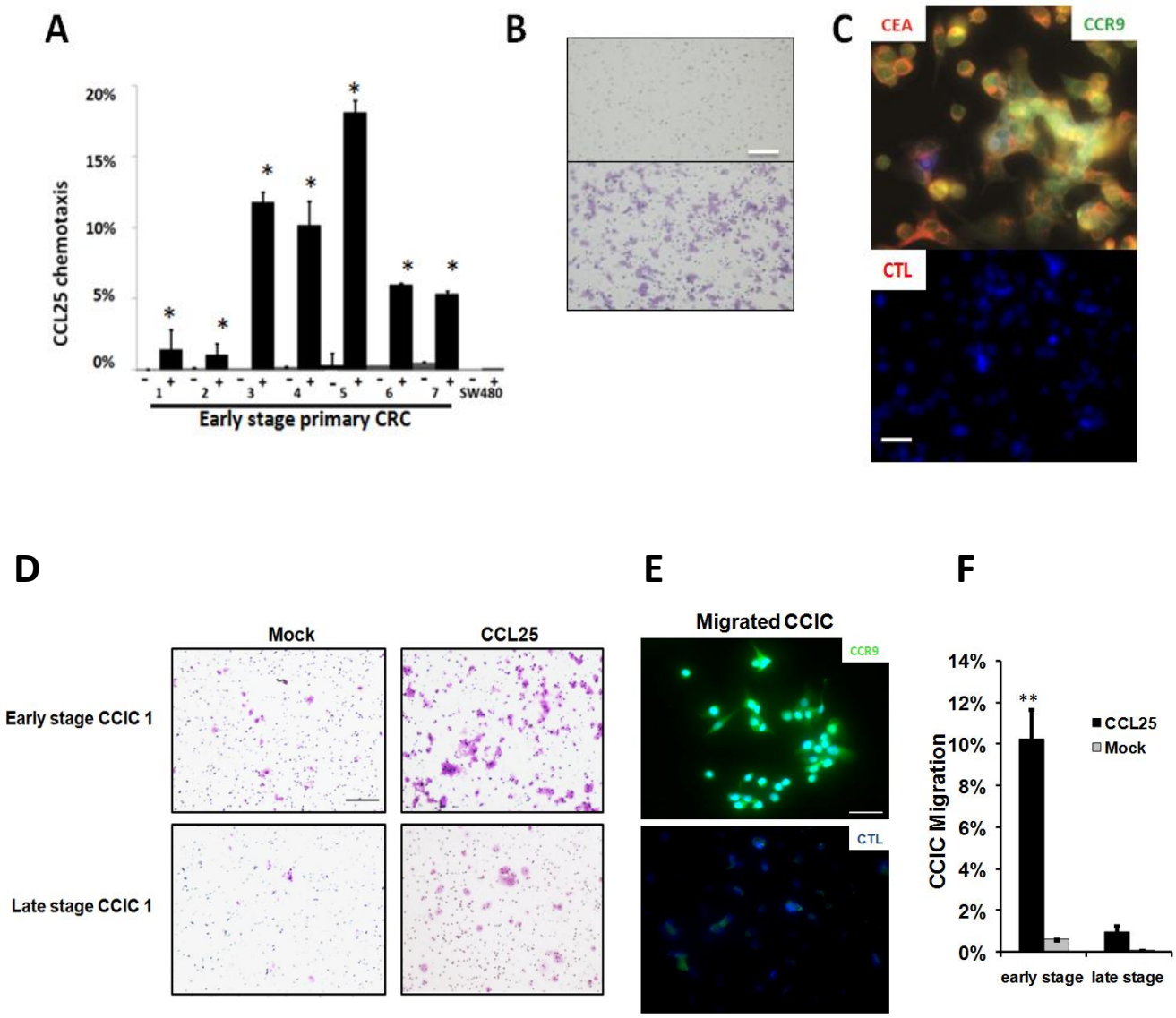

Figure 4.CCL25 dependent chemotaxisin early stage primary CRC and CCIC.
(**A)**Boyden chamber assay of 7 early stage primary CRCs chemotaxis to chamber containing CCL25. (-) CCL25 absence or (+) CCL25 presence. Error bars indicate S.E.M. *P < 0.0001 compared to matched (-) cells by one-way ANOVA (n=4). SW480 is used as a negative control. (**B**)Crystal violet staining of early stage primary CRC cells migrating into chamber with CCL25 (bottom) or mock (top).Scale bar, 50µ. (**C).**CEA (Red) and CCR9 (green) immunofluorescence of early stage primary CRC cells that migrated to chamber with CCL25. DAPI, blue. Scale bar, 10µ. IgGis negative control. (**D**) Crystal violet staining of Transwell chambers with early stage CCIC1 or late stage CCIC1(as representatives) that have migrated to CCL25or PBS (mock). Scale bar, 50µ. **(E)**CCR9 immunofluorescence of early stage CCIC that migrated to CCL25 containing chamber. CCR9 (green) and DAPI (blue).Control IgGis used as negative control. Scale bar, 10µ.**(F)** Percentage of earlyor late stage CCIC that migrated to CCL25 or mock (PBS) in Transwell assay. **P<0.001.

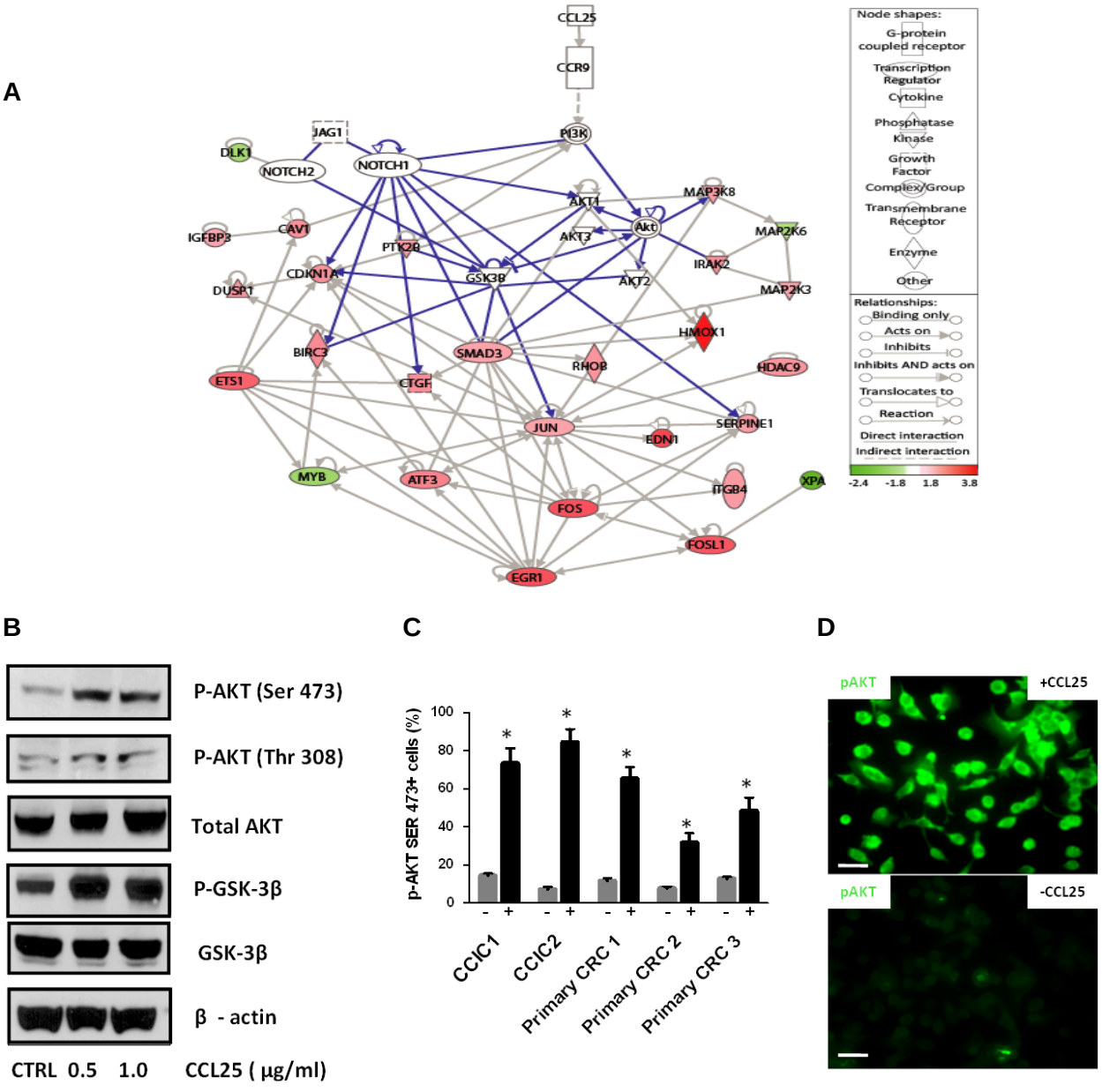

Figure 5.CCR9/CCL25 Increases AKT signaling in early stage CRC primary culture cells and CCIC.(A) Ingenuity Pathway analysis (IPA) direct interaction network of differentially expressed genes between CCR9- and CCR9+ early stage CCIC with signaling proteins known to be involved in the CCR9/CCL25 pathway(please see Method Section (SmartChip RT-PCR Procedure and Functional Analysis). Solid lines correspond to all direct interactions in IPA database. Dashed lines represent indirect interactions. Genes either with a log2 fold upregulation (red nodes) or downregulation (green nodes) are integrated in the signaling network. Blue lines correspond to direct interactions in NOTCH, AKT and GSK3β signaling pathways. (**B)**. Levels of phosphorylated AKT (Ser473 &Thr 308) and GSK-3β, which are increased by incubation with 0.5 or 1.0 µg/ml CCL25 for 30 min in early stage CCIC by western blot. β-actinis loading control. (**C)**. Levels of phospho-AKT (Ser 473) in early stage primary CRC cultured cells and early stage CCIC1 after 30 minutes of 0.5 ug/ml CCL25 treatment. Imaging analysis software Ariol SL-50 was used to evaluate immunofluorescence signals of cells (-) or (+) CCL25. * $P < 0.001$ compared to control by one way ANOVA. Error bars indicate S.E.M. (**D).**Phospho-AKT (Ser 473) in early stage primary CRC cultured cells after treatment with 0.5 ug/ml CCL25 for 30 minutes as detected by immunofluorescence (green). Scale bar, 10µ.

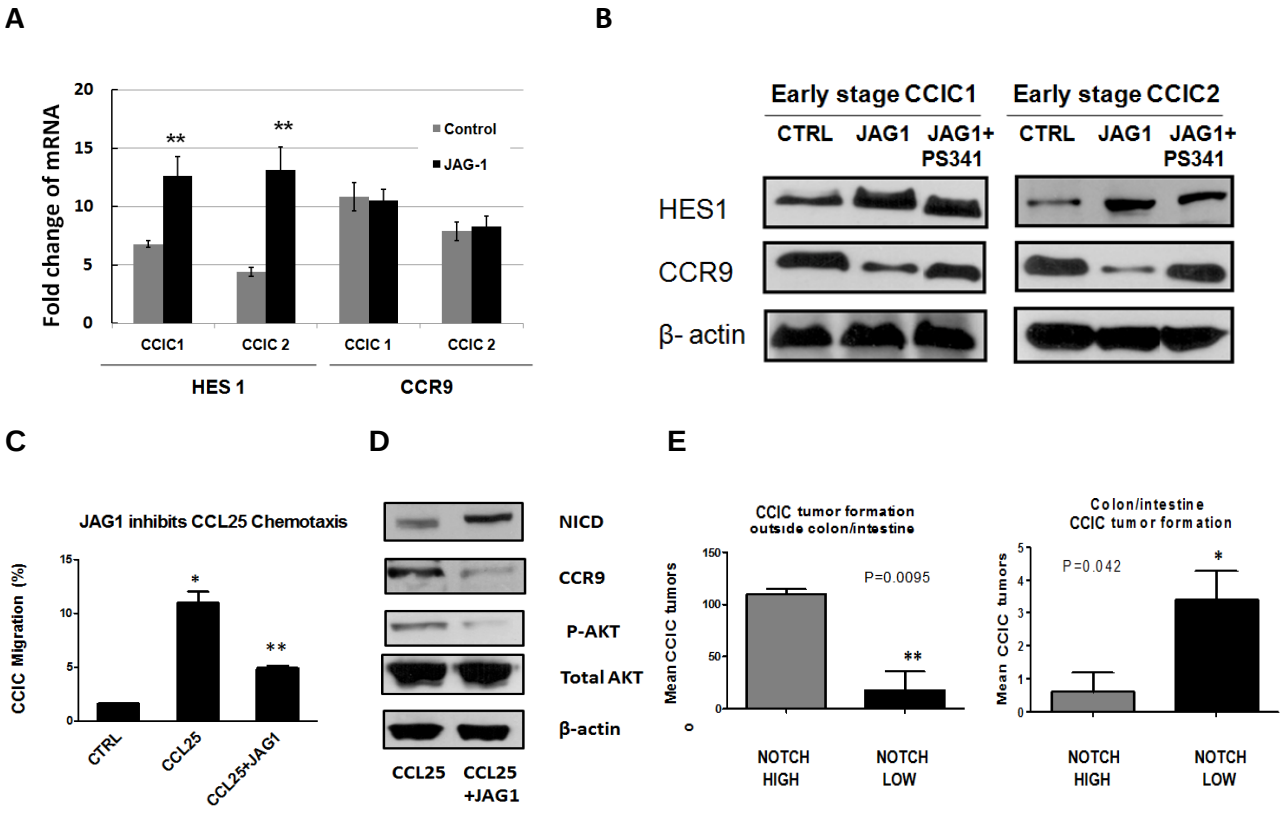

Figure 6.NOTCHdownregulates CCR9/CCL25 axis signaling in early stage CCIC and increases extra-GI tumor formation. (A)CCR9 mRNA levels in CCR9+ cells of early stage CCIC1 & CCIC2 in response to JAG1 induced NOTCH activation using quantitative PCR, HES1 is used as positive control.**(B)**CCR9 protein levels in CCR9+ early stage CCIC1 & CCIC2 co-treated with or without proteasome inhibitor (100nM PS341, 4 hours before harvest) in response to JAG1 induced NOTCH activation using western blot, HES1 is used as positive control.**(C)**Pretreatment of CCIC with 5µg/ml JAG-1 peptide for 8 hours suppresses CCL25 dependent chemotaxis in Boyden chamber assay. *P < 0.0001 vs. control by one way ANOVA; **P < 0.001 vs. CCL25 alone. (N=3). Error bars indicate S.E.M. (**D**)Pretreatment of CCR9+ CCIC with 2µg/ml *JAG1* peptide for 8 hours suppresses CCR9 protein and CCL25 inducesphospho-AKT (Ser473) levels, with essentially no change in total AKT levels. Western analysis used anti- human CCR9, phospho-AKT, total AKT (AKT 1, 2, 3), NICD and HES1 antibodies. β-actin was used as a loading control. (**E)**CCIC carrying GFP-NOTCH reporter were sorted into NOTCH high and low subpopulations by FACS and injected into NOD/SCID tail vein. NOTCH high CCICform more extra-GI tumors while NOTCH low CCIC form more GI tumors. Error bars indicate SEM. ** and * indicate statistical difference with P < 0.001 and P<0.05, respectively, comparing to each other.Also see supplemental figures 6 and 7.

Cells	# Mice	Mean Progression (weeks)	GI Tumor Incidence (%)	Mean GI Tumors / mouse	Ex-GI Tumor Incidence (%)	Mean Ex-GI Tumors/Mouse
Early Stage CCIC	**62**	**8.6**	**73.3**	**3.7**	**35.6**	**126.0**
Late Stage CCIC	**11**	**6.5***	**0***	**0***	**91.0***	**71.1***
Non-CCIC CRC lines	**24**	**11.8***	**0***	**0***	**20.0***	**66.2***

Table 1. CCIC and common CRCs form orthotopic xenograft tumors in mouse intestine, colon and other sites. colon/intestine and ex-GI tumors from mice injected with cells by tail vein. Asterisks denote statistically significant differences among CRC cell lines SW480 and LoVo, early and late stage CCIC as determined by one way ANOVA. * $P < 0.01$ compared to early stage CCICs.

Cells	# Mice	Mean Progression (weeks)	GI Tumor Incidence (%)	Mean GI Tumors / mouse	Ex-GI Tumor Incidence (%)	Mean Ex-GI Tumors/Mouse
CCR9+	8	9.4	75.0*	3.8*	25.0	8.3*
CCR9-	8	10.0	12.5	0.25	87.5	75.6
Anti-CCL25 [a] (Pre-injection)	6	11.3	28.5	1.1*	100.0	95.9
Control IgG	6	9.2	83.3	3.0	83.3	77.5
CCR9 KD [b]	7	13.0*	14.3*	0.3*	85.7	105.0*
Control shRNA	7	9.6	100.0	3.7	71.4	82.5

[a] **anti-CCL25 (pre-injection) means mice were IP injected with anti-CCL25 neutralization antibody before and concurrent with CCSC tail vein injection.**

[b] **CCIC with CCR9 shRNA knockdown were tail vein injected in mice.**

Table 2.CCR9/CCL25 is required for CCIC colon/intestine tumor formation.
mice injected with early stage CCIC.Rows1-2:Mice injected with CCR9+ CCIC or CCR9- CCIC (*P<0.001 for Row 1-2 comparison). Rows 3-4: Anti-Ccl25 antibody reduces GI tumor incidence (*P<0.05 for row 3-4 comparison). Rows 5-6: CCR9 shRNA lentiviral knockdown (KD) reduces GI tumor incidence and multiplicity, and increases ex-GI multiplicity (*P < 0.01 for row 5-6 comparison).

Cells	# Mice	Mean Progression (weeks)	GI Tumor Incidence (%)	Mean GI Tumors / mouse	Ex-GI Tumor Incidence (%)	Mean Ex-GI Tumors/Mouse
Anti-CCL25[a] (post injection)	7	7.9	71.4	2.4	42.8*	2.9*
Control IgG	7	8.7	85.7	3.3	0	0
CCR9[b] Inducible KD	8	8.1	62.5	2.2	50.0*	3.4*
Control shRNA	8	8.9	87.5	3.2	12.5	0.2

[a] **anti-CCL25 (post injection) means mice were IP injected with anti-CCL25 neutralization antibody three weeks after CCR9+ CCIC tail vein injection.**

[b] **CCR9+CCIC with CCR9 inducible shRNA were tail vein injected in mice and CCR9 knockdown were generated in vivo by administration of doxycycline three weeks later.**

Table 3. BlockingCCR9/CCL25 signaling after intestinal tumor formation increases metastasis. Mice injected with early stage CCIC. Top, after three weeks to allow GI tumors to form from injected CCR9+ early stage CCIC, mice were IP injected with 100 µg/mouse goat anti-mouse CCL25 neutralization antibody or goat control IgG every three days until moribund. The mice in anti-CCL25 groups formed extra-intestinal metastatic tumors in abdominal tissues, pancreas, kidney and liver (*P<0.001 statistically significant different to goat control IgG treatment, row 2).Bottom, after 3 weeks to allow GI tumors to form from injected CCR9+ early stage CCIC carrying either doxycycline regulatable anti-CCR9 or control shRNA, 1mg/ml doxycycline in drinking water was given to the mice every other day until moribund to induce CCR9 knockdown in tumor cells. The mice with inducible CCR9 knockdown formed extra-intestinal metastatic tumors in abdominal tissues, pancreas, kidney and liver (*P < 0.001). Also see supplemental figures 2 and 3.

SUPPLEMENTAL INFORMATION

SUPPLEMENTAL EXPERIMENTAL PROCEDURES

Immunohistochemistry For mouse experiments, histology and immunohistochemistry were performed on paraffin-embedded or frozen sections from xenograft tumors as previously described [27]. Intestinal, extra-GI tumor and corresponding normal tissues were snap frozen in OCT (Fisher Scientific, Pittsburgh, PA) and fixed in 10 % buffered formalin followed by paraffin embedding. For immunofluorescence, sections were immunostained with antibodies, counterstained with 4,6-diamidino-2-phenylindole (DAPI). H+E adjacent sections were used for comparison.

Immunocytochemistry. Cells were fixed with mixture of acetone and methanol (1:1) at -20°C for 20 min, then rinsed three times with PBS. Following cells were incubated in a blocking solution (5% BSA or normal serum (goat, rabbit or horse) and 0.1% Triton-X in PBS) for 1 hour. For single or co-immunofluorescence staining, primary antibodies diluted in blocking solution were added overnight at 4°C overnight. To ensure specificity, a no primary antibody control staining was performed. The slides were then washed in PBS and incubated with the appropriate secondary antibody for 1 hour at room temperature and counterstained/mounted with Vectashield containing DAPI (Vector Laboratories). Images were acquired on an inverted fluorescence microscope (Nikon Eclipse E800, Morrell Instruments). Ariol SL-50imaging software (Applied Imaging Instruments) was used to quantify biomarker staining. At least n=100 cells from three independent staining experiments were analyzed. Data are presented as means ± SEM and the significance was tested with the Student t test.

Fluorescent activated cell sorting (FACS) analysis FACS with anti-epithelial specific antigen (ESA, BD Pharmingen #347197) antibody was used to purify primary CRC cells [26, 66] or with anti-CCR9 antibody (BD Pharmingen Mountain View, CA) to sort CCR9+ and CCR9- CCIC, essentially as previously described [26, 66]. Cells were first incubated with anti-human CCR9 antibody for 30 minutes on ice and then were washed in 1% BSA/PBS buffer. FACS was then used to separate CCIC into CCR9 positive and negative sub-groups by signal intensity gating. Approximately 6-8 hours after sorting, CCR9+ and CCR9- subsets from 1x 10^6 CCIC were inoculated into two mice by tail vein injection and monitored as described above. GFP-NOTCH FACS sorting was performed as described (44)**.**

Western Blotting

Isolated mouse intestine, lung tissues, cultured CCIC, or ATCC CRC cell lines were homogenized in RIPA buffer and complete protease inhibitor cocktail (Roche Applied Science, Indianapolis, IN)] with brief sonication on ice, and centrifuged for 5 minutes at 14,000 r.p.m to remove large debris. Protein concentration of the supernatant was determined by Bradford protein assay (Bio-Rad Laboratories Inc, Hercules, CA). Fifty micrograms of protein derived from tissue or cell lysates were separated by SDS-PAGE and transferred to polyvinylidenedifluoride membranes. Following blocking, membranes were probed with primary antibodies to determine different levels of protein expressions. Specific antibodies targeting CCR9 (Abcam, Cambridge, MA), CCL25 (R&D systems Inc; Minneapolis, MA, Cat# AF-481-NA), AKT (Cell Signaling, Inc, Cat# 9272), phospho-AKT (ser 473, Cell Signaling, Inc, Cat# 9271), phospho-AKT (thr 308, Cell Signaling, Inc,

Cat# 9275), GSK-3β (Cell Signaling, Inc, Cat# 9315), phosphor-GSK-3β (Cell Signaling, Inc, Cat# 9336), NICD (R&D Systems, Cat# AF3647), *HES1* (Santa Cruz, Cat# sc-13842), Snail (Cell Signaling, Cat# 3879), CD26 (Calbiochem, Cat# IM1004) were used, and anti-actin antibody (Santa Cruz Biotechnology Inc, Santa Cruz, CA, Cat# sc-1616-R) was used as internal controls. Immunoreactive antibody-antigen complexes were visualized with the enhanced chemiluminescence reagents from GE Healthcare (Uppsala, Sweden). The software of Quantity One (BioRad) was used to semi-quantify protein levels in western.

Generation of CCR9 constitutive expression CRC line.

The SureTiter TM lentivector (GenTarget Inc, San Diego, CA) in which the sub-cloned human CCR9 ORF sequence (gene ID: NM_006641) and a firefly luciferase gene were under control of CMV promoter was used to generate constitutively CCR9 expressing cell lines. To generate the lentiviral particles, the above plasmids were transfected into HEK293T cells with the Genetarget lentivirus packaging mix (GenTarget Inc, San Diego, CA) according to the manufacturer's protocol. The common used CRC line HCT116 was infected with lentivirus and positive cells selected by antibiotic.

Luciferase imaging in whole animal or ex vivo tissues:

Each NOG mouse was tail vein injected with 0.5x106 CCR9 constitutively expressing or scrambled control HCT116 cells and tumor formation was determined by luciferase-IVIS imaging system every 3 days For luciferase imaging, D-luciferin of 1.5mg/10g body weight was intra-peritoneally injected into mice and 10 min later, luciferase imaging (Xenogen IVIS-200) was applied on whole-mouse body or ex vivo tissues.

Cell proliferation assay

CCR9+ primary CRC and CCIC were FACS sorted and seeded in ultro-low attachment 24-well plates for 12 hours. 100ng/ml human CCL25, 1μg/ml CCR9 neutralizing antibody (R&D systems Inc;), 2 μM pan-AKT inhibitor Triciribine (Sigma) or control goat IgG were added into culture medium and cells were continued to incubate for 36 hours. The cellular ATP (adenosine triphosphate) levels were measured to quantify cell proliferation and viability using the ViaLightPlus Kit (Lonza Rockland, Inc.) and GloMax-20/20 Single-Tube Luminometer (Promega) per manufacture instructions.

SUPPLEMENTAL INFORMATION

All experiments were done with four to eight samples per group, unless otherwise indicated, and all results were derived from at least five independent experiments. Values are expressed as mean ± SEM. For Student's t test, a 2-tailed test was used. A *p* value less than 0.05 was considered significantly. Statistical calculations were performed with the Statistical Package for the Social Sciences version 11.5 software (SPSS Inc, Chicago, IL) or GraphPad. The statistical test used for each figure or table panel is indicated.

Supplementary Figures

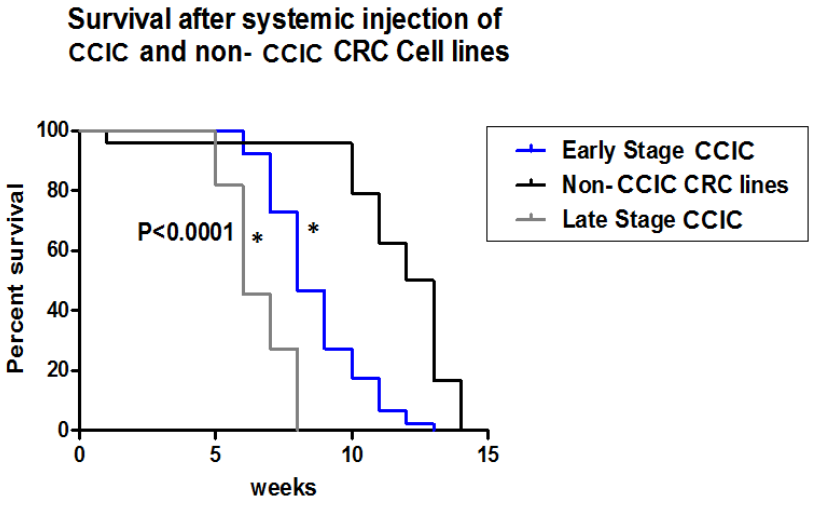

Supplemental Figure 1. Related to Figure 2. Survival of mice systemically injected with early stage CCICs, late stage CCICs and non-CCIC CRC lines. Kaplan-Meier survival analysis of mice after tail vein injection with early stage CCIC (blue), late stage CCIC (grey) or the non-CCIC commonly used CRC cell lines LoVo and SW480 (black). P<0.0001 difference between the early stage CCIC and commonly used CRC cell lines by log-rank test (Graphpad Prism software version 5).

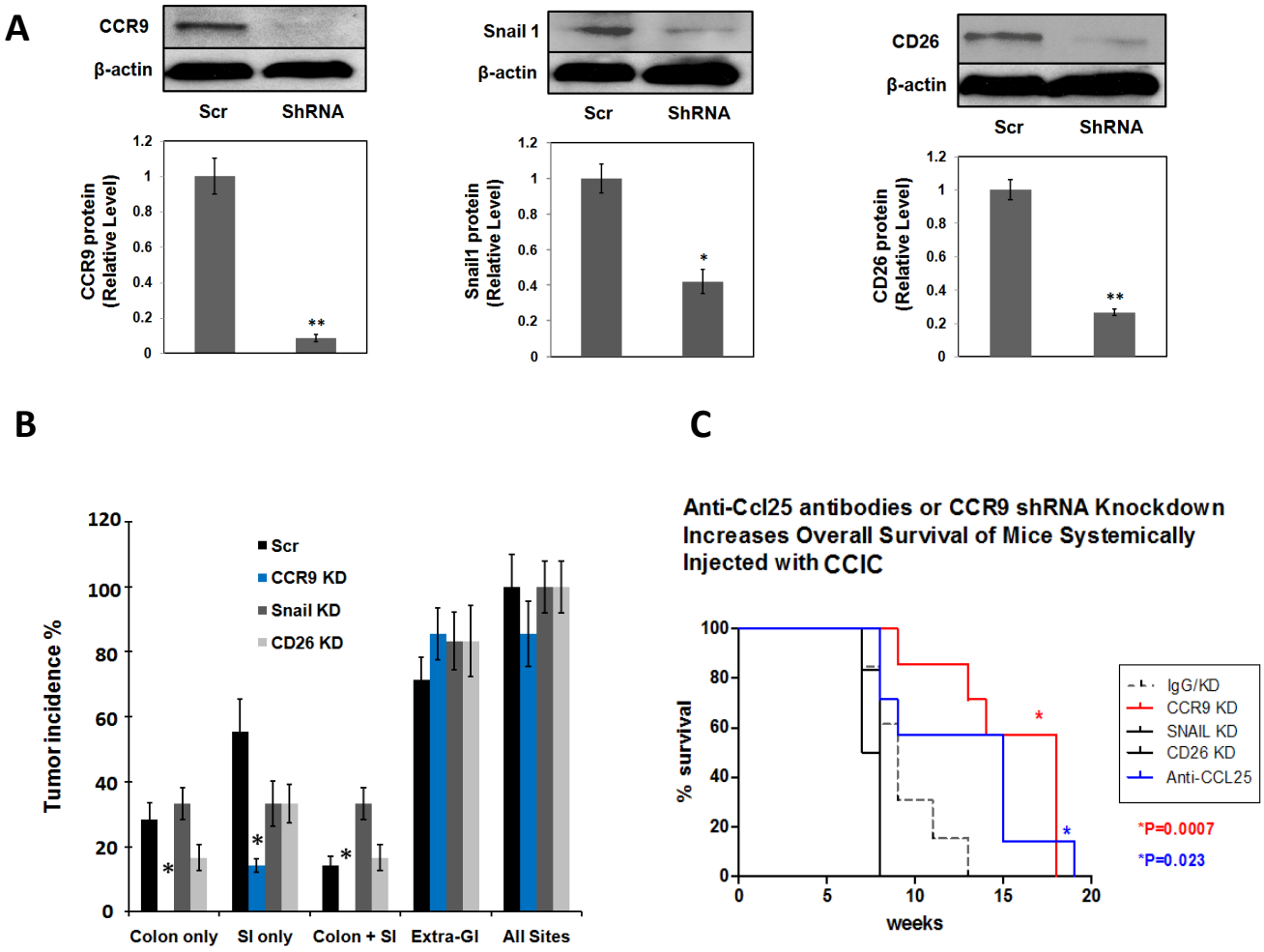

Supplemental Figure 2. Related to Figure 5. Anti-Ccl25 antibody systemic injection or shRNA knockdown of CCR9, but not CD26 or SNAIL, increases survival of mice systemically injected with CCIC. (A) shRNA constitutive knockdown efficiencies of CCR9, CD26 or SNAIL in CCIC were tested by western (left) and quantified (right) by using western quantification software of Quantitity One (BioRad). **(B)** Xenograft tumor incidence in mice injected with CCIC expressing anti-CCR9, SNAIL1 or CD26 shRNA knockdown, organized by tumor site. * P< 0.01 compared to scrambled shRNA control. Error bars indicate S.E.M**. (C)** Kaplan-Meier survival analysis of mice after tail vein injection with anti-Ccl25 antibodies or CCIC lentivirally infected with scrambled shRNA control (Mock), shRNA against CCR9, SNAIL1 or CD26. Survival curve data match Table 1. P=0.0007, Log Rank test comparison of overall survival of mice injected with CCIC expressing either scrambled shRNA control vector or anti-CCR9 knockdown sequences (Graphpad Prism version 5). P=0.023 Log Rank test comparison of overall survival of mice injected with anti-Ccl25 or IgG control (Graphpad Prism version 5).

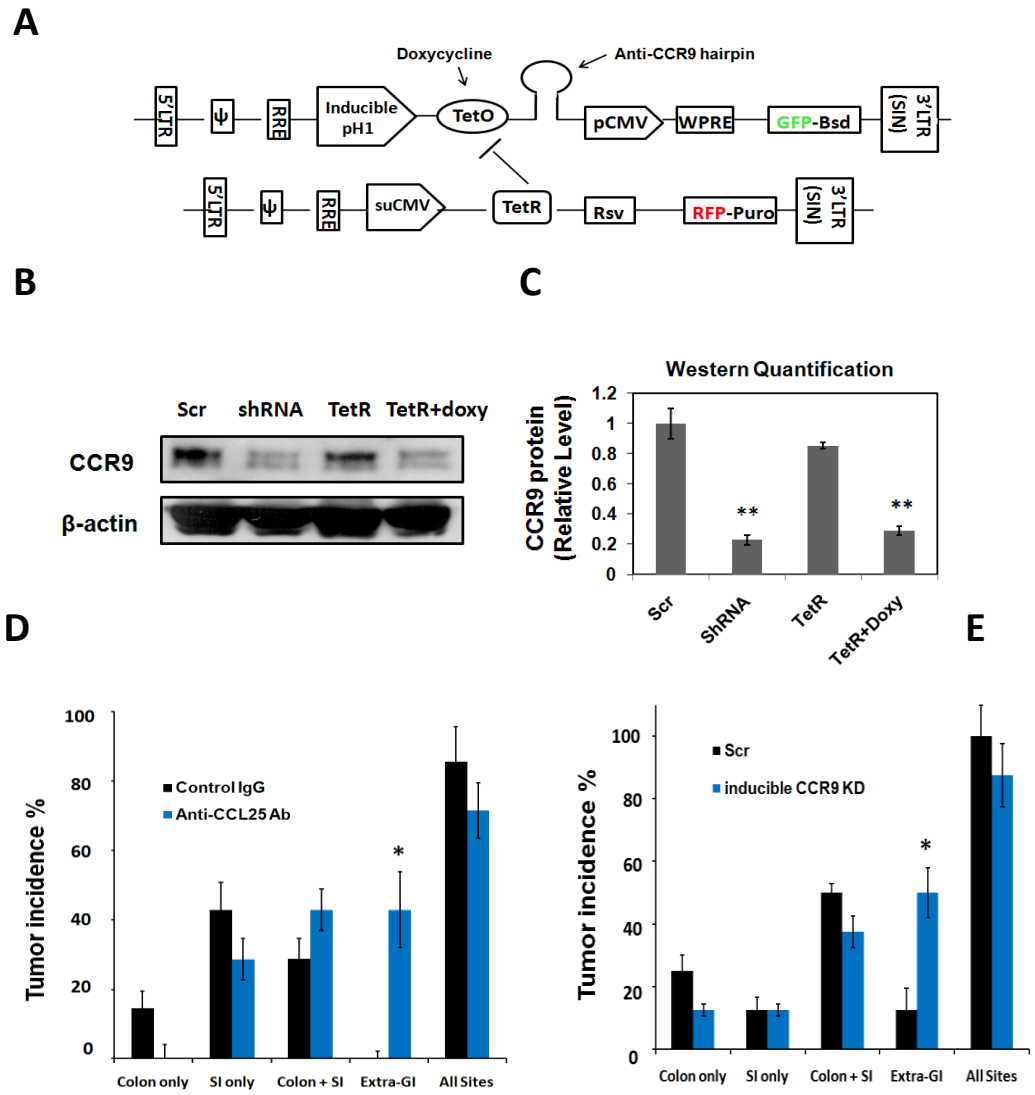

Supplemental Figure 3. related to Figure 6. CCR9/CCL25 signaling is inhibited after CCIC intestinal tumor initiation by anti-CCL25 antibody treatment or CCR9 inducible shRNA. **(A).** Schematic of CCR9 inducible shRNA, in which anti-CCR9 hairpin sequence was cloned in the 3'pH1 TetO promoter. Expression of anti-CCR9 hairpin was inhibited by TetR (Tet-repressor) and induced by tetrycycline derive doxycycline. **(B)**. Efficiency of CCR9 inducible knockdown in CCIC. The CCR9 protein levels in CCICs with only shRNAtetO vector, tetO + tetR or tetO+tetR+ doxycycline were detected by anti-human CCR9 antibody (left) and semi-quantified (right)by Quantitity One (BioRad).(**C & D**) Xenograft tumor incidence in mice injected with CCR9+ CCR9, and anti-CCL25 antibody therapy (**C**) or CCR9 inducible knockdown (or control, scr) by doxycycline (**D**) three weeks after tail vein injection organized by tumor site. * P< 0.01 compared to mock control. Error bars indicate S.E.M.

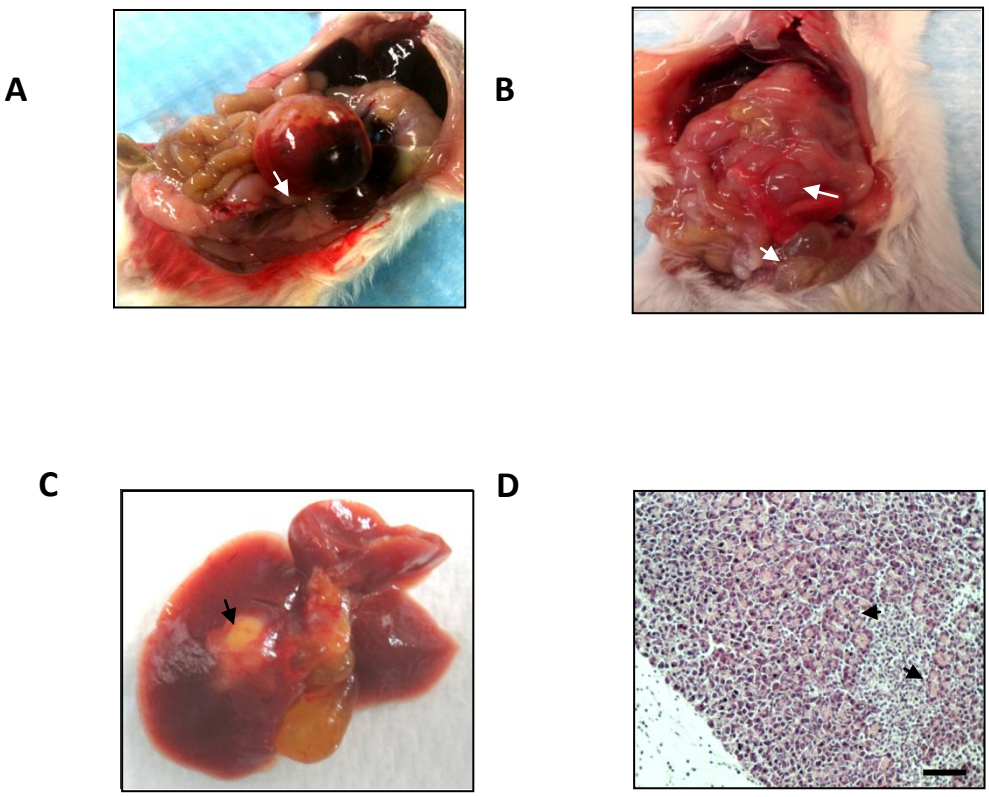

Supplemental Figure 4. related to Figure 6. CCIC extra-GI metastatic tumors are induced by anti-CCL25 treatment or CCR9 inducible knockdown. (A)and (B) Light microscopy of CCIC abdominal metastasis. **(C)** Light microscopy of CCIC liver metastasis, Metastatic foci are indicated by arrows. (**D**). H+E of CCIC metastatic tumors in pancreas. Arrows denote metastatic foci. Scale bar, 100μ.

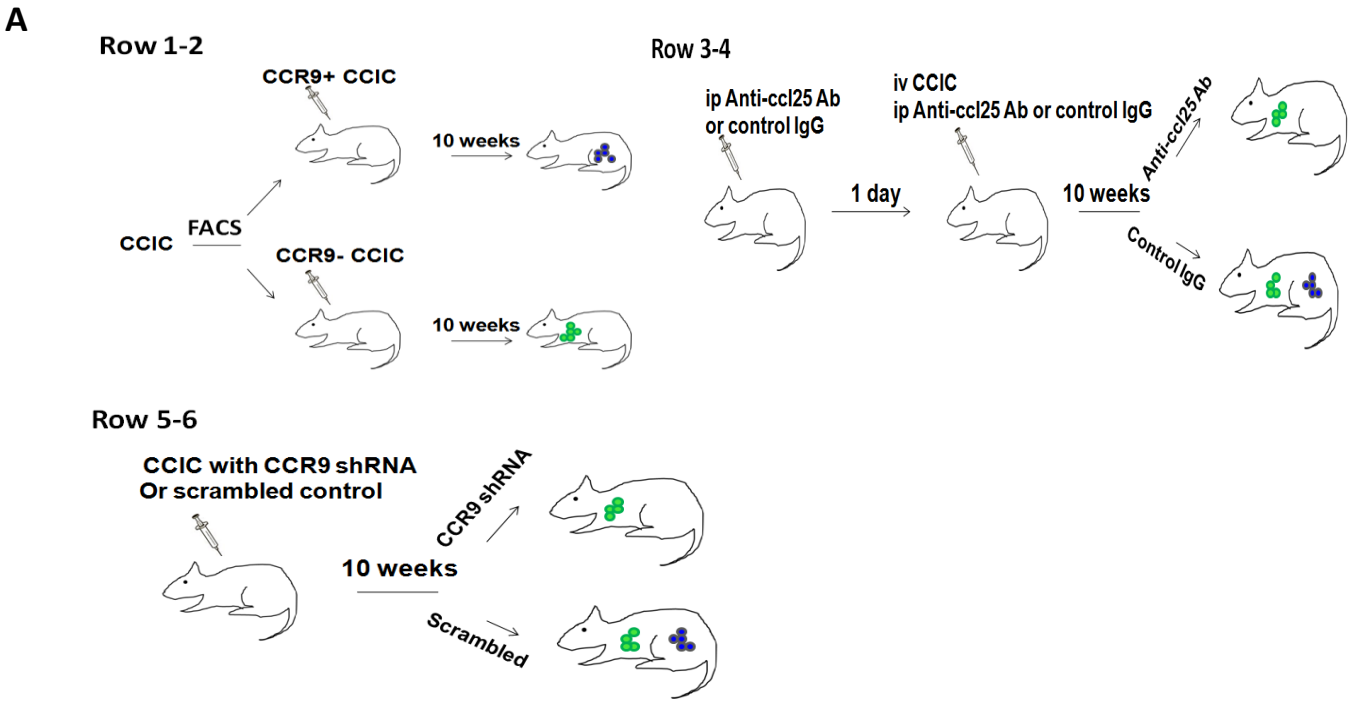

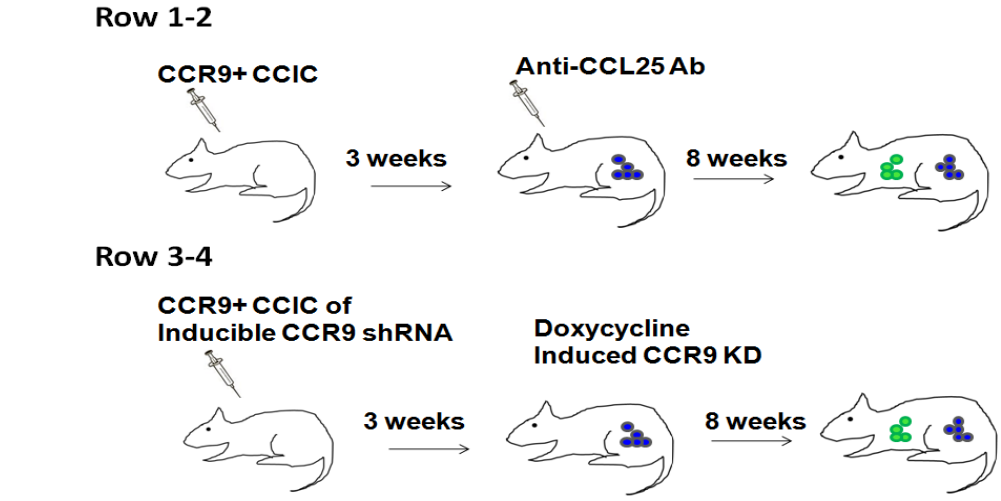

Supplemental Figure 5. related to Table 2 and 3. **(A).** Schema of the experimental procedures in Table 2. **(B)**Schema of the experimental procedures in Table 3. Colon/intestine tumors (blue) and ex-GI tumors (green) dots.

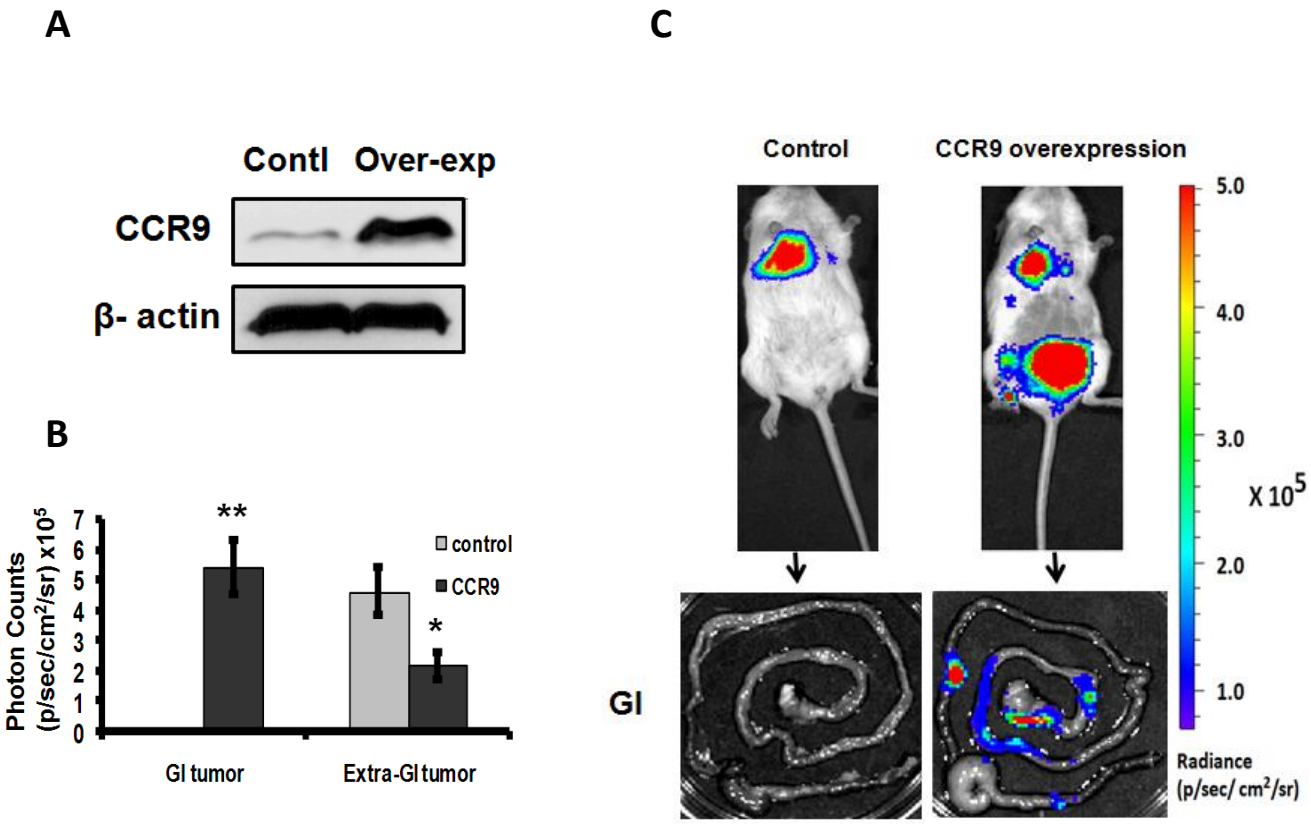

Supplemental Figure 6. Related to Figure 6. CCR9 overexpression in HCT116 significantly increased GI tumor formation and reduced extra-GI tumor formation (A). Western blot of CCR9 expression in HCT116 cells transfected with control vector or CCR9 constitutive expression vector. β-actin is loading control. (B). Quantification of GI and extra-GI tumors in mice that have HCT116 cells transfected with either CCR9 overexpression or control vector (n=6) injected by tail vein. Xenograft tumors were quantified by luciferase - photon signals with Xenogen software. ** P< 0.001; * P< 0.01 compared to the control group. Error bars indicate S.E.M. The whole-mouse (right upper panel) or an ex vivo GI (right down panel) representative imaging is shown in (C).

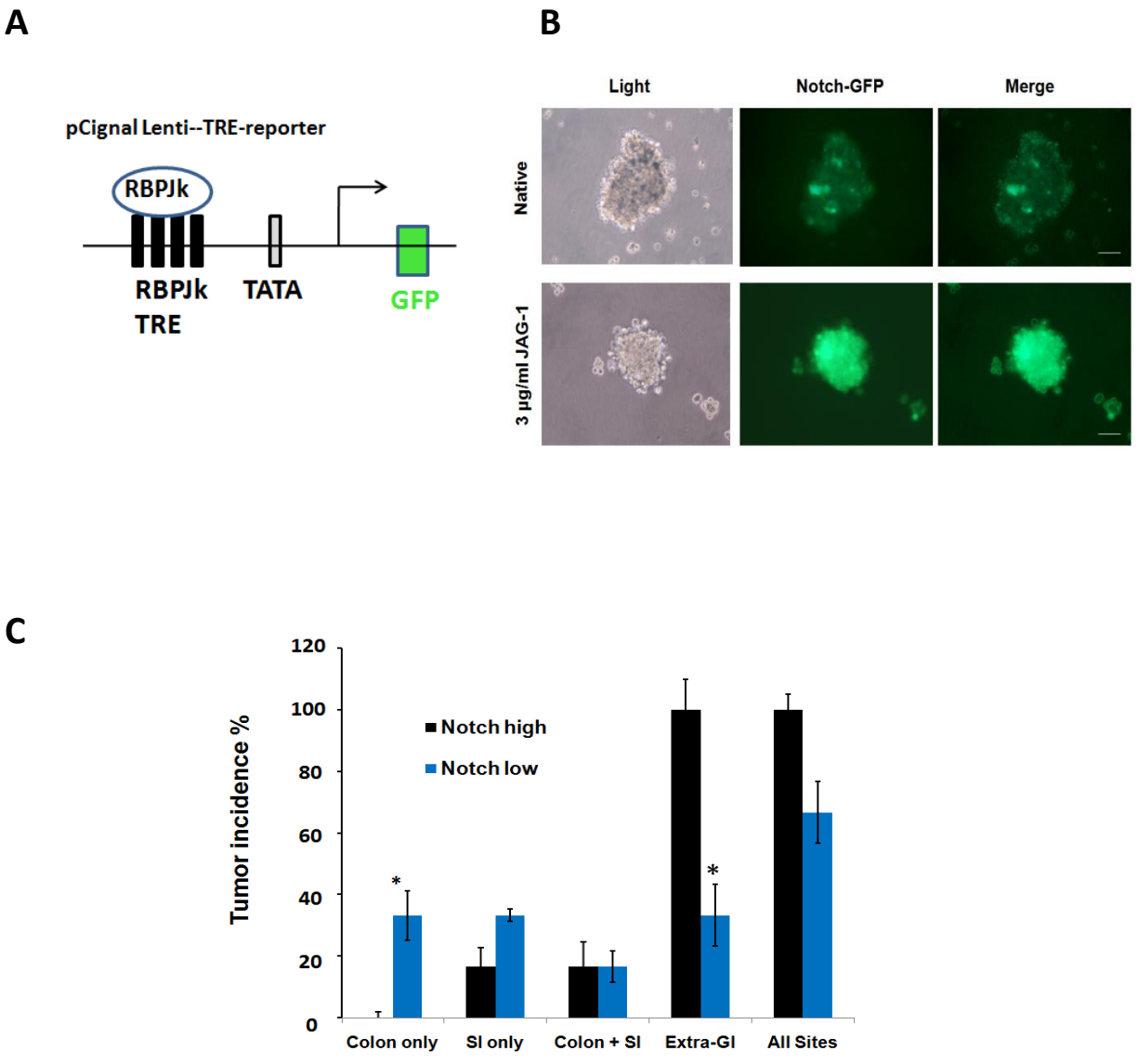

Supplemental Figure 7. related to Figure 8.CCICNotch reporter cells and *in vivo* xenografts formed by Notch high and Notch low CCICs. (A) schematic of Notch GFP reporter vector which has tandem repeats of RBP-Jk transcription responsive elements (TRE) binding to Notch downstream transcriptional factor RBP-Jk, activating promoter (TATA) and GFP expression. **(B)**CCIC Native Notch signaling was detected by GFP and increased when treated with 3µg/ml JAG1 for 4-6 hours. Scale bar, 20µ.**(C)**Xenograft tumor incidence in mice injected with FACS sorted GFP-Notch high or GFP-Notch low CCIC, organized by tumor site. * P< 0.01 compared to mock control. Error bars indicate S.E.M.

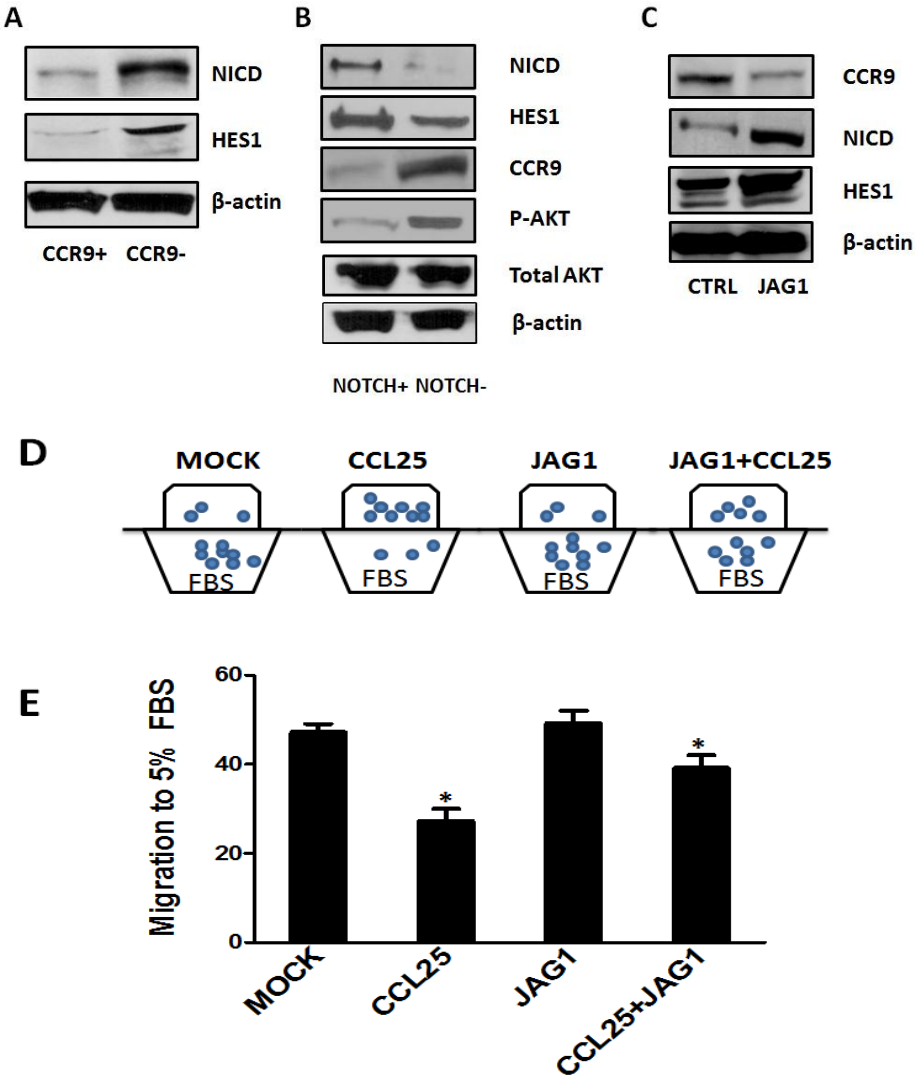

Supplemental Figure 8. Related to Figure 8. NOTCH downregulates CCR9/CCL25 axis signaling in early stage CCIC, and early stage CCIC chemotaxis to 5% FBS is inhibited by CCL25 and partially restored by *JAG1* (A)CCR9+ CCIC have lower NICD and *HES1* levels vs. CCR9- CCIC as shown by western blot. (**B).** GFP-NOTCH reporter CCIC were sorted into high and low NOTCH signaling sub-populations by FACS; CCR9 and phospho-AKT (ser 473) levels were detected higher in GFP-NOTCH- CCIC, but with no change in total AKT levels. NICD, HES1 and β-actin levels are shown for comparison. (**C)** Pre-treatment of CCR9+ CCIC with 2μg/ml *JAG1* peptide for 8 hours decreases CCR9 protein expression. NICD and HES1 levels are shown for comparison. (**D**) Schematic of CCIC incubated with different ligands in different chambers. Blue dots are representative of the relative number of cells in each chamber. FBS, 5% fetal bovine serum. (**E**) Graph of the percentage of early stage CCIC migrating to 5% FBS (%). The ligands match the schematic in (**D**). *P<0.001 by one way ANOVA for comparisons of mock control vs. CCL25 or *JAG1* vs. CCL25+*JAG1* data points.

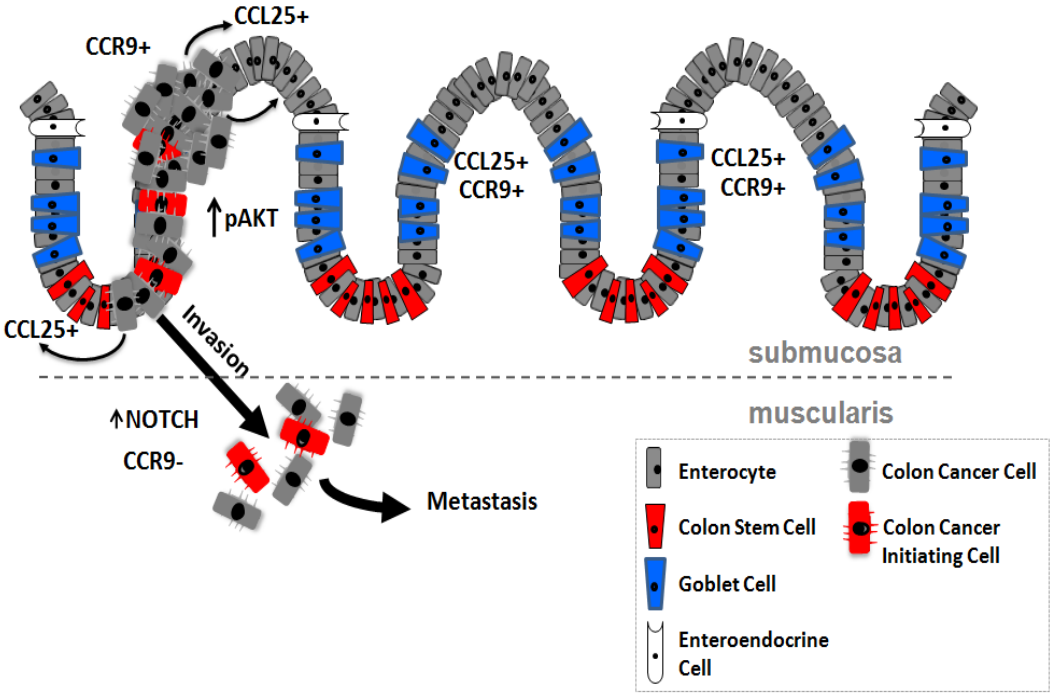

Supplemental Figure 9. Model figure of CCR9/CCL25 in the evolution of early stage to advanced CRC. Normal colon is schematized, with the crypt base on the bottom and crypt mouth at the top of the figure. A legend is given for each of the major normal colon cell types, as well as colon cancer cells and colon cancer stem cells. Early stage non-invasive CCIC and non-CCIC CRC cells upregulate the CCR9 receptor. Paracrine CCL25 from adjacent normal colon upregulates AKT signaling, proliferation, anti-apoptosis and likely superficial tumor spread along mucosal margins. As tumors progress, some cells upregulate NOTCH signaling (perhaps in response to NOTCH ligand expressing tumor associated cells such as vascular endothelium). Upregulation of NOTCH signaling causes an “invasive switch” that suppresses CCR9 and promotes NOTCH driven invasion and metastasis. Invasive and metastatic CRC tumors do not express CCR9, and CCL25 is absent from metastatic sites.

A

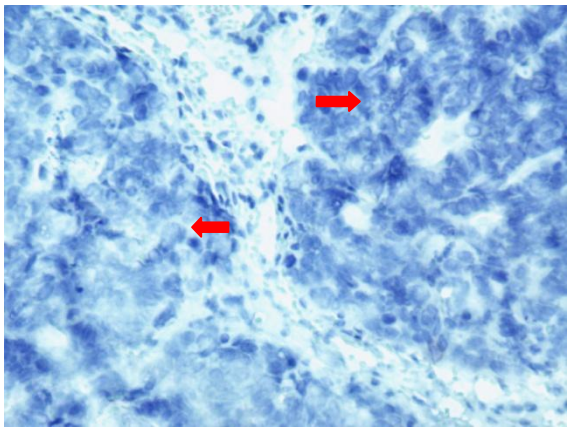

B

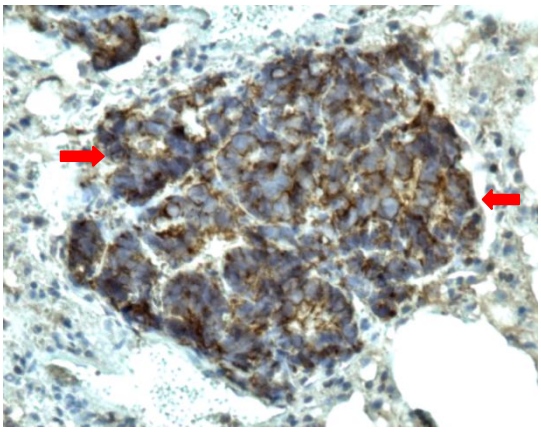

Supplemental Figure 10. CXCR4 expression in early stage CCIC extra-GI tumor. CXCR4 protein detected by immunohistochemistry in xenograft lung tumors, shown by DAB (brown), (A) IgG control; (B) anti-human CXCR4 antibody; red arrows designate tumor foci.

Supplemental Table 1: Primary human colorectal cancers used for CCR9 FACS, chemotaxis, p-AKT and cell proliferation analyses

ID	Age	Gender	Stage	Histopathology	Assays[a]
1	81	M	I	Adenocarcinoma, moderately differentiated	FACS/ p-AKT/ chemotaxis
2	74	M	I	Adenocarcinoma, moderately differentiated	FACS/ p-AKT/ chemotaxis
3	70	F	I	Adenocarcinoma, well to moderately differentiated	FACS/ p-AKT/ chemotaxis
4	86	F	II	Adenocarcinoma, well to moderately differentiated	FACS/ chemotaxis
5	58	M	II	Adenocarcinoma, well to moderately differentiated	FACS/ chemotaxis
6	63	M	I	Adenocarcinoma, well to moderately differentiated	FACS/ chemotaxis
7	59	F	II	Adenocarcinoma, poorly differentiated	FACS/ chemotaxis
8	90	F	II	Adenocarcinoma, poorly differentiated	FACS/ Proliferation
9	85	M	I	Adenocarcinoma, poorly differentiated	FACS/ Proliferation
10	40	M	II	Adenocarcinoma, poorly differentiated	FACS

[a] **The primary CRC cells were used for the assays of FACS, chemotaxis function, AKT phospholation or cell proliferation.**

Supplemental Table 2: Colorectal Cancer Initiating Cell Lines used for multiple analyses

ID	Age	Gender	Stage	Histopathology	Assays[a]
(early stage) CCIC1	57	M	I	Adenocarcinoma, well to moderately differentiated	FACS/ Mouse/ p-AKT/ Chemotaxis/ Proliferation / Western/ Q-PCR/ Microarray
(early stage) CCIC2	51	M	II	Adenocarcinoma, well differentiated	FACS/ Mouse/ p-AKT/ Chemotaxis/ Proliferation / Western/ Q-PCR
(early stage) CCIC3	74	F	I	Adenocarcinoma, well to moderately differentiated	FACS/ Mouse/ Western
(late stage) CCIC1	54	M	III	Adenocarcinoma, moderately differentiated	FACS/ Mouse/ Chemotaxis/ Western
(late stage) CCIC2	61	M	IV	Carcinoma, poor to moderately differentiated (liver metastasis)	FACS/ Mouse/ Western

[a] **The CCIC cells were used for the assays of FACS, in vivo mouse study, chemotaxis function, AKT phospholation, cell proliferation, western blot, quantative PCR, or micro-array.**

REFERENCES

1. **Bozic, I., Antal, T., Ohtsuki, H., Carter, H., Kim, D., Chen, S., Karchin, R., Kinzler, K.W., Vogelstein, B., and Nowak, M.A. Accumulation of driver and passenger mutations during tumor progression. *Proc Natl Acad Sci U S A* 2010; 107:18545-18550.**

2. **Jones, S., Chen, W.D., Parmigiani, G., Diehl, F., Beerenwinkel, N., Antal, T., Traulsen, A., Nowak, M.A., Siegel, C., Velculescu, V.E., et al. Comparative lesion sequencing provides insights into tumor evolution. *Proc Natl Acad Sci U S A* 2008; 105:4283-4288.**

3. **Johnston, M.D., Edwards, C.M., Bodmer, W.F., Maini, P.K., and Chapman, S.J. Mathematical modeling of cell population dynamics in the colonic crypt and in colorectal cancer. *Proceedings of the National Academy of Sciences of the United States of America* 2007; 104:4008-4013.**

4. **Barker, N., Ridgway, R.A., van Es, J.H., van de Wetering, M., Begthel, H., van den Born, M., Danenberg, E., Clarke, A.R., Sansom, O.J., and Clevers, H. Crypt stem cells as the cells-of-origin of intestinal cancer. *Nature* 2009; 457:608-611.**

5. **Halberg, R.B., Katzung, D.S., Hoff, P.D., Moser, A.R., Cole, C.E., Lubet, R.A., Donehower, L.A., Jacoby, R.F., and Dove, W.F. Tumorigenesis in the multiple intestinal neoplasia mouse: redundancy of negative regulators and specificity of modifiers. *Proceedings of the National Academy of Sciences of the United States of America* 2000; 97:3461-3466.**

6. **Fearon, E.R., and Vogelstein, B. A genetic model for colorectal tumorigenesis. *Cell* 1990; 61:759-767.**

7. **Merlos-Suarez, A., Barriga, F.M., Jung, P., Iglesias, M., Cespedes, M.V., Rossell, D., Sevillano, M., Hernando-Momblona, X., da Silva-Diz, V., Munoz, P., et al. The Intestinal Stem Cell Signature Identifies Colorectal Cancer Stem Cells and Predicts Disease Relapse. *Cell Stem Cell* 2011.**

8. **Dylla, S.J., Beviglia, L., Park, I.K., Chartier, C., Raval, J., Ngan, L., Pickell, K., Aguilar, J., Lazetic, S., Smith-Berdan, S., et al. Colorectal cancer stem cells are enriched in xenogeneic tumors following chemotherapy. *PLoS ONE* 2008; 3:e2428.**

9. **Ricci-Vitiani, L., Lombardi, D.G., Pilozzi, E., Biffoni, M., Todaro, M., Peschle, C., and De Maria, R. Identification and expansion of human colon-cancer-initiating cells. *Nature* 2007; 445:111-115.**

10. **Emmink, B.L., Van Houdt, W.J., Vries, R.G., Hoogwater, F.J., Govaert, K.M., Verheem, A., Nijkamp, M.W., Steller, E.J., Jimenez, C.R., Clevers, H., et al. Differentiated Human Colorectal Cancer Cells Protect Tumor-Initiating Cells From Irinotecan. *Gastroenterology* 2011.**

11. **Sonoshita, M., Aoki, M., Fuwa, H., Aoki, K., Hosogi, H., Sakai, Y., Hashida, H., Takabayashi, A., Sasaki, M., Robine, S., et al. Suppression of colon cancer metastasis by Aes through inhibition of Notch signaling. *Cancer Cell* 2011; 19:125-137.**

12. **Din, F.V., Theodoratou, E., Farrington, S.M., Tenesa, A., Barnetson, R.A., Cetnarskyj, R., Stark, L., Porteous, M.E., Campbell, H., and Dunlop, M.G. Effect of aspirin and NSAIDs on risk and survival from colorectal cancer. *Gut* 59:1670-1679.**

13. **Kabelitz, D., and Wesch, D. Features and functions of gamma delta T lymphocytes: focus on chemokines and their receptors. *Critical reviews in immunology* 2003; 23:339-370.**

14. **Youn, B.S., Kim, Y.J., Mantel, C., Yu, K.Y., and Broxmeyer, H.E. Blocking of c-FLIP(L)--independent cycloheximide-induced apoptosis or Fas-mediated apoptosis by the CC chemokine receptor 9/TECK interaction. *Blood* 2001; 98:925-933.**

15. **Wurbel, M.A., McIntire, M.G., Dwyer, P., and Fiebiger, E. CCL25/CCR9 interactions regulate large intestinal inflammation in a murine model of acute colitis. *PLoS ONE* 2011; 6:e16442.**

16. **LaPointe, L.C., Dunne, R., Brown, G.S., Worthley, D.L., Molloy, P.L., Wattchow, D., and Young, G.P. Map of differential transcript expression in the normal human large intestine. *Physiological genomics* 2008; 33:50-64.**

17. **Li, X., Madison, B.B., Zacharias, W., Kolterud, A., States, D., and Gumucio, D.L. Deconvoluting the intestine: molecular evidence for a major role of the mesenchyme in the modulation of signaling cross talk. *Physiological genomics* 2007; 29:290-301.**

18. **Hart, A.L., Ng, S.C., Mann, E., Al-Hassi, H.O., Bernardo, D., and Knight, S.C. Homing of immune cells: role in homeostasis and intestinal inflammation. *Inflamm Bowel Dis* 16:1969-1977.**

19. **Shang, L., Thirunarayanan, N., Viejo-Borbolla, A., Martin, A.P., Bogunovic, M., Marchesi, F., Unkeless, J.C., Ho, Y., Furtado, G.C., Alcami, A., et al. Expression of the chemokine binding protein M3 promotes marked changes in the accumulation of specific leukocytes subsets within the intestine. *Gastroenterology* 2009; 137:1006-1018, 1018 e1001-1003.**

20. Zaballos, A., Gutierrez, J., Varona, R., Ardavin, C., and Marquez, G. Cutting edge: identification of the orphan chemokine receptor GPR-9-6 as CCR9, the receptor for the chemokine TECK. *Journal of immunology* 1999; 162:5671-5675.

21. Amersi, F.F., Terando, A.M., Goto, Y., Scolyer, R.A., Thompson, J.F., Tran, A.N., Faries, M.B., Morton, D.L., and Hoon, D.S. Activation of CCR9/CCL25 in cutaneous melanoma mediates preferential metastasis to the small intestine. *Clinical cancer research : an official journal of the American Association for Cancer Research* 2008; 14:638-645.

22. Johnson, E.L., Singh, R., Johnson-Holiday, C.M., Grizzle, W.E., Partridge, E.E., Lillard, J.W., Jr., and Singh, S. CCR9 interactions support ovarian cancer cell survival and resistance to cisplatin-induced apoptosis in a PI3K-dependent and FAK-independent fashion. *J Ovarian Res* 2010; 3:15.

23. Johnson-Holiday, C., Singh, R., Johnson, E., Singh, S., Stockard, C.R., Grizzle, W.E., and Lillard, J.W., Jr. CCL25 mediates migration, invasion and matrix metalloproteinase expression by breast cancer cells in a CCR9-dependent fashion. *Int J Oncol* 2011; 38:1279-1285.

24. Sharma, P.K., Singh, R., Novakovic, K.R., Eaton, J.W., Grizzle, W.E., and Singh, S. CCR9 mediates PI3K/AKT-dependent antiapoptotic signals in prostate cancer cells and inhibition of CCR9-CCL25 interaction enhances the cytotoxic effects of etoposide. *Int J Cancer* 2010; 127:2020-2030.

25. Singh, S., Singh, U.P., Stiles, J.K., Grizzle, W.E., and Lillard, J.W., Jr. Expression and functional role of CCR9 in prostate cancer cell migration and invasion. *Clinical cancer research : an official journal of the American Association for Cancer Research* 2004; 10:8743-8750.

26. Sikandar, S., Dizon, D., Shen, X., Li, Z., Besterman, J and Lipkin, SM. The Class I HDAC Inhibitor MGCD0103 Induces Cell Cycle Arrest and Apoptosis in Colon Cancer Initiating Cells by Upregulating DKK-1 and Non-Canonical WNT Signaling. . *Oncotarget* 2010; 1:666-690.

27. Sikandar, S.S., Pate, K.T., Anderson, S., Dizon, D., Edwards, R.A., Waterman, M.L., and Lipkin, S.M. NOTCH signaling is required for formation and self-renewal of tumor-initiating cells and for repression of secretory cell differentiation in colon cancer. *Cancer Res* 2010; 70:1469-1478.

28. Lira, S.A., Mehrad, B., Chen, S.C., Zalamea, P., Kinsley, D.J., Wiekowski, M.T., Coronel, E.,

Vassileva, G., Manfra, D., and Jensen, K.K. Conditional transgenic models to study chemokine biology. *Methods Mol Biol* 2004; 239:105-122.

29. Pang, R., Law, W.L., Chu, A.C., Poon, J.T., Lam, C.S., Chow, A.K., Ng, L., Cheung, L.W., Lan, X.R., Lan, H.Y., et al. A subpopulation of CD26+ cancer stem cells with metastatic capacity in human colorectal cancer. *Cell Stem Cell* 2010; 6:603-615.

30. Pena, C., Garcia, J.M., Larriba, M.J., Barderas, R., Gomez, I., Herrera, M., Garcia, V., Silva, J., Dominguez, G., Rodriguez, R., et al. SNAI1 expression in colon cancer related with CDH1 and VDR downregulation in normal adjacent tissue. *Oncogene* 2009; 28:4375-4385.

31. Palmer, H.G., Larriba, M.J., Garcia, J.M., Ordonez-Moran, P., Pena, C., Peiro, S., Puig, I., Rodriguez, R., de la Fuente, R., Bernad, A., et al. The transcription factor SNAIL represses vitamin D receptor expression and responsiveness in human colon cancer. *Nature medicine* 2004; 10:917-919.

32. Kopan, R., and Ilagan, M.X. The canonical Notch signaling pathway: unfolding the activation mechanism. *Cell* 2009; 137:216-233.

33. Harrison, H., Farnie, G., Brennan, K. and Clarke, R. Breast Cancer Stem Cells: Something Out of Notching? *Cancer Res* 2010; 70:8973-8976.

34. Taketo, M.M. Reflections on the Spread of Metastasis to Cancer Prevention. *Cancer Prev Res* 2011; 4 324-328.

35. Baba, Y., Nosho, K., Shima, K., Hayashi, M., Meyerhardt, J.A., Chan, A.T., Giovannucci, E., Fuchs, C.S., and Ogino, S. Phosphorylated AKT expression is associated with PIK3CA mutation, low stage, and favorable outcome in 717 colorectal cancers. *Cancer* 2011; 117:1399-1408.

36. Yeung, T.M., Chia, L.A., Kosinski, C.M., and Kuo, C.J. Regulation of self-renewal and differentiation by the intestinal stem cell niche. *Cellular and molecular life sciences : CMLS* 2011; 68:2513-2523.

37. Fre, S., Vignjevic, D., Schoumacher, M., Duffy, S.L., Janssen, K.P., Robine, S., and Louvard, D. Epithelial morphogenesis and intestinal cancer: new insights in signaling mechanisms. *Advances in cancer research* 2008; 100:85-111.

38. Riccio, O., van Gijn, M.E., Bezdek, A.C., Pellegrinet, L., van Es, J.H., Zimber-Strobl, U., Strobl, L.J., Honjo, T., Clevers, H., and Radtke, F. Loss of intestinal crypt progenitor cells owing to inactivation of both Notch1 and Notch2 is accompanied by derepression of CDK inhibitors p27Kip1 and p57Kip2. *EMBO reports* 2008; 9:377-383.

39. Vooijs, M., Ong, C.T., Hadland, B., Huppert, S., Liu, Z., Korving, J., van den Born, M., Stappenbeck, T., Wu, Y., Clevers, H., et al. Mapping the consequence of Notch1 proteolysis in vivo with NIP-CRE. *Development* 2007; 134:535-544.

40. de Lau, W., Barker, N., and Clevers, H. WNT signaling in the normal intestine and colorectal cancer. *Frontiers in bioscience : a journal and virtual library* 2007; 12:471-491.

41. Meng, R.D., Shelton, C.C., Li, Y.M., Qin, L.X., Notterman, D., Paty, P.B., and Schwartz, G.K. gamma-Secretase inhibitors abrogate oxaliplatin-induced activation of the Notch-1 signaling pathway in colon cancer cells resulting in enhanced chemosensitivity. *Cancer Research* 2009; 69:573-582.

42. Steg, A.D., Katre, A.A., Goodman, B., Han, H.D., Nick, A.M., Stone, R.L., Coleman, R.L., Alvarez, R.D., Lopez-Berestein, G., Sood, A.K., et al. Targeting the notch ligand JAGGED1 in both tumor cells and stroma in ovarian cancer. *Clinical cancer research : an official journal of the American Association for Cancer Research* 2011; 17:5674-5685.

43. Wu, Y., Cain-Hom, C., Choy, L., Hagenbeek, T.J., de Leon, G.P., Chen, Y., Finkle, D., Venook, R., Wu, X., Ridgway, J., et al. Therapeutic antibody targeting of individual Notch receptors. *Nature* 2010; 464:1052-1057.

44. Jubb, A.M., Turley, H., Moeller, H.C., Steers, G., Han, C., Li, J.L., Leek, R., Tan, E.Y., Singh, B., Mortensen, N.J., et al. Expression of delta-like ligand 4 (Dll4) and markers of hypoxia in colon cancer. *British journal of cancer* 2009; 101:1749-1757.

45. Ridgway, J., Zhang, G., Wu, Y., Stawicki, S., Liang, W.C., Chanthery, Y., Kowalski, J., Watts, R.J., Callahan, C., Kasman, I., et al. Inhibition of Dll4 signalling inhibits tumour growth by deregulating angiogenesis. *Nature* 2006; 444:1083-1087.

46. Wang, T., Baron, M., and Trump, D. An overview of Notch3 function in vascular smooth muscle cells. *Progress in biophysics and molecular biology* 2008; 96:499-509.

47. Vooijs, M., Liu, Z., and Kopan, R. Notch: architect, landscaper, and guardian of the intestine. *Gastroenterology* 2011; 141:448-459.

48. Guilmeau, S., Flandez, M., Mariadason, J.M., and Augenlicht, L.H. Heterogeneity of Jagged1 expression in human and mouse intestinal tumors: implications for targeting Notch signaling. *Oncogene* 2010; 29:992-1002.

49. Yanall l., N., J., Ira K., Hlloka S. Kamal A.,I., and Mlzunuma N. . Dlk-1, a cellourface antigen on foetal hepatic stem/progenitor cells, is expressed in hepatocellular, colon, pancreas and breast carcinomas at a high frequency. *Journal of Biochemistry* 2010; 148:85-92.

50. Burger, J.A., and Kipps, T.J. CXCR4: a key receptor in the crosstalk between tumor cells and their microenvironment. *Blood* 2006; 107:1761-1767.

51. Rettig, M.P., Ansstas, G., and DiPersio, J.F. Mobilization of hematopoietic stem and progenitor cells using inhibitors of CXCR4 and VLA-4. *Leukemia : official journal of the Leukemia Society of America, Leukemia Research Fund, U.K* 2012; 26:34-53.

52. Rettig, M.P., Ramirez, P., Nervi, B., and DiPersio, J.F. CXCR4 and mobilization of hematopoietic precursors. *Methods in enzymology* 2009; 460:57-90.

53. Uy, G.L., Rettig, M.P., and Cashen, A.F. Plerixafor, a CXCR4 antagonist for the mobilization of hematopoietic stem cells. *Expert opinion on biological therapy* 2008; 8:1797-1804.

54. Damon, L.E. Mobilization of hematopoietic stem cells into the peripheral blood. *Expert review of hematology* 2009; 2:717-733.

55. Peled, A., Wald, O., and Burger, J. Development of novel CXCR4-based therapeutics. *Expert opinion on investigational drugs* 2012; 21:341-353.

56. Hung, K.E., Maricevich, M.A., Richard, L.G., Chen, W.Y., Richardson, M.P., Kunin, A., Bronson, R.T., Mahmood, U., and Kucherlapati, R. Development of a mouse model for sporadic and metastatic colon tumors and its use in assessing drug treatment. *Proceedings of the National Academy of Sciences of the United States of America* 2010; 107:1565-1570.

57. Wendt, M.K., Molter, J., Flask, C.A., and Schiemann, W.P. In vivo dual substrate bioluminescent imaging. *Journal of visualized experiments : JoVE* 2011.

58. Johnson, E.L., Singh, R., Singh, S., Johnson-Holiday, C.M., Grizzle, W.E., Partridge, E.E., and Lillard, J.W., Jr. CCL25-CCR9 interaction modulates ovarian cancer cell migration, metalloproteinase expression, and invasion. *World J Surg Oncol* 2010; 8:62.

59. Vermeulen, L., Todaro, M., de Sousa Mello, F., Sprick, M.R., Kemper, K., Perez Alea, M., Richel, D.J., Stassi, G., and Medema, J.P. Single-cell cloning of colon cancer stem cells reveals a multi-lineage differentiation capacity.

Proceedings of the National Academy of Sciences of the United States of America **2008; 105:13427-13432.**

60. Pastor, D.M., Poritz, L.S., Olson, T.L., Kline, C.L., Harris, L.R., Koltun, W.A., Chinchilli, V.M., and Irby, R.B. Primary cell lines: false representation or model system? a comparison of four human colorectal tumors and their coordinately established cell lines. *International journal of clinical and experimental medicine* 2010; 3:69-83.

61. Freshney, R. Isolation and culture of intestinal epithelial cells. 2002.

62. Nickoloff, B.J., Qin, J.Z., Chaturvedi, V., Denning, M.F., Bonish, B., and Miele, L. Jagged-1 mediated activation of notch signaling induces complete maturation of human keratinocytes through NF-kappaB and PPARgamma. *Cell death and differentiation* 2002; 9:842-855.

63. Weijzen, S., Velders, M.P., Elmishad, A.G., Bacon, P.E., Panella, J.R., Nickoloff, B.J., Miele, L., and Kast, W.M. The Notch ligand Jagged-1 is able to induce maturation of monocyte-derived human dendritic cells. *Journal of immunology* 2002; 169:4273-4278.

64. Ma, X.B., Jia, X.S., Liu, Y.L., Wang, L.L., Sun, S.L., Song, N., Wang, E.H., and Li, F. Expression and role of Notch signalling in the regeneration of rat tracheal epithelium. *Cell proliferation* 2009; 42:15-28.

65. Svensson, M., Marsal, J., Ericsson, A., Carramolino, L., Broden, T., Marquez, G., and Agace, W.W. CCL25 mediates the localization of recently activated CD8alphabeta(+) lymphocytes to the small-intestinal mucosa. *The Journal of clinical investigation* 2002; 110:1113-1121.

CHAPTER 2

Chemokine-Targeted Mouse Models of Human Primary and Metastatic Colorectal Cancer

(Contribution: Steven Lipkin, Huanhuan Chen and Xiling Shen designed the project; Huanhuan Chen, Jian Sun, Harry Hou Jr, Myra Arcilla, Daniel Joe, Nikolai Rakhilin, Jiahn Choi, Poornima Gadamsetty, Randy Longman and Jonlin Chen performed experiments; Huanhuan Chen, Steven Lipkin, Xi Kathy Zhou, Robert Edwards, Jian Sun, Kai Yuan Chen and Zeynep H. Gümüş analyzed the data; Steven Lipkin, Huanhuan Chen, Xiling Shen wrote the manuscript; Winfried Edelmann and Zeynep H. Gümüş, Micheal Shuler, Nozomi Nishimura helped with project discussion.)

INTRODUCTION

Colorectal cancer (CRC) is a leading cause of cancer death world wide.The most common site of CRC metastasis is the liver[67]. When CRC hepatic metastases are treated with chemotherapy, they almost invariably become chemoresistant. Consequently, five-year survival for metastatic CRC is only ~15% and, despite recent advances, current chemotherapy regimens almost never cure advanced disease.

Genetically engineered mouse models (GEMM) are powerful tools for studying CRC, but they only represent a subset of CRC driver mutations. Human subcutaneous xenograft and orthotopic models in immunodeficient mouse hosts are widely used for mechanistic studies, drug screening, and have provided many critical insights into CRC pathogenesis[27, 68-72]. However, the persistence of poor outcomes among many CRC patients highlights the need for new approaches to complement existing models.

For example, there is currently no robust non-survival surgery requiring model that recapitulates the process of human CRC cell metastasis from the GI tract to the liver, the site of more than 50% of CRC metastases. Another problem is that pre-clinical evaluation of new CRC therapies has a high false-positive success rate[69-72] and there is an urgent medical need for less chemosensitive pre-clinical models to reduce the number of futile CRC clinical trials conducted. A third problem is that human cancer cell studies *in vivo* require immunodeficient mouse hosts to avoid xeno-immunorejection, a barrier that has limited mechanistic studies of adaptive immunity in CRC progression, tumor vaccines and immunotherapies[72].

To expand the range of pre-clinical human CRC models, we created a resource of mechanistically diverse CRC cell and patient-derived xenograft (PDX)lines that collectively carry the majority of common recurrent somatic CRC mutations, represent all major molecular subtypes and robustly model primary CRCs in the native GI micro-environment via simple tail-vein injection. By controlling the CCR9-CCL25 chemokine axis, these human CRC cells traffic to the GI tract and form orthotopic tumors[73]. This minimally invasive approach avoids potential survival surgery experimental confounders (e.g. needle exit wound tracts, iatrogenic local inflammation and systemic stress), and reduces administrative compliance burden and ethical concerns of surgery associated animal morbidity.

Importantly, as proof of principle, we extended this approach to model human derived CRCs in immunoproficient mouse hosts. We microinjected human PDX CRC cells that natively express the CCR9 chemokine receptor[73] into wild-type (wt) mouse early blastocysts to form human-mouse chimeras. These humanized chimeric mice developed CRC tumors that originated from blastocyst-injected, human PDX CRC cells in the GI tract. This model allows the study of human primary CRCs in an immunoproficient GI microenvironment.

Next, we further develop this resource and demonstrate sequential metastasis of primary human CRC tumors to liver, recapitulating the anatomical route occurring in patients. Finally, we use these hepatic metastases to show that for commonly used anti-CRC therapies such as oxaliplatin, *in vivo* CRC liver metastases have elevated DKK4 levels and upregulated Notch signaling (both of which have previously been associated

with CRC chemoresistance)[74, 75]and are significantly less chemosensitive vs. paired sub-cutaneous xenografts generated from the same cells.

RESULTS

Modeling Recurrent Human Primary CRC Mutations

Chemokines are secreted ligands that regulate cell trafficking between different organs[13]. Small intestine and colon epithelia produce Chemokine 25 (CCL25), which binds to Chemokine Receptor 9 (CCR9) expressing cells[14-17]. Previously, we reported that CCR9 is up-regulated in primary tumors from early-stage CRC patients, but downregulated in invasive and metastatic CRC tumors. Furthermore, via only mouse tail-vein injection, early-stage CRC cells that endogenously express CCR9 spontaneously form primary CRCs in the colorectum and intestine, attracted by CCL25[67, 73].In contrast, blocking the CCL25-CCR9 chemokine axis by short-hairpin RNA (shRNA) or antibodies against CCL25 promotes metastasis and formation of extra-intestinal tumors.

Based on these findings, we established a Chemokine-Targeted Mouse Model (CTMM) system that can be used to study primary human CRC mechanisms of progression and chemoprevention in the native GI microenvironment. Recent genome-wide characterization studies have highlighted the extreme molecular heterogeneity among human CRCs[76]. We therefore systematically generated a panel of 15 doxycycline-inducible CCR9+ cell and PDX lines (**Supplemental Fig. 1 and Supplementary Fig. 2**) to model a diverse spectrum of primary human CRC tumors that carry the majority of common recurrent somatic mutations occurring in patients (**Supplementary Table 1**). This includes not only well-established examples (e.g. *KRAS* and *BRAF*) but also mechanistically poorly characterized recurrently mutated genes such as *ASXL1,MLL3* and *LIFR*. Orthogonally, this resource includes multiple examples from all the major

histopathological and molecularly defined CRC sub-types, such as DNA mismatch repair proficient and deficient, CpG Island Methylator Phenotype (CIMP), adenocarcinoma and mucinous sub-types. (**Supplementary Table 1**).

To facilitate quantitative experimental monitoring, each model also co-expresses constitutive luciferase and RFP reporters (**Supplementary Fig.1a**).Using tail-vein injection and luciferase monitoring (**Fig. 1a,b** and **Supplementary Fig.3**), within 3 weeks, each CTMM model forms mean1.88±0.57colorectal tumors per affected mouse host, (whereas the CCR9- parental lines rarely, if at all, form colorectal tumors (mean 0-0.15)) (**Fig. 1c and Supplementary Table 2).**

In summary, we have developed a CTMM system to model primary human CRC tumor growth and progression in the native GI microenvironment. This system includes a molecularly diverse resource that spans the majority of recurrent patient CRC somatic mutations. CTMM models can be generated easily within weeks and avoid potential experimental confounding factors from survival surgery implantation (e.g. needle tract exit wounds, iatrogenic local inflammation and systemic stress from anesthesia), as well as reduce administrative compliance burden and ethical concerns of surgery associated animal morbidity. These qualities make CTMM a potentially useful system for evaluation of early-stage CRC progression mechanisms and chemoprevention drug screening.

Human Primary Gastrointestinal CRC Tumor Formation in Immunoproficient Mouse Hosts

A current limitation of modeling human-derived cancers in mice is that immunodeficient hosts are required to avoid xenograft rejection. This is particularly problematic given our increasing appreciation of the role of the immune system in the tumor micro-environment[77]. Therefore, it will be desirable to use immunoproficient mouse hosts to model CRC when studying tumor immunology, immunotherapies or other cancer cell-microenvironment immunity cross-talk mechanisms.

First, to test whether chemokine targeting works in immunoproficient mouse hosts, we generated CCR9-expressing mouse CT26 cells. Tail-vein injection into immune-proficient Balb/c of these cells similarly generated primary CRC tumors in the colon. Co-immunofluorescence showed that the human primary tumors are infiltrated by mouse CD3+ T cells and CD20+ B cells (**Supplementary Fig.4**).

However, mouse cancer cells severely limit the scope and usefulness of CTMM. To address this limitation, we directly tested whether CTMM can model primary human CRC tumors in immunoproficient mouse hosts. Using essentially the same techniques for mouse embryonic stem cell microinjection to generate knockout mice[78, 79] we FACS sorted CCR9+ PDX cancer stem cells and injected 10-15 cells into wild-type Swiss-Webster strain mouse e3.5 blastocysts to generate human primary CRC-mouse chimeras (**Fig. 2**).

For each CCR9+ CRC cell blastocyst microinjection session into pseudo-pregnant mouse foster mothers we obtained 24-40 live mouse pups. At post-natal day 21, ~10% have IVIS detectable luciferase activity, all of which localizes to intestine/colon (**Fig. 2**). In contrast, no IVIS detectable signal is observed in pups born from blastocysts injected

with CCR9- PDX cells (data not shown). By age 3-6 months, blastocyst-injected human CRC cells form luciferase-detectable colon and small intestinal tumors in ~20% of immunoproficient mouse hosts, including locally invasive tumors that can penetrate the bowel wall (**Fig. 2**). PCR of human centromeric repeats confirmed that the dissected tumors consist of human and not rodent cells (**Supplementary Fig.5b**). Histopathological analysis confirmed that intestine/colon tumors are also RFP+, consistent with the growth of microinjected human luciferase/RFP-labeled CRC cells in the wt immunoproficient host GI microenvironment(**Fig.2 c**). In contrast, injection of CCR9- PDX cells did not form tumors anywhere in the body and were undetectable in the thoracic and visceral organs.

At the same time, no human IVIS signal or CRC cells were detected in any other organ, such as lung, liver, spleen, kidney or skeletal muscle (**Fig. 2b, Supplementary Fig. 5a** and data not shown). We also performed dual-immunofluorescence with anti-RFP and anti-mouse CD3 (a pan T cell marker) antibodies(**Fig. 2d and e**). This confirmed that mouse hosts carrying human primary CRC tumors have T cells, as well as CD20+ B cells (data not shown) infiltrating the human primary CRC malignancies. Additionally, to further confirm that mouse hosts are systemically immunoproficient, we analyzed spleen and mesenteric lymph nodes (MLNs) from human primary CRC+ mice and their control (IVIS-negative) blastocyst-non-injected littermates. This showed that T and B cells were clearly present, and the relative proportions of spleen and MLN CD3+ (T cells), CD4+ (T helper cells),CD8+ (cytotoxic T cells), CD19+ (B cells) did not significantly differ between the two groups (**Supplementary Fig.6**). Similarly, analysis of CD4+ T helper

revealed equivalent populations of $CD62L^{hi}$ $CD44^{lo}$ (naïve cells), $CD62L^{lo}$ $CD44^{hi}$ (activated memory T cells), RORγt+ (Th17), and Foxp3+ (Treg).

Overall, we have developed an orthotopic experimental system to study primary human colorectal cancer in the GI microenvironments of immunoproficient mouse hosts. This technology has the potential to significantly enhance our ability to understand and develop immunological therapies that target adaptive immune mechanisms in the GI tumor microenvironment.

Sequential primary human CRC-liver metastasis formation

Seven CTMM models (CCR9-PDX1, HT15, HCA7,SW48,Colo205, DLD1 and LS174T) spontaneously form liver tumors (mean 3.1-8.2 liver tumors/mouse by 8 weeks) but only in mice that have previously developed primary CRCs (**Fig. 3 and Supplementary Fig. 7**). IVIS imaging revealed luciferase-detectable primary CRCs (mean 1.8 weeks post-inoculation) preceded liver tumors (mean 5.8 weeks post-inoculation). In contrast, liver tumors were rarely detected in non-CTMM models, in which tail-vein injected CRC cells usually form tumors in the lung (**Fig. 3**).

These findings are potentially consistent with a model whereby CTMM promotes cells from primary CRC tumors to metastasize to liver, most likely via the portal circulation. To test this model, we tail-vein injected mice to generate primary CRC CTMM models. After primary GI tumor formation was detected by IVIS imaging, we next withdrew doxycycline to suppress CCR9 expression. In all CTMM lines tested liver tumor multiplicity was significantly higher when CCR9 levels were suppressed (**Supplementary Fig. 8a)**. Additionally, FACS of mouse liver cells 48 hours after tail

vein injection of CCR9+ CRC cells showed that RFP+ cells were essentially undetectable (**Supplementary Fig. 8b**), arguing against an alternative model in which CCR9 suppression stimulated expansion of previously resident human CRC cells in liver.

Next, to confirm that CTMM primary CRC tumor cells could enter the portal circulation, we injected mice with FITC-Dextran to label vasculature and used Multi-Photon Microscopy (MPM) to image the primary tumor and liver metastatic tumors *in vivo*. This revealed that RFP+ human CTMM cells co-localize with and travel through host blood vessels, consistent with vascular intravasation (an important step prior to entry into the portal circulation that drains to the liver) (**Supplementary Fig. 9**).

In summary, our data are consistent with a subset of molecularly well-characterized CTMM primary CRC tumors that are capable of sequentially modeling the progression of primary human CRC to liver metastases via the portal circulation that occurs in over 50% of stage IV CRC patients. Furthermore at even later time-points, luciferase+ cells spreading at additional sites such as lung were also observed (**Fig.3b** and data not shown).

Increased Chemoresistance of Human Hepatic vs. Sub-Cutaneous or Primary GI CRC tumors

One challenge for cancer drug discovery is that therapies effective against subcutaneous xenograft tumors are often ineffective in human (especially metastatic) CRC patients. For proof-of-concept, we tested whether the more clinically relevant GI

and liver microenvironments of CTMM CRCs impact chemotherapy responsiveness vs. subcutaneous xenograft models.

Oxaliplatin is an effective and widely used anti-CRC chemotherapy. We used both DNA mismatch repair proficient (pMMR) and deficient (dMMR) CIMM models to test whether the same cells have altered oxaliplatin chemosensitivity in different tumor microenvironments. We simultaneously injected mice subcutaneously or by tail vein to generate (a) subcutaneous tumors or (b) primary CRCs and sequential liver metastases. Quantitative IVIS imaging of constitutive luciferase reporters was used to directly compare tumor responses (**Fig. 4a**).

As expected, oxaliplatin treatment of mice significantly inhibited the growth of subcutaneous tumors for both pMMR and dMMR models after five weeks respectively, causing mean 53% volume reduction at week five (**Fig. 4b, c and Supplementary Fig. 10**; P=0.005). Oxaliplatin similarly inhibited the growth of primary CRCs (-33.9%; P=0.04). This difference in tumor response was not statistically significant between the two different microenvironments.

However, in the liver microenvironment, no oxaliplatin dependent growth inhibition was observed for CRC hepatic metastases generated from the same cells. The increase in oxaliplatin chemoresistance was significantly greater for liver metastases vs. either subcutaneous (P<0.001) or primary GI tumors (P=0.002).

To understand the mechanisms of CRC chemoresistance in the hepatic microenvironment, we performed RNA-seq gene expression profiling of liver and subcutaneous tumors generated from DLD-1 cells. Consistent with this comparison,

Ingenuity Pathway Analysis (IPA) revealed that the Canonical Pathway of Colorectal Cancer Metastasis Signaling was upregulated (p=0.049). Additionally, *Dickkopf 4* (DKK4)levels were dramatically upregulated(76-fold; p=0.00001) in CRC liver metastases (**Fig. 4d**)., a finding that we subsequently confirmed using qPCR (**Fig. 4e**).High DKK4 levels have previously been strongly associated with clinical CRC chemo-resistance[74]. Furthermore, Notch pathway signaling was also significantly upregulated in CRC liver metastases (p=0.012), a finding we also confirmed using qPCR for Notch pathway downstream target genes, including HES1, HES7, HEY1 and HEY2.Notch pathway signaling have also previously been associated with CRC chemoresistance[75].

In total, our CTMM model of CRC liver metastasis through the portal circulation can be performed within 5-8 weeks, does not require survival surgery and demonstrates greater oxaliplatin chemoresistance than either subcutaneous xenograft or primary GI orthotopic tumors, likely through a mechanism of upregulated DKK4 and Notch pathway signaling.

DISCUSSION

Recent comprehensive molecular studies such as TCGA have provided a broad range of insights with an unprecedented level of molecular resolution into the precise molecular alterations that drive human CRC pathogenesis and progression. However, new pre-clinical models are needed to augment existing ones and recapitulate more fully the diverse nature of both cell-autonomous signaling pathways and non-cell autonomous interactions between tumor cells and their orthotopic primary, metastasis-route and -destination site microenvironments.

Towards this goal, we systematically generated a resource of human primary CRC CTMM models that collectively carry the major recurrent somatic alterations occurring in CRC patients. This can be used to study the mechanistic role of the majority of recurrent human CRC mutations multi-dimensionally. For example, Difluoro-methylornithine (DFMO) is a potent anti-CRC chemoprevention agent that alters metabolite levels critical for DNA and histone methylation[80-83]. To study the impact of recurrently mutated epigenetic regulator genes such as the histone-lysine N-methyltransferase MLL3 or the Polycomb complex chromatin binding protein ASLX1 (**Supplementary Table 1**) on DFMO chemoprevention efficacy, mice carrying tumors from the CTMM primary CRC resource can be treated with DFMO, scored for reduced tumor multiplicity and in parallel efficacy assessed from the same dataset classified by positive vs. negative mutation status for MLL3, ASLX1 or any other epigenetic regulatorto assess the mechanistic role of each mutation and potential epistasisin DFMO chemoprevention.

Next, based on previous findings that fetal intestine and colon express the CCR9 ligand CCL25[84, 85] we extended our chemokine-targeting approach and developed an effective experimental system to model human cancer cell growth and invasion in immunoproficient mice, which has remained a challenge in the field. The precisely established mechanisms that permit immune tolerance of CCR9+ human cancer stem cells that are injected into blastocysts of wild type mice are currently poorly understood. But, perhaps similar to mechanisms allowing expression of human transgenes in genetically engineered mice, their introduction before thymus development (which also expresses CCL25) likely causes human cell antigens to be immunologically perceived as "self" by immunoproficient mouse hosts and inducing tolerance.

The ability to model human cancers in immunoproficient mouse hosts is potentially significant. We anticipate that this approach can be applied to studying other aspects of human CRC-adaptive immunity cross-talk (ex. impact of Th17 and Treg cells on primary CRC formation, liver metastasis, tumor dormancy), other cancer types (ex. chimeras targeting CXCR4+ human Acute Lymphoblastic Leukemia cells to SDF-1α expressing bone marrow), and immunotherapy screening (ex. testing anti-PD1antibodies and cancer vaccines in immunoproficient hosts).

With regard to modeling primary CRC tumor progression, current hepatic metastasis models using human CRC cells are time- and labor-intensive and technically challenging, which limits their usage for drug development. Direct injection of human CRC cells into the heart left ventricle, kidney capsule or spleen are potentially confounded by anatomical routes to the liver that do not recapitulate the microenvironment favorable for transit from the gut through the portal circulation and

lymphatics that occur in almost all advanced stage CRC patients[67]. The portal circulation is known to have distinct features that distinguish its microenvironment from other vasculature. For example, hepatic vein, lymphatic and tributary flow to the liver is unique in that it receives both oxygenated and deoxygenated blood (the latter from gut) and consequently has lower pO2 and hemodynamic perfusion pressure than other organs[86-88]. Furthermore, hypoxia can promote metastasis in multiple types of cancer[89-94]. Therefore, it is highly likely that not only GI microenvironment pre-conditioning from interactions with colon myofibroblasts, dendritic cells, the gut microbiome and native intestinal extracellular matrix impacts CRC liver metastasis, but also pre-conditioning by the portal circulation microenvironment as well.

Finally, the study of CRC cell chemoresistance is vitally important as it almost invariably occurs in the context of advanced disease. Previous experiments suggested that CRC tumors in liver are more chemoresistant than subcutaneous tumors to doxorubicin[95, 96]. But interpretation of these experiments is complicated by the fact that doxorubicin is not clinically used to treat CRC patients. We therefore used a widely prescribed, effective anti-CRC drug, oxaliplatin, and directly tested on CTMM models whether the chemosensitivity of the same cells is dependent on their microenvironment. Our data demonstrate that *in vivo* CRC liver metastases are significantly less oxaliplatin chemosensitive vs. paired subcutaneous xenografts generated from the same cells. Consistent with this finding, both the WNT pathway inhibitor DKK4 and Notch pathway signaling have been previously associated with CRC chemoresistance[74, 75] and both are significantly upregulated in CTMM CRC liver metastases.

For the past several decades, mice carrying subcutaneous xenografts have been the most commonly used pre-clinical model system to screen new chemotherapy agents. Since this approach has a high false-positive success rate[69-72], including anti-CRC drugs, and all too often fail when subsequently tested in patients, more chemoresistant CTMM models of CRC hepatic metastases have the potential to help reduce the number of futile CRC clinical trials.

Additionally, other studies have suggested that *in vitro* cultured human CRC primary tumors are more chemosensitive to 5-FU than paired hepatic metastases from the same patients[97]. However, this finding was never been validated *in vivo* in mice. Here we similarly confirmed that the same CRC cells in liver are similarly more resistant than primary CRC tumors to oxaliplatin.

In summary, we anticipate that the CTMM resources described here can help improve our mechanistic understanding of primary CRC-microenvironment interactions (particularly those involving adaptive immunity and immunotherapies), liver metastasis pre-conditioning by transit through the portal circulation, and potentially improve the clinical relevance of pre-clinical anti-CRC drug screening.

METHODS

Tissue Culture of PDX lines. Patient derived xenograft tumors were harvested and generated as previously described[27, 73, 98, 99]. Briefly, fresh patient CRC samples were collected in Medium 199 supplemented with 200 U/ml penicillin and 200 mg/ml streptomycin, immediately after patient operative resection. Fat and blood clots were removed from tissues and they were rinsed 10 times in sterile PBS. Samples were minced with sterile scalpel blades into approximately 5 mm^3 fragments. Tumor fragments were immersed into RNAlater and embedded in O.C.T. (Fisher Scientific) at -80ºC for histopathological or molecular analysis. Remaining tissue fragments were coated in Matrigel (BD Biosciences) and subcutaneously implanted into 3-4 6-week-old NOD/Shi-scid/IL-2Rγ^{null}(NOG) mice (Jackson Laboratory, Bar Harbor, Maine) After PDX tumors reached an average volume of 400 mm^3, mice were sacrificed and tumor tissue harvested. Part of tissue was passaged in new mice and the remainder was used to generated PDX cell lines using the method of collagenase /dispase enzyme digestion with slight modification, as previously described[73, 100]. Basically, tissue was minced into approximately1 mm^2 fragments and digested in DMEM/F12 containing collagenase type XI (150 U/ml, Sigma, St. Louis, MO), dispase neutral protease (40 μg/ml, Roche Applied Science) and 1% FBS, stirring at 37°C for 30 min. After centrifugation, cells were re-suspended in the DMEM/F12 containing 1% nonessential amino acids (Invitrogen), penicillin (400 U/ml;Sigma), streptomycin (400 mg/ml;Sigma), amphotericin B (1.25 mg/ml; Sigma) and heparin (4 μg/mL; Sigma), human epidermal growth factor (40 ng/mL; BD scientific), human basic fibroblast growth factor (20 ng/mL; BD scientific), B27 supplement (Invitrogen) and 5% Fetal Bovine Serum, then transferred and cultured

in the ultra-low-attachment flasks (Corning) at 37°C and 5% CO2. FACS of human ESA (epithelial specific antigen) was used to purify cancer cells and PDX cells were characterized to be able to form subcutaneous xenograftswithsimilar adenocarcinoma histomorphology to parental PDX, when injected 0.5-1 million cells / mouse in NOG mice. PDX lines were frozen in DMSO. PDX freshly thawed cells,negative for mycoplasma, were used within 10 passages for the all experiments in this study.

CCR9 inducible expression in CRC cells and PDX cells The lentiviral tetracycline-inducible protein expression system (LifeTechnologies, T-Rex System) consists of two vectors: the regulatory vector, pcDNA6/TR, which encodes the Tet repressor (TetR) under the control of the human CMV promoter; and an inducible expression vector expressing human CCR9 (CDS region (181 -1290) of gene ID: NM_031200.) or mouse Ccr9 (CDS region (296-1405) of gene ID: NM_009913) genes[101] under the control of CMV promoter and two tetracycline operator 2 (TetO2) sites. To generate the lentiviral particles, the above plasmids were transfected into HEK293T cells with the Genecopoeialentivirus packaging mix (Genecopoeia) according to the manufacturer's protocol. TetR expression lentiviruswas used to infect common CRC or PDX lines. After puromycin selection, the TetR expressing lines were then infected with the CCR9 inducible expression lentivirus and followed with blasticidin selection and RFP FACS purification. The CCR9 expression can be induced by1-1.5 ug/ml (in vitro) or 1-2mg/ml (in vivo) doxycycline (Sigma, St Louis, MO)administered in 5% sucrose-containing drinking water. The efficiency of CCR9 inducible expression in these variant colorectal lines was verified by Western Blotting using anti-human CCR9 antibody

(Abcamcat.#ab38564) or anti-mouse Ccr9 antibody (Thermo Scientific. PA1-21618) and the software of Quantity One (BioRad) was used to semi-quantify protein levels.All non-PDX cell lines used in this study were purchased from ATCC and were negative for mycoplasma.

PDX xenograft tumor formation and oxaliplatin treatment

0.5-1 x 10^6CRC cells with inducible CCR9 expression or control vectors were injected into 6-8 weeks old NOD/Shi-scid/IL-2Rγ^{null}(NOG) mice (Jackson Laboratory, Bar Harbor, Maine) by tail vein injection. Tumor incidence was monitored 2-3 times weekly by whole body IVIS imaging. When mice became moribund, they were sacrificed immediately, necropsy performed and tumors harvested using a dissecting microscope. For oxaliplatin therapy study, 1 x 10^6 CCR9+ CRC cells were tail-vein injected or subcutaneously inoculated into the left flank of 6-week NOG mice (n=8) and IVIS imaging was performed to monitor tumor formation. When GI or subcutaneous tumors reached radiance of 5 x 10^6 (p/sec/cm^2/sr), doxycycline was withdrawn to turn off CCR9 expression and oxaliplatin (6mg/kg, Sigma, St Louis, MO) or normal saline as control was given IV once weekly for 5 weeks. Tumor growth was quantified by luciferase - photon signal analysis with Xenogensoftwareuntil mice became moribund. Ex vivo IVIS imaging and necropsy were performed to further verify sizes and locations of tumor loci.

Luciferase imaging in whole animal or ex vivo tissues: For luciferase imaging, D-luciferin (The In Vivo Imaging Community.) of 1.5mg/10g body weight was injected intra-peritonealinto mice and 10 min later, luciferase imaging (Xenogen IVIS-200) was applied on whole-mouse bodies.For ex vivo imaging, mice were dissected 10 min after

luciferin injection. Intestine and other organs were quickly rinsed 3 times in PBS and place in culture dishes in which luciferase imaging was applied immediately.

Immunohistochemistry For mouse experiments, histology and immunohistochemistry were performed on paraffin-embedded or frozen sections from xenograft tumors as previously described[27]. Intestinal, extra-GI tumor and corresponding normal tissues were snap frozen in O.C.T (Fisher Scientific, Pittsburgh, PA) and fixed in 10 % buffered formalin followed by paraffin embedding. For immunofluorescence, sections were immunostained with antibodies, counterstained with 4,6-diamidino-2-phenylindole (DAPI). H+E adjacent sections were used for comparison.

Production of Human CRC-Mouse Chimeras:

The methods of blastocyst microinjection and generation of chimeric mice were modified from standard procedures[102]. Briefly, Embryonic day (E) 3.5 or Swiss Webster(CFW) blastocysts (derived from natural mating. Charles River Strain code 024) were placed in 30 ml FHM (Millipore Cat#MR-122-D) and 10-15 CCR9+ CRC cells were injected per blastocyst by transfertip(ES) (Eppendorf cat. no.: 930001040) and vacutip(Eppendorf cat. no.: 930001015) using Eppendorf TransMan NKmicromanipulatorsunder invert microscope (Nikon Diaphot). The injected blastocysts were uterine-transferred into day 2.5 pseudopregnant CD-1 recipient females (Charles River Strain Code 022) at the same day (12-15 blastocysts / female). Pups were born at day 19-21 and fostered with lactating CD-1 mice. Live IVIS imaging was performed on the chimerical mice twice every week to detect the proliferation of luciferase+ cells.

Then ex vivo IVIS and histopathology were used to confirm the tumor formation and locations.

Immune Cell Analyses in Human PDX-Mouse Chimeras 4-week old Swiss Webster mice from blastocysts injected with CCR9+ PDX-1 cells and the littermates from non-injected blastocysts as control for normal immune functions were sacrificed and the spleens and 4 mesenteric lymph nodes (MLN) / mouse were collected in cold PBS under dissecting microscope. Then MLN and spleen were immediately mechanically disrupted and passed through a 70 um cell strainer. Splenocytes and lymphocytes were collected and incubated in ACK lysis buffer (Life Technologies) to remove RBCs. Surface stainingwas performed with anti-CD3 (ebiosciences, clone:145-2C11), CD4 (ebiosciences, clone:RM4-5), CD8 (ebiosciences, clone:53.67), CD44 (ebiosciences, clone:IM7), CD62L (ebiosciences, clone:MEL-14). Intranuclear staining with anti-RORγt(ebiosciences, clone:B2D) and anti-Foxp3(ebiosciences, clone:fjk-16s) was performed according to manufacturer's protocol (Intracellular Fixation and Permeabilization Kit from eBioscienes). Prior to intracellular cytokine staining, cells were cultured in the presence of GolgiPlug (BD Biosciences) for 4 hours or stimulated with phorbolmyristate acetate (PMA; 20ng/mL) and ionomycin (1μg/mL) or IL-23 (40ng/mL; eBioscience) in the presence of GolgiPlug (BD Biosciences) for 4 hours before staining. Intracellular cytokine staining was performed according to the manufacturer's protocol (Cytofix/Cytoperm buffer set from BD Biosciences) using IFN-γPECy7 (ebiosciences, clone: XMG1.2) and IL17A FITC (ebiosciences, clone: eBio17B7). An LSR II (BD Biosciences) and FlowJo software (Tree Star) were used for flow cytometry and

analysis. Dead cells were excluded using the Live/Dead fixable aqua dead cell stain kit (Invitrogen).

Two-photon microscopy Three to six month old Balb/c male and female mice were kept under isoflurane anesthesia and a portion of the large intestine was externalized to be placed in a saline-filled, temperature-controlled chamber. The portion to image was covered with a glass coverslip and agarose for stability and imaged with a custom-built multi-photon microscope optimized for in vivo imaging. 50 mg/ml FITC-Dextran (FD2000S; Sigma-Aldrich, St. Louis, MO) was retro-orbitally injected in mice (0.25 ml / kg) and this dose allowed vasculature imaging for 1-2 hours. Simultaneous excitation with 900 nm and 1040 nm femtosecond laser light enables imaging of GFP (FITC-Dextran) and RFP (human CRC cells) at the same time.

Whole-Exome Sequencing DNA was extracted from 4 PDX lines (PDX 1-4) and common CRC lines (HT-15 and Caco-2) using DNeasy DNA extraction kit (Qiagen). Whole-Exome sequence data for the six cell lines were obtained through Agilent's G9906A HaloPlexExome Target Enrichment System kits (protocol Version A, February 2013) with Illumina HiSeq2000. Briefly, genome DNA samples were first digested by restriction enzymes to create a library of gDNA restriction fragments. Then the HaloPlexexome probe was provided as eight separate probe solutions in wells A–H of the HaloPlex Probe 8-well Strip. The circularized target DNA-HaloPlex probe hybrids, containing biotin, were captured on streptavidin beads and then DNA ligase was added to the capture reaction to close nicks in the circularized HaloPlex probe-target DNA hybrids. After a 10-minute ligation reaction period, the captured DNA libraries were diluted and PCR amplified with the PCR Master Mix. After the enrichment was validated,

the samples were pooled with different indexes, and sequenced with Illumina HiSeq2500.~ 60M 101bp pair-end reads for each sample were obtained from HiSeq2500. The mean quality score for all samples was ~ 35, and more than 90% reads were at least 30 base quality. All the raw reads were first processed with program Cutadapt[103] to remove adapter sequences from high-throughput sequencing reads. The processed sequence data were mapped to human genome (hg19) with program BWA[104]. The mapping were re-aligned and recalibrated with GATK[105]. Variants and mutations were detected with the module Unified Genotyper in GATK. Sequence data were deposited with NCBI (Accession SRP035634).

RNA sequencing and quantitative real-time PCR

Total RNAs from liver tumor or subcutaneous tumor cells were extracted by using RNeasy Kit (Qiagen, Valencia CA). For RNA-seq, library preparation and HiSeq2000 lane analysis was performed as previously described[106]. Subsequently, 75-bp paired-end read sequences were mapped to human genome (hg19) with Tophat/bowtie (version 2.1.1). Read count for each gene transcript was obtained with Genomic Features (version 1.15.9). Genes with mean read count in both liver and skin samples less than 10 were filtered out. DESeq (version 1.12.0) was used to analyze for differential expression. Fisher Exact Test was used to assess statistical significance, with adjustment using the Benjamini& Hochberg method for multiple comparisons.

For quantitative PCR, 2 μg of total RNAs were reverse-transcribed into cDNA by using RT first stand kit (SA Biosciences) and RNA levels amplified by PCR containing SYBR Green I dye (Invitrogen), normalized to β-actin as the comparative CT (cycling

threshold)= CT (target)- CT (control), were analyzed by the iCycler (Bio-Rad). Primer pairs used are (1) DKK4: F5'-CGTTCTGTGCTACATGTCGTGG and R5'-GTGTGCCATCTTGCTCATCAAGC; (2) HES1: F5'-GGAAATGACAGTGAAGCACCTCC and R5'-GAAGCGGGTCACCTCGTTCATG; (3) HES7: F5'-CATCAACCGCAGCCTGGAAGAG and R5'-CACGGCGAACTCCAATATCTCC; (4)HEY1: F5'-TGTCTGAGCTGAGAAGGCTGGTand R5'-TTCAGGTGATCCACGGTCATCTG; (5)HEY2: F5'-TGAGAAGACTTGTGCCAACTGCT and R5'-CCCTGTTGCCTGAAGCATCTTC; (6)human β-actin: F5'-CGCGAGAAGATGACCCAGAT and R5'-ACAGCCTGGATAGCAACGTACAT; (7)mouse β-actin: F5'-GATCTGGCACCACACCTTCTand R5'-GGGGTGTTGAAGGTCTCAAA.

Fluorescent activated cell sorting (FACS) analysis FACS with anti-epithelial specific antigen (ESA, BD PharmingenCat #347197) antibody was used to purify PDX cells [3,4] Cells were first incubated with anti-human ESA antibody conjugated with Alexa Fluor 488 for 30 minutes on ice and then were washed in 1% BSA/PBS buffer. FITC filter was then used to separate cells into ESA positive and negative sub-groups by signal intensity gating. The ESA+ cells were transferred into culture flasks for further growth and passages.

To detect RFP positive cells in mouse liver, 0.5 x 10^6CCR9+ RFP+ Luciferase+ CRC cells were injected into 6-week NOG mouse (n=6) by tail vein. After 48 hours, mice were sacrificed and liver pieces in the same weight were treated with collagenase / dispase (1 mg/ml, Roche Applied Science) for 0.5-1 hour to create single-cell suspension and

followed with BD Pharm Lyse (BD Scientific) treatment according to company instruction, to destroy red blood cells. RFP cells were measured as PE positive and FITC negative in FACS channels.

Transwell migration assay

Transwell Boyden chambers (BD Pharmingen Mountain View, CA) of 8-μm pore size were used to evaluate migration *in vitro*ofparental or CCR9 expression CRC cells and PDX cells. Briefly, cells were seeded at a density of 5 x 10^5 per well into the upper chamber. Culture medium as described above with 100 ng/ml recombinant mouse CCL25 protein (R&D systems Inc; Minneapolis, MA) was loaded into the lower chamber. Chambers of cells were incubated in 37^{o}C and 5 % CO_2 conditions for 12 hours. At the time of harvest, cells remaining inside the upper chambers were removed while cells attached to the lower surface of the membrane were fixed and stained with Crystal violet (Sigma, St Louis, MO) followed by imaging and cell number counting analyses.

SUPPLEMENTAL INFORMATION

Statistical Analyses

Sample sizes for all figures and tables were estimated based on our previous studies[27, 73, 100, 107]. For mouse experiments, no animals were excluded from the analyses. For each set of experiments, samples and animals were prepared for all experimental arms at the same time. For animal studies, the randomization schema had mice alternating in assignments to experimental groups. Both male and female mice were used.Values are expressed as mean ± SEM or summarized using box-plots. All

statistical tests are 2-sided.No adjustments were made for multiple comparisons. Both PIs (Lipkin and Shen) and the Study Statistician (Zhou) were blinded to experimental allocations among different experimental arms for all experiments. For all parametric statistical analyses, data were determined to be normally distributedby the D'Agostino-Pearson test. For all parametric and non-parametric tests, variances were similar between groups being compared. For comparisonbetween experimental and control groups at a specific time point or tissue site in Figures 1, 3 and Supplemental Figures 1,6, 8and 10, 2-sided Student t- test or 2-sided Mann-Whitney (MW) tests were used. In Figure 4, linear regression analysis and ANOVA was used to estimate the tumorgrowth rate in different experimental groups and study sites while adjusting for differentcell lines. Differences in tumor growth rates between Oxaliplatin treated and the controlmice at each body site and the difference in the effect of Oxaliplatin treatment on tumorgrowth rates between different sites were further evaluated using simultaneous tests forgeneral linear hypotheses (Figure 4). *P*valueswere adjusted for multiple comparisons by controlling the experiment-wise errorrate using the conservative Bonferroni-Holm method (Figure 4). Statistical calculationswere performed with the Statistical Package for the Social Sciences version 11.5software (SPSS Inc, Chicago, IL), GraphPad, or R (reference: R Core Team (2013).R: A language and environment for statistical computing. R Foundation for StatisticalComputing, Vienna, Austria. URL http://www.R-project.org/). The statistical test used foreach figure or table panel is indicated. All cell lines were purchased from ATCC in the past 2 years (or derived for PDX1-4) and were negative for mycoplasma.

Supplemental Table 2

Statistics Tests and *P* values in Figures

Cells / statistics tests	HT15	HT-29	HCA7	HCT116	SW620	SW480	SW48	Caco-2	Colo205	DLD1	LoVo	LS174T	RKO	PDX-1	PDX-2	CT26	All lines
(Fig. 1 A. Colon tumor: control VS CCR9+)																	
Name of Statistics test	MW	MW	MW	MW	MW	MW	MW	MW	MW	MW	MW	MW	MW	MW	MW	MW	Paired *t*-test
P values	0.038	0.017	0.038	0.015	0.016	0.016	0.076	0.085	0.016	0.038	0.006	0.015	0.191	0.038	0.017	0.007	0.0001
(Supplemetary Table 2. GI tumor: control VS CCR9+)																	
Name of Statistics test	MW	MW	MW	MW	MW	MW	MW	MW	MW	MW	MW	MW	MW	MW	MW	MW	Paired *t*-test
P values	0.005	0.007	0.013	0.004	0.004	0.001	0.032	0.076	0.004	0.001	0.0004	0.001	0.171	0.001	0.014	0.001	0.0001
(Supplementary Fig. 1 C migration: control VS CCR9+)																	
Name of Statistics test	*t*-test	*t*-test	*t* -test	*t*-test	*t-test*	*t-test*	*t*-test	*t*-test	*t*-test	*t*-test	*t*-test	*t*-test	*t*-test	*t*-test	*t*-test	*t*-test	*t*-test
P values	0.01	0.006	0.026	0.01	0.011	0.01	0.018	0.006	0.004	0.003	0.007	0.03	0.009	0.007	0.017	0.02	0.001

Cells / statistic tests	HT15	HCA7	SW48	Colo205	DLD1	LS174T	PDX-1	All lines
(Fig. 3D Liver tumor # : control VS CCR9+)								
Name of Statistics test	MW	MW	MW	MW	MW	MW	MW	*t*-test
P values	0.004	0.009	0.084	0.009	0.005	0.002	0.002	0.001
(Fig. 3E tumor progress time: GI VS liver)								
Name of Statistics test	MW	MW	MW	MW	MW	MW	MW	*t*-test
P values	0.003	0.008	0.029	0.004	0.002	0.002	0.002	0.001
(Supplementary Fig. 8A liver tumor #: CCR9 on VS CCR9 off)	*t*-test	*t*-test	NA	*t*-test	*t*-test	*t*-test	*t*-test	*t*-test
Name of Statistics test								
P values	0.003	0.011		0.006	0.014	0.001	0.002	0.001

In Figures 1C, 3D, 3E, Supplementary Figures 1C, 8A and Supplementary Table 2, for each data point, 6-8 week old male or female NOG mice were used for each

experimental arm (e.g. in Figure 3D 8 mice for each line's control arm and 8 mice for the CCR9+ arm).MW, 2-sided Mann-Whitney test. Paired t-test, 2-sided Student paired t test.

Study Approval

All CRC tissues used were approved by the Institutional Review Board (IRB) of Weill Cornell Medical College and Consent obtained for each participant.All animal protocols in this study were approved by the IACUC committees of Weill Cornell Medical College, Cornell Universityor Albert Einstein College of Medicine.

Accession ID

CRC cell whole exome data are deposited in NCBI GEO as SRS542031 and RNA-seq data as SRR1204492.

Acknowledgements We thank other members of the Lipkin laboratory and Shen Laboratory. This work was supported by NSF 1137269, NSF 1106153, NSF GRFP-2011131053, R01 GM095990, NIH: 2UL1 -RR024996, UH2TR000516 and a generous donation by Matthew Bell.

METHODS REFERENCES

1. Vermeulen L, Todaro M, de Sousa Mello F, et al. Single-cell cloning of colon cancer stem cells reveals a multi-lineage differentiation capacity. Proceedings of the National Academy of Sciences of the United States of America 2008;105:13427-32.

2. Pastor DM, Poritz LS, Olson TL, et al. Primary cell lines: false representation or model system? a comparison of four human colorectal tumors and their coordinately established cell lines. International journal of clinical and experimental medicine 2010;3:69-83.

3. Chen HJ, Edwards R, Tucci S, et al. Chemokine 25-induced signaling suppresses colon cancer invasion and metastasis. The Journal of clinical investigation 2012;122:3184-96.

4. Sikandar SS, Pate KT, Anderson S, et al. NOTCH signaling is required for formation and self-renewal of tumor-initiating cells and for repression of secretory cell differentiation in colon cancer. Cancer research 2010;70:1469-78.

5. Jahid S, Sun J, Edwards RA, et al. miR-23a promotes the transition from indolent to invasive colorectal cancer. Cancer discovery 2012;2:540-53.

6. Yu CR, Peden KW, Zaitseva MB, Golding H, Farber JM. CCR9A and CCR9B: two receptors for the chemokine CCL25/TECK/Ck beta-15 that differ in their sensitivities to ligand. Journal of immunology 2000;164:1293-305.

7. Nagy A. Manipulating the Mouse Embryo: A Laboratory Manual,Third Edition.: Cold Spring Harbor Laboratory Press; 2003.

8. Martin M. Cutadapt removes adapter sequences from high-throughput sequencing reads. In: EMBnetjournal; 2011.

9. Li H, Durbin R. Fast and accurate short read alignment with Burrows-Wheeler transform. Bioinformatics 2009;25:1754-60.

10. McKenna A, Hanna M, Banks E, et al. The Genome Analysis Toolkit: a MapReduce framework for analyzing next-generation DNA sequencing data. Genome research 2010;20:1297-303.

11. Cao Z, Ding BS, Guo P, et al. Angiocrine factors deployed by tumor vascular niche induce B cell lymphoma invasiveness and chemoresistance. Cancer cell 2014;25:350-65.

12. Sikandar S, Dizon D, Shen X, Li Z, Besterman J, Lipkin SM. The class I HDAC inhibitor MGCD0103 induces cell cycle arrest and apoptosis in colon

cancer initiating cells by upregulating Dickkopf-1 and non-canonical Wnt signaling. Oncotarget 2010;1:596-605.

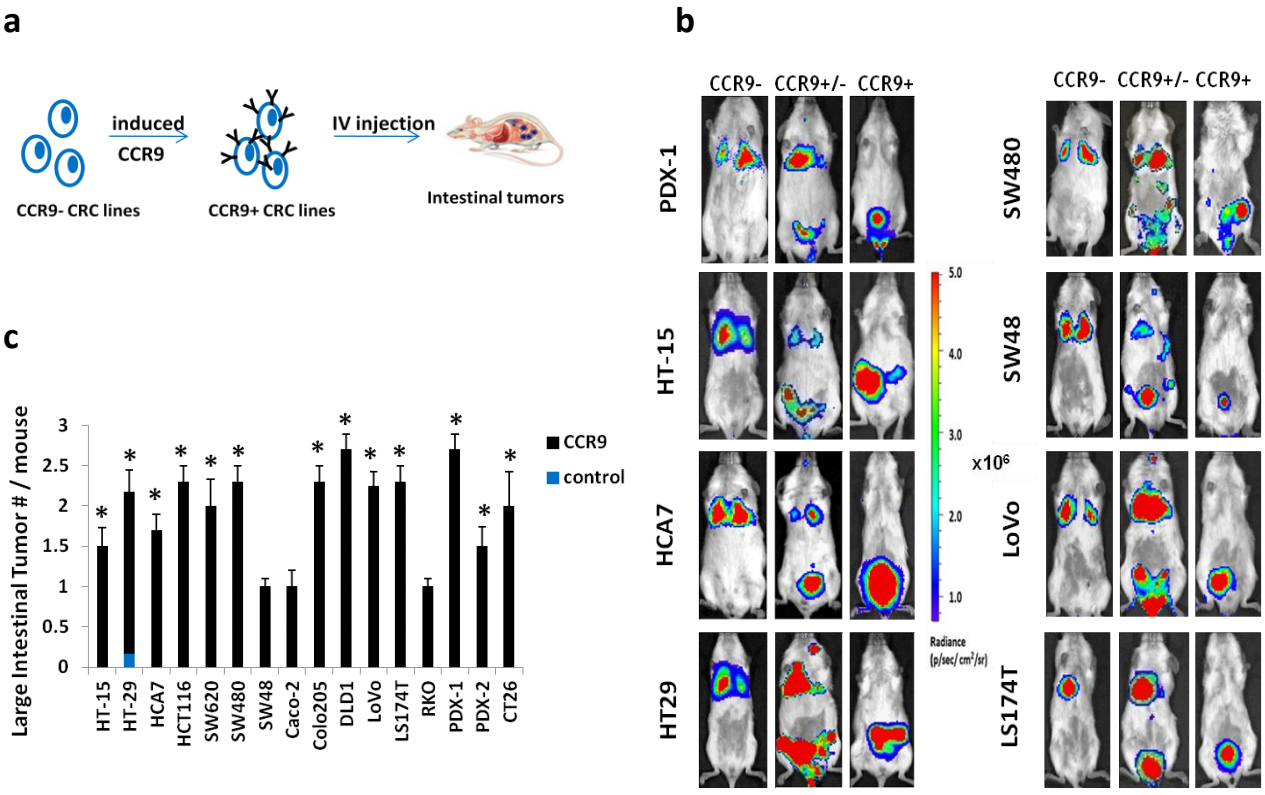

Figure 1. Modeling Primary Human CRC Recurrent Mutations in Mice without Survival Surgery (**a**).Schematic of experimental approach: Lentiviral infection with virus containing a Tetracycline inducible CCR9 expression cassette and constitutive luciferase-RFP reporter genes. After puromycin selection and FACS,0.5-1 x 10^6 CCR9+ cells were injected into 6-8 week old male or female (m/f) non-obese diabetic/severe combined immunodeficient (NOG) mice by tail vein and intestinal tumor formation monitored after 2-3 weeks by IVIS-luciferase imaging. Blue dots: GI tumors.(**b**).Representative whole body IVIS images of mice injected with CRC cells expressing a control luciferase reporter only (CCR9-), constitutive CCR9 expression and luciferase (CCR9+) or a mixture (CCR9+/-); Luciferase photon signals are shown.(**c**).Quantification of mean luciferase-detectable large intestinal tumors in 6-8 week miceinjected with CCR9 expressing cells (CCR9+) via tail vein. * P< 0.01 CCR9+ compared to the control group by 2-sided Mann-Whitney test. Error bars indicate S.E.M. (stand. error of mean). All cell lines combined control vs. CCR9+, P=0.001; Student paired t test. Also see Supplemental Table 2.

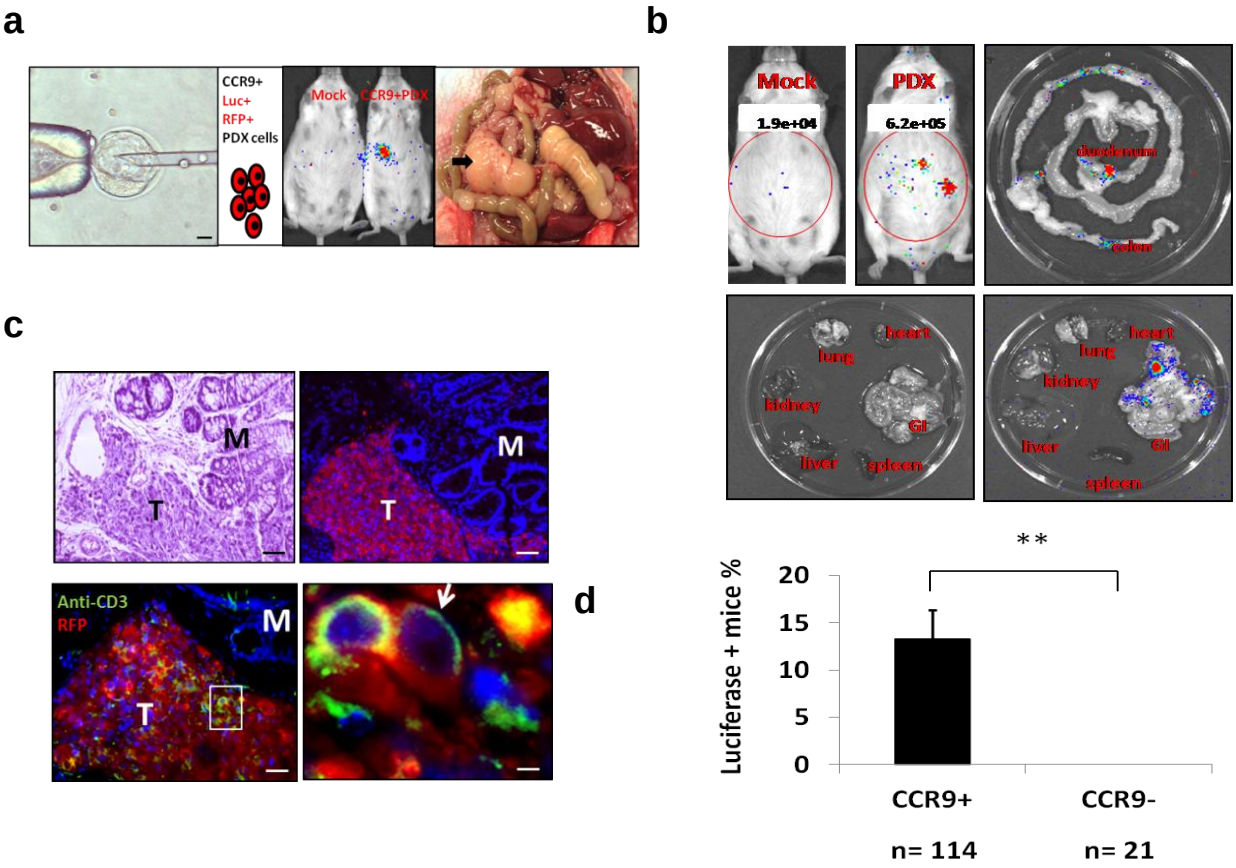
a
CCR9+
Luc+
RFP+
PDX cells
Mock
CCR9+PDX
b
Mock
1.9e+04
PDX
6.2e+05
duodenum
colon
heart
lung
kidney
GI
liver
spleen
c
M
T
Anti-CD3
RFP
d
**
Luciferase + mice %
20
15
10
5
0
CCR9+
n= 114
CCR9-
n= 21
E
Control
E9.5
E10.5
E11

Figure 2. Human Primary CRC-immunoproficient Mouse Host Chimeras (a). Left: schematic of mouse blastocyst injection with luciferase+ RFP+ CCR9+ PDX cells (10-15 cells / blastocyst); Scale bars, 20μm. **Middle:** representative whole body IVIS images of human PDX-mouse chimeras (8 weeks, Swiss Webster) generated by mouse blastocyst injection,(Luciferase - photon signal are indicated, Mock: littermate controls not injected with PDX cells.); **Right:** Three-month old human PDX-mouse chimera with abdominal tumor mass extending from intestine (4X). Arrow indicates tumor.**(b).**Representative IVIS whole-body (left upper panel) and ex vivo images (right upper and lower panels) show adult chimeras (8-weeks) with luciferase+ tumors detectable in the gastrointestinal tract but no other organs. **(c).**Anti-RFP immunofluorescence (Upper right) of caecal PDX tumor in chimeric mice (age 8 weeks).Left upper image shows Hematoxylin (nuclear: blue) and Eosin (cytoplasm: pink) (H+E) staining of the same intestinal tumor for comparison. Scale bars, 50μm. Lower panel images show double-immunofluorescence of T cells (anti-mouse CD3 antibody (green)) and human PDX cells (anti-RFP antibody (red)). Nuclei, DAPI (blue). M, mucosa; T: regions with adenocarcinoma morphology. Arrows indicate CD3+ T cells. Scale bars, 50μm (left) & 5μm (right)(**d**).Percentages of chimeric mice with luciferase positive tumors in the two groups from blastocysts injected with CCR9+ PDX cells (CCR9+) or CCR9- PDX cells (CCR9-). ** P = 0.002 by 2-sided Mann-Whitney test, Error bars indicate S.E.M. **(E).** B6-2J mouse blastocysts were microinjected with luciferase+ RFP+ CCR9+ PDX cells (15 cells/blastocyst) and uterine-transferred into day 2.5 pseudo-pregnant recipient females at the same day (12-15 blastocysts / female). Representative RFP florescent images (4X) of whole embryos at embryonic day 9.5, 10.5 and 11. Mock control: littermate controls not injected with PDX cells. White arrows designate hindgut location and black arrow designates vitelline duct location. Scale bar, 0.5 mm. Also see Supplemental Table 2.

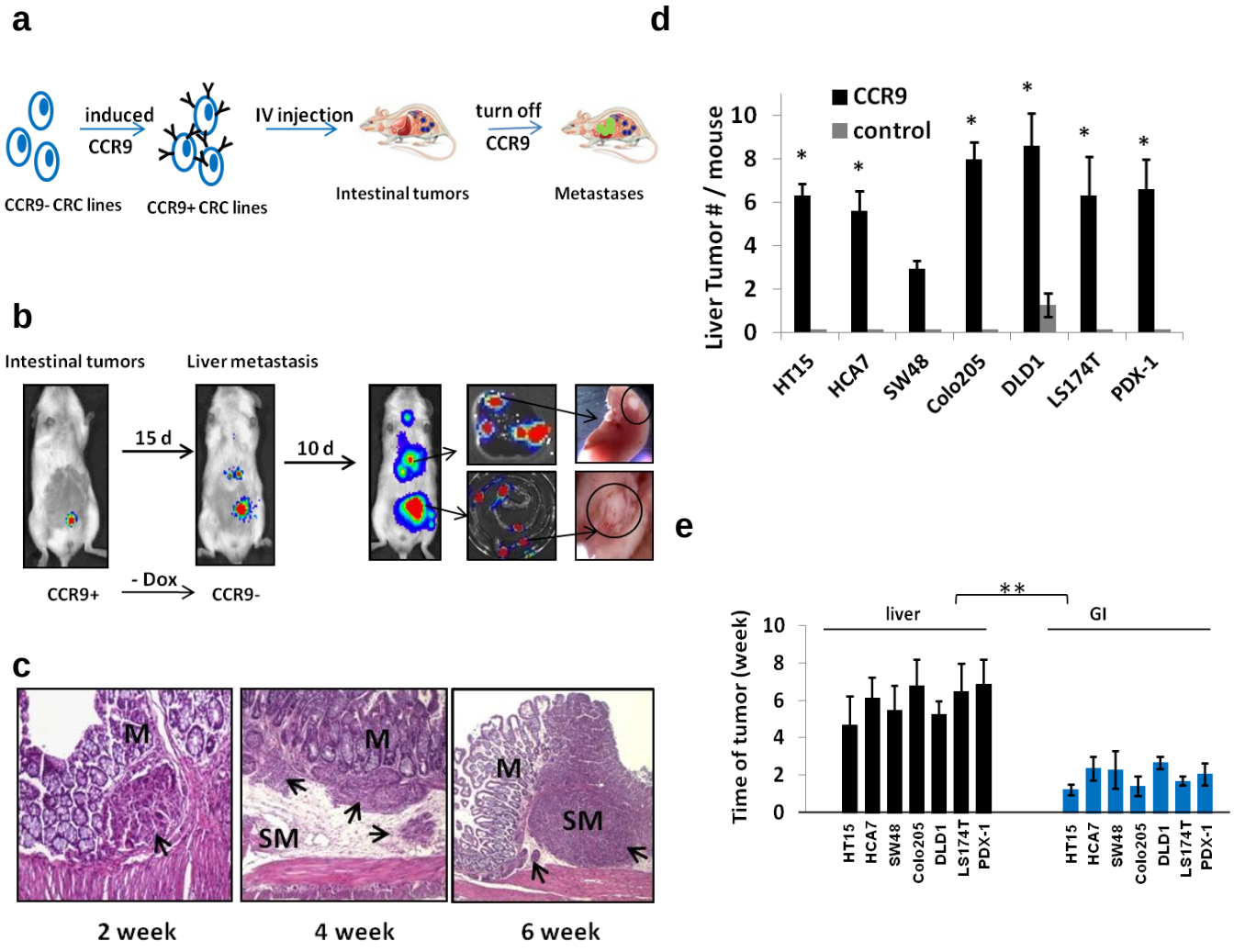
a
induced
CCR9
IV injection
turn off
CCR9
CCR9- CRC lines
CCR9+ CRC lines
Intestinal tumors
Metastases
b
Intestinal tumors
Liver metastasis
15 d
10 d
CCR9+
- Dox
CCR9-
c
M
SM
2 week
4 week
6 week
d
CCR9
control
Liver Tumor # / mouse
HT15
HCA7
SW48
Colo205
DLD1
LS174T
PDX-1
e
liver
GI
Time of tumor (week)

Figure 3.Sequential human CRC primary GI tumor- metastasis formation (a). Schematic of sequential human primary CRC and liver metastasis. Using the same approach as in **Figure 1,** in 6-8 week m/f NOG mice were injected with CCR9+ human CRC cells and monitored by IVIS imaging for primary CRC formation. Once primary GI tumors were detected, CCR9 expression was silenced by withdrawing doxycycline from drinking water. Mice were monitored using IVIS-luciferase imaging over the next 4-6 weeks and sacrificed. Blue dots: GI tumors; green dots: metastatic tumors. **(b).**Representative whole-body IVIS images(CRC line DLD1 as representative) show sequential lower abdominal and right upper quadrant abdominal detectable photons, with ex vivo confirmation of abdominal right upper quadranttumors as liver-localized(4X) (n=8 each for CCR9+ and CCR9- arm for each cell line analyzed). **(c).** Histopathology (H+E staining) examples of different primary CRC tumors detectable as submucosal (2^{nd} week), with invasion of submucosa (4^{th}week) and muscularis (6^{th} week). Arrows indicate histopathologically confirmed tumors; M, mucosa; SM, submucosa. Scale bars, 100µ. **(d).** Quantification of liver metastases in mice (n = 8 each for CCR9+ and CCR9- arm for each cell line analyzed) tail vein injected with control lentiviral vector infected CRC cells (control) or CRC cells with inducible CCR9 expression. * $P< 0.05$ compared to the control group by 2-sided Mann-Whitney test. All CCR9+ vs. control cell lines, P=0.001 2-sided Student t test. **(e).** Time post-injection of cells with inducible CCR9 expression to luciferase-detectable signal in histopathologically confirmed primary GI or liver tumors (n = 8 mice each for CCR9+ and CCR9- arm for each cell line analyzed). ** $P< 0.01$ by 2-sided Mann-Whitney test. All cell lines liver vs. GI tumors, P=0.001 2-sided Student t test. Also see Supplemental Table 2.

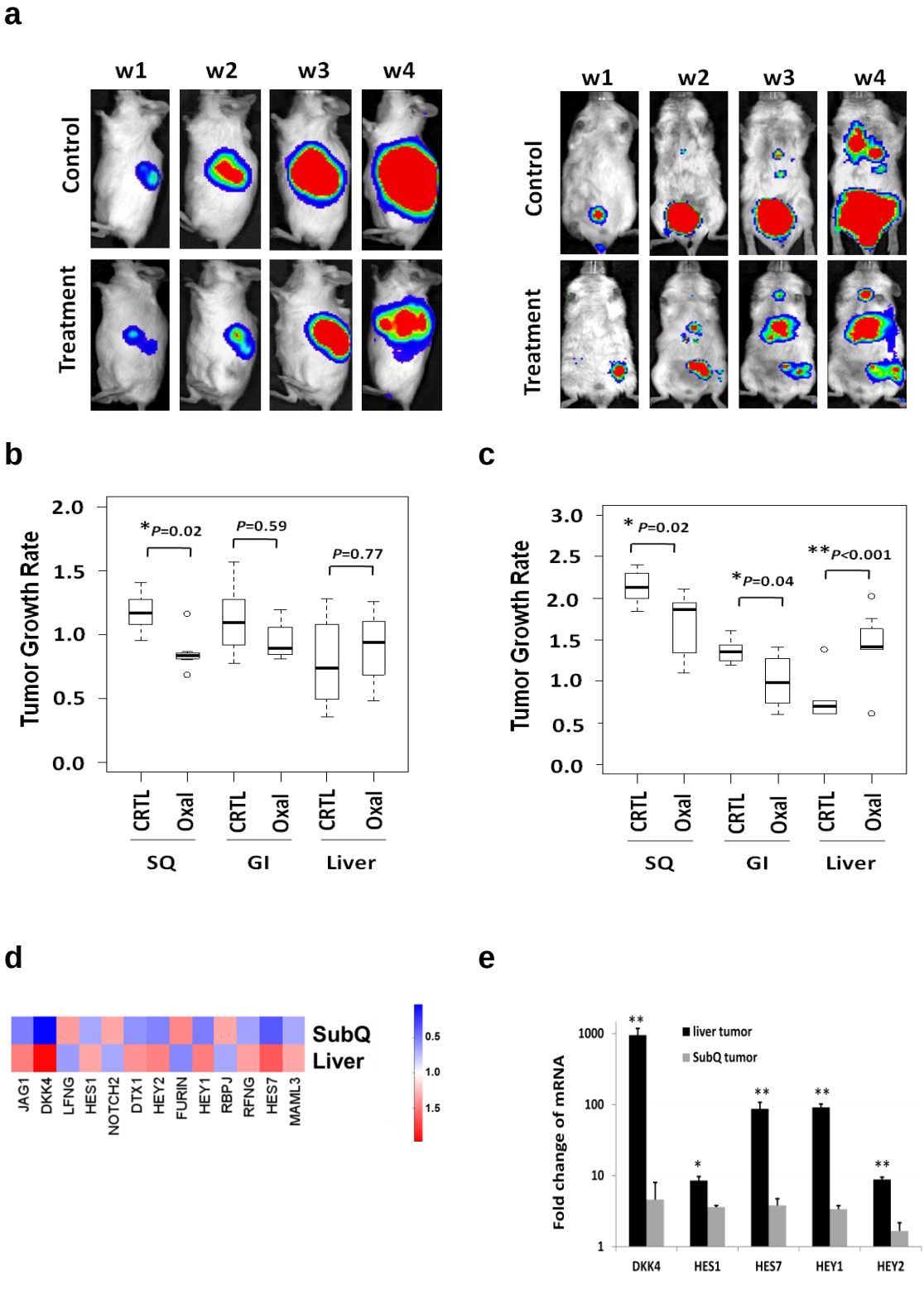
a
w1
w2
w3
w4
Control
Treatment
w1
w2
w3
w4
Control
Treatment
b
Tumor Growth Rate
2.0
1.5
1.0
0.5
0.0
*P=0.02
P=0.59
P=0.77
CRTL
Oxal
CRTL
Oxal
CRTL
Oxal
SQ
GI
Liver
c
Tumor Growth Rate
3.0
2.5
2.0
1.5
1.0
0.5
0.0
* P=0.02
*P=0.04
**P<0.001
CRTL
Oxal
CRTL
Oxal
CRTL
Oxal
SQ
GI
Liver
d
SubQ
Liver
JAG1
DKK4
LFNG
HES1
NOTCH2
DTX1
HEY2
FURIN
HEY1
RBPJ
RFNG
HES7
MAML3
0.5
1.0
1.5
e
Fold change of mRNA
1000
100
10
1
liver tumor
SubQ tumor
**
*
**
**
**
DKK4
HES1
HES7
HEY1
HEY2

Figure 4.Increased oxaliplatin chemoresistance of human CRC cells in liver vs. orthotopic or subcutaneous xenografts.1 x 10^6CCR9+ CRC cells were injected by tail-vein or subcutaneously inoculated into the left flank of 6-week NOG mice (n=8/each experimental arm) and IVIS imaging was performed to monitor tumor formation. When GI or subcutaneous tumors reached radiance of 5 x 10^6 (p/sec/cm2/sr), doxycycline was withdrawn to turn off CCR9 expression and oxaliplatin (6mg/kg) or normal saline as control was intravenously given once weekly for 5 weeks (W1-W5). Tumor growth was quantified by luciferase - photon signal analysis with Xenogen software. Real-time whole body IVIS imaging of mice with subcutaneous inoculated **(a, left panel)** or tail-vein injected CTMM cells (**a, right panel**) treated with Oxaliplatin (CRC line DLD1 as representative) (**b**) and (**c**).Quantification of the effects of Oxaliplatin on growth rate of GI, liver and subcutaneous xenograftsby luciferase -photon signal measurement with Xenogen software. Tumor growth rate is defined as the difference between week 5 tumor luciferase - photon signal (i.e., cubic transformed tumor size) and the first measurable tumor luciferase - photon signal divided by the duration of the treatment. ANOVA was used to compare change in cubic root transformed DLD1and Colo205 tumor size at week5 from week1.P-values were adjusted for multiple comparisons by controlling the experiment-wise error rate using the Bonferroni-Holm method** P< 0.001; * P< 0.05 compared to the control group. Error bars indicate S.E.M. (**b**: Colo205; **c**: DLD1).Each box-whisker plot represents 8 mice/arm. (**d**) Heat map presenting the expression level of indicated transcripts in RNA-seq comparison of non-treated DLD1 subcutaneous vs. liver metastasis tumors. The relative abundance of each gene was normalized between 0 and 2. Above 1 indicates higher expression, below 1 indicates lower expression. Red indicates upregulation. (**e**).mRNA levels of DKK4, HES1, HES7, HAY1 and HEY2 in week 5 DLD1 liver tumors (n=6) and subcutaneous tumors (n=6) using quantitative PCR. ** P< 0.01; * P< 0.05compared to subcutaneous tumors by 2-sided Mann-Whitney test.

Supplementary Figures

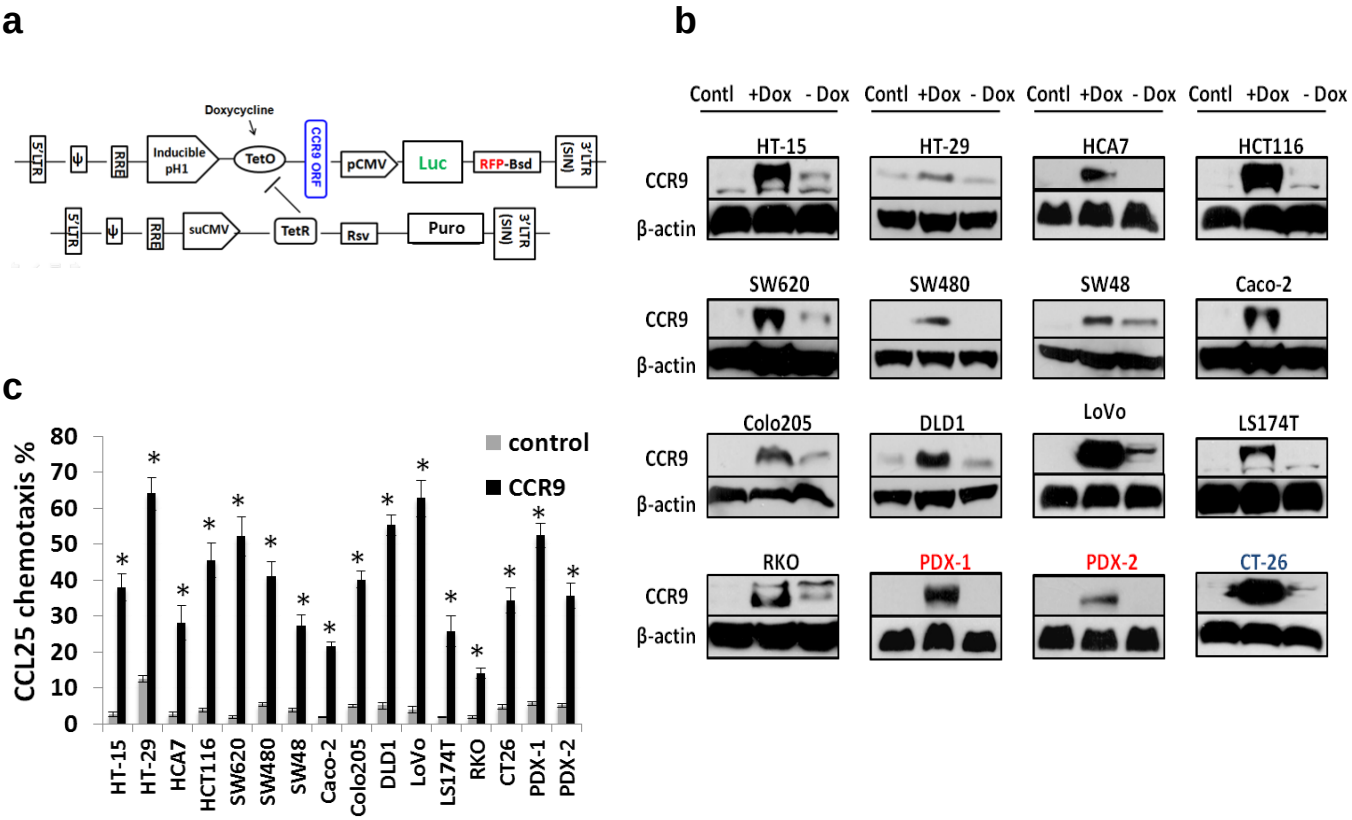

Supplementary Figure 1.Engineering inducible CCR9+ CRC lines and in vitro functionally evaluating the efficiency of CCR9+cells. (a). Schematic of inducible CCR9 expression system which consists of two vectors: the regulatory vector encoding the Tet repressor (TetR) under the control of the human CMV promoter; and an inducible expression vector expressing human CCR9 or mouse Ccr9 genes under the control of CMV promoter and two tetracycline operator 2 (TetO2) sites. This CMV promoter also drives luciferase (Luc) and Red fluorescence protein (RFP) expressions. After packaging the two vectors into lentivirus particles, TetR expression lentivirus was first used to infect common CRC or PDX lines. After puromycin selection, the TetR expressing lines were then infected with the CCR9 inducible expression lentivirus and followed with blasticidin selection and RFP FACS purification. The CCR9 expression can be induced by1-1.5 ug/ml (in vitro) or 1-2mg/ml (in vivo) doxycycline.**(b).** CCR9 protein level expression in parental CRC cells (Ctrl), CRC cells with (+ Doc) or without (- Doc) doxycycine induction were tested by using anti-human CCR9 antibody in western blots. β-actin is loading control.**(c).**In vitro migration of CRC lines toward CCL25 was significantly increased with CCR9 expression, evaluated by Boyden chamber experiments as described in METHOD section. *P< 0.01mean compared to parental CRC cells transfected with control vector by 2-sided MW test. Error bars indicate S.E.M. All cell lines control vs CCR9, P=0.001 2-sided Student t test. (n = 8 each for CCR9+ and CCR9- arm for each cell line analyzed).Also see Supplementary Table 2.

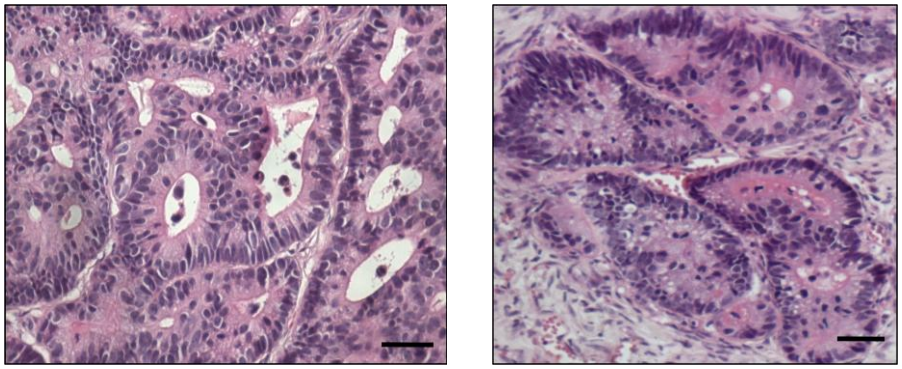

Supplementary Figure 2. Histopathology of mouse subcutaneous xenografts formed by PDX lines. 6 week NOD/SCID mice (n=6) were subcutaneously injected with 1 x 10^6PDX cells / mouse in two flanks, and tumors began to form in 6-8 weeks. H+E staining ofsubcutaneous tumors formed by PDX-1 **(Left)** or PDX-2 **(Right).**Scale bars, 50μm.

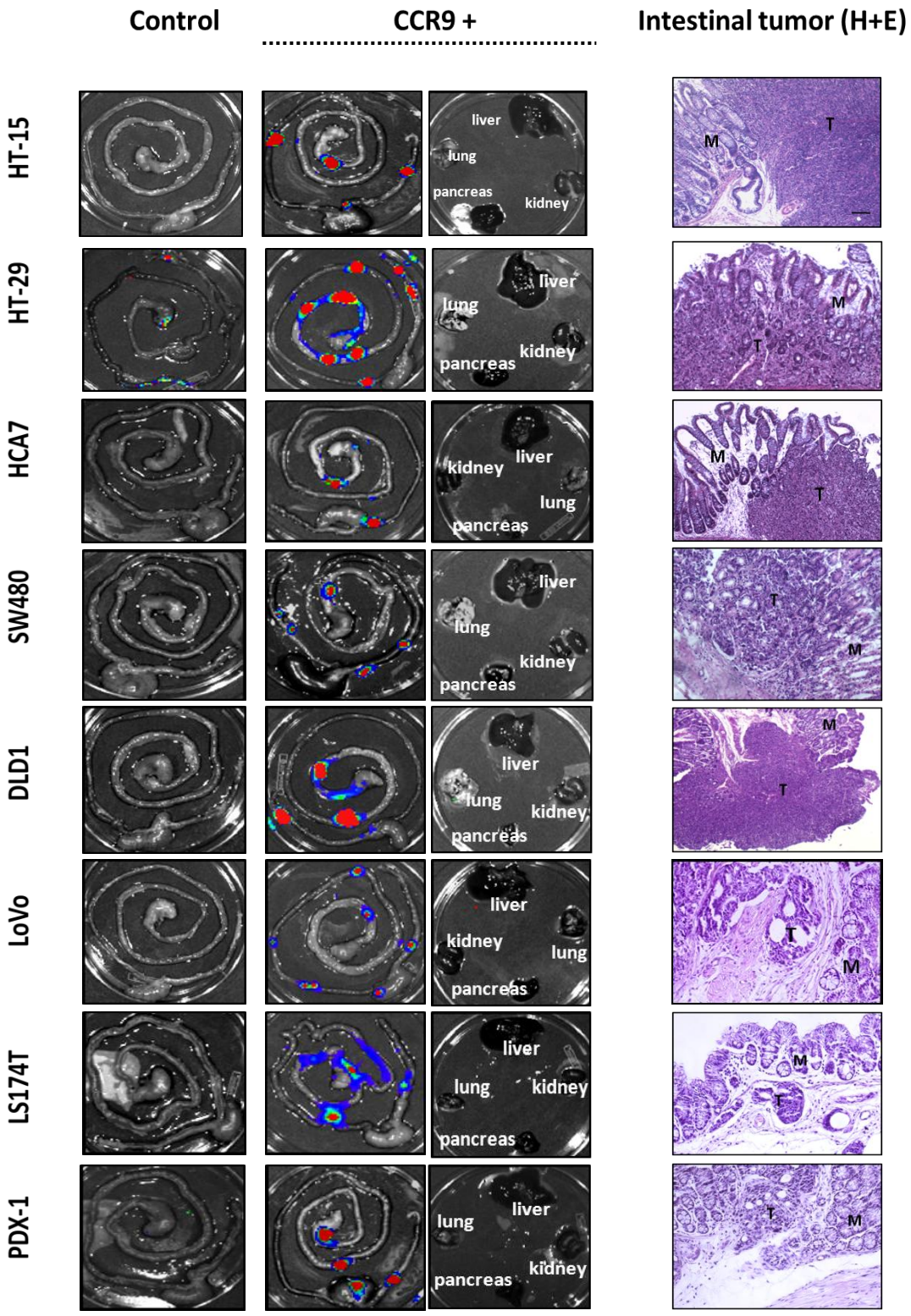
Control
CCR9 +
Intestinal tumor (H+E)
HT-15
HT-29
HCA7
SW480
DLD1
LoVo
LS174T
PDX-1
liver
lung
pancreas
kidney
M
T

Supplementary Figure 3.Ex vivo IVIS imaging and histopathology of orthotopic GI tumors formed by CCR9+ CRC lines. The specific anatomical locations of NOG mouse abdominal tumors identified by whole body IVIS imaging **(Figure 1 b)** were determined as multiple foci in the Duodenum, Jejunum, Ileum, Cecum and Colon, by both ex vivo IVIS imaging and histopathology in H+E staining (M: mucosa; T: regions with adenocarcinoma morphology).At the same time, no tumors were detectable by IVIS imaging in other organs, such as lung, liver, pancreas or kidney. Comparisons with control lines infected with non-CCR9 encoding lentivirus are shown. Scale bars, 50μm.(n = 6 for each cell line analyzed)

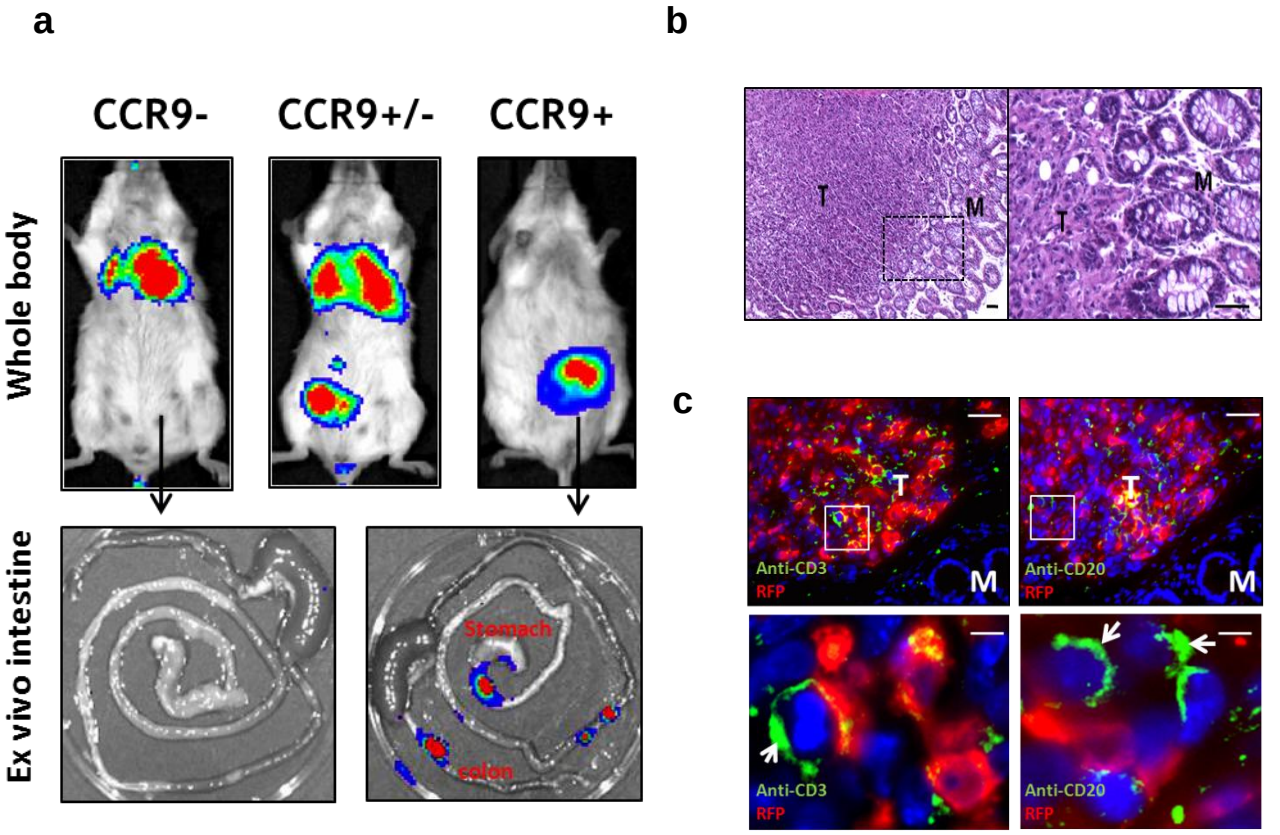

Supplementary Figure 4.Mouse CRC line with CCR9 expression formed GI tumors in immunoproficient mice with same genetic background. (a). representative whole body IVIS images (upper panel) of tail-vein injected mice with luciferase-RFP double labeled CT26 cells transfected with backbone vector (CCR9-), mixture of cells transfected with CCR9 expression vector and cells transfected with backbone vector (CCR9+/-), or CRC cells transfected with CCR9 expression vector (CCR9+); Luciferase - photon signals represent xenografts.*Ex vivo* imaging (lower panel) indicated abdominal luciferase positive tumors located in GI. **(b).**Representative H+E staining image of tumors in mouse large intestine tail vein injected with inducible CCR9+ CT26 cells. (M: mucosa; T: regions with adenocarcinoma morphology). Scale bars, 50μ**(c).**double- immunofluorescence in immune cells and tumor cells. T cell marker CD3 or B cell marker CD20 expression was detected by anti-mouse CD3 or CD20 antibody (green), tumor cells were detected by anti-RFP antibody (red) and nuclei were stained with DAPI (blue). Arrow designates T cells or B cells. Scale bars, 50μm (upper) &5μm (lower). N=6 6-8 week NOG mice.

a

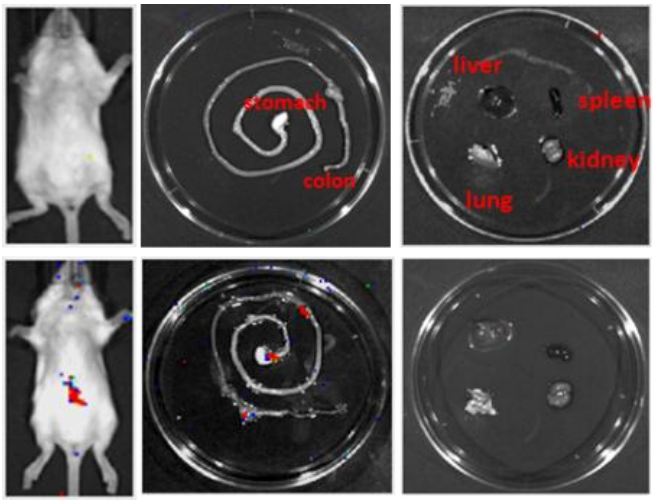

b

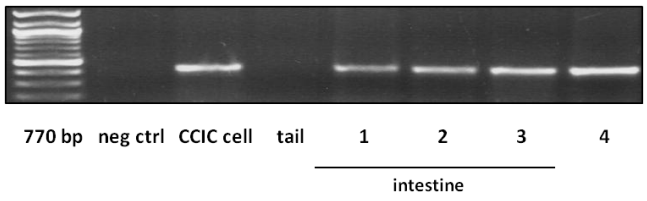

Supplementary Figure 5. Human Primary CRC-immunoproficient Mouse Host Chimeras
(a). Swiss Webstermouse blastocyst injection with luciferase+ RFP+ CCR9+ PDX cells (10-15 cells / blastocyst) and representative IVIS Whole-body (left) or ex vivo images (middle and right) from post-natal day 10 human PDX-mouse chimeras are also shown. Mock(upper panel): no injection; PDX (down panel): blastocyst injected with CCR9+PDX cells. **(b).** PCR of human centromericrepeat sequences in DNA extracted from intestinal tumors excised from human PDX-mouse blastocyst-injected chimeras (1-4), blastocyst injected mouse tail, in vitro culture PDX cells and no DNA control (negative control). Experiment was performed 3 times.

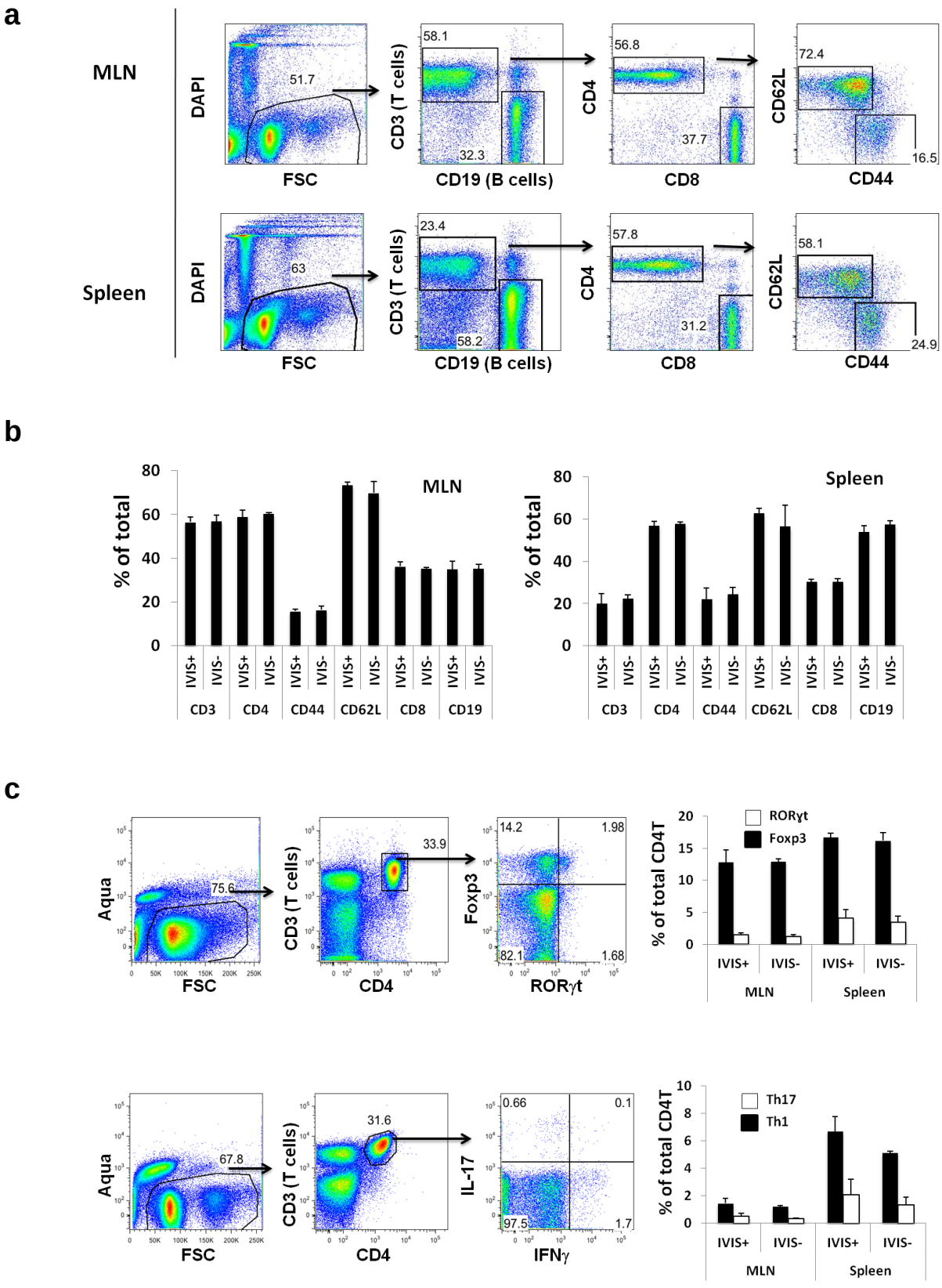
a
MLN
Spleen
DAPI
FSC
51.7
63
CD3 (T cells)
CD19 (B cells)
58.1
32.3
23.4
58.2
CD4
CD8
56.8
37.7
57.8
31.2
CD62L
CD44
72.4
16.5
58.1
24.9
b
MLN
Spleen
% of total
IVIS+
IVIS-
CD3
CD4
CD44
CD62L
CD8
CD19
c
Aqua
75.6
67.8
CD4
33.9
31.6
Foxp3
RORγt
14.2
1.98
82.1
1.68
IL-17
IFNγ
0.66
0.1
97.5
1.7
% of total CD4T
RORγt
Foxp3
Th17
Th1
MLN
Spleen

Supplementary Figure 6. Phenotypic and functional analysis of lymphocytes from the spleen and mesenteric lymph nodes (MLN) in human PDX-mouse chimeras. Spleens and 4 MLNs / mouse were collected from 4-week old mice (n=5) developed from Swiss Webster mouse blastocysts injected with CCR9+ PDX-1 cells (IVIS+). The littermates (n=5) from non-injected blastocysts were used as control for normal immune functions (IVIS-; control). **(a).** Gating strategy for phenotypic analysis is shown. Live (DAPI)-negative cells were electronically gated and CD3 (T cell) or CD19 (B cell) surface staining is shown. Electronic gating on CD3+ T cells was used to determine CD4 and CD8 expression as illustrated. CD4+ T cells were subsequently gated to determine CD62L and CD44 expression. **(B).** Relative average percentage of the parent population for each surface phenotype is shown. **(C).** Gating strategy for CD4+ T cell analysis. Live (Aqua)-negative cells were electronically gated and CD3/CD4 surface stain was used to identify CD4+ T cells. Intranuclear staining for Foxp3 and RORγt (top panel) was performed on unstimulated cells. Intracellular cytokine staining for IFNγ and IL-17 was performed of PMA/ionomycin stimulated cells. Relative percentage of mean total CD4+ T cells is displayed at right. No statistically significant differences ($P > 0.05$) between any IVIS+ vs. IVIS- groups, by 2-sided Mann-Whitney test were observed.Error bars represent standard deviation. No adjustments for multiple comparisions were made.

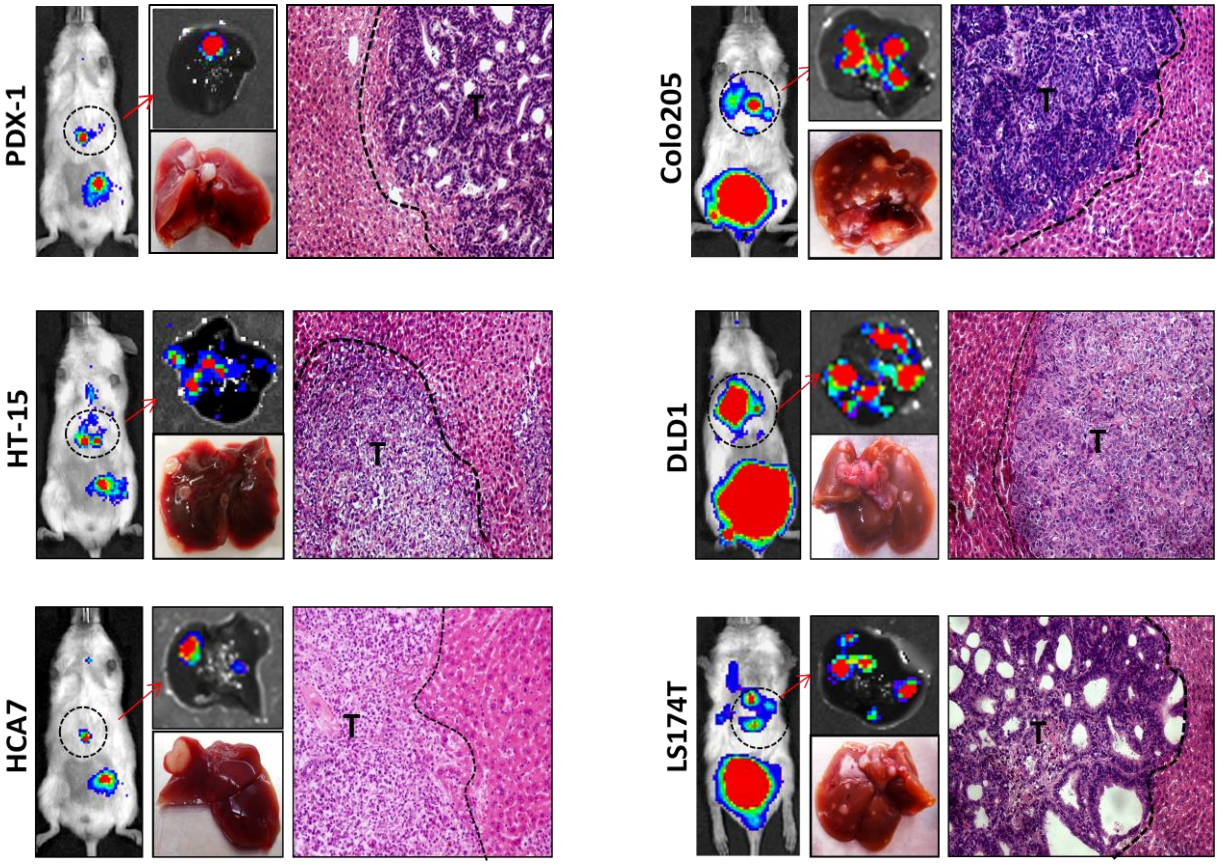

Supplementary Figure 7. Histopathological confirmation of IVIS imaged CRC liver tumors.CCR9+ CRC cells were injected via tail-vein into NOG mice and serial whole body IVIS imaging was performed to monitor tumor growth. CCR9 expression was inhibited by withdrawing doxycycline after IVIS lower abdominal tumor formation was observed at 2-4 weeks. Subsequent tumors occur primarily in liver. In each sub-panel, **Left**: representative whole-body IVIS images of GI and metastatic tumors; **Middle upper:**Ex vivo IVIS imaging of liver tumors. **Middle lower:** light microscopy of the same hepatic tumors as control. (4X)**Right:** representative images of H+E staining in hepatic human CRC tumors. (T: adenocarcinoma; Dotted lines indicate the borders between regions with hepato-cellular or tumor morphology Scale bars, 100μm. N=2-4 NOG mice/cell line.

a

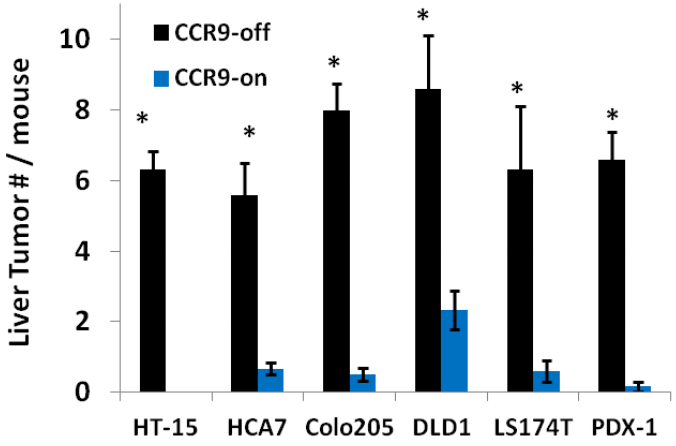

b

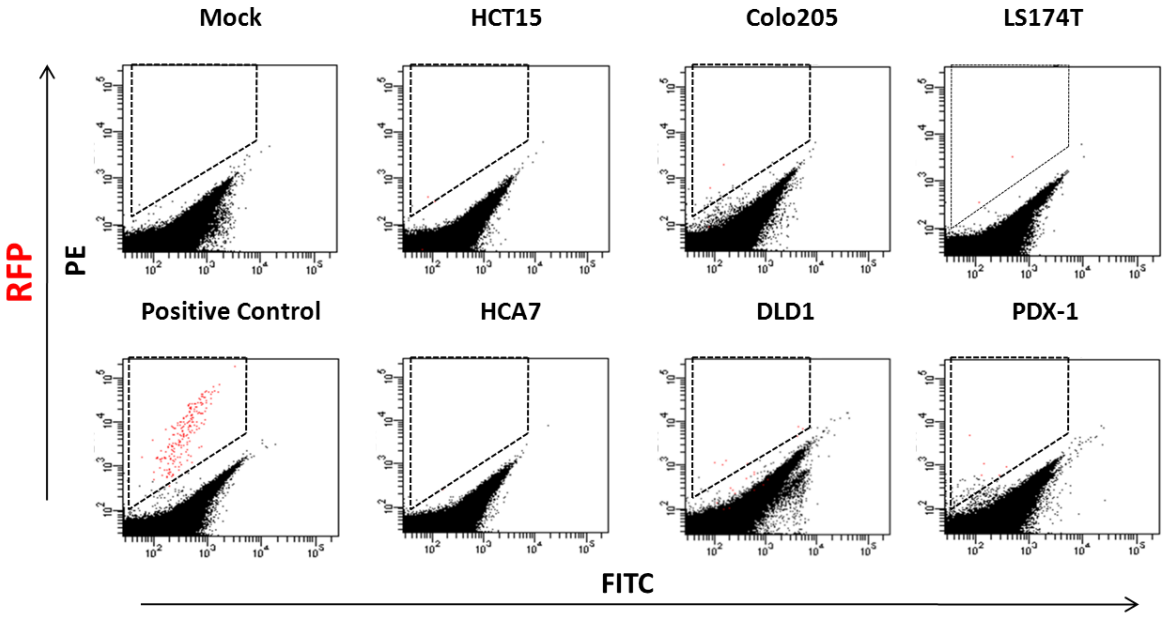

Supplementary Figure 8. Primary CRC CCR9 knockdown increases liver tumor multiplicity. (a). Quantification of liver IVIS + foci in NOG mice tail vein injected with inducible CCR9+ CRC cells. The experiment procedure is described in Figure 3. (For each cell line, CCR9-off (n=8 mice / cell line): no CCR9 expression s/p doxycycline withdrawal after lower abdominal IVIS+ signal detection; CCR9-on (n=8 mice/cell line): continuous doxycycline maintenance of CCR9 expression).* P<0.05 by 2-sided MW test. **(b).** 0.5 x 10^6 CCR9+ CRC cells were injected into 6-week NOG mouse (n=4 mice/each cell line experimental arm) by tail vein. After 48 hours, mice were sacrificed and livers were treated with collagenase and dispase to generate single-cell suspension. RFP cells were almost undetectable by FACS in mouse livers injected with RFP-labeled CCR9+ CRC cells. FACS Gates (dot windows) are set for RFP+ signal intensity; Mock: cells extracted from livers in mice injected with PBS; Positive control: GFP+ cells "spiked" in with mouse hepatic cells (200 RFP+ cells/million hepatic cells).

a.

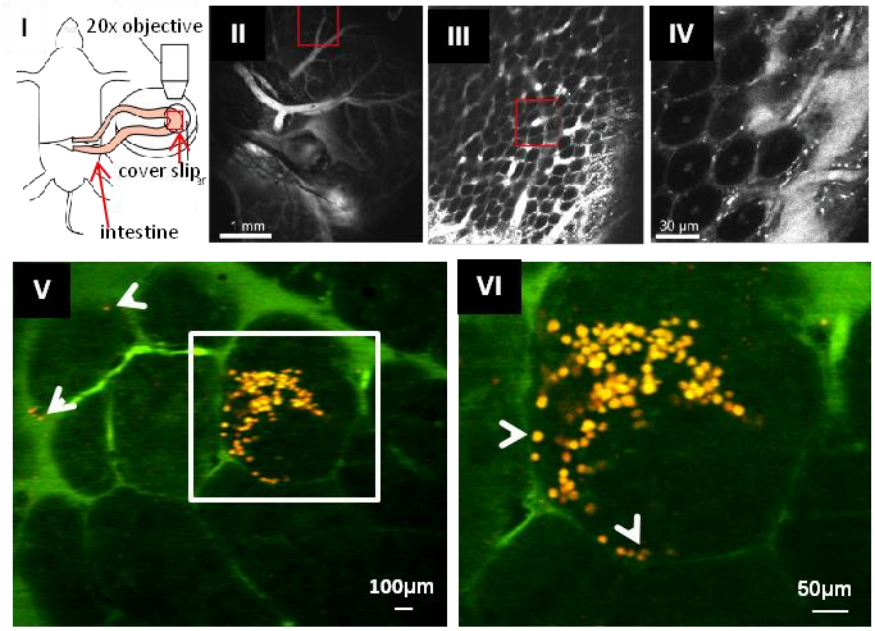

b.

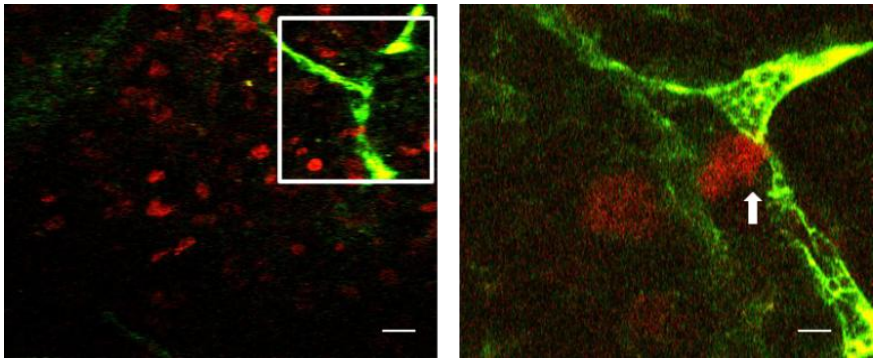

Supplementary Figure 9. Two-photon microscopy imaging of hepatic metastatic tumors. The experiment procedure to form primary CRC and sequential liver metastases was described in **Figure 3. (a).** two-photon microscopy imaging of orthotopic xenograft tumors. (representative images on tumors formed with CCR9+ DLD1 cells) (I. Schematic of surgical and imaging preparation (also referred in METHOD part); II – IV. low magnification images of intestine; V – VI. High magnificence imaging of intestinal tumors expressing RFP (red) surrounding vasculature labeled by FITC-Dextran (green).White arrows designate intravasating tumor cells.)**(b).**(Representative images on liver tumors formed with DLD1 cells)Hepatic tumor cells expressing RFP (red) surrounding vasculature labeled by FITC-Dextran (green).White arrows designate extravasating tumor cells out of blood vessel.) Scale bars, 50μm (left) & 10μm (right). N=6 mice were examined.

a

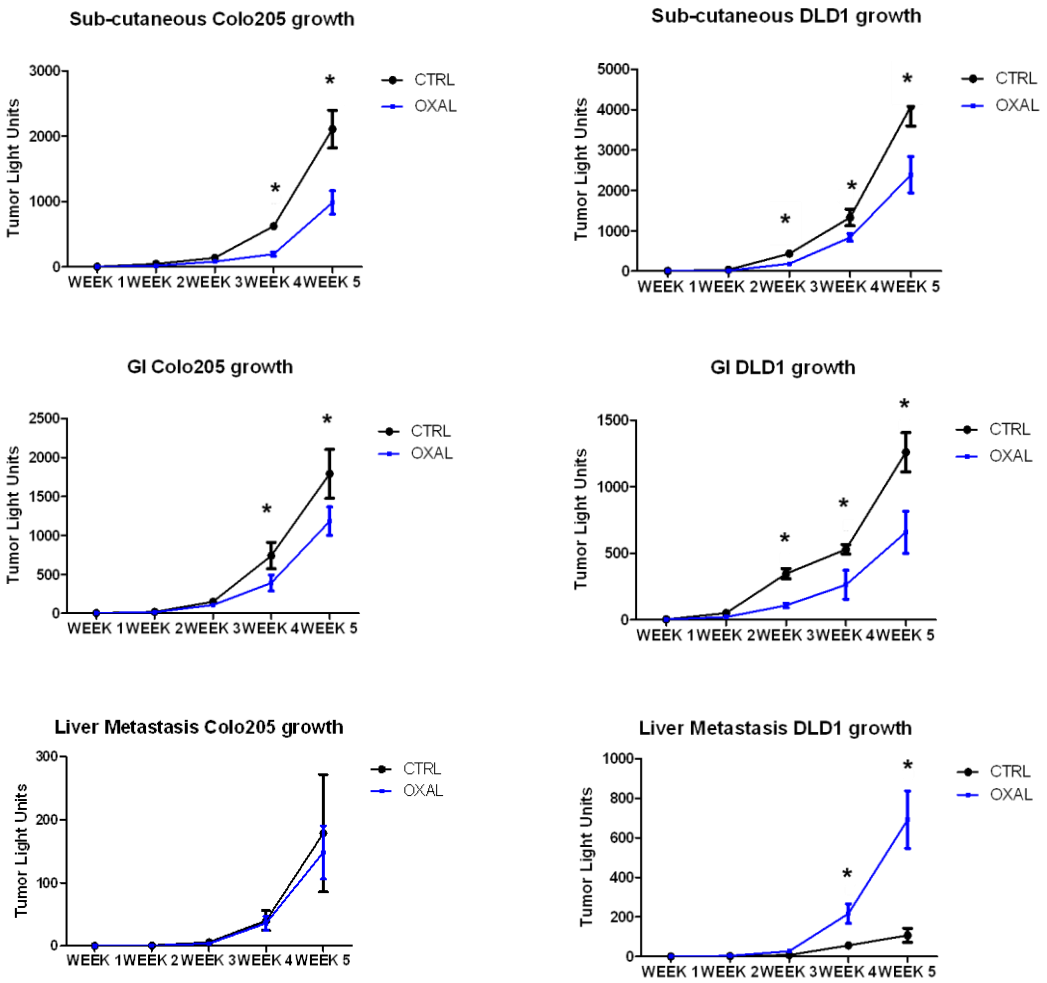
Sub-cutaneous Colo205 growth
Sub-cutaneous DLD1 growth
GI Colo205 growth
GI DLD1 growth
Liver Metastasis Colo205 growth
Liver Metastasis DLD1 growth
Tumor Light Units
CTRL
OXAL
WEEK 1
WEEK 2
WEEK 3
WEEK 4
WEEK 5

b

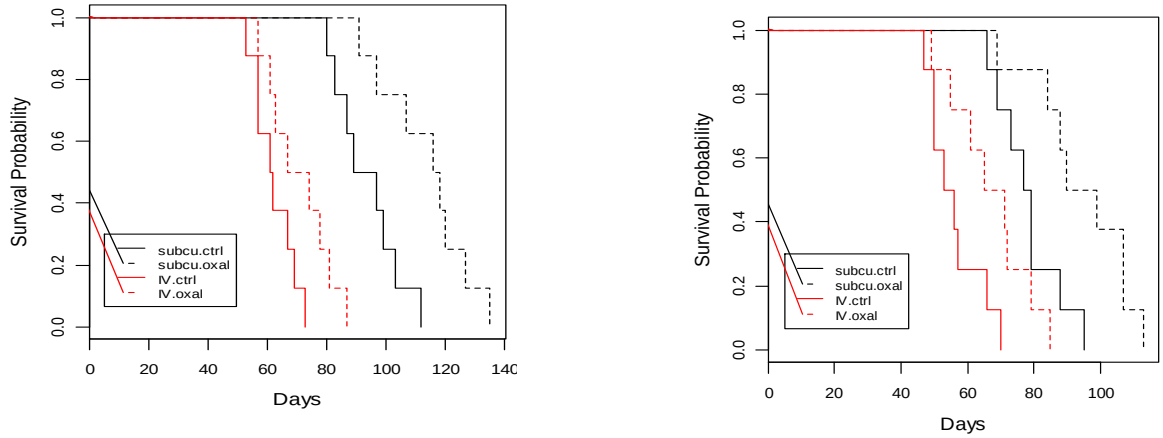
Survival Probability
Days
subcu.ctrl
subcu.oxal
IV.ctrl
IV.oxal

Supplementary Figure 10. Growth curves of human CRC cells in liver vs. orthotopic or subcutaneous xenografts, oxaliplatin chemoresistance and survival. (a). More detailed weekly growth curves of the data presented in Figure 4 are shown. 1 x 10^6CCR9+ CRC cells were tail-vein injected or subcutaneously inoculated into the left flank of 6-week NOG mice (n=8 for each experimental arm) and IVIS imaging was performed to monitor tumor formation. When GI or subcutaneous tumors reached radiance of 5 x 10^6 (p/sec/cm2/sr), doxycycline was withdrawn to turn off CCR9 expression and oxaliplatin (6mg/kg) or normal saline as control was given IV once weekly for 5 weeks. Tumor growth was quantified by luciferase - photon signal analysis with Xenogen software, with each light unit graphed representing 1 million measured light units. Real-time whole body IVIS imaging of mice at weeks 1-5 are shown for subcutaneous inoculated or tail-vein injected CTMM cells treated with Oxaliplatin. Error bars indicate S.E.M. *, No overlap of error bars at given time point**. (b).** Kaplan-Meier survival plot of mice analyzed in **(a).**

Supplementary Table 1.Mutation Profiles of CTMM CRC cell lines. The mutation status of 17 CTMM cell lines for the twenty most commonly somatically altered genes in human CRC (COSMIC Database, http://cancer.sanger.ac.uk) is given.The presence of a somatic mutation is indicated by a red bar. Whole exome sequencing analysis was performed for PDX-1 through 4, Caco-2 and HT15. PDX-3 and PDX-4 were previously described as CCIC-1 and CCIC-2 (reference 7). For the other cell lines, mutation status was previously described in the Cancer Cell Line Encyclopedia (http://www.broadinstitute.org/software/cprg/?q=node/11) or Eiden et al[108]. Cell lines were classified as MSI, microsatellite instability; MSS, microsatellite stable; Mucinous, mucinous adenocarcinoma histolopathology; CIMP,CpG Island Methylator Phenotype; CIN, chromosomal instability pathway, as previously described by D Ahmed, et al.

Cells	Mice #	Mean progression (Week)	GI tumor incidence (%)	GI tumor Locations	Mean GI tumor /mouse
Parental HT-15	9	7.8	0	NA	0
CCR9 HT-15	9	6.5	67%	small intestine, Colon	2.3 ± 0.17 *
Parental HT-29	8	7.7	37%	small intestine	0.3 ± 0.17
CCR9 HT-29	8	5.8	100%	small intestine, Colon	3.7 ± 0.34 *
Parental HCA7	8	7.6	0	NA	0
CCR9 HCA7	8	5.9	63%	small intestine, colon	3.8 ± 0.28 *
Parental HCT116	8	5.7	0	NA	0
CCR9 HCT116	8	5.2	75%	small intestine, colon	3.6 ± 0.30 *
Parental SW620	8	6.6	0	NA	0
CCR9SW620	8	5.3	75%	small intestine, colon	3.6 ± 0.38 *
Parental SW480	8	7.1	0	NA	0
CCR9 SW480	8	6.5	88%	small intestine, colon	3.1 ± 0.28 *
Parental SW48	8	7.4	0	NA	0
CCR9 SW48	8	6.0	50%	small intestine	2.0 ± 0.27 *
Parental Caco-2	8	9.2	0	NA	0
CCR9 Caco-2	8	7.5	38%	small intestine, colon	1.7 ± 0.19
Parental Colo205	8	7.2	0	NA	0
CCR9 Colo205	8	5.8	75%	small intestine, colon	3.0 ±0.33 *
Parental DLD1	8	8.2	0	NA	0
CCR9 DLD1	8	5.7	88%	small intestine, colon	3.7 ± 0.33 *
Parental LoVo	8	6.6	0	NA	0
CCR9 LoVo	8	5.1	100%	small intestine, colon	4.3 ± 0.37 *
Parental LS174T	8	7.8	0	NA	0
CCR9 LS174T	8	6.1	88%	small intestine, colon	3.6 ± 0.26 *
Parental RKO	8	5.8	0	NA	0
CCR9 RKO	8	6.7	25%	small intestine	1.5 ± 0.71
Parental PDX-1	8	8.2	0	NA	0
CCR9 PDX-1	8	6.3	88%	small intestine, colon	4.3 ± 0.31 *
Parental PDX-2	9	9.2	0	NA	0
CCR9 PDX-2	9	6.8	56%	small intestine, colon	2.4 ± 0.38 *
Parental CT26	10	7.1	0	NA	0
CCR9 CT26	12	6.5	75%	small intestine, colon	3.6 ± 0.58 *

Supplementary Table 2. Inducible CCR9+ CRCs form orthotopicxenograft tumors in mouse intestine. Colorectal and small intestine tumors formed in mice injected with cells infected with CCR9+ vector or backbone control vector by tail vein. Asterisks denote statistically significant differences between CCR9+ group and control group. * P< 0.01 compared to parental control groups by 2-sided MW test.

REFERENCES

1. Walters S, Maringe C, Butler J, Brierley JD, Rachet B, Coleman MP. Comparability of stage data in cancer registries in six countries: lessons from the International Cancer Benchmarking Partnership. International journal of cancer Journal international du cancer 2013;132:676-85.

2. Ellis LM. Preclinical data targeting vascular endothelial growth factor in colorectal cancer. Clinical colorectal cancer 2004;4 Suppl 2:S55-61.

3. Dimasi JA, Reichert JM, Feldman L, Malins A. Clinical approval success rates for investigational cancer drugs. Clinical pharmacology and therapeutics 2013;94:329-35.

4. Rubio-Viqueira B, Hidalgo M. Direct in vivo xenograft tumor model for predicting chemotherapeutic drug response in cancer patients. Clinical pharmacology and therapeutics 2009;85:217-21.

5. Sausville EA, Burger AM. Contributions of human tumor xenografts to anticancer drug development. Cancer research 2006;66:3351-4, discussion 4.

6. Siolas D, Hannon GJ. Patient-Derived Tumor Xenografts: Transforming Clinical Samples into Mouse Models. Cancer research 2013.

7. Sikandar SS, Pate KT, Anderson S, et al. NOTCH signaling is required for formation and self-renewal of tumor-initiating cells and for repression of secretory cell differentiation in colon cancer. Cancer research 2010;70:1469-78.

8. Chen HJ, Edwards R, Tucci S, et al. Chemokine 25-induced signaling suppresses colon cancer invasion and metastasis. The Journal of clinical investigation 2012;122:3184-96.

9. Ebert MP, Tanzer M, Balluff B, et al. TFAP2E-DKK4 and chemoresistance in colorectal cancer. The New England journal of medicine 2012;366:44-53.

10. Meng RD, Shelton CC, Li YM, et al. gamma-Secretase inhibitors abrogate oxaliplatin-induced activation of the Notch-1 signaling pathway in colon cancer cells resulting in enhanced chemosensitivity. Cancer research 2009;69:573-82.

11. Kabelitz D, Wesch D. Features and functions of gamma delta T lymphocytes: focus on chemokines and their receptors. Crit Rev Immunol 2003;23:339-70.

12. Youn BS, Kim YJ, Mantel C, Yu KY, Broxmeyer HE. Blocking of c-FLIP(L)--independent cycloheximide-induced apoptosis or Fas-mediated apoptosis by the CC chemokine receptor 9/TECK interaction. Blood 2001;98:925-33.

13. Wurbel MA, McIntire MG, Dwyer P, Fiebiger E. CCL25/CCR9 interactions regulate large intestinal inflammation in a murine model of acute colitis. PLoS ONE 2011;6:e16442.

14. LaPointe LC, Dunne R, Brown GS, et al. Map of differential transcript expression in the normal human large intestine. Physiol Genomics 2008;33:50-64.

15. Li X, Madison BB, Zacharias W, Kolterud A, States D, Gumucio DL. Deconvoluting the intestine: molecular evidence for a major role of the mesenchyme in the modulation of signaling cross talk. Physiol Genomics 2007;29:290-301.

16. Cancer Genome Atlas N. Comprehensive molecular characterization of human colon and rectal cancer. Nature 2012;487:330-7.

17. Quail DF, Joyce JA. Microenvironmental regulation of tumor progression and metastasis. Nature medicine 2013;19:1423-37.

18. Schneider JS VJ, Terzic A, Fraidenraich D. Blastocyst injection of embryonic stem cells: a simple approach to unveil mechanisms of corrections in mouse models of human disease. Stem Cell Rev 2009;4:369-77.

19. Eds Johan Auwerx SLA, Stephen D. Brown, Monica Justice, David D. Moore, Joseph Nadeau. Current Protocols in Mouse Biology. In: http://onlinelibrarywileycom/book/101002/9780470942390: Wiley; 2013.

20. Witherspoon M, Chen Q, Kopelovich L, Gross SS, Lipkin SM. Unbiased metabolite profiling indicates that a diminished thymidine pool is the underlying mechanism of colon cancer chemoprevention by alpha-difluoromethylornithine. Cancer discovery 2013;3:1072-81.

21. Casero RA, Jr. Say what? The activity of the polyamine biosynthesis inhibitor difluoromethylornithine in chemoprevention is a result of reduced thymidine pools? Cancer discovery 2013;3:975-7.

22. Sharma SK, Hazeldine S, Crowley ML, et al. Polyamine-based small molecule epigenetic modulators. MedChemComm 2012;3:14-21.

23. Huang Y, Marton LJ, Woster PM, Casero RA. Polyamine analogues targeting epigenetic gene regulation. Essays in biochemistry 2009;46:95-110.

24. Meurens F, Whale J, Brownlie R, Dybvig T, Thompson DR, Gerdts V. Expression of mucosal chemokines TECK/CCL25 and MEC/CCL28 during fetal development of the ovine mucosal immune system. Immunology 2007;120:544-55.

25. Meurens F, Berri M, Whale J, et al. Expression of TECK/CCL25 and MEC/CCL28 chemokines and their respective receptors CCR9 and CCR10 in porcine mucosal tissues. Veterinary immunology and immunopathology 2006;113:313-27.

26. Lautt WW. Mechanism and role of intrinsic regulation of hepatic arterial blood flow: hepatic arterial buffer response. The American journal of physiology 1985;249:G549-56.

27. Thiel H. Liver hemodynamics and portacaval shunt. Surgery, gynecology & obstetrics 1980;150:587-92.

28. Dancis J. Transport of substances across perfused organs. Acta endocrinologica Supplementum 1972;158:347-75.

29. Vanharanta S, Massague J. Hypoxia signaling--license to metastasize. Cancer discovery 2013;3:1103-4.

30. Vanharanta S, Massague J. Origins of metastatic traits. Cancer cell 2013;24:410-21.

31. Chaturvedi P, Gilkes DM, Wong CC, et al. Hypoxia-inducible factor-dependent breast cancer-mesenchymal stem cell bidirectional signaling promotes metastasis. The Journal of clinical investigation 2013;123:189-205.

32. Eisinger-Mathason TS, Zhang M, Qiu Q, et al. Hypoxia-dependent modification of collagen networks promotes sarcoma metastasis. Cancer discovery 2013;3:1190-205.

33. Erler JT, Bennewith KL, Nicolau M, et al. Lysyl oxidase is essential for hypoxia-induced metastasis. Nature 2006;440:1222-6.

34. Gilkes DM, Chaturvedi P, Bajpai S, et al. Collagen prolyl hydroxylases are essential for breast cancer metastasis. Cancer research 2013;73:3285-96.

35. Fidler IJ, Wilmanns C, Staroselsky A, Radinsky R, Dong Z, Fan D. Modulation of tumor cell response to chemotherapy by the organ environment. Cancer metastasis reviews 1994;13:209-22.

36. Wilmanns C, Fan D, Obrian C, et al. Modulation of Doxorubicin sensitivity and level of p-glycoprotein expression in human colon-carcinoma cells by ectopic and orthotopic environments in nude-mice. International journal of oncology 1993;3:413-22.

37. Okumura K, Shiomi H, Mekata E, et al. Correlation between chemosensitivity and mRNA expression level of 5-fluorouracil-related metabolic

enzymes during liver metastasis of colorectal cancer. Oncology reports 2006;15:875-82.

CHAPTER 3

Engineering Organotypic Human Colon through Recellularization:

An *ex vivo* Model for Studying Cancer Driver genes

(Contribution: Michael Shuler, Nancy Jenkins, Neal Copeland, Huanhuan Chen, Zhubo Wei, David Savage designed the project; Huanhuan Chen, Zhubo Wei, Jian Sun and Asmita Bhattacharya performed experiments; Huanhuan Chen, Zhubo Wei, Jian Sun Michael Shuler, Nancy Jenkins and Neal Copeland analyzed the data; Huanhuan Chen wrote the manuscript; Michael Shuler, Neal Copeland, Nancy Jenkins, Huanhuan Chen, Zhubo Wei, Jian Sun and Asmita Bhattacharya helped with project discussion.)

INTRODUCTION

Despite devoting more than three decades of research to improve understanding of cancer biology and development of therapeutics, the persistence of poor outcomes among cancer patients highlights the need for new approaches to complement existing research methodology [1,21,51]. One of the major obstacles arises from intrinsic limitations of existing experimental systems, which poorly translate into clinical applications due to shortage of concordance with human studies [5,12,16,24]. For instance, conventional cell culture models as research platforms lack the capacity to maintain the interactions of tumor cells with extracellular matrix (ECM) and replicate tissue-specific microenvironment, which are required for tumor pathogenesis [19, 21]. Although animal models are valuable research tools, they are costly, time-consuming, and short of appropriate resolution and sensitivity to track the dynamics of cancer progression. Animal studies can also show considerable differences from humans with regard to requirements for oncogenic transformation [36].

Another problem is that a tumor evolves heterogeneously and the numerous passenger mutations which have little function on cancer disease confound the paths of tumor-causing alterations (drivers) and this property makes most reverse genetics studies yield numerous complex genetic candidates [5,9, 10]. Therefore, testing the role of each gene in cancer pathogenesis is a critical albeit difficult task given the large number of low-frequency mutations in cancer genome. Currently large-scale high-throughput genetic approaches have facilitated the identification of genetic alterations in cancers. However, distinguishing drivers from passengers is barely successful using genome analysis alone [5, 9].

To fundamentally bypass these limitations, we have established a new system for cancer research. Recent technical advance on orthotopic organ engineering and transplantation has paved a new avenue for isolating natural matrix with preserved ECM and three-dimensional tissue-specific structure, which provide more physiologically relevant conditions [11, 17, 37, 39, 40, 49]. To truly mimic human conditions and create a refined model qualified for studying cancer genetics, we have created an organotypic cancer model using human natural matrix, and to identify low-frequency driver genes, we applied a forward genetic screen using *Sleeping Beauty (SB)* transposon- based mutagens in this cancer model [10, 14, 15, 31, 46, 47].

Here we have demonstrated the method by generating ex vivo human colon cancer tissues combined with SB mutagenesis system for studying invasion-driver genes. Found in ~80% of colorectal cancer (CRC), loss-of-function mutations in adenomatous polyposis coli (APC) gene is thought to be the initial event, which transforms normal colon epithelium into neoplasia. APC-dependent neoplasia requires additional mutations for progression from *in situ* mucosa to invasion through the muscularis layer into the submucosa where cancer cells gain access to main vascular and lymphatic systems for their systemic spreading. Thus invasion into submucosa is believed as a key feature for CRC to become malignant. As proof of principle, we first created a physiologically active model of human colon by reseeding primary colon epithelial cells, endothelial cells and fibroblasts in decellularized human colon tissues, which retain the colon's complete geometry, well preserved ECM including relatively integral vascular network, and most importantly, maintain the intactness of muscularis layer [34]. The organotypic colon was sequentially transformed into APC-null *in situ* neoplasia and then into submucosal

invasive adenoma by introducing the additional genetic elements of active K-RAS and TGF-β [22, 45, 50]. Functional analyses and molecular characterizations indicate that this bioartificial CRC model has the capacity to recapitulate the major features of tumor malignancy, including breaking muscularis layer and invading into submucosa. This CRC model, derived from genetically defined epithelium, free of redundant genetic alterations and reproducing malignancy transformation within 4 weeks, served as a new platform for studying progression-driver genes. Next, we performed a forward genetic screen using transposon- based mutagens to induce malignancy transformation in the *in situ* APC-dependent neoplasia. Our results demonstrated that the organotypic cancer model combined with transposon-based mutagenesis system allow us to achieve rapid forward genetics study in human-originated tissues and improve oncogene discovery.

RESULTS

Preparation of acellular human colon matrix

Decellularization [39,40] using sodium dodecyl sulfate (SDS) followed with Triton-X100 washing gave better results than the PEG based or DNase/enzyme based methods for removal of cellular components from human colon tissues (~5 cm^3) (Figure 1 A-D). DNA content (Supplementary Table 1) in these acellular scaffolds decreased to less than 5% of that in normal colon, while there was no difference in the quantities of the four main ECM proteins – GAG (Supplementary Table 1.), collagen (type I), laminin and fibronectin (Figure 1 I) [35]. Removal of most cellular components is further confirmed (Figure 1 I) by the observation that F-actin and nuclei are undetectable in the scaffolds by immunohistochemistry. The decellularized scaffolds successfully preserved the tissue architecture, main vasculatures and crypt niches (Figure 1 E, F and H) of the original colon. Most importantly, the colon matrix retained the intactness of muscularis layers (Figure 1 G), which form the native barrier for CRC malignancy progression and submucosa invasion.

Recellularization of acellular human colon matrix

As we have proposed earlier, one key feature of the ex vivo colon model to facilitate identification of driver genes is having a genetically defined epithelium which is free of malignant origin and secondary genetic alterations. We developed primary culture of human colon epithelial cells (hCEC) (Supplementary Figure 1 A.) from routine colonoscopy patient samples [13, 28, 43]. DNA sequencing of these cells indicated no

mutations in hotspot regions of APC, KRAS and TP53 genes. Immortalized with protein expression of the human ribonucleoprotein enzyme telomerase (hTERT), hCEC formed organoids with microcrypt structure in 3D culture (Supplementary Figure 1 A.), and were capable of self-renewal and multilineage differentiation into the various major types of functional epithelial cells [33](Supplementary Figure 1B).

The small bowel mucosa with intact crypt niches and muscularis layer can be mechanically separated from the submucosa (Supplementary Figure 3 A and B.), thus allowing to populate the acellular matrix with hCEC, human colon microvascular endothelial cells and fibroblasts (Supplementary Figure 2.) in exact physiological locations (Figure 2 B and Supplementary Figure 3 C, D). The complete organotypic human colon model was then generated by assembling the stratified mucosa and submucosa layers containing native ECM proteins and secreted stromal elements (Figure 2 B and Supplementary Figure 3 E, F). Importantly, this ex vivo colon not only remained viable, but also developed physiologically active crypts including basal stem cells and major types of functionally differentiated cells (Supplementary Figure 4).

Establishment of colon cancer model

It has been proposed that sequential alterations in several main genes and signaling pathways correlated with histological features during CRC progression. APC mutation constantly activating the *WNT* pathway is believed to be the first event transforming normal cells into an adenoma. In the adenoma-carcinoma sequence, common mutation in oncogene KRAS promotes malignant transformation of early adenoma into

intermediate adenoma. Abrogation of the TGF-β pathway, including mutations in SMAD4 and TGFBR2, is thought to occur later in CRC progression, transforming the adenoma to a carcinoma. To rapidly convert normal hCEC into cancerous cells, we introduced into the system the pathological pair of genetic elements that inhibit human APC by small- hairpin RNA and encode active KRAS by retroviral transfection. To test the tumorigenic conversion, the hCEC cells with APC null and KRAS over-expression were subcutaneously injected into immunodeficient mice and 4 weeks later, the TGF-β signaling pathway was activated by directly injecting growth factor TGF-β into the xenografts to induce tumor development. Within 6-8 weeks, tumors occurred in 60% of injection sites and presented typical epithelial CRC features with crypt-like lumen structure and microvasculature formation, but no tumor formed by parental hCEC (Supplementary Figure 5).

Based on these findings, the same sequential genetic alterations were applied to transform the ex vivo colon models to the different stages of CRC models. Tumor initiation, progression and invasion were achieved by populating the mucosa epithelium with APC- hCEC, APC-KRAS+ hCEC or APC-KRAS+ hCEC treated with TGF-β, respectively (Figure 2 A). Similar to the native human colon tissue (Figure 2 C), the ex vivo colon model recellularized with normal hCEC (Figure 2 D) was found to form single-cellular layer in crypt niches that tightly attached to the basal membrane and stromal ECM. In contrast, the APC-null colon model (Figure 2 E and F) presented dysplasia-like structure in the mucosa epithelium including cells undergoing fast proliferation to form multi-cellular layers and distorted crypt structure with multi-lumenal fusion, a typical phenotype in early stage adenoma. The APC-null neoplasias formed in

only 2 weeks and were *in situ* restricted to mucosa layer. Next, the CRC model further demonstrated that constant expression of KRAS functioned synergistically with the activated TGF-β pathway to promote the APC-dependent neoplasia growth into large adenoma, breaking through the muscularis layer and invading into submucosa, a key feature of malignant CRC (Figure 2 G-I).This malignant transformation occurred within 4 weeks from the onset of the *in situ* APC-null neoplasia.

In summary, we have developed a colon cancer model using human natural matrix and genetically defined primary colon cells. This pathophysiologically active CRC model recapitulated the key features in tumor initiation, progression and malignant transition from mucosa in situ to submucosa invasion. The different stages of oncogenic transformation can be generated easily within weeks, correlating well with histological features and avoiding redundant passenger mutations. The ex vivo system also can provide single-cell resolution and time-lapse sensitivity for anatomically tracking and dissecting disease steps within CRC progression. These qualities make the ex vivo CRC model a potentially useful system for high-throughput genetics or therapeutics study.

Identification of CRC driver genes

In our previous study, *SB* transposon-based mutagenesis has been successfully used as a genetic modification tool to model many types of human cancer in mice and this forward genetics study facilitated the exploration of many novel genes and signaling pathways driving cancer in mice [7,8,10,14,15, 26, 27,31,36,46,47,48] . Here we extend

the *SB* mutagenesis system to model cancer diseases in human-origin tissues, which allows for identification of cancer driver genes in real human conditions. In order to create an active human *SB* transposition system covering broad target range on the low-frequency mutant genes of CRC, we made some improvements to the current T2/Onc transposition system used in mice. We added the dual selection markers of GFP and neomycin between the two inverted repeats/direct repeats in the transposon gene and this allowed the purification of the cell population with transposon insertions. We also replaced the *SB10* transposase in the transposition system with *SB100X*, the most effective transposase currently available [20]. In the combination system of T2/Onc and *SB100X*, 500 ng transposon donor plasmids and 100 ng transposase helper plasmids were found to function best for hCEC cells for reaching the peak activity of transposase and avoiding the effect of overproduction inhibition (OPI) [20](Supplementary Figure 6 A). Each hCEC cell had on an average 4 ± 3 transposon copies inserted in its host genome after 4 weeks of antibiotics selection (Supplementary Figure 6 B).

The adenoma undergoing submucosa invasion developed within 6-7 weeks in the colon matrix with APC-null SB-inserted hCEC seeded in the crypt niches (Figure 3 D and E). The average number of invasion loci in every 10 cm^2 matrix was 5.5 ± 1.9 which is significantly higher than that of the matrix with APC-null hCEC transfected with transposon donor plasmid alone (Figure 3 F), and indicated that SB-based mutagenesis system was physiologically functional in generating genetic hits during CRC progression. The ex vivo system demonstrated that colon tumors in multiple disease stages can be sequentially reproduced and time-lapse tracked to single-cell resolution (Figure 3 G - I).

In this study, 21 invasive neoplasias in total from 15 independent recellularized matrixes were excised by laser-capture microdissection to minimize the contaminations with non-invasive tumor tissues. For analysis of transposon insertion sites, ligation-mediated PCR (LM-PCR) [4] was performed to specifically amplify the transposon integrated genomic fragments which were then sequenced by illumine sequencing. Low mapping quality reads (values less than 30) were filtered out for the following analysis. Among the high mapping quality reads, about half of them were mapped at the “TA” dinucleotide sites. Further analysis was focused on these consensus SB insertion sites. From the distribution of read depth at the insertion sites, it was clear that majority of the insertion sites resulted from background insertion events or PCR artifacts. We considered the top 10% of the deepest insertion sites as clonal insertion sites. We mapped these clonal insertion sites in each sample to the human genome annotation file, refGene, and picked the sites that were within 1000bp of known transcripts in refGene. In addition to this, big dye terminator sequence was used to confirm the transposon insertion sites [20].

This forward genetics screen identified a total of 39 candidate genes which, when mutated, probably contributed through cooperation with APC mutations to the malignant transformation of the ex vivo CRC (Supplementary Table 2). All the candidate genes have been documented in the human colon cancer cataloged TCGA database, highlighting the strong concordance of the ex vivo CRC models to the real clinical aspect of the disease. Intriguingly, 17 of the 39 genes were found to have been identified earlier to contribute majorly in CRC progression and these included TCF7L2 and WNT9B (two members in WNT pathway), DNA mismatch repair gene MSH2;

TWIST2 (associated with the phenomenon of epithelial to mesenchymal transition), JAK1and STAT3 in JAK-STAT signaling pathway; DCC (a common deletion gene in CRC) (Table 1). Among the remaining 22 genes which have not previously been implicated in CRC progression, we selected 10 genes (ASXL1, CAMTA1, CSTF3, DDX20, FXR1, LATS2, MITF, PAX7, PRKG1, and RPAP1) for validating the driver function of causing tumor malignant transformation. siRNA was used to down-regulate the gene expressions in APC-null hCEC or colon cancer cell line SW480. SW480 line was derived from early-stage adenocarcinoma and harbors APC mutation similar to that of hCEC in our model, thus used as a suitable cellular tool to test the candidate functions in real CRC cells. It was observed that 7 genes promoted cell proliferation, 4 increased cell mobility and 7 enhanced cell invasions through matrigel matrix (Figure 4).

Discussion

We have described a new methodology that allows unbiased forward genetics studies performed in human-origin tissues under real human conditions. The decellularized human native matrix can provide major tissue-required elements, including complex tissue-specific structure, cell-matrix interaction, and physiological co-location of multiple types of cells and these make our method advanced to conventional assays of cell migration or invasion though synthetic matrigel or collagen layer which does not exist in real tissues. Compared to the complex bioreactor and medium formula desired to generate native functional organs for orthotopic transplantation, we used simpler systems that fulfill minimal requirements for developing tissue-level tumor models, enabling low-cost and large-scale cancer study.

Currently, very few animal models have been developed to study malignant events and test late-stage CRC, mainly because the intestinal-specific and inducible gene modifications in mice are available in only some of the genes relevant to human CRC and most global genetic manipulations barely cause colon-specific cancer phenotypes. Through introducing sequential pathologically-paired genetic elements, the ex vivo CRC model was able to recapitulate most features in different disease stages and developed malignant transformation within weeks, suggesting it to be a valuable complement to current cancer models. Genetic alteration patterns required for oncogenic transformation in human systems are different to animal systems. For instance, it is estimated that average 5-12 somatic mutations are required for a normal human cell to undergo malignant transformation, but only 2-4 mutations are sufficient for mouse cells.

The ex vivo cancer models generated from human native matrix and primary cells may serve as a more accurate and efficient research platform from which the results derived may be applied directly to the human circumstance, bridging the gaps between animal models and clinical diseases.

Transposon-based insertion mutagenesis system is believed as an unbiased and high-throughput genetic tool for cancer gene discovery. *SB* system has been used to model many types of mouse cancers. However our studies, to our best knowledge, at the first time demonstrate *SB* is capable to induce human cancer development under human native conditions. Identification of malignancy driving genes that will lead to developing not only drug targets but also diagnosis markers, therefore, is critically important for improving clinical outcomes. Currently, studying malignancy driver genes remains as a challenge and a tractable system that enables recapitulating the dynamic malignancy transition within a clear diver alteration context would largely facilitate oncogene discovery. The ex vivo CRC models we described here were created with normal primary cells free of redundant mutations and have the capacity to reproduce tumor initiation, promotion and progression by sequentially introducing APC, KRAS and TGF-β genetic alterations. Based on the tractable model system, we applied *SB*-mediated mutagenesis to simulate multiple hits during cancer evolution and the mutations correlated to CRC development were promptly detected by pathological features and efficiently identified by high-throughput LM-PCR.

To provide the proof of principle for the forward genetic study based on the approach of “engineering oncology”, we identified 39 candidate driver genes involved in CRC submucosal invasion though cooperation with mutations in APC. All of the genes have

been listed in the TCGA-colon cancer database, suggesting the highly relevance of the ex vivo model to clinical CRC diseases and among these genes, 17 have been previously reported correlated to CRC progression, indicating the effectiveness and accuracy of the model system as a functional platform and feasibility of ex vivo SB-based forward genetic screen for studying cancer genetics. Besides functional assays, the known functions of the candidate genes also provide evidence for some of them to be the drivers in CRC development. ASXL2 [30], for example, is a member of ASXL family that are epigenetic scaffolding proteins with functions of epigenetic regulations by recruitment of the polycomb-group repressor complex (PRC) and trithorax-group (trxG) activator complex and of histone modification by assembling transcription factors to specific genetic domains. ASXL2 as well as ASXL1, another ASXL family member, BRCA1 and YY1 are binding partners of BAP1 that is a nuclear de-ubiquitinating enzyme and strongly associated with metastasis as a tumor suppressor. Truncation mutations of ASXL2 have been correlated to poor prognosis in prostate cancer, pancreatic cancer and breast cancer. Additionally, ASXL1 has been involved in the malignant progression of multiple cancers including CRC with microsatellite instability (MSI).

Another candidate CAMTA1 was previously identified as a putative tumor suppressor in neuronal cancers [23]. CAMATA1 decreases glioblastoma cell growth by stimulating the expression of anti-proliferative peptide NPPA and regulates neuroblastoma cell mobility through increasing expressions of β3 (TUBB3) tubulin, microtubule associated protein 2 (MAP2) and neurofilament light chain (NEFL). CAMTA1 may function through Ca^{2+} signaling pathway and mediate Ca^{2+} - dependent processes in cell differentiation.

Particularly, decreased expression of CAMTA1 was observed frequently in CRCs and was previously reported to be substantially associated with poor survival as an independent indicator [32]. Consistent to previous findings, our both in vitro and ex vivo functional assays that decreased CAMTA1 expression substantially promoted cell proliferation and invasion in hCEC and SW480 lines, further indicated that CAMTA1 may play a tumor-suppressor role in CRC malignancy transformation.

Because of the heterogeneity during cancer evolution and diversity in personal genomic background, the 39 candidates identified in this screen are sort of specificity to the patients that these three colon epithelial cell lines were derived from. Theoretically, this model system can discover broader ranges of novel oncogenes by using various patient cell sources or generating initial pools covering different mutation profiling through different rounds of *SB* mutagenesis. Although now mutations in tumors can be identified on a whole-genome scale, elucidating the roles of genetic alterations in tumorigenesis is still challenging. Here we demonstrated the potential value of the ex vivo cancer models to complement existing in vitro cell lines and in vivo animal models for studying the mechanistic roles of the recurrent human cancer mutations multi-dimensionally. The new methodology of engineering ex vivo cancer models developed in this research also offers more opportunities to create specialized physiological microenvironment for mimicking real clinical diseases. For instance, further engineering vascular network, immune system and organ-specific microbes may be selected to incorporate into the miniaturized cancer tissues depending on variant research goals to achieve. In addition, this new engineering process also might be extent to generating other types of ex vivo cancer organs [38, 42], such as lung, liver, skin and kidney and

potentially provide new research strategy in many fields of oncology from developing biomarkers for diagnosis and prognosis to screening drugs, chemicals, pathogens and toxins for personalized medication.

METHODS

Decellularization of human colon tissues.

All primary normal colon tissues in this study were taken from the normal parts of CRC tissues collected by the Weill Cornell Colon Cancer Biobank, approved by the Institutional Review Board (IRB) of Weill Cornell Medical College. Pathological study has been used to check the normal origin by tissue morphology. Briefly, fresh patient colon tissues were collected in Medium 199 supplemented with 200 U/ml penicillin and 200 mg/ml streptomycin, immediately after patient operative resection. Fat and blood clots were removed from tissues and they were rinsed 5 times in sterile PBS. Samples were cut into 5 cm x 2 cm pieces and incubated in sterile 1% SDS (Fisher Scientifics) in deionized water for 4-6 hours at room temperature and gently shaking condition. Sterile 1% Triton –X100 (Sigma) in deionized water was applied to rinse the tissues for 1 hour and the acellular matrix was then washed in sterile PBS containing penicillin/streptomycin/amphotericin at 37°C for the first 5 hours changing the PBS every 30 minutes and the other 5 days changing the PBS every day. The decellularized matrix can be freshly used for the following recellularization or stored in – 80 °C for up to 6 months.

Quantification of DNA and Glycosaminoglycan (GAG)

To assess total DNA or GAG content within the native colon and decellularized colon matrix, 6 X 100mg (wet weight) specimens were used for the following measurements.

For DNA measurement, specimens were minced and homogenized in 1 ml lysis buffer consisting of 50 mM TriseHCl (pH 8), 50 mM EDTA, 1% SDS and 10 mM NaCl, and then digested with Proteinase K for overnight, followed by phenol/chloroform extraction.

The total DNA was precipitated and washed with 70% ethanol and dissolved in RNA-free water. Subsequently, DNA purity and concentrations were charaterized by nanodrop (Thermo Scientific 2000c).

The sulfated GAG content from both native and acellular colon tissues was quantified using Blyscan GAG Assay Kit (Biocolor, UK). GAG concentrations were calculated by the absorbance at 595 nm using a microplate reader (Tecan Infinity) and compared to standards made from bovine tracheal chondroitin-4-sulfate.

Culture of primary human colon cells

With proved of IRB at Weill Cornell Medical College, Colon biopsies (0.5-1 cm^3) without visible adenomas by pathology were obtained from patients undergoing colonoscopy screening. The techniques of isolation and primary culture of human colon epithelial cells (hCEC) were slightly modified from the previous studies. Briefly, Colonic specimens were immersed in cold X medium (HyClone) supplemented with 2 % penicillin/streptomycin, immediately after patient operative procedure and rinsed with sterile PBS with antibiotics/ antimycotic (invitrogen) for 5 times. The tissues were minced into small pieces (~1mm in size) and crypts were gently exacted by digestion in X medium containing collagenase type XI (150 U/ml, Sigma, St. Louis, MO), dispase neutral protease (40 μg/ml, Roche Applied Science), stirring at 37°C for 15-30 min. The crypt cells were cultured in X medium with growth supplements of 5% FBS, EGF (25ng/ml R&D systems), insulin (5.0 μg/ml, Sigma), hydrocortisone (1.0 μg/ml Sigma), transferring (2 μg/ml Sigma), BPE (50 μg/ml Sigma), B27 supplement (Invitrogen), R-spondin 1 (200 ng/ml, R&D systems) and Noggin (50ng/ml, Peprotech) in collagen-I coated flasks (BD scientific) incubated at 33°C, 5% CO2. After 48 hour culture,

fibroblast Inhibitory reagent (Human Colon FibrOut™ from CHI Scientific) was applied to the culture medium for 2-3 days to reduce fibroblast growth. After cell colonization was observed, cells were transfected with retroviral hTERT and followed with the characterization by 3D matrigel culture into organoid growth and expression of stem cell marker Lgr5 and differentiation markers. Co-culture with human colon fibroblasts was required to develop tight-junction in hCEC.

Human colon myofibroblasts and endothelial cells were primary cultured from the normal tissue parts of CRC patient surgical specimens and characterized by CD31 marker for endothelial cells and α-smooth muscle actin for myofibroblasts.

DNA sequencing of hCEC indicated no mutations in hotspot regions of APC, KRAS and TP53 genes and the primers are listed as following:

Oligonucleotide sequences and PCR conditions used to amplify exons 1-14 of *APC*. Amplification was performed in the 25µl amplification mixture containing 100-200ng DNA, 1.5mM $MgCl_2$, 0.2mM of each dNTP, 0.5mM of each primer and 1.25U of Taq DNA polymerase.

Exon	Primer	Sequence 5′→3′	Size (bp)	Amplification conditions*
1	F	AACCTTATAGGTCCAAGGGTAG	234bp	A
	R	ACCTCAAGTTTACAAGAGGGAA		
2	F	AAATACAGAATCATGTCTTGAAGT	212bp	B
	R	ACACCTAAAGATGACAATTTGAG		
3	F	GACCCAAGTGGACTTTTCAGG	423bp	B
	R	ACAATAAACTGGAGTACACAAGG		
4	F	GAGAAGTTTGCAATAACAACTGATG	291bp	A
	R	TTATCCTGAATTTTAATGGATTACCT		

5	F	AACCTCACTCTAACTGGACCAA	481bp	A
	R	AACAGAGCTGTAATTCATTTTATTCC		
6	F	GGTAGCCATAGTATGATTATTTCT	204bp	B
	R	CTACCTATTTTTATACCCACAAAC		
7	F	AAGAAAGCCTACACCATTTTTGC	238bp	B
	R	GATCATTCTTAGAACCATCTTGC		
8	F	GACACTTCATTTGGAGTACCTTAACA	222bp	A
	R	GGCATTAGTGACCAGGGTTT		
9	F	AGTCGTAATTTTGTTTCTAAACTC	394bp	B
	R	TTTGAAACATGCACTACGAT		
10	F	TTGCTCTTCAAATAACAAAGCAT	192bp	A
	R	TCCACCAGTAATTGTCTATGTCA		
11	F	GATGATTGTCTTTTTCCTCTTGC	215bp	B
	R	CTGAGCTATCTTAAGAAATACATG		
12	F	TGACAAAGGAAGAACAGATAGCA	390bp	B
	R	GCAGTGAGCTGAGATTGCAC		
13	F	TTTCTATTCTTACTGCTAGCATT	306bp	B
	R	ATACACAGGTAAGAAATTAGGA		
14	F	AGGGACGGGCAATAGGATAG	390bp	A
	R	GGTCTTTTTGAGAGTATGAATTCTG		

*A: an initial denaturation at 94ºC for 2min, followed by 40 cycles at 94ºC for 30", (50ºC, for exon 10, and 55ºC) for 45" and 72ºC for 1min, and a final extension step at 72ºC for 7min.

B: The touchdown PCR protocol consists on: an initial denaturation at 94ºC for 2 min, followed by 3 cycles (94ºC for 30s, 60ºC for 40s and 72ºC for 30s), 3 cycles (94ºC for 30s, 58ºC for 40s and 72ºC for 30s), 25 cycles (94ºC for 30s, 55ºC for 40s and 72ºC for 30s) and a final extension step at 72ºC for 7 min.

15-1 5'GTTACTGCATACACATTGTGAC3'
5'TGTGGTTGGAACTTGAGGTG3'
1375bp 15 IVS15-54 -3275

15-2 5'CAGATGAGCAGTTGAACTC 3'
5'GATTTGGTTCTAGGGTGC 3'
907bp 15 3095-4001

15-3 5’ACAGGAAGCAGATTCTGC 3’
5’GAGCCTCATCTGTACTTCTGC3’
1223bp 15 3879-5101

15-4 5’AGTGATCTAACAATCGAATCC3’
5’CACCCTTGAGTCTTGAAGGG3’
1204bp 15 4972-6175

*** *KRAS* mutational analysis by PCR & sequencing**

The genomic region harboring mutational sites was amplified using three different primer data set to obtain respectively 198 bp, 181 bp and 162 bp amplicons:

* *KRAS* 198 bp forward: 5´ GGTACTGGTGGAGTATTTGATAGTG 3´ and reverse: 5´ GTTGGATCATATTCGTCCACAA 3´

* *KRAS* 181 bp forward: 5´ GGTACTGGTGGAGTATTTGATAGTG 3´ and reverse: 5´ CCACAAAATGATTCTGAATTAGC 3´

* *KRAS* 162 bp forward: 5´ TGTAAAACGACGGCCAGTGGCCTGCTGAAAATGACTGAA 3´and reverse: 5´ CAGGAAACAGCTATGACCGGTCCTGCACCAGTAATATGC 3´

PCR was performed in 50-µl reaction volumes containing 1X AmpliTaq ® Gold DNA Polymerase Buffer (Applied Biosystems, CA, USA); 2 mM of $MgCl_2$; 0.02 mM of each deoxynucleotide; 0.2 µM of each primer; 5 units AmpliTaq Gold ® DNA Polymerase (Applied Biosystems) and 80 ng of DNA template. PCR reactions to amplify *KRAS* 198-bp amplicons were performed by incubating the samples at 95°C for 10 min, followed by 40 cycles of 95°C for 30 s, 58°C for 30 s and 72°C for 1 min. The final extension step was performed for 10 min at 72°C and the samples were then chilled to 4°C. The amplification of *KRAS* 181-bp and 162-bp PCR fragments was obtained with the same conditions, but using 2.5 mM $MgCl_2$. PCR reactions were run in a Veriti PCR apparatus (Applied Biosystems).

The sequence data were analyzed using the Sequencer software Version 4.8 (Gene Codes Corporation, MI, USA) to identify mutations and to assign genotypes to individual DNA samples. The identified DNA changes were compared with a reference sequence of *KRAS* (Gene Bank accession NM_004449.3). Sequence results were scored by visual inspection of the chromatograms, performed by three independent analysts (Nicola Normanno, Pietro Carotenuto, Cristin Roma or Anna Maria Rachiglio). A mutation was called when three independent observers agreed.

*** *TP53* mutational analysis by PCR & sequencing**

DNA fragments were amplified by PCR using primer pairs previously described (http://www-p53.iarc.fr), with the exception of the primers used to sequence exons 2 and 3 (Table S1).

Lentivirus transduction of primary hCEC.

The lentiviral vector pEco-CMV-H1-shRNA-GFP encoding a shRNA hairpin sequence (5"-gatccccGCTCTGCTGCCCATACACAttcaagagaTGTGTATGGGCAGCAGAGCtttttggaaa-3" and 5"-agcttttccaaaaaGCTCTGCTGCCCATACACAtctcttgaaTGTGTATGGGCAGCAGAGCggg-3".) was used for knockdown of APC expression. The psi-LVRH1GP (CMV-H1-APC shRNA-SV40-KRAS^{G12D} - neomycin) encoding both APC- shRNA hairpin sequence and human KRAS^{G12D} sequence was used for knockdown of APC expression and over-expression of KRAS ^{G12D} in hCEC. To generate the lentiviral vectors, the above plasmids were transfected into HEK293T cells with the Gentarget lentivirus packaging mix (GenTargetInc, San Diego, CA) according to the manufacturer's protocol. High titer virus particles were used to transduce hCEC in serum free conditions and the efficiency

of APC knockdown and KRAS expression was verified by Western Blotting after antibiotic selection.

Recellularization of acellular colon matrix

The mucosa layer of decellularized colon matrix was physically separated from submucosa by forceps and seeded human endothelial cells by microinjection of 1000 cells/side into four sides of 1 cm^3 mucosa layer. After 5 days culture in endothelial cell medium, 0.2 million hCEC were planted to the 1 cm^3 mucosa evenly with cells seated in crypt niches and cultured for 10 days in epithelial cell medium with 1:1 matrix of endothelial cell basal medium. The myofibroblasts were seeded in the opposite surface of mucosa and continue culturing for another 10-15 days. Last, the mucosa layers were assembled with submucosa part and returned back to culture in epithelial cell medium with 1:1 matrix of endothelial cell basal medium for certain time until developing CRC in different stages.

Establishment of SB – TIM system in hCEC

Insertion of CMV-GFP-Puromycin into T2/Onc vector

- Use BglII and BsaBI to cut T2/Onc vector.

Double Digest Recommendation(s) for BglII + BsaBI:

- Digest in NEBuffer 3 at 37°C with BglII, then add BsaBI and raise temperature to 60°C.

  At least one enzyme has < 100% activity in this buffer, so additional units of enzyme and/or longer incubation time may be necessary.
- Design PCR primers with BgLII and BsaBI ends for the CMV-GFP-Puro: add BglII in CMV end and BsaBI in Puromycin end.

LEFT PRIMER TGACCTTACGGGACTTTCCTAC
RIGHT PRIMER CAGCGTATCCACATAGCGTAAA
PRODUCT SIZE: 2754, PAIR ANY COMPL: 5.00, PAIR 3' COMPL: 2.00

So the end with BglII is: 5'- agatctTGACCTTACGGGACTTTCCTAC– 3'

GC% = 46%, Tm = 60C

The end with BsaBI is: 5'- gatnnnnatcCAGCGTATCCACATAGCGTAAA – 3'

(in T2/Onc VECTOR the BsaBI site is 5'… gattatgatc … 3')

= 5'- GATTATGATCCAGCGTATCCACATAGCGTAAA – 3'

GC% = 41%, Tm = 61C

TOTAL LENGTH IS 2754bp

Perform PCR amplification of the DNA piece of CMV-GFP-Puro with BglII and BsaBI ends

PCR conditions:

Initial denaturation: 95 C for 2 min

30 cycles: 95C for 30S

55 C for 30S

68 C for 4 min

Final extension: 72C for 7 min

Hold: 4 C

Ligation of the two DNA fragments by T4 ligase

The Schema map of T2/Onc – CMV-GFP-Puro

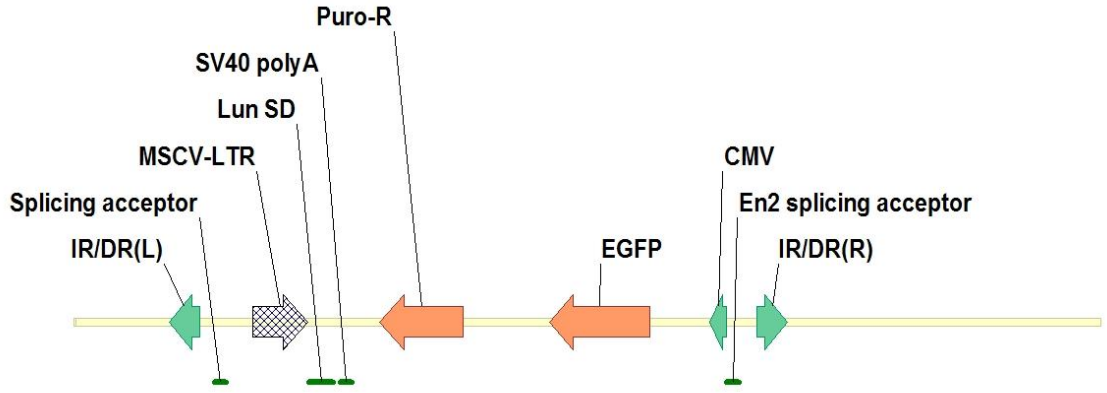

pT2/Onc2-PURO-EGFP

7362 bp

Transfection of hCEC

50,000 hCEC cells with APC shRNA were seeded into 24 well plates one day prior to transfection. 500 ng transposon T2/Onc – GFP-Puro and 100 ng transposase SB 100X were used to transfect hCEC in each well with presence of Lipofectamine 3000 (invitrogen) and after 3 days incubation, cells were transferred into collagen-I coated flasks for continuing culture starting with puromycin selection. After 3 weeks antibiotic selection, the hCEC cells were used immediately for populating the 3D colon matrix.

Laser-capture microdissection

The cells undergoing submucosal invasion were harvested by laser-capture microdissection according to the company instruction (Carl Zeiss MicroImaging, Germany) and DNA was exacted from the samples using QIAamp DNA MicroKit (#56304, Qiagen).

LM-PCR amplification and preparation for illumina sequencing

Restriction digest

1. Digest 1µg of tumor DNA with *Nla*III (IRR) or AluI (IRL). Do not use more than 2 µg of genomic DNA as this
will lead to concatomerization of genomic fragments during the ligation step. Less than 1 µg of genomic
DNA can be used, but the final volume should be scaled to maintain a similar DNA concentration in the
reaction.
1 µL enzyme
4 µL buffer
4 µL 10X BSA (if needed)
X µL H2O
Y µL DNA
20 µL Total

2. Incubate at least 3 hours at 37°C.

3. Heat inactivate enzyme.
The restriction digest can be incubated overnight. In this case, heat inactivation of the enzyme is not required.
However, overnight incubation should be performed in a 37°C incubator (not a water bath) to prevent

evaporation of the sample.

Ligation

1. Prepare the adaptor by mixing the linker+ and linker- primers (each at 100μM) at a 1:1 ratio (see below for
primer details). Linkers should be re-suspended at 100μM when stored. Heat the primer solution at 95°C
for 5 minutes. Turn off the heat and allow the primers to slowly cool to room temperature. This allows the
single-stranded oligos to anneal and form the double-stranded adaptor.
2. Set up ligations:
10.0 μL digested genomic DNA
2.0 μL 10X NEB buffer 4
2.0 μL 10 mM ATP
1.5 μL adaptor
1.0 μL T4 ligase (2,000U)
3.5 μL dH2O
20.0 μL Total
ligate 2-3 hours at room temperature or overnight at 16°C
3. Heat inactivate the T4 ligase (65°C for 10 minutes).
4. Digest ligation with *BamHI*. This prevents the fragment from transposons within the concatomer from being
amplified. *BamHI* solution is made in a 10μL volume per tube. To each tube add:
1.0 μL *Bam*HI
1.0 μL NEB Buffer 4
3.0 μL 10X BSA
5.0 μL dH2O
10.0 μL Total
If the digest ligation is performed overnight at 37**°**C then column purification is not required as the *Bam*HI has degraded. Otherwise, a column purification is needed to remove the *Bam*HI enzyme.

PCR

2.00 μL ligation reaction Step 1 98°C 30 seconds
10.00 μL 5X buffer
1.00 μL 10 mM dNTPs Step 2 98°C 10 seconds
1.50 μL primer 1 (10 μM) 63°C 20 seconds
1.50 μL primer 2 (10 μM) 72°C 30 seconds
0.25 μL Phusion polymerase (NEB) repeat Step 2 for 25 cycles
33.75 μL H2O
50.00 μL Total Step 3 72°C 2 minutes
Hold at 4°C
- dilute 3 μL of PCR reaction in 147 μL H2O (1:50 dilution)
- store remaining primary PCR reaction at 4°C
Set up secondary PCR
4.00 μL diluted primary PCR (diluted 1:50 in H2O)
20.00 μL 5X buffer
2.00 μL 10 mM dNTPs
3.00 μL nested primer 1 (10 μM)

3.00 µL nested primer 2 (10 µM)
1.00 µL Phusion polymerase (NEB)
67.00 µL H2O
100.00 µL Total
- perform PCR using the same cycle conditions as primary PCR (25 cycles)

- Analyze 25 µL of PCR product on 1.5% agarose gel.
- Purify remaining PCR product to remove excess primers/dNTPs.
- Determine concentration of purified PCR products (Nanodrop or UV spec is sufficient)
- Pipet 25 ng of each PCR product pool into a single tube to be run on a single lane on the Illumina
- platform
- Adjust the final concentration of the mixed sample to be ~20-25 ng/µL.
- Incubate the diluted products at 37-42°C for 30 minutes
- Submit sample for sequencing

Primers to generate adaptors:
IRDRR adaptor
NlaIII linker+ 5'-GTAATACGACTCACTATAGGGCTCCGCTTAAGGGACCATG-3'
NlaIII linker- 5'-Phos-GTCCCTTAAGCGGAG-C3spacer-3'
IRDRL adaptor
AluI linker+ 5'-GTAATACGACTCACTATAGGGCTCCGCTTAAGGGAC-3'
AluI linker- 5'-Phos-GTCCCTTAAGCGGAG-C3spacer-3'
All adaptor primers are resuspended in STE* buffer at 100µM. All PCR primers were used at 10 µM
concentration. C3spacer modification is available from Integrated DNA Technologies.

Primers for IRR amplification (NlaIII-digested DNA):
Primary PCR
IRR 5'GGATTAAATGTCAGGAATTGTGAAAA 3'
linker primer 5'GTAATACGACTCACTATAGGGC 3'

Primers for IRL amplification (BfaI and AluI-digested):
Primary PCR
IRL 5'AAATTTGTGGAGTAGTTGAAAAACGA 3'
linker primer 5'GTAATACGACTCACTATAGGGC 3'

Secondary PCR (for IRR and IRL)
IR-A1
5'AATGATACGGCGACCACCGAGATCTACACTCTTTCCCTACACGACGCTCTTCCGATCT
(barcode)TGTATGTAAACTTCCGACTTCAACTG
Linker-A2
5'CAAGCAGAAGACGGCATACGAGCTCTTCCGATCTAGGGCTCCGCTTAAGGGAC 3'

Then the DNA samples are ready for direct illuma sequencing

CIS analysis

For analysis of transposon insertion sites, ligation-mediated PCR (LM-PCR) was performed to specifically amply the transposon integrated genomic fragments which were then sequenced by illumine sequencing. Low mapping quality reads (values less than 30) were filtered out for the following analysis. Among the high mapping quality reads, about half of them were mapped at the “TA” dinucleotide sites. Further analysis was focused on these consensus SB insertion sites. From the distribution of read depth at the insertion sites, it was clear that majority of the insertion sites resulted from background insertion events or PCR artifacts. We considered the top 10% of the deepest insertion sites as clonal insertion sites. We mapped these clonal insertion sites in each sample to the human genome annotation file, refGene, and picked the sites that were within 1000bp of known transcripts in refGene. In addition to this, big dye terminator sequence was used to confirm the transposon insertion sites.

Knockdown candidate genes through siRNA

siRNA was used to knockdown expressions of candidate genes in hCEC or SW480 cells with Lipofectamine RNAiMAX (invitrogen) and Q-PCR was used to test the knockdown efficiency.

Gene symbol	Q-PCR primers	siRNA sequences
PAX7-F	GGAGGATGAAGCGGACAAGAAG	GCGAGAGCGAGAGAAUAAAUAUATA
PAX7-R	AGGTCAGGTTCCGACTCCACAT	AGAAUCAAGUUCGGGAAGAAAGAGG
LATS2-F	GTTCTTCATGGAGCAGCACGTG	GGAACUCAGUUUAACUAUUAUUUAT
LATS2-R	CTGGTAGAGGATCTTCCGCATC	CCCGAGGAAUGAGCAGAUUGUGCGG
RPAP1-F	GGATAGCCTCACTGCTCACTCT	AGAGAACAUAGCAAGACUGCAGGCC
RPAP1-R	CAGACACCTGTGTCCAAGTGAC	GGAGUGAAGAGUGGCUUAGCUAUTT
CSTF3-F	CTCTTCGTACAGAGGATCAGACC	ACUGUACAUUGAAGCAGAGGUUACT
CSTF3-R	CTTGACTGCTCAAGATACTGGGC	CGCACGUUGUAAUCAGCUGAGGCCA
PRKG1-F	GAGTTGGAGGTTTCGGACGAGT	AGAUUACUAUGGUACAGAAACUGGG
PRKG1-R	GATGTGCTCCTGCTGTCTTGTG	GGGAUAUAGACUUCUAAUGUAUUTC
CAMTA1-F	CATCTCCAACTCGGTGGTGTTTG	ACCGAAGUUAUAAGAAAUGUGGCAA
CAMTA1-R	CTCTCCATCTGCTCCAGTCGTT	GGAAUUCCAAAGAUCUUUACAUUGG
DDX20-F	AATCAGCGTCTTGATGCTATGGC	CCCAGAAAUGUAAUAUCAACCUUCT
DDX20-R	ACAACCAGATTCACCTTCTCAGC	ACAAAGUACAUGAGAGAUCCCACTT
MITF-F	GGCTTGATGGATCCTGCTTTGC	CCAAGUACCACAUACAGCAAGCCCA
MITF-R	GAAGGTTGGCTGGACAGGAGTT	CCAAGUACCACAUACAGCAAGCCCA
ASXL2-F	GGACAGAATCCAGGTGCGAAAAG	GGAGACUAAUAUGAAAGAACCUCTA
ASXL2-R	GATGGAGACTGGAAAACGAGCC	GCCAUGGAAAGAACAAUUCUUUGAA
FXR1-F	GGTCTCGTAGACGAAGGACTGA	GGACUAAUAUGAACAGCAAAUUGGA
FXR1-R	TGTCTGCTCTGAGACTCAGCTC	CGCUACUUACAAUGAAAUAGUCACA

FIGURES

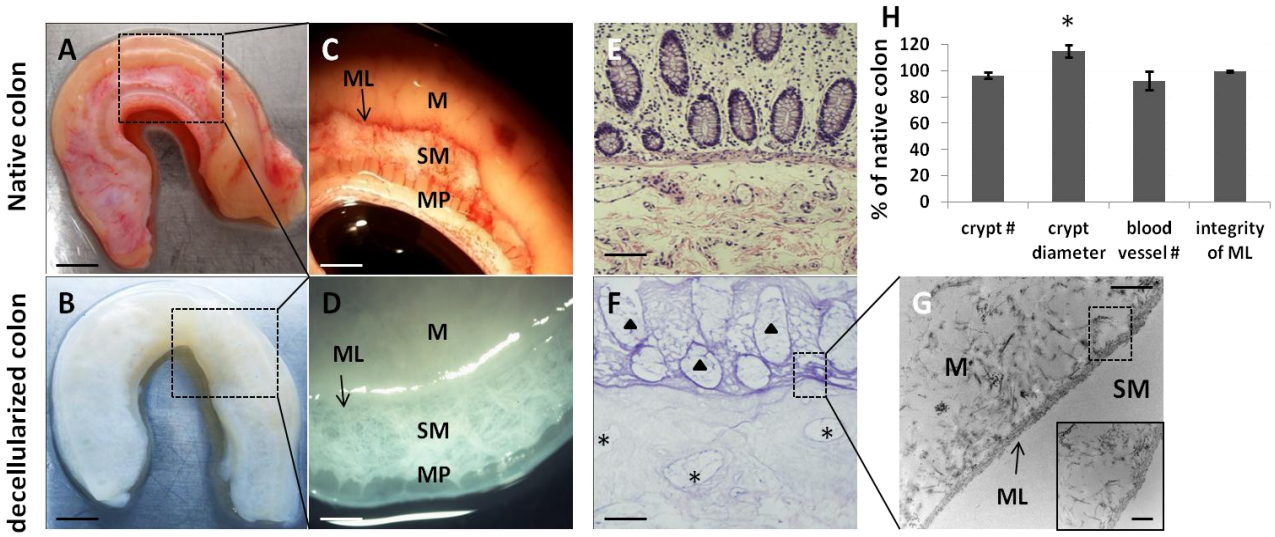
Native colon
decellularized colon
A
B
C
D
ML
M
SM
MP
E
F
G
H
% of native colon
120
100
80
60
40
20
0
*
crypt #
crypt diameter
blood vessel #
integrity of ML

I

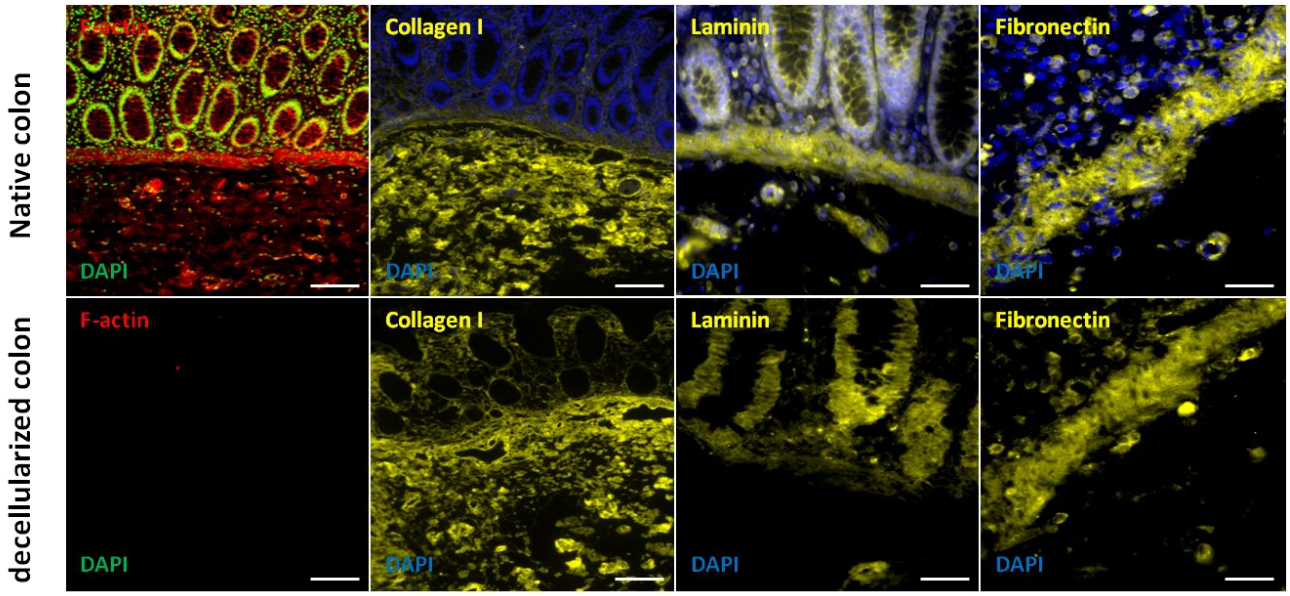
Native colon
decellularized colon
F-actin
Collagen I
Laminin
Fibronectin
DAPI

Figure 1. Preparation and characterization of acellular human colon matrix. (B) and (D) representative images of decellularized human colon; comparison with **(A) and (C)** native human colon tissues. H+E staining of decellularized colon matrix **(F)** and native colon tissue **(E),** Acellular colon matrix well preserved vasculature (Asterisks), &crypt niches (Triangles). **(G)** Electron microscope image of acellular mucosa preserved integral muscularis layer (ML); **M:** mucosa area; **SM:** submucosa area. **(H)** Quantification of crypt numbers and diameters, blood vessel number and ML integrity in native tissue and acellular matrix. **(I)** Representative immunostaining images of left to right: F-actin for cell skeleton, DAPI for cell nuclei, collagen-I, laminin and fibronectin in acellular matrix (down) and native tissues (up).

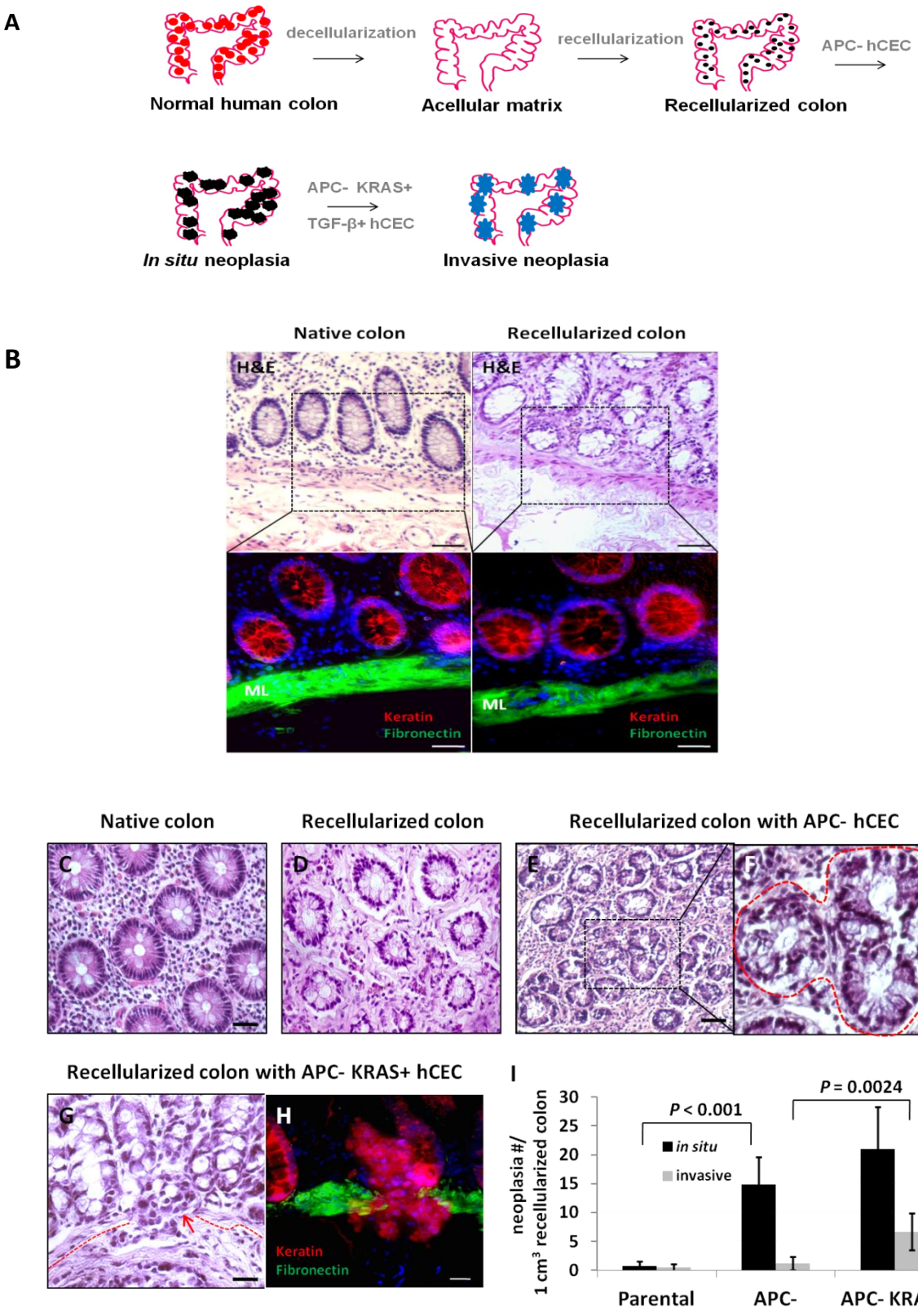
A
decellularization
recellularization
APC- hCEC
Normal human colon
Acellular matrix
Recellularized colon
APC- KRAS+
TGF-β+ hCEC
In situ neoplasia
Invasive neoplasia
B
Native colon
Recellularized colon
H&E
H&E
ML
Keratin
Fibronectin
ML
Keratin
Fibronectin
Native colon
Recellularized colon
Recellularized colon with APC- hCEC
C
D
E
F
Recellularized colon with APC- KRAS+ hCEC
G
H
Keratin
Fibronectin
I
P < 0.001
P = 0.0024
in situ
invasive
neoplasia #/
1 cm³ recellularized colon
30
25
20
15
10
5
0
Parental
APC-
APC- KRAS+

Figure 2. Creation of organotypic human colon model and transformation into CRC cancer models. (A) Schematic of creating ex vivo colon model through recellularization and transforming normal colon models into CRC models; **(B)** representative images of H+E staining (up) and dual immunostaining (down) of cytokeratin & fibronectin in recelluarized colon or native colon tissues. **ML:** Muscularis layer; Representative images of native colon **(C),** recellularized colon with hCEC **(D),** APC-null hCEC **(E) & (F),** APC-null-KRAS-overexpression hCEC which is also treated with TGF-β **(G) & (H). (I)** Quantification of in situ neoplasia and invasive neoplasia.

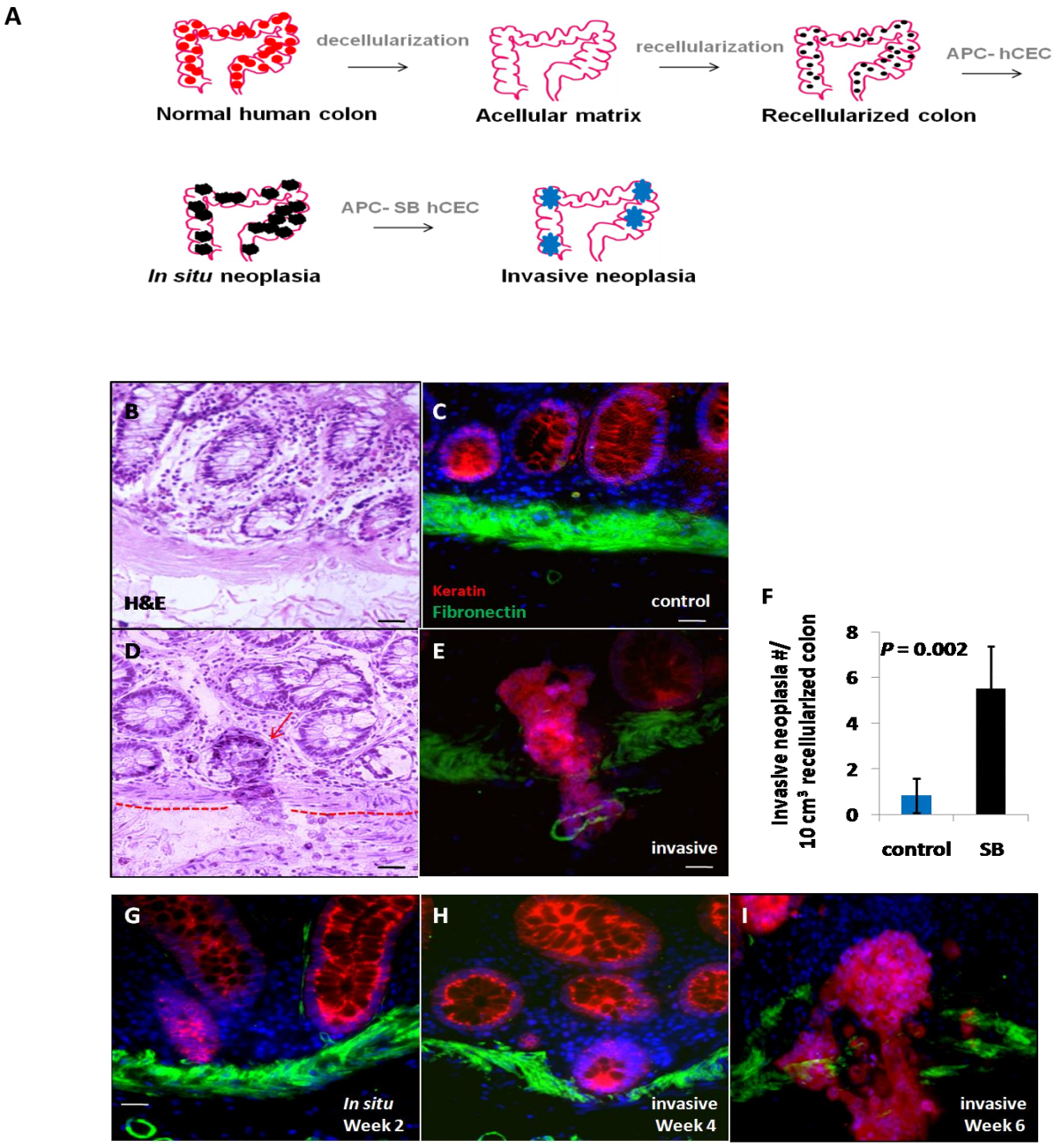

Figure 3. Invasive adenoma induced by SB transposon-based mutagenesis. (A) Schematic of different stage CRC models induced by SB transposon-based mutagenesis; Representative images (H+E in **B & D**; immunostaining of keratin & fibronectin in **C & E**) of CRC models recellularized with APC-null hCEC transfected with SB transposition system (down) or only SB transposon donor plasmids (up, as negative control). **(F)** Quantification of invasive neoplasia formation in the samples with SB mutagenesis system or in the negative control. **(G-I)** representative images (dual immunostaining in keratin & fibronectin) of neoplasia progression from in situ to submucosal invasion.

Gene symbol	Number of insertions *	Invasive neoplasia with insertions **	Predicted effects on gene ***	Function
AKTIP	1	1	Loss	AKT signaling
DCC	1	1	Loss	Cell adhesion/apoptosis signaling
EPHB1	1	1	Loss	Cell migration and adhesion
EPHB2	1	1	Loss	Cell migration and adhesion
FSTL5	1	1	NP	Calcium ion binding
JAK1	1	1	NP	STAT signaling
LATS2	2	2	Loss	P53 signaling
MAML3	1	1	Loss	*NOTCH* signaling
MSH2	1	1	Loss	DNA mismatch repair
NRCAM	1	1	NP	Cell adhesion
PTPRD	2	3	Loss	Cell growth and differentiation
ROCK1	1	1	Gain	Cell motility
STAT3	1	1	Gain	STAT signaling
TCF7L2	1	2	NP	*WNT* signaling
TTN	1	1	NP	Cell motility
TWIST2	1	1	NP	Epithelial to mesenchymal transition
WNT9B	1	1	Gain	*WNT* signaling

Table 1. Candidates have been previously identified as malignancy driving genes in CRC. * copy number of transposons inserted in each gene; ** number of invasive neoplasia with the same insertion. *** Genetic functions affected by transposon insertions.

A

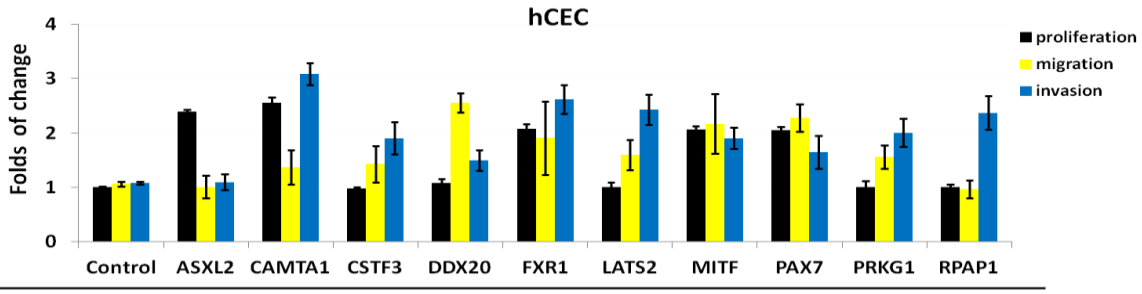

	Control	ASXL2	CAMTA1	CSTF3	DDX20	FXR1	LATS2	MITF	PAX7	PRKG1	RPAP1
Proliferation		+	+			+		+	+		
Migration					+			+	+		
Invasion			++			+	+			+	+

+: two folds; ++: three folds

B

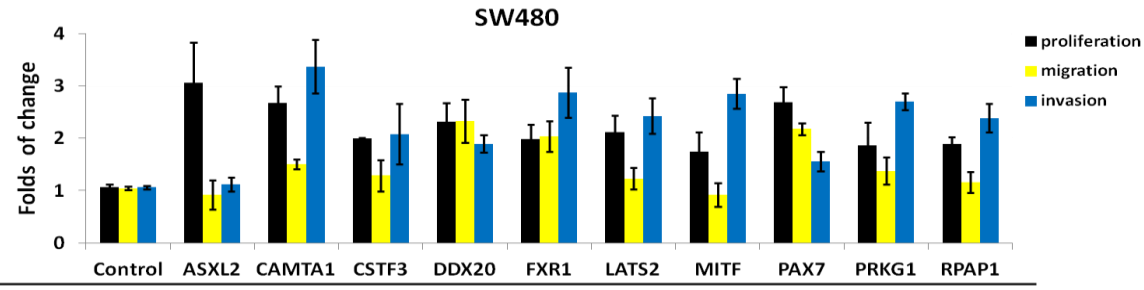

	Control	ASXL2	CAMTA1	CSTF3	DDX20	FXR1	LATS2	MITF	PAX7	PRKG1	RPAP1
Proliferation		++	+		+		+		++		
Migration					+	+			+		
Invasion			++	+		+	+	+		+	+

+: two folds; ++: three folds

Figure 4. In vitro and ex vivo functional validation of candidate genes. Evaluated the effects of 10 genes on APC-null hCEC **(A)** or colon cancer cell line SW480 **(B)** in cell proliferation, migration and invasion through matrigel in Boyden chamber, when gene expressions were down regulated by siRNA.

Supplementary Figures

	Native human colon tissue (n=6)	Acellular human colon tissue (n=6)	p-value
DNA (ng/mg wet weight)	**432.7 ± 35.3**	**17.8 ± 5.0**	**< 0.0001**
GAG (ng/mg wet weight)	**50.4 ± 5.2**	**46.5 ± 4.1**	**0.085**
SDS	**N.A.** *	**N.D.** **	**N.A**
Triton-100	**N.A.**	**N.D.**	**N.A**

*** Value Not Available**

**** Value Not Distinguishable from Zero.**

Supplementary Table 1. Molecular characterization of acellular human colon matrix.

A

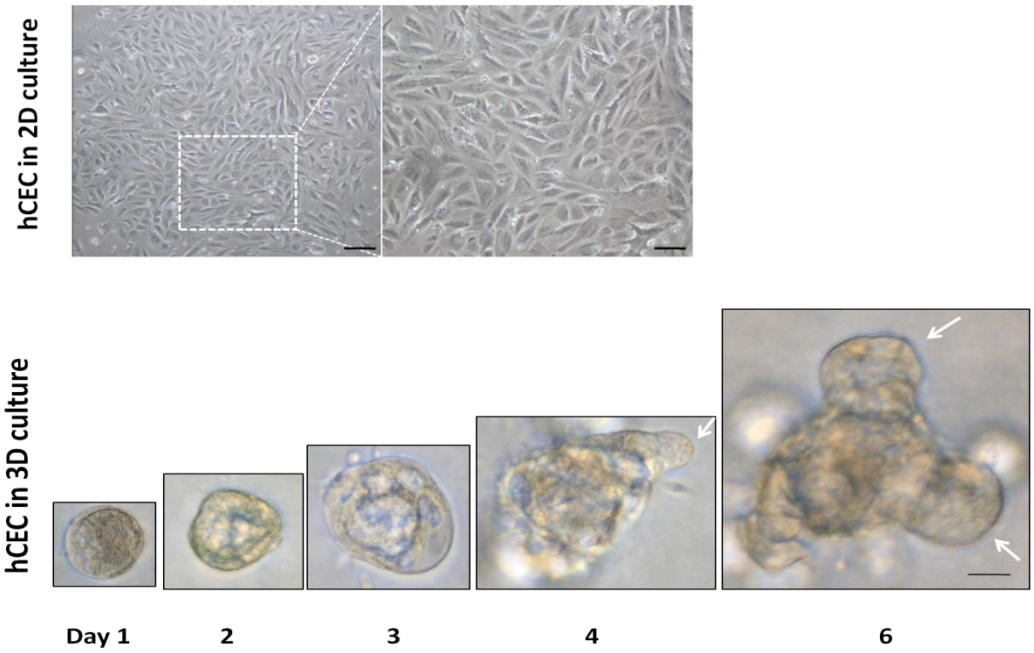
hCEC in 2D culture
hCEC in 3D culture
Day 1
2
3
4
6

B

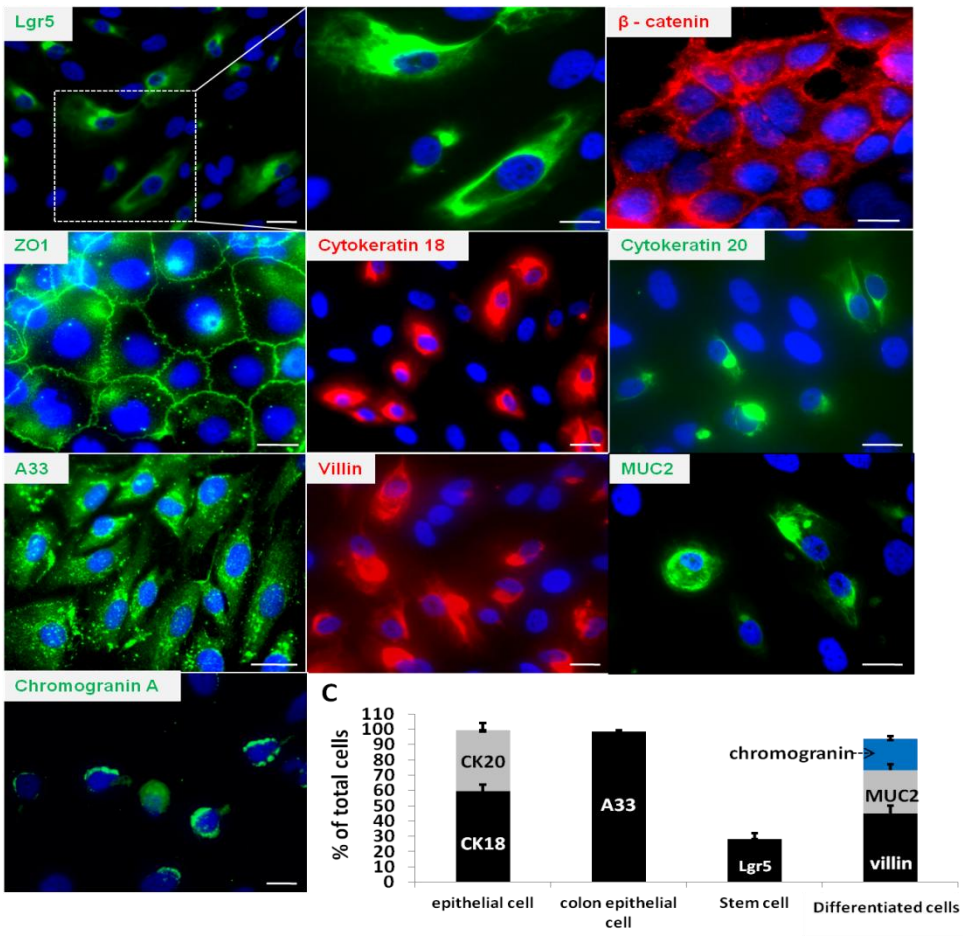
Lgr5
β - catenin
ZO1
Cytokeratin 18
Cytokeratin 20
A33
Villin
MUC2
Chromogranin A
C
% of total cells
CK20
CK18
A33
Lgr5
chromogranin
MUC2
villin
epithelial cell
colon epithelial cell
Stem cell
Differentiated cells

Supplementary Fig 1. Characterization of primary human colon epithelial cells (hCEC). (A) representative images of hCEC cells in 2D flask culture or 3D matrigel culture. In matrigel culture, (left to right) individual hCEC progressively form organiod-type structure. **(B)** Expressions of stem cell marker Lgr5, epithelial markers cytokeratin 18 & 20, zonula occludens-1 (ZO-1), A33, and differentiation markers villin, mucin 2 and chromogranin; **(C)** Quantification of stem cells and differentiated functional cells.

A

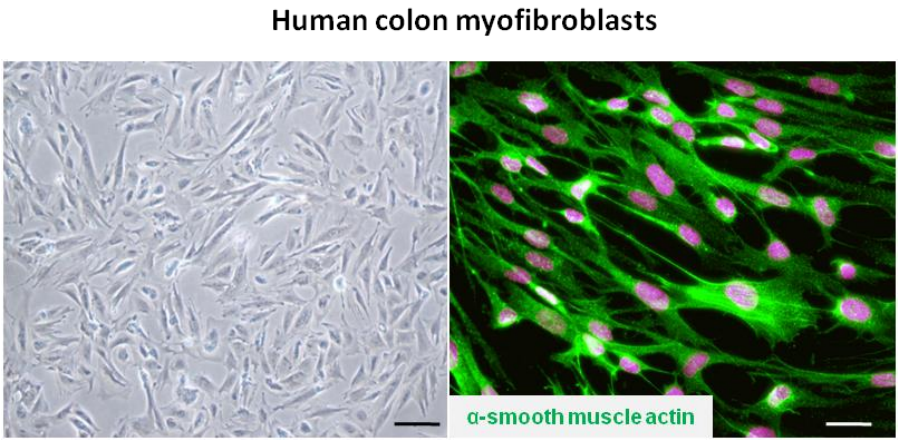

B

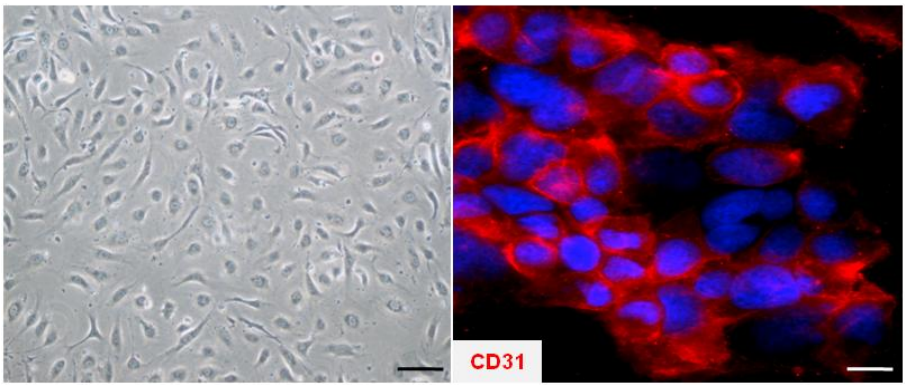

Supplementary Fig 2. Characterization of primary human colon microvascular endothelial cells and fibroblasts. (A) Primary cultured colon fibroblasts in light microscope (left) or stained with anti-α smooth muscle actin (right). **(B)** Primary cultured colon microvascular endothelial cells in light microscope (left) or stained with anti-CD31 (right).

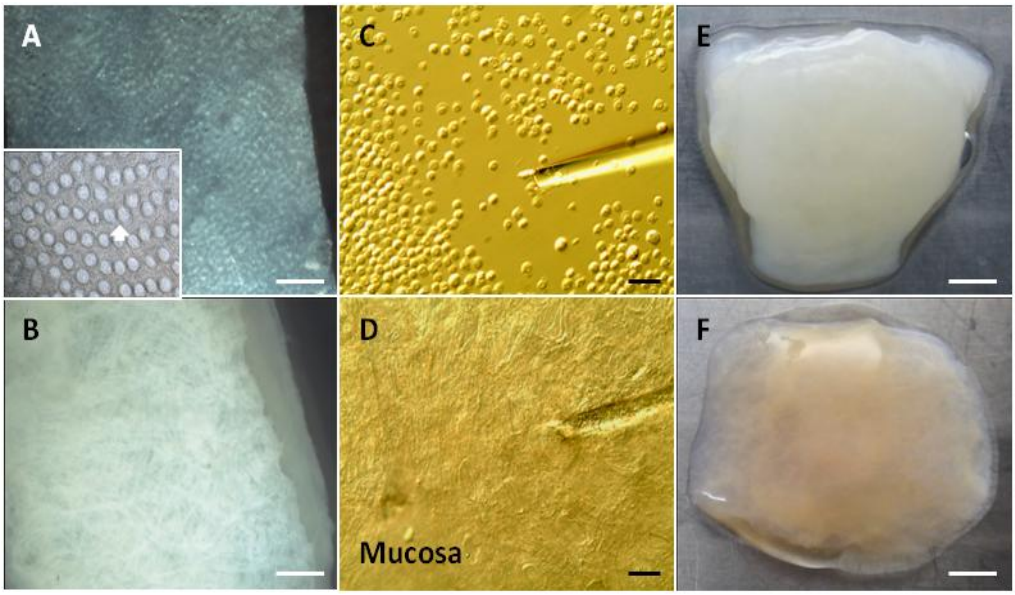

Supplementary Fig 3. Engineering organotypic human colon model through microinjection

The acellular colon matrix was physically separated into mucosa layer **(A)** with 20x in big window and 40 x in small window, and submucosa layer **(B);** white arrow designated the intact epithelial crypt niches. **(C)** And **(D)** representative images of the microinjection procedure that the endothelial cells was microinjected into mucosa layer. **(F)** Colon matrix was populated with hCEC, endothelial cells and fibroblasts after 4 week in vitro culture, compared to the acellular matrix **(E).**

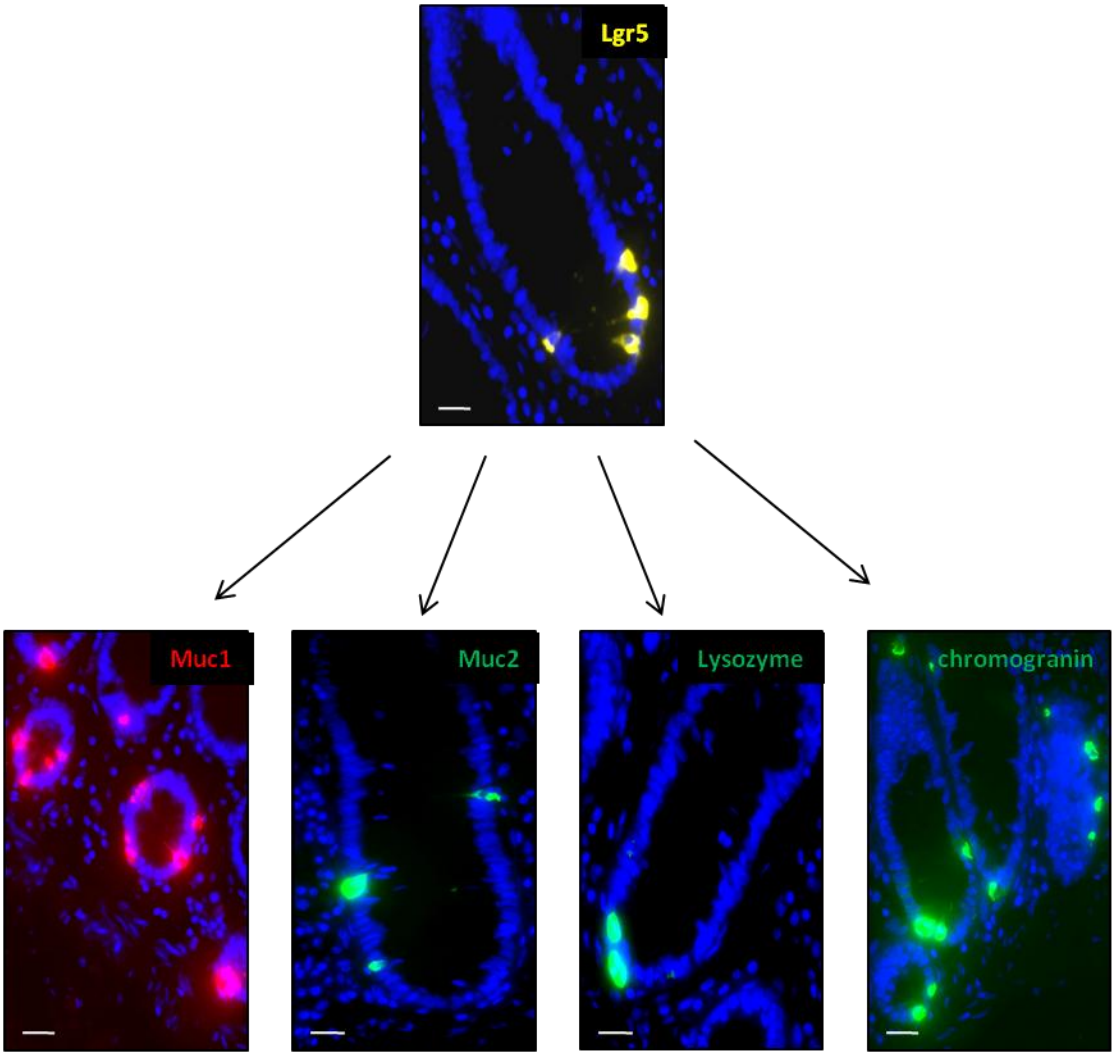

Supplementary Fig 4. Molecular characterization of physiological active crypts recellularized with hCEC. Immunostaining of intestinal stem cell marker Lgr5, and other differentiation biomarkers (MUC1 for non-terminally differentiated colonic epithelial cells MUC2 for goblet cells; Lysozyme for paneth cells; chromogranin for enteroendocrine) in the colon models recellularized with immortalized hCEC.

A

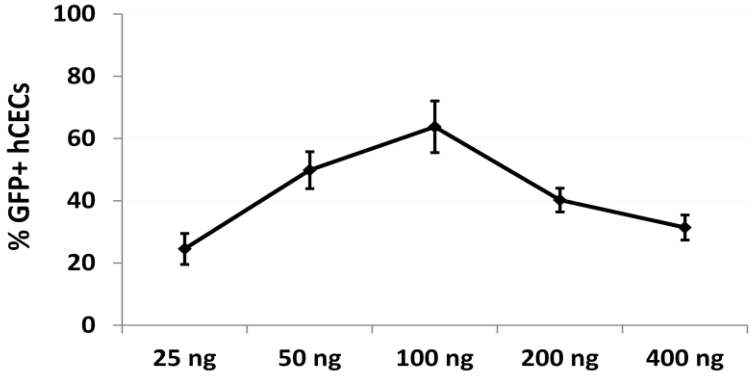

B

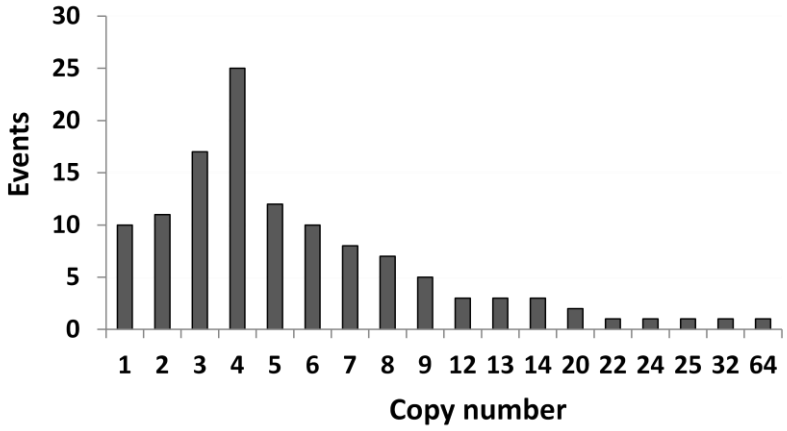

Supplementary Fig 6. Creation of transposition system by T2/Onc and SB100X in hCEC. (A) quantification of transposition activity in fixed dose of tranposon-donor plasmids (500 ng of T2/Onc) under variant doses of transposase-plasmids (SB 100X); **(B)** average transposon copy numbers in hCEC individual colonies.

Supplementary Table 2. Candidate genes identified by *SB* – based forward genetics screen. * listed in TCGA – colon cancer database; ** identified as driver genes in Dvoli et, al list

Gene symbol	Chromosome	Number of insertions	Invasive neoplasia with insertions	Mutation in TCGA*	Identified as driver genes in Dvoli et.al list**
AFF3	2	1	1	X	
AKTIP	16	1	1	X	
ANTXR1	2	1	1	X	
ASXL2	2	1	1	X	X
CAMTA1	1	1	1	X	
CSTF3	11	1	2	X	
DBF4	7	1	1	X	
DCC	18	1	1	X	
DDX20	1	1	1	X	
DENND2C	1	1	1	X	
DMXL2	15	1	1	X	X
EPHB1	3	1	1	X	
EPHB2	1	1	1	X	
FGF13	X	1	1	X	
JAK1	1	1	1	X	
SFI1	22	1	1	X	
FSTL5	4	1	1	X	
FXR1	3	1	1	X	X
GRM8	7	1	2	X	
KDM2B	12	1	2	X	
LATS2	13	2	2	X	
LPP	3	1	1	X	
MAML3	4	1	1	X	
MITF	3	1	1	X	
MSH2	2	1	1	X	X
NRCAM	7	1	1	X	
PAX7	1	1	2	X	
PDE4DIP	1	1	1	X	
PRKG1	10	1	1	X	
PTPRD	9	2	3	X	
ROCK1	18	1	1	X	
RPAP1	15	1	1	X	
SEMA6D	15	1	1	X	
SFI1	22	1	1	X	
STAT3	17	1	1	X	
SUPT3H	6	1	1	X	
TCF7L2	10	1	2	X	X
TTN	2	1	1	X	
TWIST2	2	1	1	X	
WNT9B	17	1	1	X	

REFERENCE

1. Arrowsmith, J., *Trial watch: Phase II failures: 2008-2010.* Nat Rev Drug Discov, 2011. **10**(5): p. 328-9.

2. Bates, R.C., *Colorectal cancer progression: integrin alphavbeta6 and the epithelial-mesenchymal transition (EMT).* Cell Cycle, 2005. **4**(10): p. 1350-2.

3. Bates, R.C. and A.M. Mercurio, *The epithelial-mesenchymal transition (EMT) and colorectal cancer progression.* Cancer Biol Ther, 2005. **4**(4): p. 365-70.

4. Brett, B.T., et al., *Novel molecular and computational methods improve the accuracy of insertion site analysis in Sleeping Beauty-induced tumors.* PLoS One, 2011. **6**(9): p. e24668.

5. Cancer Genome Atlas, N., *Comprehensive molecular characterization of human colon and rectal cancer.* Nature, 2012. **487**(7407): p. 330-7.

6. Chen, H.J., et al., *Chemokine 25-induced signaling suppresses colon cancer invasion and metastasis.* J Clin Invest, 2012. **122**(9): p. 3184-96.

7. Collier, L.S., et al., *Cancer gene discovery in solid tumours using transposon-based somatic mutagenesis in the mouse.* Nature, 2005. **436**(7048): p. 272-6.

8. Collier, L.S. and D.A. Largaespada, *Hopping around the tumor genome: transposons for cancer gene discovery.* Cancer Res, 2005. **65**(21): p. 9607-10.

9. Collier, L.S. and D.A. Largaespada, *Transforming science: cancer gene identification.* Curr Opin Genet Dev, 2006. **16**(1): p. 23-9.

10. Copeland, N.G. and N.A. Jenkins, *Harnessing transposons for cancer gene discovery.* Nat Rev Cancer, 2010. **10**(10): p. 696-706.

11. Crapo, P.M., T.W. Gilbert, and S.F. Badylak, *An overview of tissue and whole organ decellularization processes.* Biomaterials, 2011. **32**(12): p. 3233-43.

12. de Jong, G.M., et al., *Animal models for liver metastases of colorectal cancer: research review of preclinical studies in rodents.* J Surg Res, 2009. **154**(1): p. 167-76.

13. Deveney, C.W., et al., *Establishment of human colonic epithelial cells in long-term culture.* J Surg Res, 1996. **64**(2): p. 161-9.

14. Dupuy, A.J., et al., *Mammalian mutagenesis using a highly mobile somatic Sleeping Beauty transposon system.* Nature, 2005. **436**(7048): p. 221-6.

15. Dupuy, A.J., et al., *A modified sleeping beauty transposon system that can be used to model a wide variety of human cancers in mice.* Cancer Res, 2009. **69**(20): p. 8150-6.

16. Francia, G., et al., *Mouse models of advanced spontaneous metastasis for experimental therapeutics.* Nat Rev Cancer, 2011. **11**(2): p. 135-41.

17. Gilbert, T.W., T.L. Sellaro, and S.F. Badylak, *Decellularization of tissues and organs.* Biomaterials, 2006. **27**(19): p. 3675-83.

18. Gomes, C.C., et al., *Assessment of TP53 mutations in benign and malignant salivary gland neoplasms.* PLoS One, 2012. **7**(7): p. e41261.

19. Gout, S. and J. Huot, *Role of cancer microenvironment in metastasis: focus on colon cancer.* Cancer Microenviron, 2008. **1**(1): p. 69-83.

20. Grabundzija, I., et al., *Comparative analysis of transposable element vector systems in human cells.* Mol Ther, 2010. **18**(6): p. 1200-9.

21. Hanahan, D. and R.A. Weinberg, *Hallmarks of cancer: the next generation.* Cell, 2011. **144**(5): p. 646-74.

22. Helm, J., et al., *Current and evolving strategies for colorectal cancer screening.* Cancer Control, 2003. **10**(3): p. 193-204.

23. Henrich, K.O., et al., *CAMTA1, a 1p36 tumor suppressor candidate, inhibits growth and activates differentiation programs in neuroblastoma cells.* Cancer Res, 2011. **71**(8): p. 3142-51.

24. Hung, K.E., et al., *Development of a mouse model for sporadic and metastatic colon tumors and its use in assessing drug treatment.* Proc Natl Acad Sci U S A, 2010. **107**(4): p. 1565-70.

25. Hunter, D.D., et al., *A laminin-like adhesive protein concentrated in the synaptic cleft of the neuromuscular junction.* Nature, 1989. **338**(6212): p. 229-34.

26. Ivics, Z., et al., *Molecular reconstruction of Sleeping Beauty, a Tc1-like transposon from fish, and its transposition in human cells.* Cell, 1997. **91**(4): p. 501-10.

27. Ivics, Z., et al., *Transposon-mediated genome manipulation in vertebrates.* Nat Methods, 2009. **6**(6): p. 415-22.

28. Jung, P., et al., *Isolation and in vitro expansion of human colonic stem cells.* Nat Med, 2011. **17**(10): p. 1225-7.

29. Kalluri, R. and R.A. Weinberg, *The basics of epithelial-mesenchymal transition.* J Clin Invest, 2009. **119**(6): p. 1420-8.

30. Katoh, M., *Functional and cancer genomics of ASXL family members.* Br J Cancer, 2013. **109**(2): p. 299-306.

31. Keng, V.W., et al., *A conditional transposon-based insertional mutagenesis screen for genes associated with mouse hepatocellular carcinoma.* Nat Biotechnol, 2009. **27**(3): p. 264-74.

32. Kim, M.Y., et al., *Recurrent genomic alterations with impact on survival in colorectal cancer identified by genome-wide array comparative genomic hybridization.* Gastroenterology, 2006. **131**(6): p. 1913-24.

33. Kosinski, C., et al., *Gene expression patterns of human colon tops and basal crypts and BMP antagonists as intestinal stem cell niche factors.* Proc Natl Acad Sci U S A, 2007. **104**(39): p. 15418-23.

34. Liotta, L.A., *Tumor invasion and metastases: role of the basement membrane. Warner-Lambert Parke-Davis Award lecture.* Am J Pathol, 1984. **117**(3): p. 339-48.

35. Lohi, J., et al., *Laminins, tenascin and type VII collagen in colorectal mucosa.* Histochem J, 1996. **28**(6): p. 431-40.

36. March, H.N., et al., *Insertional mutagenesis identifies multiple networks of cooperating genes driving intestinal tumorigenesis.* Nat Genet, 2011. **43**(12): p. 1202-9.

37. Mertsching, H., et al., *Engineering of a vascularized scaffold for artificial tissue and organ generation.* Biomaterials, 2005. **26**(33): p. 6610-7.

38. Mishra, D.K., et al., *Human lung cancer cells grown in an ex vivo 3D lung model produce matrix metalloproteinases not produced in 2D culture.* PLoS One, 2012. **7**(9): p. e45308.

39. Ott, H.C., et al., *Regeneration and orthotopic transplantation of a bioartificial lung.* Nat Med, 2010. **16**(8): p. 927-33.

40. Ott, H.C., et al., *Perfusion-decellularized matrix: using nature's platform to engineer a bioartificial heart.* Nat Med, 2008. **14**(2): p. 213-21.

41. Pusch, J., et al., *The physiological performance of a three-dimensional model that mimics the microenvironment of the small intestine.* Biomaterials, 2011. **32**(30): p. 7469-78.

42. Ridky, T.W., et al., *Invasive three-dimensional organotypic neoplasia from multiple normal human epithelia.* Nat Med, 2010. **16**(12): p. 1450-5.

43. Roig, A.I., et al., *Immortalized epithelial cells derived from human colon biopsies express stem cell markers and differentiate in vitro.* Gastroenterology, 2010. **138**(3): p. 1012-21 e1-5.

44. Schraivogel, D., et al., *CAMTA1 is a novel tumour suppressor regulated by miR-9/9* in glioblastoma stem cells.* EMBO J, 2011. **30**(20): p. 4309-22.

45. Smith, G., et al., *Mutations in APC, Kirsten-ras, and p53--alternative genetic pathways to colorectal cancer.* Proc Natl Acad Sci U S A, 2002. **99**(14): p. 9433-8.

46. Starr, T.K., et al., *A transposon-based genetic screen in mice identifies genes altered in colorectal cancer.* Science, 2009. **323**(5922): p. 1747-50.

47. Starr, T.K., et al., *A Sleeping Beauty transposon-mediated screen identifies murine susceptibility genes for adenomatous polyposis coli (Apc)-dependent intestinal tumorigenesis.* Proc Natl Acad Sci U S A, 2011. **108**(14): p. 5765-70.

48. Su, Q., et al., *A DNA transposon-based approach to validate oncogenic mutations in the mouse.* Proc Natl Acad Sci U S A, 2008. **105**(50): p. 19904-9.

49. Totonelli, G., et al., *A rat decellularized small bowel scaffold that preserves villus-crypt architecture for intestinal regeneration.* Biomaterials, 2012. **33**(12): p. 3401-10.

50. Trobridge, P., et al., *TGF-beta receptor inactivation and mutant Kras induce intestinal neoplasms in mice via a beta-catenin-independent pathway.* Gastroenterology, 2009. **136**(5): p. 1680-8 e7.

51. Valastyan, S. and R.A. Weinberg, *Tumor metastasis: molecular insights and evolving paradigms.* Cell, 2011. **147**(2): p. 275-92.

52. Wilson, C.H., et al., *Nuclear receptor binding protein 1 regulates intestinal progenitor cell homeostasis and tumour formation.* EMBO J, 2012. **31**(11): p. 2486-97.

53. Worm, J., et al., *Genetic and epigenetic alterations of the APC gene in malignant melanoma.* Oncogene, 2004. **23**(30): p. 5215-26.

54. Wurbel, M.A., et al., *CCL25/CCR9 interactions regulate large intestinal inflammation in a murine model of acute colitis.* PLoS One, 2011. **6**(1): p. e16442.

55. Youn, B.S., et al., *Blocking of c-FLIP(L)--independent cycloheximide-induced apoptosis or Fas-mediated apoptosis by the CC chemokine receptor 9/TECK interaction.* Blood, 2001. **98**(4): p. 925-33.

CHAPTER 4

Future Recommendation

Project 1 (in chapter 1)

Common cancer cell lines that are adapted for long-term in vitro culture and have accumulated numerous passenger mutations barely retain the native properties of primary cancer cells. One of the advantages in our study is that we established working protocols for deriving primary culture colon cancer cells directly from clinical patient samples at different disease stages and keeping these primary cells in low-passage and native conditions for most of our experiments. The benefits of using primary cells were demonstrated in the findings that CCR9 expression, as an adaptive phenotype in native colon cancers, was retained at high levels only in early-stage non-invasive primary CRC cells, which enabled a functional response to its ligand CCL25, while CCR9 expression could not be detected in most common cell lines. The relationship of chemokine CCL25 – CCR9 signaling regulating CRC progression, otherwise, could not been studied effectively using common CRC lines.

In this project, we revealed the crosstalk between NOTCH-JAG1 signaling and CCL25-CCR9 signaling that activated NOTCH by JAG1 directly down-regulated CCR9 levels in CRC cells through CCR9 proteosomal degradation. What we found was NOTCH activation decreased CCR9 expression in protein level, but not in RNA level, and the CCR9 protein decrease can be blocked by proteosome inhibitor PS-341. Based on the current data, it is difficult to draw the conclusion that CCR9 protein is one of the direct downstream targets of NOTCH pathway and further investigation is necessary to understand whether the CCR9 protein restored by blocking proteosome function is

exactly the one regulated by NOTCH signaling, or due to the different CCR9 protein, because of blocking the proteosomal degradation of other signaling pathways which otherwise would have decreased CCR9 expression.

Project 2 (in chapter 2)

Through engineering inducible CCR9+ expression in CRC cells, orthotopic mouse intestinal tumors could be formed with many common CRC lines or primary cultured CRC cells through tail vein injection. CTMM models are relatively fast, low-cost and robust in developing GI tumors and metastases within several weeks, and this property makes CTMM a valuable model for tracking and studying multiple steps in CRC progression from cancer cell invasion, migration, blood vessel intravasation, traveling in circulation system, extravasation to colonization in distant organs. Furthermore, similar to the engineering approach of CTMM, other types of chemokine and cell trafficking markers could be used to generate orthotopic cancer models in various types of organs. For instance, CXCR4 could be utilized to target the growth of leukemia cells specifically in bone marrow which express ligand SDF-1, or CCR6 could be applied to guide human hepatocellular carcinoma cells to specifically grow in mouse liver, which is one of the major organs secreting CCR6 ligand CCL20.

Another interesting finding is that we demonstrated liver metastases are more chemoresistant than orthotopic GI tumors or subcutaneous xenografts, and explored the potential molecular mechanisms of increased DKK4 level and NOTCH signaling involved in the chemoresistance to Oxaliplatin, as consistent to the study using clinical patient samples. Our RNA-Sequencing and quantitative RCP double confirmed that DDK4 level was 80 times up-regulated in metastasis than that in primary GI tumors,

indicating there could be a sort of “on” and “off” switch of genetic regulation involved in DKK4 signaling. Further studied will be required to reveal the broader signaling network involved in CRC chemoresistance, such as the regulation of DKK4 mediated TFAP2E-dependent resistance, or the DKK4 activation of WNT pathways with crosstalk of NOTCH pathway. These results also highlight the concordance of our CTMM to the clinical CRC diseases, and further studies might be performed to interdict the detailed molecules and signaling network undergoing in CRC chemoresistance. In addition, CTMM could be applied as an advanced pre-clinical model for middle-throughput screening of potential drugs, chemicals, toxin and other therapeutics, or studying biomarkers for prevention and diagnosis.

The technology of engineering humanized orthotopic cancer in immunoproficient mice through blastocyst injection shed more light on creating humanized chimera models. CCR9+ CRC cells could be substantially incorporated into and grow along with mouse embryos at a successful rate, having RFP+ human cells detected in the hindgut and co-localized with regions expressing ccl25. Comparing to embryos, it is much more difficult to detect the RFP+ human cells in adult mouse intestines and this could be due to the immune rejection by mature adult immune system or the dormancy of human cells losing the capability of proliferation. Nevertheless, our methodology demonstrated the proof of principle that CCR9 expression promoted human CRC cells survive in mice with normal immune system. Our research provide the potential approaches of engineering humanized organs or tissues through chemokine targeting, and similar to the CCR9 procedure, other chemokines such as CXCR4 or CCR6 could be applied to engineer humanized mouse bone marrow or liver tissues.

Another interesting question is how the CCR9+ human cells evade xeno-immune rejection from mouse hosts. Immunologically, the chimeric mice represent a complicated situation. T cells are educated in the thymus on mouse Major Histocompatibility Complex (MHC) and this would make human antigens only cross-presented by mouse antigen presenting cells. However these T cells would be unable to recognize the human cells with human MHC. One possibility to test the mechanism of central immune tolerance is to identify whether colonized human CRC cells exist in the thymus in the chimeric mice. If true, there could be neonatal central tolerance to the human cells. If not, peripheral tolerance mechanisms might be operative, especially when mouse T cell, not negatively selected for xenogenic (human) MHC, encounter human MHC in the periphery under non-acute inflammatory conditions. To test this, the same CRC cells coud be grafted subcutaneously in the chimeras at 6 weeks of age when the mouse immune system becomes mature. If the xenografts occur, this would prove the immune-proficiency versus systemic tolerance.

Project 3 (in chapter 3)

Decellularization removed cellular components from the human colon tissue while retaining intact tissue architecture, blood vessel network and ECM. The integral vasculature provided a possibility for modeling angiogenesis in cancer tissues. Moreover, future technical improvements are necessary to complement the current decellularization method for preserving native soluble molecules, growth factors and other biomaterials along with the acellular matrix.

In addition to three types of colon cells: epitheial cell, endothelial cells and fibroblasts, other types of cells such as lymphocytes, adipocytes, or microbes could be potentially

incorporated into the ex vivo colon model system for achieving various research goals. The ex vivo CRC models can also be personalized and retain the pathological and genetic features in individual patients by having the normal colon epithelial cells replaced with patient-derived primary CRC cells. Furthermore, because of its properties of single-cell resolution, time-lapse sensitivity and easy genetic manipulation, the ex vivo CRC model could be applied for exploring sophisticated questions in genetics, and proteomics, such as fate determination of stem cells, cellular behaviors in complete tissue context as well as the reciprocal effects between cells and ECM.

It was quite amazing to perform forward genetics study in real human conditions and we demonstrated that many novel genes and signaling steps were successfully identified through transposon-based forward screens in the ex vivo human CRC models. However, carefully designed functional validations are critical to analyze the candidate genes identified from ex vivo models. Here for testing driver genes in malignant transformation, the ideal model will be APC^{min} mouse models and further studies could be developed to investigate the tumor progression through knockdown or over-expressing the candidate genes in intestine-specific conditions.

Through this forward screen, we identified a total of 22 novel candidate genes. In addition to functional assays, the known functions of the candidate genes provided evidence for some of these to be the drivers in CRC development. At least 5 of them are promising since they have already been implicated in other types of cancers or independently correlated to clinical patient outcome. Further studies are recommended for exploring the molecular mechanisms of each candidate in CRC progression. Another interesting finding is that besides insertions in genetic coding regions, *SB* also inserted

in non-coding regions and some of them target gene promoters or the genomic “dark” area such as the domains related to transcriptions of microRNA or long non-coding RNA. It will be good to know the exact functions of these mciroRNA and long non-coding RNA in CRC progression through further mechanistic studies.

APPENDIX

Engineering Colorectal Cancer and Metastasis Models for Mechanism And Therapeutic Studies

Thesis Dissertation Proposal presented to Professors Xiling Shen, Micheal Shuler, Steven Lipkin and Robert Weiss in May. 2013 in partial fulfillment of the requirements for the admission to Ph. D. Candidacy exam (A exam)

Abstract

Whereas Primary colorectal cancers (CRC) can be cured by surgery, metastasis is the major cause of CRC mortality. To effectively treat CRC diseases largely depends on precisely interdicting the mechanisms of metastasis and developing drugs targeting the mechanisms. However, we currently lack advance in vivo and in vitro research systems to accurately model metastatic CRC diseases and test therapies.

Here, we engineered orthotopic and metastatic CRC mouse models utilizing chemokine switch. Based on our former study that early stage CRC cells are CCR9 positive and they spontaneous form GI tumors by tail vein injection, we created primary and commercial CRC lines with inducible CCR9 expressions and show these cells were able to form tumors in mouse intestine simple through tail vein injection. After forming orthotopic tumors, CRC cells are free to metastasize from the primary tumor after CCR9 turns off, if they possess the intrinsic ability to metastasis. This model recapitulates the most features of CRC metastasis progression directly from primary GI locations to distant organs. In addition, we broadly engineered CCR9 expressing cell lines representing all major CRC molecular subtypes in TCGA list, to form orthotopic CRC

accounting for clinical patient genetic diversity. At last we indicated that the new CRC mouse models facilitate mechanism study by combining with whole body IVIS imaging as well as multi-photon microscopy and also provide effective and efficient platform for pharmaceutics study. (This project is close to end and we currently prepare paper submission.)

In the other hand, we created an in vitro organotypic human colon by reseeding primary colon epithelial, endothelial cells and fibroblasts in decellularized human colon tissues, which retain colon's complete geometry, preserves the extracellular matrix including relative intact vascular network, and most importantly, maintains the integrity of muscularis layer. The organotypic colon can then be transformed into APC-null invasive neoplasia in CRC-associated genetic pathways. Functional analyses and molecular characterizations indicate the bioartificial organ has the ability to recapitulate the major features of CRC malignant progression.

Our future research plan is to use the pathophysiologically relevant bioartificial human CRC as a culture platform to identify invasion driving genes. We will apply SB transposon systems as mutagens to induce submucosa invasion of APC *in situ* neoplasia in the bioartificial colon. Then we will perform in vitro and in vivo functionally validations to corfirm the invasion driver genes we captured. (For this part, we collaborate with Copeland & Jenkins lab, and Zalton Ivics group and we suppose to finish in ~ 1.5 years.) Overall, my PhD research goal is to engineer in vivo and in vitro CRC models which can fill the gaps between conventional 2D cell culture and animal models, serving as better research platforms for mechanism and therapeutics studies.

Part A: Inducible Colorectal Cancer Metastasis Mouse Model via a Chemokine Switch

Background

Colorectal cancer (CRC) is a major public health source of morbidity and mortality, with proximately 150,000 new diagnoses each year in the United States[109]. 25% CRC patients eventually die from metastatic diseases. CRC progresses through multiple distinct stages. Firstly, inappropriate proliferation cause colon stem or progenitor cells to transform into colon cancer stem cells, which start with adenoma formation and evolve into carcinoma in situ[110]. Then, pre-invasive CRCs by accumulating more genetic mutations, acquire the ability to invade through the submucosa and muscularis, metastasize, and survive outside the colon microenvironment niche and in the distant organs[111, 112]. Precisely understanding mechanisms of CRC formation, transition from localized to metastatic stages and developing drugs to block the mechanisms are criticalpre-requirements to improve patient outcomes. While current CRC animal models, as basal research tools, have their weaknesses whichretardus from fully understanding metastasis mechanisms and developing effective drugs.

Genetically engineered mouse model (GEMM, transgenetic mice) is a very powerful tool for cancer study. However, it is relatively expensive and time consuming to create. Also, due to its over-simple genetic background, GEMM hardly captures all the features of the genetic mutations and epigenetic regulations in human CRC diseases. For example, mouse screens for cooperating mutations are not always concordant with TCGA (The Cancer Genome Atlas) results to identify the most common mutations, genomic rearrangements and epigenetic in the corresponding human cancers. Subcutaneous

xenograft models, the currently workhorse for drug screening, lack the native gut microenvironment [113, 114]and the property of distant metastasis, thus lead to many false positive cures.Surgical implantation of CRC cells under the kidney capsule, or orthotopic implantation through intra-cecum or rectal injection overcomes this limitation. However, injection needle tracts create potential artifacts for cell egress, disturb the extracellular matrix and artificially generate a local inflammatory microenvironment, which confound the research results. Additionally, we currently do not have robust, consistent models of CRC liver metastasis from primary intestinal sites[115, 116]. Therefore, advance methods are required to model more accurately CRC metastasis and therapeutics[117].

Approaches

Here, we create an inducible colorectal cancer metastasis mouse model via a Chemokine Switch. Chemokines are a family of secreted ligands that play important roles for trafficking lymphocytes in the body to different organs, including bone marrow, skin, thymus, intestine,liver and other sites.The G protein–coupled chemokine receptor 9 (CCR9) and its ligand chemokine 25 (CCL25) comprise a signaling axis that is particularly important for the small intestine and colon[15]. Intestinal epithelial cells produce CCL25, which attracts circulating CCR9+ T cells to intravasateinto the gut toward the CCL25 source.Normal colon epithelial cells also are CCR9+. Recently our study[73]showed that early but not late stage CRCs are CCR9+ and when injected by tail vein can spontaneously form gut tumors.Thus, our working hypothesis is by making inducible CCR9 expression in human CRC cells, we can have the CRC cells forming tumors in the native mouse gut microenvironment simply through tail vein injection and

then metastasizing to the most common anatomical sites when CCR9 expression turns off. We used this as a platform to develop a more general metastasis system.Solid tumors are heterogeneous and this is a problem for metastasis study becauseof over-extrapolating results from a limit diversity of genetic backgrounds. To address this issue, we made a series of CCR9+ lines that cover the major CRC molecular subtypes as defined in TCGA. This should be a useful research resources or tools for mechanistic studies and drug screening.These inducible CCR9+ lines also have luciferase and fluorescence double labeling for real time in vivo tracking by IVIS system for middle-throughput drug screening and time lapse imaging to study deep metastatic mechanisms like tumor cell intra-/extravasations, epithelial mesenchymal transition. Finally, we evaluateoxaliplatin effects, one of the first line drugs in clinical CRC therapy, using the inducible CRC metastasis model as well as current standard subcutaneous xenograft model.

Experimental Designs and Results

1. Engineering inducible CCR9+ primary or commercial CRC lines and In vitro evaluating the efficiency of inducible CCR9 expression, migration to CCL25, cell growth and death with CCR9 expression.

We first constructed an inducible CCR9 expression lentivirus vector, in which the open reading frame (ORF) of human or mouse CCR9 and a Red fluorescence protein (RFP) marker are sub-cloned under a CMV promoter**(Figure 1 A).** The CMV promoter is tetracycline inducible promoter (conditional knock-in) which means the CCR9 gene is silent until certain amounts of tetracycline derive doxycycline is given in vivo or in vitro. Then we infected a panel of human or mouse CRC lines with the lentivirus particles and

test the CCR9 expression is inducible with doxicyclineby western blots**(Figure 1 B).**The boyden chamber experiment was then performed to functionally evaluate the in vitro migration of CCR9+ cellstoward CCL25**(Figure 1 D).** Additionally, we tested that CCR9 expression has no significanteffects on CRC cell proliferation[14] and apoptosis by the cellular ATP (adenosine triphosphate) levels**(Figure 1 C).**

2. **Qualify and quantify GI (gastrointestinal) vs extra-GI tumor formationby engineered CRC lines.**

We performed whole body IVIS imaging on mice iv injected with CCR9- (parental) only, CCR9+/- (mixture) and CCR9+ only CRC cells**(Figure 2 B and Figure 1 A** is the experiment schema). Most CCR9- cells developed tumors in lung locations, and the CCR9+/- mixture cells formed tumors in both lung and abdominal sites, while the pure CCR9+ cells only formed tumors in abdominal sites. The abdominal tumors were further confirmed**(Figure 3)**by ex vivo IVIS imaging and histopathology asmultiple foci along intestinal system from Duodenum, Jejunum, Ileum, cecum to colon.We totally engineered 13 CCR9+ commercial human CRC lines and 2 CCR9+ primary CRC lines derived from clinical patient samples**(Figure 2 C),** among which 12 commercial lines and 2 primary lines formed tumors in GI. We then quantified**(Table 1)** extra-GI, small intestinal and large intestinal tumors formed by different CRC lines, in multiplicity, sizes, and rates, compared to their parental lines.

3. **Broadly engineering human CCR9+ cell lines representing all major CRC molecular subtypes in TCGA list and a mouse CRC lines to develop murine orthotopic CRC model in immunoproficient environment.**

We expanded the CCR9+ engineering in 13 human commercial CRC lines and 2 primary CRC lines which harbor most top 20 genetic mutations in TCGA list**(Table 2).** The orthotopic CRC mouse models developed by these lines may serve as practical research resources or platforms for genetic subtype CRC study and drug development targeting specific molecular signaling. They also enable studying CRC tumor in its orthotopic organ site, with higher resolution and allows tracking of dynamics. As a demonstration, we performed in vivo multi-photon imaging of the gut tumor**(Figure 5).** We also created a CCR9+ murine CRC line CT26**(Figure 4),** which formed intestinal tumors and liver metastasis in the same BALB/C genetic background through CCR9+ controlling. This orthotopic mouse CRC model in immunoproficient conditions could be a useful tool to study the effects of immune system on CRC progression.

4. **Create the inducible metastasis models that orthotopic CRC tumors metastasize after CCR9 expression turns off and use the models to demonstrate the dynamics of CRC metastasis progression.**

We performed real time whole body IVIS imaging on mice iv injected with CCR9+ CRC cells**(Figure 6).** The CCR9 expression was turned off after lower abdominal tumor formation and subsequently metastasis occurred mainly in liver which is the most common organ the human CRC diseases metastasize. The CCR9 expression shutting down returns the engineered CRC lines back into their parental stages and the metastasis was caused by cell native properties. EX VIVO imaging combining histopathology**(Figure 7 A)** were used to further quantify the locations and numbers of primary and metastasis tumors, comparing to the control. The histological analyses of H+E staining **(Figure 7 B)** indicate the primary tumor undergoing progression from *in*

situ carcinoma (Stage I), submucosa invasion (stage II), to muscularis invasion (stage III). We also compare**(Figure 8)**the occurring time and numbers of liver metastasis foci between doxycline-keep group (CCR9-on) and withdrew group (CCR9-off). The data showing the doxycline withdrew group develop more liver metastatic foci in shorter period of time indicate metastasis correlates with doxycycline induction. In total, **(Figure 8 B)**three commercial CRC lines and one primary CRC line were able to develop the inducible metastasis mouse models. Furthermore, most liver tumors by CCR9 engineered lines occur later than their primary GI tumors and also later than those liver tumors developed by wild-type lines, indicating it is possible that most liver tumors are the metastases from GI tumors **(Figure 8 C).**In addition, we show the dynamic tumor growths in primary and metastatic locations can be time-lapse monitored by luciferase - IVIS imaging, indicate this model can be used more practically for drug screening

5. **The chemokine inducible CRC metastasis models (CIMM) serve as a powerful platform for imaging the dynamics of the metastasis progress.**

Combining multi-photon microscopy, we apply real-time imaging on primary GI as well as liver metastasis tumors. Since vasculature was labeled by green fluorescent dyes and engineered CRC cells have RFP marker, it is possible to track the tumor cell intravasation and extravasation, as important steps in metastasis generation**(Figure 5 and Figure 9).** Similarly, the interaction between tumor cells and microenvironment, dynamic alternation of molecular markers and signaling pathway associated with metastasis progress could be more directly and practically studied in this system.

6**. CIMM models have the similar drug responses to that of clinical CRC diseases.**

Oxaliplatin is an alkylating agent breaking DNA strand and causing cell apoptosis, which combined with 5-fluorouracil is the first line drug in clinical CRC therapy regimen. We applied the CRC mouse models in therapeutic study**(Figure 10 and Figure 11).** We tested oxaliplatin treatment on subcutaneous, orthotopic and liver metastatic xenograft tumors by Colo205 (CIN type) and DLD1 (MIS type) and evaluate therapy efficiency by tumor growth inhibition and mouse survival rates. The study show metastatic tumors are more chemoresistantthan primary GI tumors and subcutaneous xenografts. Interestingly, we also found oxaliplatin treatment is intended to induce further metastases probably by having more effects on primary tumors than metastatic tumors or promoting chemoresistant subpopulation amplification by eradicating the chemosensitive group.

To evaluate whether CIMM model produce similar drug responses to those of CRC patients, we studied 14 patients with primary colorectal cancer and 11 patients with liver metastases **(Figure 12 and Figure 13).** Chi-Square tests in tumor volume or growth dynamics indicate there is significant difference in drug responses between primary CRC tumors and metastatic tumors, proving the similar conclusion that metastatic tumors are more chemoresistant than primary CRC tumors.

Conclusion

We develop a novel CRC metastatic model. The CIMM system, in which human CRC cells form primary tumors in native gut microenvironment and metastasize to the most common anatomical sites, recapitulates most features of CRC metastasis progression. This model is easy to handle (tail-vein injection), is repeatable, and generates metastasis robustly, which has not been achieved by other CRC models.In CIMM system, chemokine engineering does not affect cellular native capability to metastasize

because chemokine expression in CIMM is inducible and controllable, meaning the engineered cell lines could be changed back to parental stage right after seeding in the primary gut sites and metastasis is generated by cellular native properties.

We generated a broad panel of CIMM systems with all the major molecular CRC subtypes in TCGA, as research platforms for specific mechanism study on different genetic background and evaluating drugs that target specific molecular signaling.

Furthermore, we demonstrate that CIMM combined with multiple-photon microscopy can be applied to study the dynamic interaction between CRC cells and vasculatures, and the CRC metastatic progress under native microenvironment.

Low-cost, surgery-free, repeatable and capturing the most features of primary CRC formation and metastasis progression, CIMM can be anovel and practical tool for pharmaceutical screening, by filling the gaps between subcutaneous xenograft and clinical trials.

Part B: In Vivo Imaging of Epithelial Mesenchymal Transition (EMT) in CIMM models

Background

An epithelial mesenchymal transition (EMT) is a biological process that allows the polarized epithelial cells to functionally undergo multiple biochemical changes into migratory mesenchymal cells secreting ECM components[118]. EMT is required for embryonic development, tissue remodeling, and wound repair. Recently, accumulating evidence indicates that tumor progression, invasion, and metastasis involve theinduction of EMT. During EMT, the loss of E-cadherin facilitates tumor cells dissociated from cell-cell or cell-extracellular matrix adhesions, and the induction of mesenchymal markers such as N-cadherin or vimentin leads to the reorganization of cellular skeleton and acquisition of a motile and invasive capacity.

EMT research raises the hypothesis that the tumor cells undergoing EMT are supposed to have higher invasive and metastatic capability than those cells that do not, thus closely associated with metastasis formation. While, up to date, this hypothesis [119]is still short of direct evidence to prove and this difficulty partly comes from the lack of a reliable metastatic model that recapitulates the most properties of metastasis (CRC invasion and intravasation from the primary tumor) and that allows real-time monitoring of this dynamic process in single cell resolution.

Approaches

Here, we utilize the combination of CIMM model and multiphoton microscopy to explore the above questions. We first develop CIMM models with E-/N-cadherin dual reporter cell lines, which could designate EMT by fluorescence colors. By the promoter reporters, we could further determine whether the invasive cells intravasing into vasculature are undergoing functional EMT, how the occurrence of EMT coincides with distant metastasis.

Experimental Designs and Results

1. In vivo imaging of CRC cells undergoing EMT in CIMM mice.

First, we engineered two EMT reporter CRC lines (CCR9-SW480 and CCR9-SW620) which are transfected with DNA plasmids of E-cadherin promoter driving GFP and N-cadherin promoter driving mCherry**(Figure 14).** Then multi-phone microscopy will be performed in CIMM mice to visualize the CRC cells in primary GI and liver locations. The cells undergoing EMT can be captured by GFP and mCherry dual markers.

2. Quantity of the EMT cells correlated with invasion, intravasation and metastasis

Furthermore, we will study the relationships between EMT cells and CRC progression. We will quantify the EMT cells in different GI positions: mucosa *in situ*, submucosa invasion and muscular invasion. The intravasating EMT CRC cells also will be identified and the percentage of EMT cells will be quantified in the total amount of CTC cells which is in RFP marker.

Conclusion

We apply CIMM model to explore some critical questions in CRC fields, which are hard to study using conventional animal models. EMT correlated with CRC cancer metastasis is hypothesized, based on the research well studied in vitro cell culture models, while it has not been completely proved in vivo[120]. These hypotheses have significant implications for anti-metastasis therapies. The difficulty largely lies in the lack of a reliable metastatic model that recapitulates the onset of metastasis (CRC invasion and vascularintravasation from the primary tumor) and that allows real-time monitoring of thisdynamic process.Here, we try to fill the gap by directly visualizing the EMT phenomena in orthotopic CRC and study the correlation between EMT and tumor progression by using CIMM models.

Part C:Identification of Invasion Driver Genes Utilizing a Bioartificial Colorectal Cancer Model with Transposon Mutagenesis

Background

Human colorectal cancers (CRC) generally can be divided into two classes based on the genetic background displaying chromosomal instability (CIN) or microsatellite instability (MSI), in which CIN phenotype occurs in 80-90% CRC cases. CRC displaying CIN frequently harbor loss-of-function mutations in adenomatous polyposis coli (APC) which transforms normal colon epithelium into neoplasia. APC neoplasia requires gaining additional mutationsin order to progress from *in situ* mucosa and invade through the basement membrane (muscularis layer) into the submucosa where cancer cells get access to the vascular and lymphatic systems for their systemic spreading[121]. Invasion into submucosa is therefore considered the first checkpoint in CRC becoming malignancy, and identification of invasion driving mutations is critical to illuminate CRC mechanisms and to develop potential therapeutic targets, which could eventually improve patient outcomes.

However, limited progress has been made to date due to three difficulties: 1.Conventional cell or animal-based research platforms have intrinsic limitations[122]. The former could not recapitulate intercellular interactions and tissue microenvironment, which are required for tumor malignancy. While animal models are not only costly and time-consuming, they also lack the appropriate resolution and sensitivity to track or monitor the dynamic and transientmalignant transition. 2. The difference between human and animal makes the results from animal studies usually inconsistent to clinical patient data. 3. Although second generation sequencing facilitates reverse gene studies,

tumor heterogeneous evolutions and numerous passenger mutations confound the curves of driver alterations.Therefore, animal or patient based reverse genetic studies generally yield numerous and complex genetic candidates, including both driver and passenger mutations that makes hard for functional validation.

Approaches

To overcome the first two difficulties, we will utilize a pathophysiologically relevant model[123] of bioartificial human colon as the research platform, which provides sufficient resolution, time-lapse monitoring for rapid gene screening, and also because of human tissue, produces responses that are more predictive of humans than animal models. First, we create an organotypic human colonby reseeding primary colon epithelial, endothelial cells and fibroblasts in decellularized human colon tissues[124, 125], which retain colon's complete geometry, preserves the extracellular matrix including relative intact vascular network, and most importantly, maintains the integrity of muscularis layer. Then we transform the organotypic colon into APC-null invasive neoplasias by deregulating APC expression, upregulatingK-RAS expression and TGF-β treatment[126, 127]. Functional analyses and molecular characterizations indicate the bioartificial organ has the ability to recapitulate the major features of CRC malignant progression.

To overcome the third difficulty, we will perform forward, instead of reverse, gene screen using transposon-based insertional mutagenesis (TIM).Transposons are discrete DNA elements including transposon and transposase, which have the unique ability to change their genomic position through "cut and paste" mechanism and leave 5 bp

common insertion sites (CIS) in the hostgenome after transposition.To our knowledge, the TIM system has been considered non-biased, efficient, and thus the best mutagen system to date to simulate somatic mutations in cancer models.We plan to use the Sleeping Beauty (SB) DNA transposon systemdeveloped by the Copeland & Jenkins lab[128] at Methodist Research Institute, as mutagen to simulate the additional insertion hits on the APC-null *in situ*neoplasia.During the same time, we will perform time-lapse microscopy monitor on the neoplasia and capture the cells undergoing invasion into submucosa. By analyses of SB CIS in the invasive subgroup cells, we can identify the invasion driving genes. Finally, we will cross outside human databases such as TCGA (The Cancer Genome Atlas) of APC subtype CRC or murine datasets of APC dependent intestinal tumorigenesis[129], to verify and narrow down our driver candidates for further functional validation.

Experimental Designs and Results

1. Create acellular human colon bioscaffolds by decellularization.

We performed detergent-based decellularization slightly modified from D.A.Taylor. Nat. Med. 2008[130], whichaccording to our pilot experiment results[131], works best to remove cellular components in human colon tissues than othermethods**(Figure 15).**DNA content **(Figure 17)**in decellular scaffolds decreased to less than 5% of that in normal colon, while there was no difference in GAG, Collagen (collagen I)[132], laminin[133] and fibronectin[134] contents. Removal of most cellular components is further conformed **(Figure 18)** that F-actin and nuclei are undetectable in the scaffolds by immunohistochemistry. As expected, the decellular scaffolds **(Figure 16)**leaved main

vasculatures and crypt niches intact and retained the integrity of basal membranes (muscularis layers).

2. Primary cultures of human colon epithelial cells, myofibroblasts and microvascular endothelial cells and identification.

Subsequently, we did primary cultures of human colon epithelial cells (hCEC)[135, 136], myofibroblasts and endothelial cells, the main cast needed for scaffold recellularization**(Figure 19)**. In order to maintain long-term in vitro culture, hCEC have to be immortalized by overexpression of the non-oncogenic gene of telomerase reverse transcriptase (TERT) by retrovirus infection. We succeeded to grow out and maintain three hCEC primary lines in vitro which form microcrypt/villi in matrigel 3D culture**(Figure 20)** andexpress markers of colonic epithelial cells such as pan cytokeratins, zonula occludens-1, mucins-2, antigen A33, chromogranin A and stem cell marker Lgr5**(Figure 21)**. Interestingly, about 20 % hCECs form crypt-like structure when keep cultured in 3-D mitrigel without high Wnt/ Notch signaling stimulation[137] for 5-6 days, indicating harboring stem cell like cells. Myofibroblasts are identified as more than 90% cells expressingα- smooth muscle actin and similarly vascular endothelial cells are positive in CD31 expression.

3. Bioscaffoldrecellularization and characterization.

Before recellularization, the mucosa layers with complete muscularis layers were physically separated from submucosa**(Figure 15).**For the mucosa fabrication, we then seededhCECs in the crypt niches and the mixture of endothelial cells andmyofibroblasts (1:1) in the extracellular matrix outside crypt niches by capillary injection of hand-pulled glass needles or microinjection needles**(Figure 22)**. After the cells attached to the

extracellular matrix and start proliferation, the myofibroblasts were planted on the muscularis layer opposed to the mucosa**(Figure 22)**. In addition, we seed endothelial cells in the submucosa scaffolds. The two scaffolds of mucosa and submucosa were physiologically placed together and mounted in proper culture medium. After 20-30 day culture, both morphology**(Figure 23)** (H+E staining) and molecular markers**(Figure 24)**(immunohistochemistry) were applied to test the physiological properties and differentiation of the recellularizedorganotypic colon.

4. The organotypic colon recapitulates the feathers of APC-dependent malignant transition from mucosa *in situ* to submucosa invasion.

We then performed functional analysis whether the organotypic colon can be transformed into APC -dependent invasive neoplasias. We generatedthree groups of organotypic colons fabricated with APC knockdown hCEC, APC knockdown + K-Ras overexpression hCEC or APC knockdown + K-Ras overexpressionhCEC + TGF-β treatment, and firstly APC knockdown + K-Ras overexpression hCECs were subcutaneously implanted in immunodeficient (NSG) mice to test the tumorigenesis capability by xenograft formation(Figure 25). Subsequently, in order to test whether the organotypic colon has the ability to transform normal epithelial cells into APC-null invasive neoplasia in CRC-associated genetic pathways, the three subgroups of hCECs were seeded in the crypt niches of decellular scaffolds along with endothelial cells and fibroblasts. After 20-30 day culture, we observed neoplasia*in situ* formation in APC knockdown group **(Figure 26)** and with additional K-Ras overexpression, the neoplasia became larger, making crypt shape deformed and mucosa disorganized **(Figure 26)**.Furthermore, in the third group of APC knockdown + K-Ras overexpressionhCEC +

TGF-βtreatment developedsubmucosainvasive neoplasias in the organotypiccolon system **(Figure 26).**Functional analyses and molecular characterizations will be performed to prove the bioartificial organ has the ability to recapitulate the major features of CRC malignant progression.

Future plan:

Apply sleeping beauty (SB) insertion mutations in the APC-dependent neoplasias and capture the invasion driving genetic signatures.

Currently I and Zhubo Wei, the postdoc in Copeland & Jenkins labs have been working together to transfect SB transposon vectors (the transposon plasmid T2/Onc2 and transposase plasmid SB100x) in hCECs with enough gene copies inserted in host genome, which ensure SB can be mobilized at frequencies high enough to induce submucosa invasion**(Figure 27).**APC-null hCECs transfected with SB, along with endothelial cells and fibroblasts will be seeded in the acellular colon matrix to form colon neoplasia. During the same time, time-lapse monitoring will be performed to track and capture the cells undergoing invasion into submucosa. A modified splinkerette PCR method by barcoded primers will be used to amplify the SB CIS from the invasive hCECs, and the mutation sites, types, and copy number variations can be identified by sequencing PCR products. We currently collaborate with the SB transposon discoverer[138] and geneticist, Dr. ZoltánIvics, who provides technical support withhuman cellular SB CIS mapping to identify the candidate mutations[139, 140]. Then we will cross outside human databases such as TCGA (The Cancer Genome Atlas) of APC subtype CRC or murine datasets of APC dependent intestinal tumorigenesis, to

verify and narrow down our driver candidates for further functional validation in the next step**(Figure 28).**

6. Functional validation of the gene signatures.

For functional validation of the driver genes, we will use siRNA to silence the candidate oncogenes and use DNA vectors to knockin the candidate suppressor genes in APC –null hCECs or common CRC cell lines. Subsequently, in vitro cell proliferation, migration and invasion assays will be performed to test the driver genes. If time and funds allow, an APC^{min} knockout mouse model will be used to verify the drivers of invasive progression by monitoring histological changes in the CRC tissues **(Figure 28).**

Conclusion

To our knowledge, this is the firstorganotypic human colon created to be a natural platform by de-/re-cellularization[141], as a third research model to fill the gap between 2D cell culture and animal models. This will be also the first tumor model[142]developed on a bioartificial colon and induced from genetically defined primary colon epithelial cells. The APC-dependent neoplasias created from the organotypic colon will recapitulate the features of invasive malignancy and serve as an ex vivo platform to screen genetic signaling driving tumor progression.

Moreover, this study will be the first application of SB transposon-mediated forward gene screen in human organotypic system for cancer research. It was reported by Copeland & Jenkins group and othersthat SB transposon germlineinsertions, as mutagens to mimic somatic mutations, enable to inducevariant types of tumors in mice. This forward gene screen that tumors result from SB insertion mutagenesis, facilitates the identification of the gene and signaling pathways that drive tumor formation[143,

144]. However, the forward gene screens based on transposon systems can beonly applied[145] in non-human systems, which have quite different genetic background and mechanisms of tumorigenesis than human body. Here, we try to explore the forward genetic study of the SB transposon mutagenesis in human systems, the physipathological relevant bioartificial colon, to identify CRC invasion driving genes, providing a potential way to bridge the gaps between animal and human study.

Reference

1. Bozic, I., et al., *Accumulation of driver and passenger mutations during tumor progression.* Proc Natl Acad Sci U S A, 2010. **107**(43): p. 18545-50.

2. Jones, S., et al., *Comparative lesion sequencing provides insights into tumor evolution.* Proc Natl Acad Sci U S A, 2008. **105**(11): p. 4283-8.

3. Johnston, M.D., et al., *Mathematical modeling of cell population dynamics in the colonic crypt and in colorectal cancer.* Proceedings of the National Academy of Sciences of the United States of America, 2007. **104**(10): p. 4008-13.

4. Barker, N., et al., *Crypt stem cells as the cells-of-origin of intestinal cancer.* Nature, 2009. **457**(7229): p. 608-11.

5. Halberg, R.B., et al., *Tumorigenesis in the multiple intestinal neoplasia mouse: redundancy of negative regulators and specificity of modifiers.* Proceedings of the National Academy of Sciences of the United States of America, 2000. **97**(7): p. 3461-6.

6. Fearon, E.R. and B. Vogelstein, *A genetic model for colorectal tumorigenesis.* Cell, 1990. **61**(5): p. 759-67.

7. Merlos-Suarez, A., et al., *The Intestinal Stem Cell Signature Identifies Colorectal Cancer Stem Cells and Predicts Disease Relapse.* Cell Stem Cell, 2011.

8. Dylla, S.J., et al., *Colorectal cancer stem cells are enriched in xenogeneic tumors following chemotherapy.* PLoS ONE, 2008. **3**(6): p. e2428.

9. Ricci-Vitiani, L., et al., *Identification and expansion of human colon-cancer-initiating cells.* Nature, 2007. **445**(7123): p. 111-5.

10. Emmink, B.L., et al., *Differentiated Human Colorectal Cancer Cells Protect Tumor-Initiating Cells From Irinotecan.* Gastroenterology, 2011.

11. Sonoshita, M., et al., *Suppression of colon cancer metastasis by Aes through inhibition of Notch signaling.* Cancer Cell, 2011. **19**(1): p. 125-37.

12. Din, F.V., et al., *Effect of aspirin and NSAIDs on risk and survival from colorectal cancer.* Gut. **59**(12): p. 1670-9.

13. Kabelitz, D. and D. Wesch, *Features and functions of gamma delta T lymphocytes: focus on chemokines and their receptors.* Critical reviews in immunology, 2003. **23**(5-6): p. 339-70.

14. Youn, B.S., et al., *Blocking of c-FLIP(L)--independent cycloheximide-induced apoptosis or Fas-mediated apoptosis by the CC chemokine receptor 9/TECK interaction.* Blood, 2001. **98**(4): p. 925-33.

15. Wurbel, M.A., et al., *CCL25/CCR9 interactions regulate large intestinal inflammation in a murine model of acute colitis.* PLoS One, 2011. **6**(1): p. e16442.

16. LaPointe, L.C., et al., *Map of differential transcript expression in the normal human large intestine.* Physiological genomics, 2008. **33**(1): p. 50-64.

17. Li, X., et al., *Deconvoluting the intestine: molecular evidence for a major role of the mesenchyme in the modulation of signaling cross talk.* Physiological genomics, 2007. **29**(3): p. 290-301.

18. Hart, A.L., et al., *Homing of immune cells: role in homeostasis and intestinal inflammation.* Inflamm Bowel Dis. **16**(11): p. 1969-77.

19. Shang, L., et al., *Expression of the chemokine binding protein M3 promotes marked changes in the accumulation of specific leukocytes subsets within the intestine.* Gastroenterology, 2009. **137**(3): p. 1006-18, 1018 e1-3.

20. Zaballos, A., et al., *Cutting edge: identification of the orphan chemokine receptor GPR-9-6 as CCR9, the receptor for the chemokine TECK.* Journal of immunology, 1999. **162**(10): p. 5671-5.

21. Amersi, F.F., et al., *Activation of CCR9/CCL25 in cutaneous melanoma mediates preferential metastasis to the small intestine.* Clinical cancer research : an official journal of the American Association for Cancer Research, 2008. **14**(3): p. 638-45.

22. Johnson, E.L., et al., *CCR9 interactions support ovarian cancer cell survival and resistance to cisplatin-induced apoptosis in a PI3K-dependent and FAK-independent fashion.* J Ovarian Res, 2010. **3**: p. 15.

23. Johnson-Holiday, C., et al., *CCL25 mediates migration, invasion and matrix metalloproteinase expression by breast cancer cells in a CCR9-dependent fashion.* Int J Oncol, 2011. **38**(5): p. 1279-85.

24. Sharma, P.K., et al., *CCR9 mediates PI3K/AKT-dependent antiapoptotic signals in prostate cancer cells and inhibition of CCR9-CCL25 interaction enhances the cytotoxic effects of etoposide.* Int J Cancer, 2010. **127**(9): p. 2020-30.

25. Singh, S., et al., *Expression and functional role of CCR9 in prostate cancer cell migration and invasion.* Clinical cancer research : an official journal of the American Association for Cancer Research, 2004. **10**(24): p. 8743-50.

26. Sikandar, S., Dizon, D., Shen, X., Li, Z., Besterman, J and Lipkin, SM, *The Class I HDAC Inhibitor MGCD0103 Induces Cell Cycle Arrest and Apoptosis in Colon Cancer Initiating Cells by Upregulating DKK-1 and Non-Canonical WNT Signaling. .* Oncotarget, 2010. **1**(7): p. 666-690.

27. Sikandar, S.S., et al., *NOTCH signaling is required for formation and self-renewal of tumor-initiating cells and for repression of secretory cell differentiation in colon cancer.* Cancer Res, 2010. **70**(4): p. 1469-78.

28. Lira, S.A., et al., *Conditional transgenic models to study chemokine biology.* Methods Mol Biol, 2004. **239**: p. 105-22.

29. Pang, R., et al., *A subpopulation of CD26+ cancer stem cells with metastatic capacity in human colorectal cancer.* Cell Stem Cell, 2010. **6**(6): p. 603-15.

30. Pena, C., et al., *SNAI1 expression in colon cancer related with CDH1 and VDR downregulation in normal adjacent tissue.* Oncogene, 2009. **28**(49): p. 4375-85.

31. Palmer, H.G., et al., *The transcription factor SNAIL represses vitamin D receptor expression and responsiveness in human colon cancer.* Nature medicine, 2004. **10**(9): p. 917-9.

32. Kopan, R. and M.X. Ilagan, *The canonical Notch signaling pathway: unfolding the activation mechanism.* Cell, 2009. **137**(2): p. 216-33.

33. Harrison, H., Farnie, G., Brennan, K. and Clarke, R., *Breast Cancer Stem Cells: Something Out of Notching?* Cancer Res, 2010. **70**: p. 8973-8976.

34. Taketo, M.M., *Reflections on the Spread of Metastasis to Cancer Prevention.* Cancer Prev Res, 2011. **4** p. 324-328.

35. Baba, Y., et al., *Phosphorylated AKT expression is associated with PIK3CA mutation, low stage, and favorable outcome in 717 colorectal cancers.* Cancer, 2011. **117**(7): p. 1399-408.

36. Yeung, T.M., et al., *Regulation of self-renewal and differentiation by the intestinal stem cell niche.* Cellular and molecular life sciences : CMLS, 2011. **68**(15): p. 2513-23.

37. Fre, S., et al., *Epithelial morphogenesis and intestinal cancer: new insights in signaling mechanisms.* Advances in cancer research, 2008. **100**: p. 85-111.

38. Riccio, O., et al., *Loss of intestinal crypt progenitor cells owing to inactivation of both Notch1 and Notch2 is accompanied by derepression of CDK inhibitors p27Kip1 and p57Kip2.* EMBO reports, 2008. **9**(4): p. 377-83.

39. Vooijs, M., et al., *Mapping the consequence of Notch1 proteolysis in vivo with NIP-CRE.* Development, 2007. **134**(3): p. 535-44.

40. de Lau, W., N. Barker, and H. Clevers, *WNT signaling in the normal intestine and colorectal cancer.* Frontiers in bioscience : a journal and virtual library, 2007. **12**: p. 471-91.

41. Meng, R.D., et al., *gamma-Secretase inhibitors abrogate oxaliplatin-induced activation of the Notch-1 signaling pathway in colon cancer cells resulting in enhanced chemosensitivity.* Cancer Research, 2009. **69**(2): p. 573-82.

42. Steg, A.D., et al., *Targeting the notch ligand JAGGED1 in both tumor cells and stroma in ovarian cancer.* Clinical cancer research : an official journal of the American Association for Cancer Research, 2011. **17**(17): p. 5674-85.

43. Wu, Y., et al., *Therapeutic antibody targeting of individual Notch receptors.* Nature, 2010. **464**(7291): p. 1052-7.

44. Jubb, A.M., et al., *Expression of delta-like ligand 4 (Dll4) and markers of hypoxia in colon cancer.* British journal of cancer, 2009. **101**(10): p. 1749-57.

45. Ridgway, J., et al., *Inhibition of Dll4 signalling inhibits tumour growth by deregulating angiogenesis.* Nature, 2006. **444**(7122): p. 1083-7.

46. Wang, T., M. Baron, and D. Trump, *An overview of Notch3 function in vascular smooth muscle cells.* Progress in biophysics and molecular biology, 2008. **96**(1-3): p. 499-509.

47. Vooijs, M., Z. Liu, and R. Kopan, *Notch: architect, landscaper, and guardian of the intestine.* Gastroenterology, 2011. **141**(2): p. 448-59.

48. Guilmeau, S., et al., *Heterogeneity of Jagged1 expression in human and mouse intestinal tumors: implications for targeting Notch signaling.* Oncogene, 2010. **29**(7): p. 992-1002.

49. Yanall l., N., J., Ira K., Hlloka S. Kamal A.,I., and Mlzunuma N. , *Dlk-1, a cellourface antigen on foetal hepatic stem/progenitor cells, is expressed in hepatocellular, colon, pancreas and breast carcinomas at a high frequency.* Journal of Biochemistry, 2010. **148**: p. 85-92.

50. Burger, J.A. and T.J. Kipps, *CXCR4: a key receptor in the crosstalk between tumor cells and their microenvironment.* Blood, 2006. **107**(5): p. 1761-7.

51. Rettig, M.P., G. Ansstas, and J.F. DiPersio, *Mobilization of hematopoietic stem and progenitor cells using inhibitors of CXCR4 and VLA-4.* Leukemia : official journal of the Leukemia Society of America, Leukemia Research Fund, U.K, 2012. **26**(1): p. 34-53.

52. Rettig, M.P., et al., *CXCR4 and mobilization of hematopoietic precursors.* Methods in enzymology, 2009. **460**: p. 57-90.

53. Uy, G.L., M.P. Rettig, and A.F. Cashen, *Plerixafor, a CXCR4 antagonist for the mobilization of hematopoietic stem cells.* Expert opinion on biological therapy, 2008. **8**(11): p. 1797-804.

54. Damon, L.E., *Mobilization of hematopoietic stem cells into the peripheral blood.* Expert review of hematology, 2009. **2**(6): p. 717-33.

55. Peled, A., O. Wald, and J. Burger, *Development of novel CXCR4-based therapeutics.* Expert opinion on investigational drugs, 2012. **21**(3): p. 341-53.

56. Hung, K.E., et al., *Development of a mouse model for sporadic and metastatic colon tumors and its use in assessing drug treatment.* Proceedings of the National Academy of Sciences of the United States of America, 2010. **107**(4): p. 1565-70.

57. Wendt, M.K., et al., *In vivo dual substrate bioluminescent imaging.* Journal of visualized experiments : JoVE, 2011(56).

58. Johnson, E.L., et al., *CCL25-CCR9 interaction modulates ovarian cancer cell migration, metalloproteinase expression, and invasion.* World J Surg Oncol, 2010. **8**: p. 62.

59. Vermeulen, L., et al., *Single-cell cloning of colon cancer stem cells reveals a multi-lineage differentiation capacity.* Proceedings of the National Academy of Sciences of the United States of America, 2008. **105**(36): p. 13427-32.

60. Pastor, D.M., et al., *Primary cell lines: false representation or model system? a comparison of four human colorectal tumors and their coordinately established cell lines.* International journal of clinical and experimental medicine, 2010. **3**(1): p. 69-83.

61. Freshney, R., *Isolation and culture of intestinal epithelial cells.* 2002.

62. Nickoloff, B.J., et al., *Jagged-1 mediated activation of notch signaling induces complete maturation of human keratinocytes through NF-kappaB and PPARgamma.* Cell death and differentiation, 2002. **9**(8): p. 842-55.

63. Weijzen, S., et al., *The Notch ligand Jagged-1 is able to induce maturation of monocyte-derived human dendritic cells.* Journal of immunology, 2002. **169**(8): p. 4273-8.

64. Ma, X.B., et al., *Expression and role of Notch signalling in the regeneration of rat tracheal epithelium.* Cell proliferation, 2009. **42**(1): p. 15-28.

65. Svensson, M., et al., *CCL25 mediates the localization of recently activated CD8alphabeta(+) lymphocytes to the small-intestinal mucosa.* The Journal of clinical investigation, 2002. **110**(8): p. 1113-21.

66. Sikandar, S., Edwards, R., Lyles, K., Waterman, M. and Lipkin, SM, *NOTCH signaling is required for colon cancer initiating cell tumor formation, self-renewal and repression of secretory cell lineage differentiation.* Cancer Research, 2010. **70**(4): p. 1469-78.

67. Walters, S., et al., *Comparability of stage data in cancer registries in six countries: lessons from the International Cancer Benchmarking Partnership.* Int J Cancer, 2013. **132**(3): p. 676-85.

68. Ellis, L.M., *Preclinical data targeting vascular endothelial growth factor in colorectal cancer.* Clin Colorectal Cancer, 2004. **4 Suppl 2**: p. S55-61.

69. Dimasi, J.A., et al., *Clinical approval success rates for investigational cancer drugs.* Clin Pharmacol Ther, 2013. **94**(3): p. 329-35.

70. Rubio-Viqueira, B. and M. Hidalgo, *Direct in vivo xenograft tumor model for predicting chemotherapeutic drug response in cancer patients.* Clin Pharmacol Ther, 2009. **85**(2): p. 217-21.

71. Sausville, E.A. and A.M. Burger, *Contributions of human tumor xenografts to anticancer drug development.* Cancer Res, 2006. **66**(7): p. 3351-4, discussion 3354.

72. Siolas, D. and G.J. Hannon, *Patient-Derived Tumor Xenografts: Transforming Clinical Samples into Mouse Models.* Cancer Res, 2013.

73. Chen, H.J., et al., *Chemokine 25-induced signaling suppresses colon cancer invasion and metastasis.* J Clin Invest, 2012. **122**(9): p. 3184-96.

74. Ebert, M.P., et al., *TFAP2E-DKK4 and chemoresistance in colorectal cancer.* N Engl J Med, 2012. **366**(1): p. 44-53.

75. Meng, R.D., et al., *gamma-Secretase inhibitors abrogate oxaliplatin-induced activation of the Notch-1 signaling pathway in colon cancer cells resulting in enhanced chemosensitivity.* Cancer Res, 2009. **69**(2): p. 573-82.

76. Cancer Genome Atlas, N., *Comprehensive molecular characterization of human colon and rectal cancer.* Nature, 2012. **487**(7407): p. 330-7.

77. Quail, D.F. and J.A. Joyce, *Microenvironmental regulation of tumor progression and metastasis.* Nat Med, 2013. **19**(11): p. 1423-37.

78. Schneider JS, V.J., Terzic A, Fraidenraich D., *Blastocyst injection of embryonic stem cells: a simple approach to unveil mechanisms of corrections in mouse models of human disease.* Stem Cell Rev, 2009. **4**: p. 369-77.

79. Eds Johan Auwerx, S.L.A., Stephen D. Brown, Monica Justice, David D. Moore, Joseph Nadeau, *Current Protocols in Mouse Biology*, in http://onlinelibrary.wiley.com/book/10.1002/9780470942390. 2013, Wiley.

80. Witherspoon, M., et al., *Unbiased metabolite profiling indicates that a diminished thymidine pool is the underlying mechanism of colon cancer chemoprevention by alpha-difluoromethylornithine.* Cancer Discov, 2013. **3**(9): p. 1072-81.

81. Casero, R.A., Jr., *Say what? The activity of the polyamine biosynthesis inhibitor difluoromethylornithine in chemoprevention is a result of reduced thymidine pools?* Cancer Discov, 2013. **3**(9): p. 975-7.

82. Sharma, S.K., et al., *Polyamine-based small molecule epigenetic modulators.* Medchemcomm, 2012. **3**(1): p. 14-21.

83. Huang, Y., et al., *Polyamine analogues targeting epigenetic gene regulation.* Essays Biochem, 2009. **46**: p. 95-110.

84. Meurens, F., et al., *Expression of mucosal chemokines TECK/CCL25 and MEC/CCL28 during fetal development of the ovine mucosal immune system.* Immunology, 2007. **120**(4): p. 544-55.

85. Meurens, F., et al., *Expression of TECK/CCL25 and MEC/CCL28 chemokines and their respective receptors CCR9 and CCR10 in porcine mucosal tissues.* Vet Immunol Immunopathol, 2006. **113**(3-4): p. 313-27.

86. Lautt, W.W., *Mechanism and role of intrinsic regulation of hepatic arterial blood flow: hepatic arterial buffer response.* Am J Physiol, 1985. **249**(5 Pt 1): p. G549-56.

87. Thiel, H., *Liver hemodynamics and portacaval shunt.* Surg Gynecol Obstet, 1980. **150**(4): p. 587-92.

88. Dancis, J., *Transport of substances across perfused organs.* Acta Endocrinol Suppl (Copenh), 1972. **158**: p. 347-75.

89. Vanharanta, S. and J. Massague, *Hypoxia signaling--license to metastasize.* Cancer Discov, 2013. **3**(10): p. 1103-4.

90. Vanharanta, S. and J. Massague, *Origins of metastatic traits.* Cancer Cell, 2013. **24**(4): p. 410-21.

91. Chaturvedi, P., et al., *Hypoxia-inducible factor-dependent breast cancer-mesenchymal stem cell bidirectional signaling promotes metastasis.* J Clin Invest, 2013. **123**(1): p. 189-205.

92. Eisinger-Mathason, T.S., et al., *Hypoxia-dependent modification of collagen networks promotes sarcoma metastasis.* Cancer Discov, 2013. **3**(10): p. 1190-205.

93. Erler, J.T., et al., *Lysyl oxidase is essential for hypoxia-induced metastasis.* Nature, 2006. **440**(7088): p. 1222-6.

94. Gilkes, D.M., et al., *Collagen prolyl hydroxylases are essential for breast cancer metastasis.* Cancer Res, 2013. **73**(11): p. 3285-96.

95. Fidler, I.J., et al., *Modulation of tumor cell response to chemotherapy by the organ environment.* Cancer Metastasis Rev, 1994. **13**(2): p. 209-22.

96. Wilmanns, C., et al., *Modulation of Doxorubicin sensitivity and level of p-glycoprotein expression in human colon-carcinoma cells by ectopic and orthotopic environments in nude-mice.* Int J Oncol, 1993. **3**(3): p. 413-22.

97. Okumura, K., et al., *Correlation between chemosensitivity and mRNA expression level of 5-fluorouracil-related metabolic enzymes during liver metastasis of colorectal cancer.* Oncol Rep, 2006. **15**(4): p. 875-82.

98. Vermeulen, L., et al., *Single-cell cloning of colon cancer stem cells reveals a multi-lineage differentiation capacity.* Proc Natl Acad Sci U S A, 2008. **105**(36): p. 13427-32.

99. Pastor, D.M., et al., *Primary cell lines: false representation or model system? a comparison of four human colorectal tumors and their coordinately established cell lines.* Int J Clin Exp Med, 2010. **3**(1): p. 69-83.

100. Jahid, S., et al., *miR-23a promotes the transition from indolent to invasive colorectal cancer.* Cancer Discov, 2012. **2**(6): p. 540-53.

101. Yu, C.R., et al., *CCR9A and CCR9B: two receptors for the chemokine CCL25/TECK/Ck beta-15 that differ in their sensitivities to ligand.* J Immunol, 2000. **164**(3): p. 1293-305.

102. Nagy, A., *Manipulating the Mouse Embryo: A Laboratory Manual,Third Edition.* 2003.: Cold Spring Harbor Laboratory Press.

103. Martin, M. *Cutadapt removes adapter sequences from high-throughput sequencing reads.* EMBnet.journal, 2011.

104. Li, H. and R. Durbin, *Fast and accurate short read alignment with Burrows-Wheeler transform.* Bioinformatics, 2009. **25**(14): p. 1754-60.

105. McKenna, A., et al., *The Genome Analysis Toolkit: a MapReduce framework for analyzing next-generation DNA sequencing data.* Genome Res, 2010. **20**(9): p. 1297-303.

106. Cao, Z., et al., *Angiocrine factors deployed by tumor vascular niche induce B cell lymphoma invasiveness and chemoresistance.* Cancer Cell, 2014. **25**(3): p. 350-65.

107. Sikandar, S., et al., *The class I HDAC inhibitor MGCD0103 induces cell cycle arrest and apoptosis in colon cancer initiating cells by upregulating Dickkopf-1 and non-canonical Wnt signaling.* Oncotarget, 2010. **1**(7): p. 596-605.

108. Ahmed, D., et al., *Epigenetic and genetic features of 24 colon cancer cell lines.* Oncogenesis, 2013. **2**: p. e71.

109. Helm, J., et al., *Current and evolving strategies for colorectal cancer screening.* Cancer Control, 2003. **10**(3): p. 193-204.

110. Hanahan, D. and R.A. Weinberg, *Hallmarks of cancer: the next generation.* Cell, 2011. **144**(5): p. 646-74.

111. Valastyan, S. and R.A. Weinberg, *Tumor metastasis: molecular insights and evolving paradigms.* Cell, 2011. **147**(2): p. 275-92.

112. *Comprehensive molecular characterization of human colon and rectal cancer.* Nature, 2012. **487**(7407): p. 330-7.

113. Gout, S. and J. Huot, *Role of cancer microenvironment in metastasis: focus on colon cancer.* Cancer Microenviron, 2008. **1**(1): p. 69-83.

114. Arrowsmith, J., *Trial watch: Phase II failures: 2008-2010.* Nat Rev Drug Discov, 2011. **10**(5): p. 328-9.

115. de Jong, G.M., et al., *Animal models for liver metastases of colorectal cancer: research review of preclinical studies in rodents.* J Surg Res, 2009. **154**(1): p. 167-76.

116. Francia, G., et al., *Mouse models of advanced spontaneous metastasis for experimental therapeutics.* Nat Rev Cancer, 2011. **11**(2): p. 135-41.

117. Hung, K.E., et al., *Development of a mouse model for sporadic and metastatic colon tumors and its use in assessing drug treatment.* Proc Natl Acad Sci U S A, 2010. **107**(4): p. 1565-70.

118. Kalluri, R. and R.A. Weinberg, *The basics of epithelial-mesenchymal transition.* Journal of Clinical Investigation, 2009. **119**(6): p. 1420-1428.

119. Bates, R.C. and A.M. Mercurio, *The epithelial-mesenchymal transition (EMT) and colorectal cancer progression.* Cancer Biol Ther, 2005. **4**(4): p. 365-70.

120. Bates, R.C., *Colorectal cancer progression: integrin alphavbeta6 and the epithelial-mesenchymal transition (EMT).* Cell Cycle, 2005. **4**(10): p. 1350-2.

121. Liotta, L.A., *Tumor invasion and metastases: role of the basement membrane. Warner-Lambert Parke-Davis Award lecture.* Am J Pathol, 1984. **117**(3): p. 339-48.

122. Xu, B.J.G., et al., *Identification of Early Intestinal Neoplasia Protein Biomarkers Using Laser Capture Microdissection and MALDI MS.* Molecular & Cellular Proteomics, 2009. **8**(5): p. 936-945.

123. Crapo, P.M., T.W. Gilbert, and S.F. Badylak, *An overview of tissue and whole organ decellularization processes.* Biomaterials, 2011. **32**(12): p. 3233-43.

124. Gilbert, T.W., T.L. Sellaro, and S.F. Badylak, *Decellularization of tissues and organs.* Biomaterials, 2006. **27**(19): p. 3675-83.

125. Mertsching, H., et al., *Engineering of a vascularized scaffold for artificial tissue and organ generation.* Biomaterials, 2005. **26**(33): p. 6610-7.

126. Smith, G., et al., *Mutations in APC, Kirsten-ras, and p53--alternative genetic pathways to colorectal cancer.* Proc Natl Acad Sci U S A, 2002. **99**(14): p. 9433-8.

127. Trobridge, P., et al., *TGF-beta receptor inactivation and mutant Kras induce intestinal neoplasms in mice via a beta-catenin-independent pathway.* Gastroenterology, 2009. **136**(5): p. 1680-8 e7.

128. Dupuy, A.J., et al., *Mammalian mutagenesis using a highly mobile somatic Sleeping Beauty transposon system.* Nature, 2005. **436**(7048): p. 221-6.

129. March, H.N., et al., *Insertional mutagenesis identifies multiple networks of cooperating genes driving intestinal tumorigenesis.* Nat Genet, 2011. **43**(12): p. 1202-9.

130. Ott, H.C., et al., *Perfusion-decellularized matrix: using nature's platform to engineer a bioartificial heart.* Nat Med, 2008. **14**(2): p. 213-221.

131. Totonelli, G., et al., *A rat decellularized small bowel scaffold that preserves villus-crypt architecture for intestinal regeneration.* Biomaterials, 2012. **33**(12): p. 3401-10.

132. Lohi, J., et al., *Laminins, tenascin and type VII collagen in colorectal mucosa.* Histochem J, 1996. **28**(6): p. 431-40.

133. Hunter, D.D., et al., *A laminin-like adhesive protein concentrated in the synaptic cleft of the neuromuscular junction.* Nature, 1989. **338**(6212): p. 229-34.

134. Kosinski, C., et al., *Gene expression patterns of human colon tops and basal crypts and BMP antagonists as intestinal stem cell niche factors.* Proc Natl Acad Sci U S A, 2007. **104**(39): p. 15418-23.

135. Deveney, C.W., et al., *Establishment of human colonic epithelial cells in long-term culture.* J Surg Res, 1996. **64**(2): p. 161-9.

136. Roig, A.I., et al., *Immortalized epithelial cells derived from human colon biopsies express stem cell markers and differentiate in vitro.* Gastroenterology, 2010. **138**(3): p. 1012-21 e1-5.

137. Jung, P., et al., *Isolation and in vitro expansion of human colonic stem cells.* Nat Med, 2011. **17**(10): p. 1225-7.

138. Ivics, Z., et al., *Molecular reconstruction of Sleeping Beauty, a Tc1-like transposon from fish, and its transposition in human cells.* Cell, 1997. **91**(4): p. 501-10.

139. Ivics, Z., et al., *Transposon-mediated genome manipulation in vertebrates.* Nat Methods, 2009. **6**(6): p. 415-22.

140. Grabundzija, I., et al., *Comparative analysis of transposable element vector systems in human cells.* Mol Ther, 2010. **18**(6): p. 1200-9.

141. Pusch, J., et al., *The physiological performance of a three-dimensional model that mimics the microenvironment of the small intestine.* Biomaterials, 2011. **32**(30): p. 7469-78.

142. Ridky, T.W., et al., *Invasive three-dimensional organotypic neoplasia from multiple normal human epithelia.* Nat Med, 2010. **16**(12): p. 1450-5.

143. Starr, T.K., et al., *A transposon-based genetic screen in mice identifies genes altered in colorectal cancer.* Science, 2009. **323**(5922): p. 1747-50.

144. Su, Q., et al., *A DNA transposon-based approach to validate oncogenic mutations in the mouse.* Proc Natl Acad Sci U S A, 2008. **105**(50): p. 19904-9.

145. Copeland, N.G. and N.A. Jenkins, *Harnessing transposons for cancer gene discovery.* Nat Rev Cancer, 2010. **10**(10): p. 696-706.